Experimental and Techno-economic Studies of Pipeline Hydro-transport of Agricultural Residue Biomass to a Biorefinery

by

Mahdi Vaezi

A thesis submitted in partial fulfillment of the requirements for the degree of

Doctor of Philosophy

Department of Mechanical Engineering
University of Alberta

© Mahdi Vaezi, 2014

Abstract

Pipeline hydro-transport of agricultural residue biomass to bio-based energy facilities, e.g. a bio-refinery, is considered to be a more economically favorable method than truck delivery. Pipeline hydro-transport not only benefits from economy of scale, but also reduces the environmental and traffic congestion issues compared to truck delivery. In this research, a 25 m closed-circuit lab-scale pipeline facility was designed and fabricated to experimentally investigate pipeline hydro-transport of knife-milled and pre-classified wheat straw and corn stover agricultural residues. Agricultural residue particle-water mixtures (or slurries) were prepared over a wide range of particle size, slurry solid mass content, and slurry bulk velocity, and were pumped into the closed-circuit. Several morphological and mechanical parameters were measured prior to and during pipelining agricultural residue particles through the pipeline. The main objectives of the research were to (1) study the particle size, particle size distribution, and morphological features of agricultural residue biomass; (2) study the technical feasibility of replacing truck with pipeline in agricultural residue biomass delivery; (3) experimentally investigate friction loss and rheological behaviors of agricultural residue biomass slurry through a pipeline at various slurry solid mass content, slurry bulk velocity, and agricultural residue biomass particles types and sizes; (4) develop an empirical correlation to predict the agricultural residue biomass slurry pressure drop across the pipeline; (5) evaluate the performance of centrifugal slurry pumps handling agricultural residue biomass slurry; and finally (6) conduct a series of techno-economic analyses on pipeline hydro-transport of agricultural residue biomass. Based on the results obtained in the study, agricultural residue biomass particles studied here were found to be fibrous in nature, and the slurry of fibrous

agricultural residue biomass particles exhibited unique drag-reduction characteristics for more concentrated slurries at elevated velocities. In addition, the proposed empirical correlation was found capable of precisely predicting the longitudinal pressure gradient of the flow of agricultural residue biomass slurry in pipes, and the efficiency of the pump handling small (<3.2 mm) wheat straw particles was found to be more than the efficiency of the same pump handling pure water only. Finally, all the pipelines hydraulically transporting agricultural residue biomass with capacities of 1.0 M dry t/yr and more were found to have lower fixed and incremental costs compared to alternatives of hauling by truck. The results obtained here would help in optimizing the design and operation of commercial agricultural residue biomass pipeline hydro-transport processes and the development of large-scale bio-based energy facilities.

Preface

The pipeline facility referred to in chapter 3 was originally fabricated by H. Safaei and J. Luk in the Large Scale Fluids Lab and was further modified by me. All other technical apparatus referred were designed, fabricated, and calibrated by me with the assistance of Dr. A. Kumar. All of the modeling, data analyses, and concluding remarks in chapters 4 to 8 are my original work, as well as the literature review in chapter 2.

Chapter 3 of this thesis was published as *Vaezi, M., Pandey, V., Kumar, A., and Bhattacharyya, S., "Lignocellulosic biomass particle shape and size distribution analysis using digital image processing for pipeline hydro-transportation," Biosystems Engineering, Volume 114 (2013), Pages 97-112*. I was responsible for the data collection and analysis as well as the manuscript composition. V. Pandey assisted with the data collection. A. Kumar was the supervisory author and was involved with concept formation and manuscript composition. S. Bhattacharyya was a supervisory author as well.

Chapter 4 of this thesis was published as *Vaezi, M., Katta, A.K., and Kumar, A., "Investigation into the mechanisms of pipeline transport of slurries of wheat straw and corn stover to supply a bio-refinery," Biosystems Engineering, Volume 118 (2014), Pages 52–67.* I was responsible for the performance of the experiments and analysis of the data as well as the manuscript composition. A.K. Katta assisted with some viscosity measurements. A. Kumar was the supervisory author and was involved with concept formation and manuscript composition.

Chapter 5 of this thesis was published as *Vaezi, M. and Kumar, A., "The flow of wheat straw suspensions in an open-impeller centrifugal pump," Biomass and Bioenergy, Volume 69 (2014), Pages 106-126.* I was responsible for the performance of the experiments and analysis of the data as well as the manuscript composition. A. Kumar was the supervisory author and was involved with concept formation and manuscript composition.

This thesis is dedicated to my parents,

Mohammad and Massoumeh,

for their unconditional love, support, and encouragement.

Acknowledgment

First and foremost, I would like to express sincere gratitude to my research supervisor, Dr. Amit Kumar, without whose endless support, invaluable advice, and active participation in every step of the process this thesis may never have been completed. Not only did he give generously of his time and expertise while carrying out the experiments, he also remained particularly involved while I wrote the papers and this thesis. I have been extremely fortunate to work with Dr. Kumar, whose enthusiasm for science and understanding of/kindness to people has set the norm for my future career.

I am thankful to my supervising committee, Dr. Michael Lipsett and Dr. Rajender Gupta. Their discussions and comments during the candidacy exam were extremely beneficial in the completion of this thesis.

Special recognition must be given to Prof. Geoff Duffy at The University of Auckland for offering helpful feedback on the pump performance evaluation, as well as guides and suggestions on the numerical modeling section of this dissertation.

This work could not have been completed without the support of the staff at the Department of Mechanical Engineering. Special thanks must be made to Teresa Gray and Richard Groulx for their administrative support, as well as to Roger Marchand, Rick Bubenko, and Ryan Shoults at the Machine Shop and Rick Conrad in the Electrical Lab for their technical advice and all the time spent in my lab to fabricate, program, and calibrate devices.

I truly appreciate my summer students Vivek Pandey, Rohit Ragupal, Anil Katta, and Jonathan Down, also my lab assistants Abrar Foad, Tanveer Hassan, Asif Ankur, and Md. Abdul Mirdad, whose contributions in experimental measurements were extremely notable.

I wish to acknowledge Astrid Blodgett for editing/proofreading countless pages from my papers and thesis.

I would like to thank all my friends at the University of Alberta, all former and current graduate students in the Sustainable Energy Research Group for their support. My heartfelt gratitude particularly to the people in Ring House # 3 for their pure friendship, for all the pleasant days spent, parties thrown, and memories colored together.

The author is grateful to Alberta Agriculture, Alberta Innovates – Bio Solutions, and the National Sciences and Engineering Research Council of Canada (NSERC) for the financial support to carry out this project.

Above all, I wholeheartedly thank my mighty God for giving me the vision, power, spirit, and endurance to complete this interesting research.

Table of Contents

List of Figures

List of Tables

CHAPTER 1

Introduction

1.1. Background

With the depletion of fossil fuels and their undesirable impacts on the environment, biomass is receiving increased attention as a potential source of renewable energy. Biomass refers to a renewable fuel derived from a currently living organism or by-product of a currently living organism. These could be forest-based (e.g., whole tree, forest harvest residues, mill residues), agriculture-based (e.g., grains, straw, corn stover), animal-based (e.g., animal waste, manure), and energy crops (e.g. switchgrass, miscanthus, willow, poplar). Biomass is considered one of the promising amongst renewable resources for fuel production as it is considered a renewable resource and is nearly carbon neutral [1]. Today, commercial scale biomass-based (bio-based) liquid fuel production facilities mostly operate on grain-based (starchy) biomass (e.g., canola, corn, wheat) and are at capacities significantly below those of current fossil-fuel based plants. The liquid fuel production plants based on lignocellulosic biomass (e.g., straw, corn stover, wood chips) are at various stages of development and currently not operating commercially on a large scale. This is partly because of immature conversion technologies but mainly due to the high cost of transporting feedstock by truck to the plants [2-4].

In the use of lignocellulsic biomass for the production of fuels, there is a trade-off between the capital cost of production per unit output and the costs of transportation. Such a trade-off results in an economic optimum size of the field/forest-sourced bio-based energy facilities at which the cost of the production of fuels or chemicals is minimum [5]. Currently, most bio-based energy facilities are constructed below such economic optimum size, making them uncompetitive with fossil fuel-based facilities. Low biomass bulk density, the high cost of biomass transportation by truck, security of supply, traffic congestion issues of supplying large-scale plants, and anticipated local

community oppositions are major barriers towards increasing the scale of bio-based energy facilities [3].

In terms of traffic issues, approximately one chip van (36 tonne capacity) is required every four minutes by a plant using 4.3 M t/yr of wood chips to produce 900 MW electricity [6], and 15 standard highway trucks (20 tonne capacity) per hour are required by a plant using 2 M dry t/yr of corn stover to produce up to 960 ML/yr of ethanol [7], a very small production capacity compared to 25 GL/yr capacity of a typical oil refinery [4, 8]. In terms of economic issues, the transport and logistics arrangements of biomass from its point of availability, i.e., farm or forest, to its point of use, e.g., bio-based energy facility, contribute significantly to the total delivered cost of biomass. This cost is directly proportional to the number and frequency of trucks required and the distance over which the fuel has to be moved, factors that increase with increasing scale, i.e., economies of scale do not apply to truck delivery. Allen and Browne [9] reported the cost of transporting biomass to be 29%, 22%, 17%, and 12% of the total delivered cost of straw, forest biomass, coppice, and miscanthus, respectively. Epplin [10] estimated the cost to transport switchgrass to a conversion facility to be 8.8 $/dry t or 24% of the total delivered cost. Morey et al. [11] found the truck transport of round bales of corn stover to contribute 24.9% to the total cost. Aden et al. [2] showed that the contribution of corn stover delivery to the total delivered cost was 24%. Perlack and Turhollow [12] reported the cost of truck delivery to contribute as much as 45% to the delivered cost of corn stover at a bio-ethanol plant with a capacity of less than 1 M dry t/yr and a hauling distance of 50 to 80 km [13]. Mobile pelleting stations for biomass densification was investigated by Krishnakumar and Ileleji [14] as well, when the cost of truck delivery did not decrease drastically because of the new cost incurred in pelleting and handling. The sustainability of the delivery system thus requires a more cost-effective mode of transport to replace truck delivery to resolve the traffic congestion issue and improve the cost-competitiveness of the bio-energy sector.

Pipeline transport of agricultural residue biomass (e.g., wheat straw and corn stover) in the form of slurry (chopped straw- or wood chip-water mixture) can be considered as an alternative approach to enable bio-based energy facilities to achieve higher capacities;

such transport both creates benefits from economies of scale [15] and reduces traffic congestion issues of overland transportation. Although such an approach comes with limitations for applications involving combustion [15], there is no penalty in pipeline hydro-transport of biomass in the form of a solid-liquid mixture (slurry[1]) for bio-ethanol production purposes via fermentation [4], hydrothermal liquefaction [16], hydrothermal hydrolysis [17], or hydrothermal pre-treatment process where the process itself is aqueous. In these cases, most of the equipment at the pipeline inlet facility replaces equipment at the bio-refinery that would otherwise be required if biomass were directly delivered to the plant, e.g., washing, shredding, sizing, and slurrying machines [4]. Biomass slurry would contain almost the required amount of process water, and the slurry would enter the facility directly with or without minor adjustments in the biomass-water ratio, depending on the concentration at which the slurry is pipelined [18]. The pipeline system would be comprised of a number of local receiving facilities, which use pipelines to hydro-transport biomass to a central bio-ethanol refinery. These receiving facilities would receive biomass from fields by trucks. That would result in small-scale short hauls over a limited rural area instead of frequent large-scale truck deliveries between farms and refineries via main urban roads. In other words, pipeline hydro-transport could be an integrated operation of truck and pipeline with the initial transport of biomass by trucks using existing rural roads [3, 15], but it would not be a truck-independent procedure.

Through a series of techno-economic analyses, Kumar et al. [3, 4, 15] studied various scenarios of pipelining wood chips and corn stover biomass. They investigated one-way and two-way pipeline scenarios wherein a one-way pipe would discharge/use the carrier liquid at the receiving facility and a two-way pipe would return all or a portion of the carrier liquid to the inlet facility. They found the cost of transporting wood chips by pipeline at a solid volume content of 30% to be less than the midrange distance cost of truck delivery (0.1167 $/t.km - 2000 U.S. dollar basis) at capacities above 0.5 M dry t/yr for a one-way pipeline and 1.25 M dry t/yr for a two-way pipeline. They also studied the cost of pipeline hydro-transport of corn stover agricultural residue (lignocellulosic) biomass at a 20% solids volume content, compared it with the cost of truck delivery, and

[1]The terms ″slurry″ and ″suspension″, ″fibre″ and ″particle″, ″pressure drop″ and ″friction loss″, ″size″ and ″diameter″ are used interchangeably throughout the thesis.

found that pipeline hydro-transport costs less than truck delivery at capacities above 1.4 M dry t/yr for a one-way pipeline and 4.4 M dry t/yr for a two-way pipeline. However, while the economic feasibility of agricultural residue biomass pipeline hydro-transport has been proved, its technical and chemical feasibility have been never studied before. Furthermore, pressure drop correlations used to obtain the pipeline cost estimates for corn stover had been originally proposed for transporting wood chip-water mixtures in pipes [19, 20]. Corn stover and wood chips are of diverse shapes; the former is fibrous in nature with a wide aspect ratio [21]; the wide aspect ratio gives rise to a variety of unique mechanisms in slurry flow (e.g., drag reduction) [18, 22] that are often not encountered in classical solid-liquid slurry systems.

Although a number of hypotheses has been proposed to explain certain aspects of observed phenomena in slurry flows of fibrous particles, more complete expressions of the functional relationships between the numerous variables governing the hydro-transport of fibrous materials in pipes were achieved based upon purely empirical correlations. Mohamadabadi [23] investigated the effect of long time exposure to water during pipeline transport on the physical properties of wheat straw particles. Luk et al. [24], using the same experimental facility as the one used in the current research, studied the technical feasibility of pipelining wheat straw slurries. The present research attempts to, for the first time, experimentally investigate pipeline hydro-transport of slurries of fibrous agricultural residue biomass, specifically wheat straw and corn stover, and to study technical limitations, potential advantages, governing equations, and economic feasibilities. The output of the research will help others design and operate future agricultural residue biomass pipelines.

1.2. Objectives of the Research

While the overall objective of the research was to experimentally investigate various aspects of agricultural residue biomass pipeline hydro-transport, the specific objectives of the research are:

a) To study the technical feasibility of replacing truck by pipeline in the large-scale agricultural residue biomass transport sector, assess the potential difficulties in handling

agricultural residue biomass slurries, and propose a standard operating procedure for pipelining irregular-shaped agricultural residue biomass particles.

b) To investigate the dimensions, size distributions, size distribution algorithms, morphological features (including shape factors, the effect of knife mill operating factors on particle dimensions, particle size reduction effect during pipelining), and micro-scale surface features of knife-milled pre-classified wheat straw and corn stover.

c) To investigate the effect of fine (<50 μm) particles on the viscosity of the carrier liquid of the agricultural residue biomass slurry during pipeline hydro-transport, critically examine the applicability of wood chips pressure drop correlations to calculate friction losses while hydro-transporting wheat straw and corn stover particles, study the mechanical behavior, specifically the pressure drop, of agricultural residue biomass slurry at various slurry solid mass contents, slurry flow rates, and agricultural residue biomass particles types and sizes, and try to obtain the optimum operating conditions.

d) To establish the effect of slurries of fibrous wheat straw biomass particles over a range of slurry solid mass contents on performance characteristics of centrifugal slurry pumps, particularly on produced head, efficiency, and power consumption of the pump, and develop an empirical correlation to predict the agricultural residue biomass slurry pressure drop throughout the pipeline.

e) To conduct a series of techno-economic analyses on biomass pipeline hydro-transport using empirically obtained technical features and pressure drop correlation and compare the results with previously published analyses.

1.3. Scope and Limitations

- For the present research, the experiments were conducted in a pipeline of diameter of 50 mm (or 2″) only. While the pipe diameter is not considered an experimental variable, efforts have been made to extrapolate the results for larger diameter pipelines.

- The range of slurry bulk velocity studied here varies between 0.5 m/s and 5.0 m/s. Instrument and technical limitations prevented achieving lower and higher velocities.

- The size (d_{50}) of particles studied here is limited to 1.9 to 8.3 mm. The authors are not able to extend the results obtained here to the particles out of this range.

- The experimental measurements were limited to the study of corn stover and wheat straw slurries.

1.4. Organization of the Thesis

The thesis consists of eight chapters, six of which are based on published/submitted papers. This thesis is a consolidation of papers, each chapter of which is intended to be read independently. As a result, some concepts and data are repeated.

The current chapter provides a background on the economic challenges of pipeline hydro-transport of biomass materials to bio-based energy facilities and outlines the objectives and limitations of this research.

The second chapter reviews the literature published on the technical, modeling, and economic aspects of pipeline hydro-transport of biomass (mainly wood chips) particles.

Chapter three investigates particle size, particle size distribution (PSD), and corresponding parameters, PSD functions, morphological features, and micro-scale features of knife-milled pre-classified wheat straw and corn stover.

Chapter four critically examines the applicability of wood chips pressure drop correlations to calculate friction losses while hydro-transporting wheat straw and corn stover particles in pipes and studies mechanical behavior of biomass slurry at various slurry solid mass contents, slurry flow rates, and agricultural residue biomass particles types and sizes.

Chapter five attempts to establish the effect of concentrated slurries of fibrous wheat straw biomass particles over a wide range of slurry solid mass contents on the performance characteristics of a centrifugal slurry pump specifically produced head, efficiency, and power consumption of the centrifugal pump.

In chapter six, an empirical correlation is developed based on experimental measurements to predict longitudinal pressure gradients of the flow of the slurry of agricultural residue biomass in a 50 mm diameter pipeline. The pressure gradient correlation is then scaled up to account for pipe diameters larger than 50 mm.

In chapter seven, the technical parameters and constraints as well as the empirical correlations obtained through the course of experimental study, together with the pipeline economic structure proposed by Kumar et al. [15, 25, 26], are used to develop a data-intensive techno-economic model to estimate the cost of pipeline hydro-transport of wheat straw and corn stover agricultural residue biomass to bio-ethanol refinery.

Finally, chapter eight presents the conclusions and provides recommendations for future research.

References

[1] UN. Green energy: biomass fuels and the evironment. Geneva, Switzerland United Nations; 1991.

[2] Aden, A., Ruth, M., Ibsen, K., Jechura, J., Neeves, K., Sheehan, J., et al. Lignocellulosic biomass to ethanol process design and economics utilizing co-current dilute acid prehydrolysis and enzymatic hydrolysis for corn stover (Report No TP-510-32438). National Renewable Energy Laboratory (NREL); 2002.

[3] Kumar, A., Cameron, J.B., Flynn, P.C. Large-scale ethanol fermentation through pipeline delivery of biomass. Applied Biochemistry and Biotechnology, 2005 (a); 121: 47-58.

[4] Kumar, A., Cameron, J.B., Flynn, P.C. Pipeline transport and simultaneous saccharification of corn stover. Bioresource Technology, 2005 (b); 96: 819-29.

[5] Ruth, M. Large Scale Ethanol Facilities and Short Cut for Changing Facility Size. Internal Report, National Renewable Energy Laboratory Technical Memo; 1999.

[6] Kumar, A., Cameron, J.B., Flynn, P.C. Biomass power cost and optimum plant size in western Canada. Biomass and Bioenergy, 2003; 24: 445-64.

[7] Sokhansanj, S., Turhollow, A., Cushman, J., Cundiff, J. Engineering aspects of collecting corn stover for bioenergy. Biomass & Bioenergy, 2002; 23: 347-55.

[8] Wallace, B., Yancey, M., Easterly, J. Bioethanol co-location with a coal-fired power plant. 25th Symposium on Biotechnology for Fuels and Chemicals Breckenridge, CO; 2003.

[9] Allen, J., Browne, M. Logistics management and costs of biomass fuel supply. International Journal of Physical Distribution & Logistics Management, 1998; 28: 463-77.

[10] Epplin, F.M. Cost to produce and deliver switchgrass biomass to an ethanol-conversion facility in the Southern Plains of the United States. Biomass & Bioenergy, 1996; 11: 459-67.

[11] Morey, R.V., Kaliyan, N., Tiffany, D.G., Schmidt, D.R. A biomass supply logistics system. 2009, p. 4802-14.

[12] Perlack, R.D., Turhollow, A.F. Assessment of options for the collection, handling, and transport of corn stover. Available from: http://bioenergy.ornl.gov/pdfs/ornltm-200244.pdf. Report no ORNL/TM-2002/44; 2002.

[13] Glassner, D., Hettenhaus, J., Schechinger, T. Corn stover collection project. Bioenergy 1998; 1998.

[14] Krishnakumar, P., Ileleji, K.E. A Comparative Analysis of the Economics and Logistical Requirements of Different Biomass Feedstock Types and Forms for Ethanol Production. Applied Engineering in Agriculture, 2010; 26: 899-907.

[15] Kumar, A., Cameron, J.B., Flynn, P.C. Pipeline transport of biomass. Applied Biochemistry and Biotechnology, 2004; 113: 27-39.

[16] Zhu, Y., Biddy, M.J., Jones, S.B., Elliott, D.C., Schmidt, A.J. Techno-economic analysis of liquid fuel production from woody biomass via hydrothermal liquefaction (HTL) and upgrading. Applied Energy, 2014; 129: 384-94.

[17] Thangavelu, S.K., Ahmed, A.S., Ani, F.N. Bioethanol production from sago pith waste using microwave hydrothermal hydrolysis accelerated by carbon dioxide. Applied Energy, 2014; 128: 277-83.

[18] Vaezi, M., Katta, A.K., Kumar, A. Investigation into the mechanisms of pipeline transport of slurries of wheat straw and corn stover to supply a bio-refinery. Biosystems Engineering, 2014; 118: 52-67.

[19] Hunt, W.A. Friction factors for mixtures of wood chips and water flowing in pipelines,. 4th International Conference on the Hydraulic Transport of Solids in Pipes. Alberta, Canada; 1976., p. 1-18.

[20] Wasp, E.J., Aude, T.C., Thompson, T.L., Bailey, C.D. Economics of chip pipelining. Tappi, 1967; 50: 313-18.

[21] Vaezi, M., Pandey, V., Kumar, A., Bhattacharyya, S. Lignocellulosic biomass particle shape and size distribution analysis using digital image processing for pipeline hydro-transportation. Biosystems Engineering, 2013; 114: 97-112.

[22] Duffy, G.G., Lee, P.F.W. Drag reduction in turbulent flow of wood pulp suspensions. Appita, 1978; 31: 280-86.

[23] Mohamadabadi, H.S. Characterization and pipelining of biomass slurries University of Alberta; 2009.

[24] Luk, J., Mohammadabadi, H.S., Kumar, A. Pipeline transport of biomass: Experimental development of wheat straw slurry pressure loss gradients Biomass and Bioenergy, 2014; 64: 329-36.

[25] Kumar, A., Flynn, P.C., Cameron, J.B. Large-scale ethanol fermentation through pipeline delivery of biomass. Applied Biochemistry and Biotechnology, 2005; 121: 47-58.

[26] Kumar, A., Flynn, P.C., Cameron, J.B. Pipeline transport and simultaneous saccharification of corn stover. Bioresource Technology, 2005; 96: 819-29.

CHAPTER 2

Pipeline Hydraulic Transport of Biomass Materials: A Review[1]

2.1. Introduction

Hydraulic transport (hydro-transport) of solids in pipes has been the subject of investigations since the turn of the last century. Nora Blatch (1906) was probably the first person to conduct a systematic investigation on solid-liquid mixture flows through a 25 mm horizontal pipe [1]. Since then, particularly owing to the improvements in centrifugal pump design and the advances in solid-liquid mixture flow knowledge in the 1960s [2], a number of short and long solid-liquid mixture pipelines have been constructed to hydraulically transport a variety of solids, from coal to limestone to complex bitumen. The technical and economic advantages of pipeline hydro-transport have encouraged various sectors to consider replacing conventional modes of transport, e.g., road and rail, with pipelines for long-distance transport purposes. Major advantages include benefits from economies of scale in the construction of the pipeline and associated equipment, large transportation volume (e.g., 2273 Mt/yr of phosphate concentrate [1, 3]), excellent safety record (fewer than two incidents per 10,000 km of pipeline reported per year [4]), continuous operation, and reduced in-transit inventory.

While, to the best knowledge of the authors, there is no large-scale long-distance biomass pipeline in operation at the moment, the pulp and paper industry uses hydro-transport for wood pulp fibres for on-site processing over short distances [5-8]. The pulp and paper industry has also conducted some laboratory-scale research projects on wood chip pipeline hydro-transport for feedstock supply purposes [9-11]. Besides the pulp and paper industry, pipeline hydro-transport of biomass, more specifically lignocellulosic biomass, is now receiving new interest as an alternative means of delivering biomass to bio-based plants [12-18] that can potentially reduce the cost of feedstock delivery [13] and enable bio-based energy facilities to reach higher capacities.

[1] Paper submitted to the Journal of Biomass and Bioenergy, 2014

Wood pulp fibre is not a natural biomass but a mechanically or chemically processed biomass, and, therefore, its hydro-transport is not reviewed here. This paper instead reviews the literature published on pipeline hydro-transport of unprocessed biomass in the pulp and paper industry as well as in the bio-based energy sector. The literature is reviewed in chronological order and is classified into experimental measurements, modeling studies, and techno-economic analyses. All the costs reported in the economic analysis section have been inflated to the 2014 U.S. dollar. Table 2-1 lists the research activities conducted in this field and reviewed here. The objectives of this review are to understand the technical challenges and mechanical limitations as well as the economy of biomass pipeline hydro-transport and also to identify gaps in the knowledge of biomass pipeline hydro-transport for future research.

Table 2-1: Historical development of biomass slurry pipelines

Organization	Time	Location	Biomass Feedstock	Pipeline Length	Pipeline Diameter	Particle Dimension	Reference No.
D.T. Elliott and W.H. de Montmorency Pulp and Paper Institute of Canada	1958	Quebec, Canada	Spruce and balsam fir wood chips	160 m	200 mm	d_{50} = 6.4 mm	[9, 19]
Shell Pipeline Company	1962	Texas, U.S.	Wood chips	1220 m	200 mm	---	[20, 21]
R.R. Faddick Queen's University	1963	Ontario, Canada	Wood chips	---	100 mm	---	[10]
A. Brebner Queen's University	1964	Ontario, Canada	Jack pine and spruce wood chips	120 m	100 mm	d_{50} = 6.4 mm	[22]
E.J. Wasp Bechtel Crop.	1967	California, U.S.	Wood chips	---	200 mm	19 mm×12.7 mm×2.54 mm	[23]
A. Soucy Laval University	1967	Quebec, Canada	Wood chips	---	150 mm	---	[24]
R.R. Faddick Montana State University	1970	Montana, U.S.	Uniform-sized plastic chips	210 m	75 mm 100 mm	12.7 mm×9.5 mm×2.54 mm	[25]
J.L. Gow Montana State University	1971	Montana, U.S.	Lodgepole pine wood chips	---	100 mm 150 mm	d_{50} = 9.5 mm	[11]
W.A. Hunt Montana State University	1976	Montana, U.S	Lodgepole pine wood chips	91 m 183 m	200 mm 300 mm	d_{50} = 28.4 mm	[20]
Kinki University	2011	Japan	Balsa square timber wood chips	100 mm 850 mm 600 mm	32 mm 50 mm 65 mm	d_{50} = 3.0 mm	[15]
University of Leeds University of Kent	2012	U.K.	Flour, willow, wood, bark	3.85 m	49 mm	0.35 mm to 5.6 mm	[26]

2.2. Experimental Measurements

2.2.1. Wood Chip-Water Mixtures in Pipes

Elliott and de Montmorency [9, 19] at the Pulp and Paper Research Institute of Canada (PAPRICAN) were the first to install a laboratory-scale experimental facility to study the hydro-transport of wood chips in pipes. The facility was composed of 160 m of 200 mm diameter aluminum pipe, and the chips consisted of spruce and balsam fir, with d_{50} of 6.4 mm that, at a fully saturated condition, attained a moisture content (water mass content) of 68% to 70% and specific gravity of 1.03 to 1.06 [9]. Elliott [19] observed a deterioration (also referred to as degradation or particle size reduction) caused mainly by the pump and reported the production of wood chips smaller than 12.7 mm to be 39% compared to 10% in control chips from the original batch after four hours of circulation. The optimum mixture solid volume content was reported to be about 30%, since at a solid volume content of 35% the pump power consumption began to increase slightly and at 47% the mixing operation became erratic because the equipment was not designed for such a heavy mixture. Considering pressure drop measurements, Elliot and de Montmorency [9], using a pressure drop-velocity plot, showed that with increasing velocity the curves corresponding to the mixtures above 20% solid volume contents go through a minimum of friction loss, where chips along the bottom start to build up toward plugging conditions. Afterwards, the curves straighten and become parallel/close to the pure water line where chips are in complete suspension.

The research and development section of the Shell Pipeline Company [21] studied hydro-transport of wood chip-water mixtures on a closed-circuit pipeline facility of 1220 m length and 200 mm diameter in Houston, Texas, U.S.A. The results were inconclusive and the system was later dismantled; further experiments were conducted on shorter and smaller clear plastic pipelines 50 mm in diameter. The results, however, were proprietary and not released [20].

Faddick [10] conducted an experimental investigation on wood chip-water mixtures on a 100 mm diameter pipeline. Later, he tried to simulate the pipeline hydro-transport of

wood chips using uniform-sized plastic chips instead [25] (discussed in a subsequent section).

To verify the feasibility of the concept of wood chip hydro-transport and to determine the empirical laws relating various variables, Brebner [22] performed a series of experiments on a test circuit that was made up of 120 m of 100 mm diameter aluminum pipe. He used standard jack pine and spruce chips with d_{50} of 6.4 mm, which at fully saturated conditions attained a moisture content of 70% and specific gravity of 1.15. Considering slurry flow regimes, Brebner observed three regimes at velocities between 1.5 and 4.5 m/s consisted of ″suspension″ for solid volume contents below 5%, ″discontinuous sliding bed with saltation″ for solid volume contents between 5% and 12%, and ″continuous sliding bed″ for solid volume contents above 12%. In the latter, chips were physically interlocked while loose chips progressed at a slightly faster rate above the sliding bed.

Wasp et al. [23] conducted an experiment on conveying wood chips of specific gravity of (fully saturated) 1.13 and dimensions of 19 mm×12.7 mm×2.5 mm through a 200 mm diameter pipe at 3.0 m/s velocity. They applied the homogeneous-heterogeneous model [27] (see section 3, Eqs. 5 and 6) to identify the flow regime and mixture solid volume content across the pipe cross section.

Soucy [24], using 150 mm diameter acrylic pipes, conducted a series of experiments to measure the pressure drop of wood chip-water mixtures in pipes. Soucy's data were later used by Faddick [25] and Gow [11].

In 1962, the Montana State University entered into a cooperative aid agreement with the U.S. Forest Service to conduct a series of technical and economic analyses to establish criteria to design, construct, and operate wood chip pipeline systems to feed the pulp and paper industry [11, 25, 28]. As a part of this study and to simulate the pipeline hydro-transport of wood chips as well as investigate friction loss parameters, Faddick [25] transported uniform-sized plastic chips of a specific gravity of 0.92 and 1.05 and dimensions of 12.7 mm×9.5 mm×2.5 mm through 75 mm and 100 mm diameter and 210 m long acrylic pipes. Later, Gow [11] modified Faddick's laboratory pipeline system to

study wood chip-water mixtures and correlated experimental friction loss data over a range of mixture velocities, pipe diameters, wood chip sizes, and mixture solid volume contents. The use of lodgepole pine wood chips with d_{50} of 9.5 mm, a fully saturated moisture content of 50%, and a specific gravity of 1.015 resulted in the mixture velocity's being limited to 3.3 m/s and 1.3 m/s through 100 mm diameter acrylic plastic and 150 mm diameter aluminum pipes, respectively. Gow's investigation was directly comparable to Faddick's experimental data [10] (the two experiments were conducted with a 100 mm diameter pipe). Gow concluded that at a given mixture velocity, the friction factor increases in magnitude with increasing solid volume content. Also at a given mixture velocity and solid volume content, the friction factor decreases with increasing pipe diameter. However, Gow noted the dependence of friction factor on pipe diameter was non-linear for high solid volume contents and insignificant at high velocities. An abrupt change was also observed in friction factor in which the corresponding velocity (critical velocity) depended on mixture solid volume contents and was due to the change in the mode of transport of wood chips from ″heterogeneous discontinuous sliding bed with saltation″ to ″continuous sliding bed.″ This study employed the terms ″pseudo-laminar″ and ″pseudo-turbulent″ to refer to sliding bed and saltation flows, respectively, to distinguish these phenomena from classical laminar and turbulent pipe flows.

Hunt [20] studied the hydro-transport of wood chip-water mixtures using elongated oblong plate-shaped lodgepole pine wood chips with d_{50} of 28.4 mm and approximate specific gravity of 1.0 to 1.05. He used 200 mm and 300 mm diameter and 91 m and 183 m long steel pipes in order to scale up the experiments conducted on 75 mm, 100 mm, and 150 mm diameter pipes and to examine the applicability of the extrapolation approach to friction loss correlations proposed by others [11, 25]. The friction loss correlation proposed by Hunt will be reviewed in the next section.

Sawai et al. [15] studied the hydro-transport of wood chip-water mixtures in sloped pipelines to understand the mechanism of wood chip blockade and effects of wood chip density, carrier liquid (water) flow rate, pipe diameter, and the inclination angle of the pipeline on maximum flow rate of wood chip-water mixtures. Using balsa square timber wood chips with d_{50} of 3.0 mm and (fully saturated) specific gravity of 0.6 to 1.0, they

designed the sloped (hilly terrain) pipeline in three sections: the upstream section with an incline of 30 degrees and length of 100 mm, the midstream section mounted horizontally or with an upward or downward incline of 2.0 degrees and length of 850 mm, and the downstream section with an incline of 30 degrees and length of 600 mm; all three sections were available in diameters of 32 mm, 50 mm, and 65 mm. Fig. 2-1(a) shows the flow pattern of wood chip-water flow through the midstream section using a pipe diameter of 50 mm, incline angle of 2.0 degrees, and wood chip density of 1296 kg/m^3. Flowing through the midstream section, the carrier liquid changed from supercritical to subcritical flow, which was then followed by a drastic increase in the depth and width of liquid film (hydraulic jump) in which the maximum wood chip flow rate ($Q_{s,max}$) was recorded and a blockade of wood chips subsequently occurred. The stagnation of wood chips was observed right after the hydraulic jump; however, the wood chips arranged in layers were slowly transported with the carrier liquid. In the midstream section, which was mounted upward with an incline of 2.0 degrees, it was not possible to transport the wood chips with carrier liquid in any of the flow conditions. Fig. 2-1(b) presents the variation of maximum wood chip flow rate with carrier liquid rate for various wood chip densities. The maximum flow rate for wood chips with densities larger than water density was larger than the flow rate for wood chips with densities smaller than that of water. However, the general effect of wood chip density on the wood chip maximum flow rate was negligible. Sawai et al. [15] also studied the effect of pipe diameter on maximum wood chip flow rate and observed that the flow rate decreased as the pipe diameter decreased. They also analytically investigated the maximum flow rate of wood chips when a midstream section was mounted horizontally.

Using a pipe with a diameter of 49 mm and length of 3.85 m, Gubba et al. [26] studied pneumatic pipeline transport of biomass particles on burner feeding applications in biomass-coal co-firing power plants and compared the results with those obtained through computational fluid dynamics (CFD) techniques. Because the particle-particle, particle-air, and particle-wall interactions generate a net electrostatic charge on the particles, the electrostatic sensing and correlation techniques were applied to measure particle velocity and solid volume content distribution. Flour was substituted for coal (for health and safety regulations) and mixed with willow, wood, or bark. The mixture was

eventually injected into the pipeline with a flour-biomass mass flow rate of 0.42 g/s and 0.9 g/s and an air flow velocity ranging from 15 to 25 m/s. It was observed that, due to physical properties and gravitational effects, the biomass particles traveled slower near the bottom of the pipe and the flour flow ran slightly slower on the sides of the pipe than it did in the central portion. Furthermore, the root mean square (r.m.s.) charge levels of various flour-biomass mixtures measured by the electrodes showed that the particle charge level increased as the mass flow rate increased.

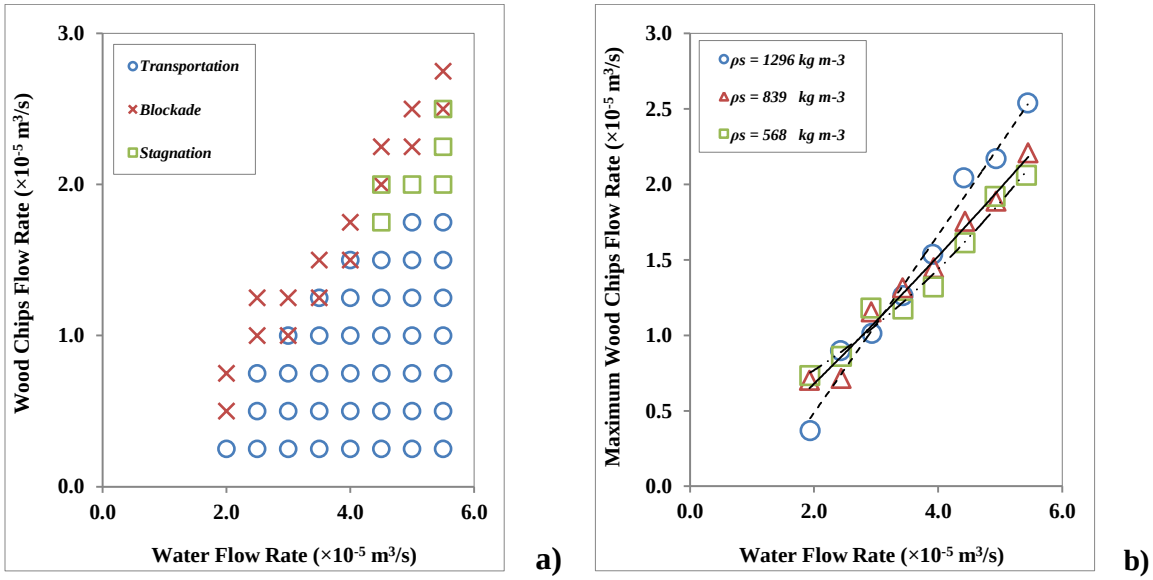

Fig. 2-1: a) Flow pattern map of a wood chip-water mixture flow (Q_s vs. Q_l) through a pipe with a diameter of 50 mm, incline angle of 2.0 degrees, and wood chip density of 1296 kg/m^3, b) The variation of maximum wood chip flow rate ($Q_{s,max}$) vs. carrier liquid (water) flow rate (Q_l) through a pipe with a diameter of 50 mm and incline angle of 2.0 degrees for various wood chip densities. *Figures reproduced with the permission of Sawai et al. [15]*

2.2.2. Agricultural Residue Biomass Slurries in Pipes

Mohammadabadi [29] was the first person who experimentally studied the feasibility of pipelining biomass materials in the form of solid-liquid mixtures (slurries). Mohammadabadi designed, fabricated, and instrumented a 50 mm diameter and 25 m long closed-circuit lab-scale pipeline facility at the Large-scale Fluids Lab at the University of Alberta and successfully pumped wheat straw-water mixtures up to a solid

volume content of 30%. Mohammadabadi mainly focused on the change in wheat straw particles' physical properties through exposure to water. For instance, the change in wet-basis moisture content of particles with nominal dimensions of 3.2 mm and 19.2 mm was measured while the particles were being soaked and mechanically mixed for 192 hours. The samples containing small size particles absorbed water faster, the final moisture level (saturation level) of the samples of large size particles was greater (81.2% vs. 81.0%), and mechanical mixing compared to soaking increased the magnitude of absorption (82.4% vs. 81.2% for 19.2 mm particles) as well as the rate of absorption of water into wheat straw particles. In addition, the saturated particle density of wheat straw samples was found to be greater for smaller particles compared to larger ones (1050 kg/m^3 vs. 1030 kg/m^3) and greater after 192 hours of mixing compared to the density obtained after the same amount of soaking time (1060 kg/m^3 vs. 1050 kg/m^3 for 3.2 mm particles). The lab-scale closed-circuit pipeline facility created by Mohammadabadi was used later by Luk et al. [30, 31] and Vaezi et al. [16, 17] to experimentally investigate the hydraulics of pipeline hydro-transport of agricultural residue biomass.

Luk et al. [30, 31] studied the pressure drop behavior of wheat straw-water mixtures for wheat straw particles of dimensions of 3.2, 6.4, and 19.2 mm, solid mass contents (dry matter) of 1.92, 3.90, and 5.94%, and slurry bulk velocities of 1.5 to 3.0 m/s. Luk et al. realized that fibre-like wheat straw particles can suppress the flow turbulence at elevated velocities of more concentrated flows and cause the pressure drop to fall below the pressure drop of water alone (the drag-reducing effect).

2.2.3. Summary

A series of experiments has been conducted on pipeline hydro-transport of wood chips for a wide range of variables, including pipeline materials of aluminum, clear plastic, and acrylic; pipeline lengths of 91 to 1220 m; pipeline diameters of 50 to 300 mm; wood chip moisture contents of 50 to 70%; wood chip diameters (d_{50}) of 3.0 to 28.4 mm; and wood chip-water mixture velocities of 0.5 to 4.5 m/s. Economic and technical issues limited the maximum mixture solid volume content achieved to 30%, where at solid volume contents above 20% and mixture velocities above 1.5 m/s the wood chip-water mixture friction

losses dropped to close to pure water. It was found that mounting the pipeline horizontally, increasing the pipe diameter, and decreasing mixture solid volume content bring about optimum pipeline conditions and reduce the probability of a wood chip blockade throughout the pipe.

Researchers have studied pipeline hydro-transport of wheat straw agricultural residue biomass on a 50 mm diameter and 25 m long closed-circuit lab-scale pipeline facility. Changes in physical properties of wheat straw particles due to long-time exposure to water and general friction loss behavior of wheat straw-water mixture have been studied. However, differences between pressure drop behavior of agricultural residue biomass-water mixtures and conventional solid particles slurries; changes in friction loss and rheological behaviors of agricultural residue-water mixtures with changes in biomass particles type (wheat straw and corn stover), particle dimension, slurry solid mass content, and slurry velocity; and the performance of the centrifugal pumps handling slurries of agricultural residue biomass need to be yet investigated.

2.3. Modeling Studies

In 1952 Durand and Condolios [32] presented a universal correlation to estimate the friction loss in solid-liquid pipelines (Eq. 1). α and β constants were later empirically determined by Worster [33] and Gibert [34]. The former found constants of 81 and -1.5 for coal-water mixtures, and the latter found constants of 180 and -1.5 for sand- and gravel-water mixtures. Following a study on hydro-transport of spruce and balsam fir wood chips, Elliott and de Montmorency [9, 19] modified the Durand equation and proposed an empirical correlation (Eq. 2) for estimating friction loss in wood chip-water mixtures flowing in pipes. They also recommended a pumping velocity close to 1.2 m/s where the friction losses were high enough to be technically and economically satisfactory.

$$\frac{i_m - i_w}{C_v . i_w} \cong \alpha \left[\frac{V_m^2}{gD(s-1)}\sqrt{C_d}\right]^{\beta} \quad (1)$$

$$\frac{i_m - i_w}{C_v . i_w} = 211 \left[\frac{\sqrt{D}}{V_m}\right]^{2.25} \quad (2)$$

Faddick [10] presented the following Durand-type correlation (Eq. 3) for friction loss in wood chip pipelines based on experimental studies. Faddick's results appeared to give predicted friction loss values as much as 30% higher than those of Elliot and de Montmorency [20].

$$\frac{i_m - i_w}{C_v . i_w} = 2.51 \left[\frac{4gD}{V_m^2}\right]^{1.42} \quad (3)$$

Brebner [22] experimentally studied the feasibility of hydro-transporting jack pine and spruce wood chips and measured the friction loss throughout the pipe. With results similar to Elliott's [9, 19], Brebner reported the hydraulic gradients of wood chip-water mixtures in a Durand-type equation as follows:

$$\frac{i_m - i_w}{C_v . i_w} \cong 18 \left[\frac{V_m^2}{gD}\right]^{-1.5} \quad (4)$$

While adopting the Durand equation (Eq. 1) for wood chip results in an equation constant of 6.0, Brebner measured a three-times-larger friction loss with a constant of 18.0. Brebner attributed his findings to the interlocking sliding bed mode of transport. He also successfully tried a pumping velocity as low as 1.5 m/s in which, since it was the commonly accepted velocity for water alone, he found no advantage going below such velocity.

Wasp et al. [27] introduced a model that is widely used in coal pipeline hydro-transport to classify the particles as either uniformly distributed (homogeneous) or with solid volume fraction gradient across a cross section (heterogeneous or partially stratified). Wasp's model calculates the friction loss per unit pipe length as the sum of losses due to water+suspended fine particles flow (Eq. 5) and water+coarse particles flow (Eq. 1) together with the amount of suspended particles contributing to the former flow (Eq. 6).

Following an experimental study on pipeline hydro-transport of wood chips [23], Wasp investigated solid volume content distribution and calculated the solid volume fraction at the top (C_{top}) and middle (C_{mid}) of the pipe. It was found that for every 7 chips at the top, there were 100 chips at the center. This implied that the solid volume content distribution was non-uniform and that the nature of the flow was heterogeneous.

$$i_f = \frac{(0.0032 + 0.221Re_f^{-0.237})\, V_m^2}{2D}\rho_f \tag{5}$$

$$log\frac{C_{top}}{C_{mid}} = -1.8\,(\frac{V_\infty}{\beta k V_m\sqrt{f_f/8}}) \tag{6}$$

Wasp et al. [27] examined the compatibility of the Durand correlation with the published data of Elliott and de Montmorency. While a good agreement was observed for 10-20% solid volume content, a systematic trend for the Durand equation to predict high values for low concentrates (i.e., 5% solid volume content) and low values for high concentrates was found. Zandi and Govatos [35] proposed a criterion to determine the transition in flow regimes from heterogeneous (suspension) to discontinuous sliding bed with saltation and improved the original Durand equation by eliminating the corresponding saltation data. Observing the apparent inconsistency between Elliott and de Montmorency's [9] and Faddick's [10] experimental results, Wasp et al. also attempted to refine the Durand equation by modifying its constants, as proposed by Zandi and Govatos [35]. However, the Wasp correlation did not fit the data any better than the old Durand equation, which pointed out the need for additional experimental work.

Faddick [25] simulated the pipeline hydro-transport of wood chips using uniform-sized plastic chips to investigate friction loss parameters. With the data from four sets of experiments using plastic chips and three sets of experiments (by other researchers) using wood chips, Faddick proposed calculating the friction loss in wood chip pipelines using the Darcy-Weisbach equation and evaluated the mixture friction factor using curve-fitting techniques as follows:

$$log f_D = a_1 C_v (\frac{d}{D})^x + a_2 log(Re_m) + a_3 C_v (\frac{d}{D})^y \log(Re_m)^2 \quad (7)$$

where a_1, a_2, a_3, x, and y are empirical coefficients determined experimentally.

Metzner and Reed [36] developed a semi-theoretical correlation to analyze friction loss of laminar non-Newtonian fluids (Eq. 9), and Dodge and Metzner [37] extended their method to include turbulent non-Newtonian fluids (Eq. 10). Gow found Metzner and Reed's method for laminar non-Newtonian flows to be capable of analyzing the friction loss data for wood chip-water mixtures in pseudo-laminar flow (sliding bed) conditions, where *n* and *K* coefficients were obtained from wood chip-water mixture friction loss data as functions of solid volume contents. Gow also indicated that the ratio of friction factors of two various pipe diameters equals the reciprocal ratio of the pipe diameters to the *n* power (Eq. 11).

$$Re_g = \frac{D^n V_m^{2-n} \rho_w}{8^{n-1} K} \quad (8)$$

$$f_F = \frac{16}{Re_g} \quad (9)$$

$$\frac{1}{\sqrt{f_F}} = \frac{4}{n^{0.75}} \log\left(Re_g {f_F}^{1-n/2}\right) - \frac{0.4}{n^{1.2}} \quad (10)$$

$$\frac{f_{F,1}}{f_{F,2}} = (\frac{D_2}{D_1})^n \quad (11)$$

However, the correlation for turbulent non-Newtonian flows proposed by Dodge and Metzner [37] was not applicable for wood chip-water mixtures in pseudo-turbulent (saltation flow) regions. Because of the similarity between friction loss curves for wood chip-water mixtures in pseudo-turbulent regions and clear water lines defined by Prandtl's universal law of friction for turbulent pipe flow (Eq. 12), Gow [11] proposed a new correlation (Eq. 14) where, with friction loss experimental data, a plot of $1/\sqrt{f_F}$

versus $\log(Re_w\sqrt{f_F})$ gives the constant value A and the quantity $(E - A\log\emptyset)$ as the slope and the ordinate intercept, respectively. Assuming Eq. 13 to be valid, Gow found the coefficients A and $\log\varphi$ to be 4.0 and 0.0 for a 0% solid volume content and E to be -4.0 for all the mixture solid volume contents. Gow also observed that the wood chip-water mixture viscosity, as defined by Eq. 13, increased with increasing mixture solid volume contents and became larger for larger chip sizes. Gow found such viscosity variation to be the result of increased particle-wall interaction due to increased solid volume content and decreased turbulent intensity due to increased chip size.

$$\frac{1}{\sqrt{f_F}} = 4\ \log\left(Re_w\sqrt{f_F}\right) - 0.4 \tag{12}$$

$$\mu_m/\mu_0 = \emptyset(C_v, V_m, D, \rho_m, d_{50}) \tag{13}$$

$$\frac{1}{\sqrt{f_F}} = A\ \log\left(Re_w\sqrt{f_F}\right) + E - A\log\emptyset \tag{14}$$

Hunt [20] studied the hydro-transport of wood chip-water mixtures and examined the applicability of the extrapolation approach to friction loss correlations proposed by Gow [11] and Faddick [25]. Hunt found the failings on previously developed correlations to be: (1) the difficulty in calculating the wood chip specific gravity and drag coefficients for Eq. 1 by Durand; (2) the lack of inclusion of the effect of particle-to-pipe size ratio for Eq. 2 by Elliott and de Montmorency and Eq. 3 by Faddick; (3) the non-consideration of the viscosity of the carrier liquid (water) for Eqs. 1, 2, and 3; (4) the lack of convergence to the clear water friction factor for a mixture solid volume content of 0% for Eq. 7 by Faddick; and (5) the inconsistency with values reported by Elliott and de Montmorency in 200 mm pipes [9] for Eq. 9 and by Gow for Eq. 14. To correct these deficiencies, Hunt proposed a correlation (Eq. 16) to predict the wood chip-water mixture friction loss in terms of an excess friction factor (f_m/f_w -1) as a function of four dimensionless parameters (Eq. 15). In the selection of a mathematical model for fitting the data into a single equation including all four dimensionless groups of Eq. 15, Hunt modified the mixture solid volume content (C_v) and particle-to-pipe size ratio (P) to satisfy two boundary

conditions; the mixture friction factor should be identical with that of clear water when the mixture solid volume content equals zero, and the mixture friction factor for a given mixture solid volume content should increase with an increase in the particle-to-pipe size ratio. Hunt's expression for a wood chip-water mixture friction factor brings about a standard deviation of about 12% from previously reported data [9, 11, 24, 25] on pipes of 75 mm, 100 mm, 150 mm, 200 mm, and 300 mm diameter.

$$\frac{f_m}{f_w} - 1 = G[(V_m^3/\nu g), (D^{1.5} g^{0.5}/\nu), C_v, (d_{50}/D)] \tag{15}$$

$$\frac{f_m}{f_w} - 1 = 197\left(\frac{D^{0.97}\, g^{1.312}\, \nu^{0.342}}{V_m^{2.964}}\right)\left(\frac{C_v}{1-C_v}\right)^{0.838+0.930\ln(1-P)} \tag{16}$$

Gubba et al. [26] used Reynolds-averaged Navier Stokes (RANS) methodology and the Direct Phase Model (DPM) through ANSYS FLUENT to carry out continuous phase and particulate phase CFD modeling, respectively, on the pneumatic pipeline transport of four types of biomass particles: flour, wood, bark, and willow. An estimated particle shape factor based a non-spherical drag model and a modified stochastic inter-particle collision method accounted for the biomass particles' morphological features and inter-particle collisions. Gubba first compared the gas phase axial velocity with the experimental measurements to validate the CFD calculations, and then compared the CFD simulation results with available experimental data. He observed the variations in particle velocities in the upper, central, and lower regions of the pipe as well as particle distribution across the pipe cross section. A good agreement was reported between numerically simulated and experimentally measured data.

2.3.1. Summary

Several investigators proposed correlations to predict the friction loss of laminar and turbulent wood chip-water mixture flows of various regimes (e.g., heterogeneous, discontinuous sliding bed with saltation) in pipes. A deviation of 30% between estimated values of the friction loss of the same mixture using various correlations and a deviation of 300% between estimated values and experimental measurements were reported in

literature, both of which pointed out the need for additional experimental work. Wood chip size, and density and viscosity of the carrier liquid were the variables not considered in some of the proposed correlations. However, all the effective variables were included in the more recently developed equations, where a standard deviation of only 12% from previously obtained experimental data was reported.

2.4. Techno-economic Analyses

Following an empirical study on pipeline hydro-transport of pulpwood chips, Elliot and de Montmorency [9, 19] studied the economic feasibility of wood chip transport via a hypothetical system of pipelines leading from a landing to the mill (Fig. 2-2). The forest field included a productive area of 2300 km^2 with an annual cut of 0.9 Mm^3. The aluminum pipeline was composed of surface-laid branch pipelines converging into a buried feeder line that discharged into a buried main line. Elliot and de Montmorency argued that the amount of water required, e.g., 2.5 Mm^3/yr to transport 1.5 Mm^3/yr of wood chips in a 40% solid volume content mixture, was not exceptionally large in terms of the amount of resources available on most timber limits. Further, they presented the power loss per kilometer distance for 150 mm, 200 mm, and 250 mm diameter pipes carrying wood chips at mixture solid volume contents of 20%, 30%, and 40%. It was shown that power and operating costs could be lowered by increasing the mixture solid volume content and decreasing the pumping velocity, which would also increase capital investments. The direct economic benefits named by researchers included low unit transportation costs for an annual capacity over 0.7 Mm^3, a minor increase in transportation costs over a period of 20 years due to low labor requirements, low depreciation compared to new road or rail construction, and a drastic reduction in mill, forest, and in-transit inventories.

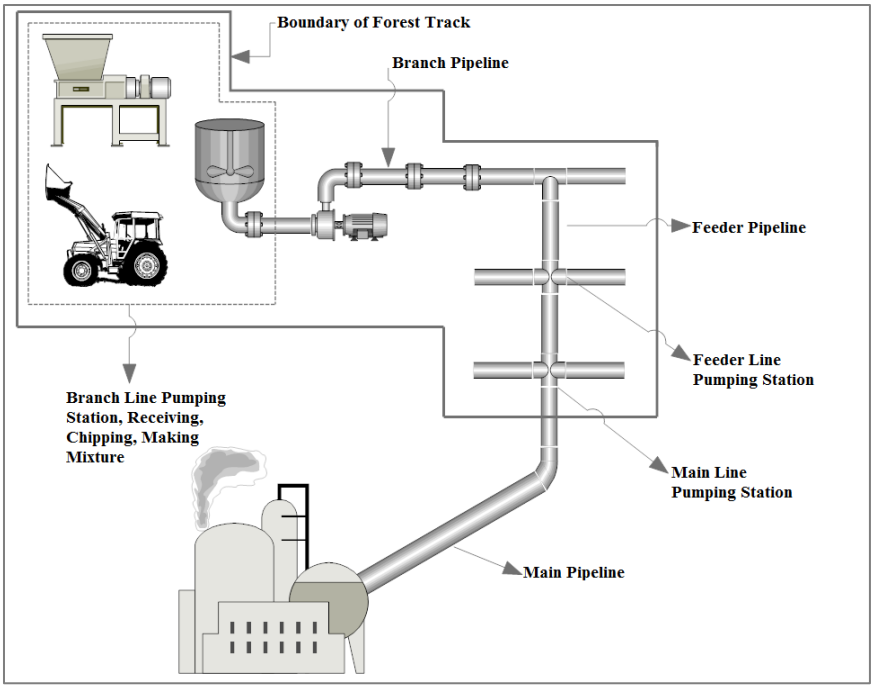

Fig. 2-2: Schematic of the proposed system by Elliot and de Montmorency [9, 19] for the pipeline hydro-transport of wood chips

Using only the friction losses found experimentally, Brebner [22] calculated the cost of transport of a 35% solid volume content wood chip-water mixture in a 200 mm diameter pipeline at 2.0 m/s pumping velocity and 55% pump/motor efficiency to be 0.095 $/t.km. No measurements of wear, corrosion, or erosion in the pipe (all of which could increase capital costs) were taken by Brebner.

Wasp et al. [23], while reviewing wood chip pipelining, discussed the related economics. Fig. 2-3(a) presents the investment cost and Fig. 2-3(b) shows the capital costs (including carbon steel pipe, external coating, installation costs, positive displacement pump stations and related facilities, communication system, water supply system, chip injection facilities, terminal dewatering facilities, and indirect costs including a contingency allowance, interest during construction, working capital, and engineering management) and the operating costs (including electrical power costs for driving the pumps and mixing, costs of operating personnel for the pipeline system, an allowance for chemical corrosion inhibitors, supplies and maintenance for the pipeline and pump stations, administration costs, and a contingency allowance) of such pipelines based on a 100 km

long pipeline capable of hydro-transporting various amounts of so-called green (35% moisture content) wood chips at 20% solid volume content. Wasp also found the sensitivity to change in length to be quite low, e.g., a 50% reduction in length causes a 7% increase in total unit transportation costs. In addition to showing the concept of economy of scale, which is found to be highly applicable to pipeline systems, Fig. 2-3 shows that capital charges account for more than 70% of the total transportation cost, i.e., once the pipeline is constructed, 70% of the transportation costs are not subject to escalation. This is a distinct advantage of pipeline hydro-transport over nearly every other mode of transport. To achieve these results, Wasp used Elliot and de Montmorency's [9] friction loss data. Using Faddick's [10] data increased the total and capital costs by 25%.

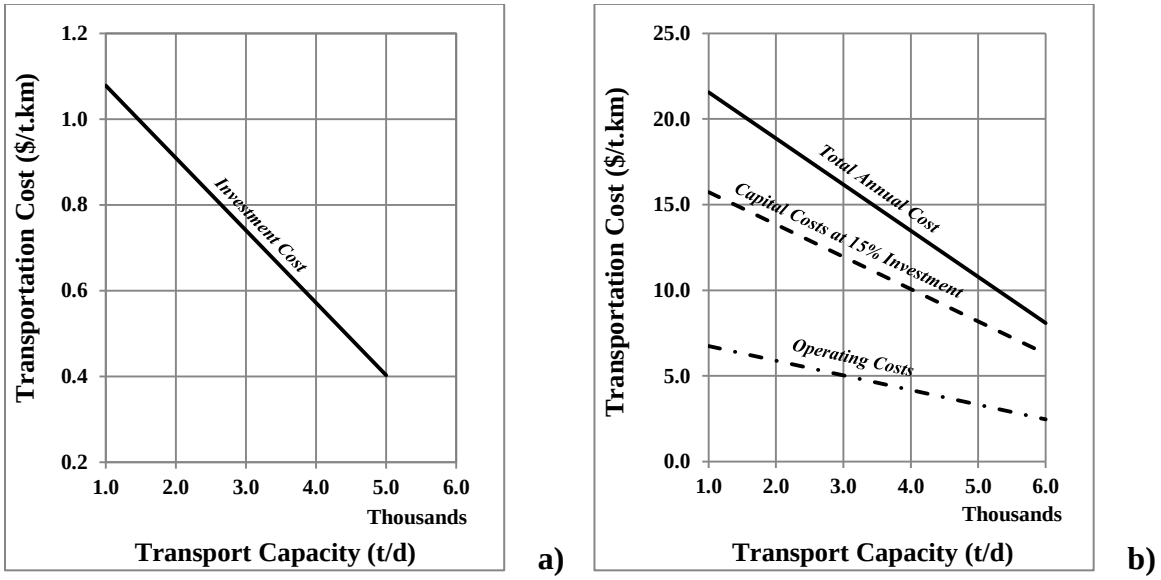

Fig. 2-3: Wood chip pipeline capital and operating costs vs. pipeline capacity based on a 100 km pipeline for green chips at 35% moisture content, 20% wood chip-water mixture solid volume content, and 310 operation days per year (operating factor 85%) [23], *Figures reproduced with the permission of Technical Association of the Pulp and Paper Industry (TAPPI)*

Hunt [38, 39] conducted an analysis to determine the conditions under which a pipeline system might be economically competitive with other methods of transporting wood chips to processing plants. The economic model to determine the cost of transporting one tonne of wood chips for one kilometer by a given transportation system included the

capital investment, operating expenses, and associated overhead charges. Hunt subdivided the costs into seven groups, each depending on one or more of the 23 variables selected to formulate the algebraic expressions that relate the hydraulic properties of the pipeline and physical properties of the wood chips to the economics of the system. Using Brebner's friction loss equation [22], the total cost per one tonne of wood chips per unit distance can be found with Eqs. 20 to 27 for each of the seven cost groups previously mentioned.

$$S_m = C_v[(MC + 1)S_{odc} - 1] + 1 \tag{17}$$

$$\lambda = \frac{1}{216gD^5}\frac{W}{C_v S_{odc}} \tag{18}$$

$$H_T = 31{,}680(0.547\lambda^{-1.42} + 1)f_W\lambda + \frac{Z_T}{L} \tag{19}$$

$$X_T = \sum_{M=1}^{7} X_m \tag{20}$$

$$X_1 = 0.000753\ \frac{R_1}{e\ S_{odc}}\frac{S_m\, H_T}{C_v} \tag{21}$$

$$X_2 = \frac{R_2\, D}{365\ W}(crf) \tag{22}$$

$$X_3 = 0.000000115\ \frac{R_3}{e\ S_{odc}}\frac{S_m\, H_T}{C_v}(crf) \tag{23}$$

$$X_4 = \frac{R_4 + R_5}{365\ L}(crf) \tag{24}$$

$$X_5 = \frac{R_6}{365\ W\ L} \tag{25}$$

$$X_6 = \frac{1}{365\,W}\,R_7\,\frac{H_T}{H_{sa}} + R_8 \tag{26}$$

$$X_7 = 0.000240\,\frac{1 - C_v}{C_v}\frac{R_9}{S_{odc}\,L} \tag{27}$$

Table 2-2: Data for a generalized economic model by Hunt [38] (Originally presented in imperial units). *Table reproduced with the permission of Forest Products Research Society*

Item	Value	Unit	Item	Value	Unit	Item	Value	Unit
crf	0.200		S_{odc}	0.40		R_5	107.8	\$/t.d
e	0.650		Z_T	0	m	R_6	323,400	\$/yr
f	0.018		R_1	0.05	\$/kWh	R_7	51,000	\$/per pump station
g	9.8	m/s^2	R_2	615,600	\$/m.km	R_8	425.3	\$/km.yr
H_{sa}	244	m	R_3	1430	\$/kW	R_9	0.1423	$\$/Mm^3$
M	1.80		R_4	53.9	\$/t.d			

Developing a computer program and using the cost data listed in Table 2-2, Hunt obtained the cost per tonne per unit distance for transporting various amounts of wood chips per day (500 t, 1000 t, and 2000 t). An investigation of the effect of mixture solid volume content, pipe diameter, pipe length, and wood chip transport capacity per day on the total cost per tonne per unit distance (e.g., Fig. 2-4(a)) showed a 10% reduction in the unit cost when the same volume was transported in a line twice as long and a 30% reduction in the unit cost when the volume was double for a given distance. 20-22% mixture solid volume content was found to be the maximum working solid volume content for wood chip pipelines. Hunt also indicated that the optimum solid volume content to transport 500 t/d of wood chips over 160 km was approximately 21% for 200 mm diameter, 14% for 250 mm diameter, and 9% for 350 mm diameter pipelines.

Hunt [40] collected data for the cost of transportation by truck and rail from 43 pulp mills in the Great Lake states, as well as northwest, northeast, and southern regions in U.S., and compared the cost per tonne per unit distance for pipeline hydro-transport of wood chips with that for truck and rail haul (Fig. 2-4(b)). It was found that hydro-transport of wood chips in quantities greater than 1000 t/d could compete economically with the rates for truck haul and northern railroad haul for distances up to 88 km. However, if the cost

of the construction of highways and railroads was also included in Hunt's transportation cost database, the cost of pipeline hydro-transport would be much more favorable.

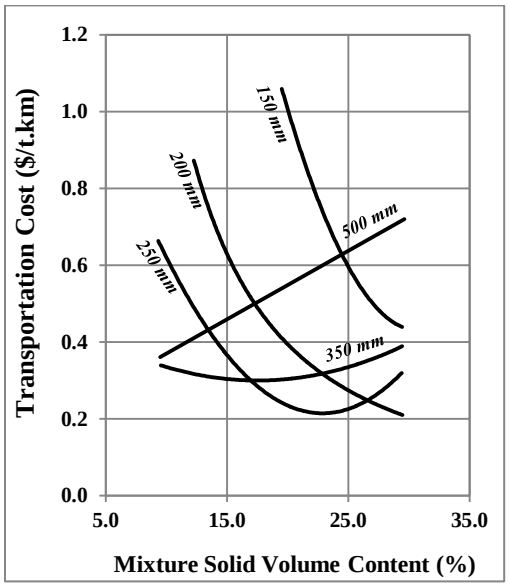

a)

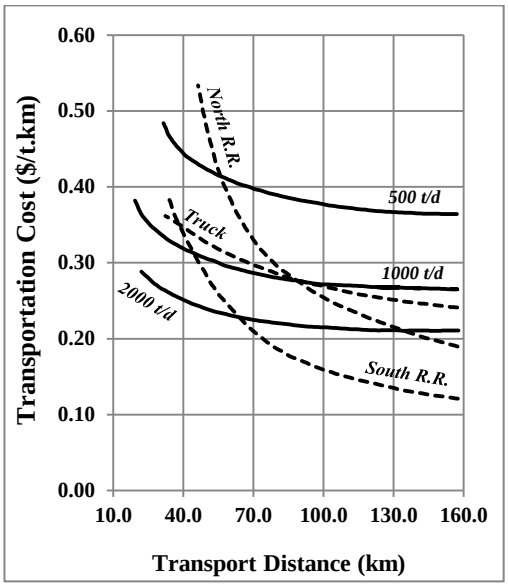

b)

Fig. 2-4: a) The cost of pipeline hydro-transport as a function of pipeline diameter and mixture solid mass content for capacities of 1000 t/d over 160 km, b) Comparative transportation costs (both the graphs are based on 365 operation days per year) [38], *Figures reproduced with the permission of Forest Products Research Society*

Kumar et al. [12-14] conducted a series of techno-economic analyses on pipeline hydro-transport of wood chips and pipeline hydro-transport and simultaneous saccharification of corn stover. Drawing on the works of Wasp et al. [23] on pipelining wood chips and Liu et al. [41] on pipelining compressed coal cylinders, Kumar et al. [14] developed pipeline cost estimates for transporting wood chip-water mixtures; these estimates are shown on Table 2-3 and Fig. 2-5(a). Comparing the cost of truck delivery of wood chips with the cost of pipeline transport of a wood chip-water mixture with solid volume content of 30% over an arbitrary pipeline length of 160 km, the marginal cost of pipeline hydro-transport was found to be higher than truck delivery cost at capacities <0.5 M dry t/yr for a pipeline without the return line for the carrier liquid (one-way). The corresponding minimum capacity for a pipeline with the return line for the carrier liquid (two-way) was 1.25 M dry t/yr. It was shown that the minimum length of the pipeline to recover the fixed costs of a pipeline with a capacity of 2.0 M dry t/yr was 75 km for a one-way pipeline and 470

km for a two-way pipeline (in addition to the initial 35 km truck haul to the pipeline inlet). In addition, the authors investigated the drop in the lower heating value (LHV) of biomass because of the take-up of the carrier liquid and discussed the limited application of pipeline hydro-transport of biomass to supply aqueous-based processes only, e.g., bio-ethanol production or supercritical water gasification.

Table 2-3: Economic and technical parameters used by Kumar et al. to estimate the capital and operating costs of a wood chip-water mixture pipeline [13], *Table reproduced with the permission of Springer Publication*

Item	Value	Unit
Life of pipeline	30	yr
Contingency cost	20	% of total cost
Engineering cost	10	% of total capital cost
Discount rate	10	%
Operating factor	0.85	
Power cost	50	$/MWh
Velocity of slurry	1.5	m/s
Velocity of water in water return line	2.0	m/s
Maximum pressure	4100	kPa
Pump efficiency	80	%
Scale factor applied to inlet, outlet, and booster station facilities excluding pumps	0.75	

Kumar et al. [14] also investigated the pipeline hydro-transport of corn stover and found the one-way pipeline at a scale of 1.0 to 2.0 M dry t/yr and mixture solid volume content of above 15% to cost less than truck delivery (Fig. 2-5). To estimate the corn stover-water mixture friction factor in pipes, Kumar et al. used Hunt's correlation [20], which was originally proposed for wood chip-water mixtures in pipes. However, they examined the sensitivity to friction factor parameter and found that a variation of -50% to +100% in friction factor results in a -16% to +31% change in the distance variable cost of pipeline hydro-transport of corn stover, a sensitivity that did not invalidate the conclusion of the study.

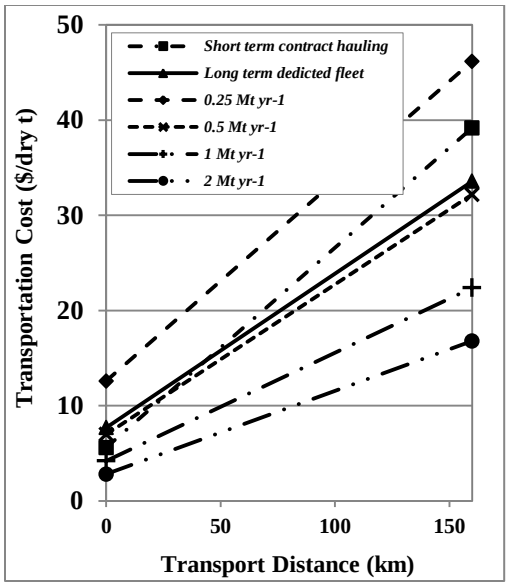

a)

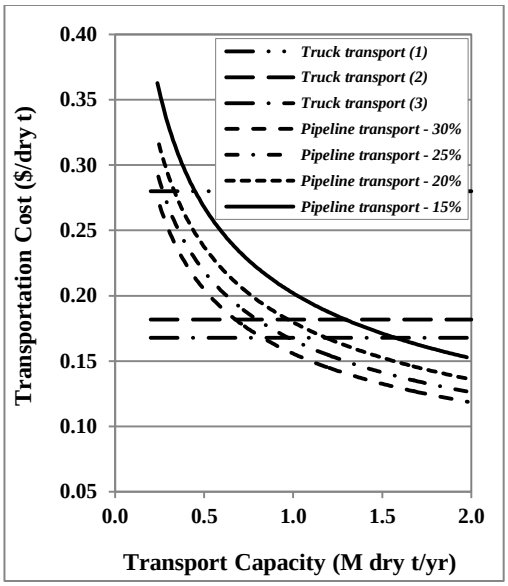

b)

Fig. 2-5: a) Truck and pipeline hydro-transport costs of wood chips without the return line for the carrier liquid [13], b) Distance variable cost of truck and pipeline hydro-transport of corn stover at different solid volume contents without the return line for the carrier liquid [14], truck transport (1): study by Marrison and Larson [42], truck transport (2): study by Jenkins et al. [43] and Kumar et al. [44], truck transport (3): study by Glassner et al. at NREL [45], *Figures reproduced with the permission of Springer and Elsevier Publications*

Ellis et al. [46] considered the possibility of partial processing-in-transit through solid-liquid mixture pipelines. Nardi [47] suggested a similar technique for wood chips to inject the chemicals into a heated section near the receiving facility. Kumar et al. [14] examined the simultaneous saccharification and transport (SST) on a corn stover hydro-transport pipeline. It was found that, since the current cellulase enzyme (that converts starch into sugar) causes an acidic environment in the pipe, the SST requires a prohibitively expensive stainless steel pipeline that makes it technically and economically inapplicable. Furthermore, residence time and mixture temperature are critical factors, as National Renewable Energy Laboratory (NREL) suggests a contact time of 35 hr at a saccharification temperature of 65°C [48]. The fuel cost for heating a corn stover-water mixture by 40°C using natural gas at 5 $/GJ was estimated to be more than 0.069 $/L of produced ethanol. Insulation might also be required, specifically for smaller capacity pipelines buried in the soil. Furthermore, it was found that insulating a 100 mm diameter

pipeline carrying 1.5 M dry t/yr with 25 mm of foam would cause an approximately 15% increase in the installed cost of a corn stover-water mixture pipeline and a 10% increase in the distance variable cost.

Sawai et al. [15], while investigating hydro-transport of wood chips by hilly terrain pipelines, compared the energy required for pipeline hydro-transport systems with that for cable logging systems. While Harada [49] estimated the energy required by cable logging and mobile tower yarder to transport trees between forest and forestry road to be about 500 MJ/t, Sawai found the energy required to transport wood chips through a pipeline of 200 m length and 300 mm diameter across a terrain of 30° inclination to be only about 5.0 MJ/t.

2.4.1. Summary

Based on experimental measurements and empirical correlations reported in the literature, a few researchers studied the economic feasibility of pipelining wood chip-water mixtures to processing plants. The concept of economy of scale was found to be highly applicable to pipeline systems, the water required at the pipeline inlet was reported to be not exceptionally large (in relation to the amount of resources available on most timber limits), and a 25% variation in the total cost of a pipeline system was obtained by using various pressure drop correlations. It was shown that the power required and, accordingly, the operating costs of the pipeline system would decrease and the capital costs of the pipeline system would increase with an increase in solid volume content, decrease in mixture velocity, and increase in pipeline length. Furthermore, capital charges were reported to account for more than 70% of the total transportation cost.

2.5. Conclusion

The potential of biomass-based fuels as economically viable replacements for fossil fuels is being increasingly recognized. Using pipeline hydro-transport to replace traditional truck delivery is a major step towards building large-scale bio-based fuel production facilities. This paper reviewed the literature published on pipeline hydro-transport of wood chips and agricultural residue biomass for pulp and paper production, as well as for

fuel and energy generation. The technical challenges and economic issues were reviewed, and correlations to predict biomass-water mixture mechanical behavior were introduced.

None of the studies conducted either experimentally or theoretically considered wear, corrosion, or erosion in a pipeline, all of which could impact the mechanical specifications (e.g., friction loss) and economic features (e.g., capital cost) of the pipeline and which should be measured/calculated in future studies. As described in this paper, pipeline hydro-transport of wheat straw biomass has been experimentally studied on a 50 mm diameter and 25 m long (laboratory-scale) horizontal pipeline facility. Scaling up such a pipeline must be studied to understand how the change in pipeline diameter and orientation would change the slurry mechanical behavior. More research needs to be conducted to develop empirical correlations to estimate corresponding slurry friction loss. Such correlations could be used to study the economy of agricultural residue pipelines, as previous studies on this field used friction loss correlations originally proposed for wood chip-water mixtures instead. Water mixtures of other sorts of biomass materials could be also investigated to understand how biomass physical specifications would change slurry mechanical behavior. Chemical processing-in-transit through pipeline hydro-transport of biomass materials is another interesting issue that, although its economic viabilities have been analyzed, needs its mechanical and chemical feasibility to be experimentally investigated.

Nomenclature

d_1, d_2, d_3	dummy variables, dimensionless
a_1, a_2, a_3	empirical coefficients, dimensionless
x, y	empirical coefficients, dimensionless
α, β	empirical coefficients, dimensionless
m	number of cost group, from 1 to 7
e	combined efficiency of motor-pump drivers, %
g	gravitational acceleration, m/s^2
k	von Karman constant (0.4 in this paper)
s	specific gravity, dimensionless
d	representative chip dimension defined, m
n	fluid behavior index, dimensionless
z	distance from the pipe invert, m
v	kinematic viscosity of the carrier liquid, m^2/s
crf	charge on capital investment to cover interest, depreciation, etc.
$r.m.s.$	root mean square
K	fluid consistency index, units consistent with those in generalized Reynolds number
A	empirical constant, dimensionless
E	empirical constant, dimensionless
P	ratio of characteristic particle dimension (here d_{50}) to pipe diameter, dimensionless
D	pipe internal diameter, m
W	tonnes per day of oven-dry chips, dry t/d
L	length of the pipeline, km
MC	moisture content of wood chips, %
LHV	lower heating value, J/kg
X_1	energy cost, $/t.km
X_2	installed cost of pipeline and its appurtenance (valves, meters, flow controls), $/t.km
X_3	installed cost of pump station, $/t.km
X_4	installed cost of injection and separation system, $/t.km
X_5	cost of fixed salaries, wages, and operations that are independent of length of pipeline or number of pump stations, $/t.km
X_6	cost of variable salaries, wages, and operations that are dependent on the length of the pipeline and the number of pumping stations, $/t.km
X_7	cost of water treatment, $/t.km
X_m	each of the 7 cost groups, $/t.km
X_T	total cost of pipeline hydro-transport, $/t.km
R_1	cost of electrical energy, $/kWh
R_2	installed cost of pipeline, including right-of-way, $/m.km
R_3	cost of pump station and controls, $ per installed kW
R_4	cost of wood chip injection system, $/dry t.d
R_5	cost of wood chip separation system, $/dry t.d
R_6	annual cost of fixed salaries, wages, and operation maintenance, exclusive of pipeline maintenance and pump station operation
R_7	annual wages, salaries, etc., for pump stations, $ per pump station
R_8	annual maintenance cost of pipeline, $/km

Nomenclature (Cont'd)

R_9	cost of water and treatment, \$/Mm^3
d_{50}	particle length at respective 50% cumulative number fraction of particles, mm
Z_T	difference in elevation between inlet and discharge of the pipe, m
S_m	specific gravity of wood chip-water mixture, dimensionless
H_T	head due to friction and difference in elevation, m_{H2O}/km
H_{sa}	total head developed per pump station, m_{H2O}
S_{odc}	specific gravity of oven-dried wood chips, dimensionless
C_v	solid volume content, %
C_d	particle drag coefficient, dimensionless
C_{top}	solid volume content at $z/D = 0.92$ (z is the vertical position from the pipe bottom)
C_{mid}	solid volume content at $z/D = 0.5$
Q_l	carrier liquid (water) flow rate, m^3/s
Q_s	wood chip flow rate, m^3/s
$Q_{s,max}$	maximum wood chip flow rate, m^3/s
Re_f	Reynolds number of water and suspended fine particles flow, dimensionless
Re_g	generalized Reynolds number, dimensionless
Re_m	mixture Reynolds number, dimensionless
Re_w	clear water Reynolds number, dimensionless
V_m	mean mixture velocity, m/s
V_∞	particle settling velocity, m/s
i_m	hydraulic gradient of mixture, m_{H2O}/m_{pipe}
i_w	hydraulic gradient of water, m_{H2O}/m_{pipe}
i_f	hydraulic gradient of water and suspended fine particles flow, m_{H2O}/m_{pipe}
f_F	Fanning friction factor, dimensionless
f_D	Darcy-Weisbach friction factor, dimensionless
f_m	mixture friction factor, dimensionless
f_f	friction coefficient of the water and fins particles flow, dimensionless
f_w	clear water friction factor, dimensionless
μ_0	dynamic viscosity of clear water, N.s/m^2
μ_m	viscosity of mixture, N.s/m^2
ρ_f	density of water and suspended fine particles mixture, kg/m^3
ρ_w	density of clear water, kg/m^3
ρ_m	density of mixture, kg/m^3
φ	the ratio of mixture viscosity to clear water viscosity, dimensionless

References

[1] Abulnaga, B. Slurry systems handbook: McGraw-Hill, New York, NY; 2002.

[2] Bain, A.J., Bonnington, S.T. The hydraulic transport of solids by pipeline: Pergamon Press, New York, NY, US; 1970.

[3] Weston, M.D., Worthen, L. Chevron phosphate slurry pipeline commissioning and start-up. 12th International Conference on Coal and Slurry Technology. Washington, DC; 1987.

[4] TRAPIL, Petrolum pipeline transport company, How pipelines work? Available from http://www.trapil.fr/uk/comcamarche4.asp. Accessed April 2013.

[5] Duffy, G.G. Measurement, mechanisms, and models: some important insights into the mechanisms of flow of fibre suspensions. Annual Transaction of Nordic Rheology Society, 2006; 14: 19-31.

[6] Lee, P.F.W., Duffy, G.G. Analysis of drag reducing regime of pulp suspension flow. Tappi, 1976 (a); 59: 119-22.

[7] Moller, K. Correlation of pipe friction data for paper pulp suspensions. Industrial and Engineering Chemistry Process Design and Development, 1976; 15: 16-19.

[8] Paul, T., Duffy, G., Chen, D. New insights into the flow of pulp suspensions. Tappi Solutions, 2001; 1.

[9] Elliott, D.R., de Montmorency, W.H. The transportation of pulpwood chips in pipelines. Report of an exploratory study. Montreal: Pulp and Paper Institute of Canada; 1963.

[10] Faddick, R.R. The aqueous transport of pulpwood chips in a four inch aluminum pipe. Kingston, Ontario: Queen's University; 1963.

[11] Gow, J.L. Hydraulic transport of woodchips in pipelines. Bozeman: Montana State University; 1971.

[12] Kumar, A., Cameron, J.B., Flynn, P.C. Large-scale ethanol fermentation through pipeline delivery of biomass. Applied Biochemistry and Biotechnology, 2005; 121: 47-58.

[13] Kumar, A., Cameron, J.B., Flynn, P.C. Pipeline transport of biomass. Applied Biochemistry and Biotechnology, 2004; 113: 27-39.

[14] Kumar, A., Cameron, J.B., Flynn, P.C. Pipeline transport and simultaneous saccharification of corn stover. Bioresource Technology, 2005; 96: 819-29.

[15] Sawai, T., Kajimoto, T., Ohmasa, M., Shibue, T., Nishi, K. Hydraulic transportation system of chips by Hilly Terrain Pipelines. 22nd International Symposium on Transport Phenomena. Delft, The Netherlands 2011.

[16] Vaezi, M., Katta, A.K., Kumar, A. Investigation into the mechanisms of pipeline transport of slurries of wheat straw and corn stover to supply a bio-refinery. Biosystems Engineering, 2014; 118: 52-67.

[17] Vaezi, M., Kumar, A. The flow of wheat straw suspensions in an open impeller centrifugal pump. Biomass and Bioenergy, 2014; XX: XX.

[18] Vaezi, M., Pandey, V., Kumar, A., Bhattacharyya, S. Lignocellulosic biomass particle shape and size distribution analysis using digital image processing for pipeline hydro-transportation. Biosystems Engineering, 2013; 114: 97-112.

[19] Elliott, D.R. The transportation of pulpwood chips in pipelines. Pulp and Paper Magazine of Canada, 1960; 61: 170-75.

[20] Hunt, W.A. Friction factors for mixtures of wood chips and water flowing in pipelines. 4th Hydrotransport Internatinoal Conference. Banff, AB, Canada; 1976.

[21] O'donnell, J.P. Diversification of owners is common in products pipeline. Oil and Gas Journal, 1964; 62: 88-100.

[22] Brebner, A. On pumping of wood chips through 4 inch aluminum pipe-line. Canadian Journal of Chemical Engineering, 1964; 42: 139-42.

[23] Wasp, E.J., Aude, T.C., Thompson, T.L., Bailey, C.D. Economics of chip pipelining. Tappi, 1967; 50: 313-18.

[24] Soucy, A. Data supplied to R.R. Faddick by Laval University. Quebec City, Quebec; 1968.

[25] Faddick, R.R. Hydraulic transportation of solids in pipelines. Bozeman: Montana State University; 1970.

[26] Gubba, S.R., Ingham, D.B., Larsen, K.J., Ma, L., Pourkashanian, M., Qian, X., et al. Investigations of the transportation characteristics of biomass fuel particles in a horizontal pipeline through CFD modelling and experimental measurement. Biomass & Bioenergy, 2012; 46: 492-510.

[27] Wasp, E.J., Regan, T.J., Withers, J., Cook, P.A.C., Clancey, J.T. Crosscountry coal pipeline hydraulics. Pipeline News, 1963; 35: 20-28.

[28] Schmidt, R.E. An investigation of the effects of pressure and time on the specific gravity, moisture content, and volume of wood chips in a water slurry. Civil Engineering: Montana State University; 1965.

[29] Mohamadabadi, H.S. Characterization and pipelining of biomass slurries. University of Alberta; 2009.

[30] Luk, J., Mohammadabadi, H.S., Kumar, A. Pipeline transport of biomass: Experimental development of wheat straw slurry pressure loss gradients Biomass and Bioenergy, 2014; 64: 329-36.

[31] Luk, J. Pipeline transport of wheat straw slurry. University of Alberta; 2010.

[32] Durand, R., Condolios, G. The hydraulic trasnport of coal and solids in pipes. Hydraulic Transport of Coal Conference London; 1952.

[33] Worster, R.C. Hydraulic transport of solids. Hydraulic transport of coal conference London; 1952.

[34] Gibert, R. Hydraulic transport and discharge of mixtures in pipes. Report by Annals of Roads and Bridges; 1960.

[35] Zandi, I., Govatos, G. Hetrogeneous flow of solids in pipelines. ASCE Journal of the Hydraulic Devision, 1967; 93: 145-59.

[36] Metzner, A.B., Reed, J.C. Flow of non-Newtonian fluids - correlation of the laminar, transition, and turbulent flow regions. Aiche Journal, 1955; 1: 434-40.

[37] Dodge, D.W., Metzner, A.B. Turbulent flow of non-Newtonian systems. Aiche Journal, 1959; 5: 189-204.

[38] Hunt, W.A. Economic analysis of wood chip pipeline. Forest Products, 1967; 17: 68-74.

[39] Hunt, W.A. Continuous flow transport of low value forst products by hydraulic pipeline [Unpublished report to Intermountain Forest and Range Experiment Station]. Bozman, Montana; 1962.

[40] Scheer, A.C. Survey on wood chips transportation charges [Unpublished report to Intermountain Forest and Range Experiment Station]. Bozman, Montana; 1962.

[41] Liu, H., Noble, J., Zuniga, R., Wu, J. Economic analysis of coal log pipeline transportation of coal. Report No 95-1. Capsule Pipeline Research Center (CPRC), University of Missouri, Columbia, USA; 1995.

[42] Marrison, C.I., Larson, E.D. Cost versus scale for advanced plantation-based biomass energy systems in the US and Brazil. Proceeding of Second Biomass Conference of the Americas: Energy, Environment, Agriculture, and Industry; 1995, p. 1272-90.

[43] Jenkins, B.M., Dhaliwal, R.B., Summers, M.D., Bernheim, L.G., Lee, H., Huisman, W., et al. Equipment performance, costs, and constraints in the commercial harvesting of rice straw for industrial applications. American Society of Agricultural Engineers (ASAE) Conference; 2000.

[44] Kumar, A., Cameron, J.B., Flynn, P.C. Biomass power cost and optimum plant size in western Canada. Biomass & Bioenergy, 2003; 24: 445-64.

[45] Glassner, D., Hettenhaus, J., Schechinger, T. Corn stover collection project. Bioenergy Conference. Madison, WI, USA; 1998, p. 1100-10.

[46] Ellis, H.S., Redberger, P.J., Bolt, L.H. Slurries: basic principles and power requirements. Industrial and Engineering Chemistry, 1963; 55: 18-26.

[47] Nardi, J. Pumping solids through a pipeline. Pipeline News, 1959: 26-33.

[48] Aden, A., Ruth, M., Ibsen, K., Jechura, J., Neeves, K., Sheehan, J., et al. Lignocellulosic biomass to ethanol process design and economics utilizing co-current dilute acid prehydrolysis and enzymatic hydrolysis for corn stover, Report no. NREL/TP-510-32438. National Renewable Energy Laboratory; 2002.

[49] Harada, T. Energy consumption in utilization of woody biomass. Wood Industry, 2002; 57: 480-83.

CHAPTER 3

Lignocellulosic Biomass Particle Shape and Size Distribution Analysis Using Digital Image Processing for Pipeline Hydro-transportation[1]

3.1. Introduction

Pipeline hydro-transport of agricultural residue biomass (e.g., wheat straw or corn stover) in the form of solid-liquid mixture (slurry) involves chopping of feedstock, classifying based upon size, mixing with water up to certain solid mass content (concentration) levels, and pumping through a pipeline [1-3]. Apart from several factors affecting initial and operating parameters, biomass particles shape and size are critical factors in slurry pipeline transport. Above certain slurry solid mass contents, the decrease in size of the particles increases the slurry pressure drop [4-6]. Similarly, decrease in size of the particles increases the sugar-release from the biomass during the pipeline hydro-transport. These observations illustrate the importance of particle size in the pipeline hydro-transport. Hence, investigating particle size distribution (PSD) and morphological features, not only helps to analyse slurry flow behaviour, but also helps to modify the slurry preparation processes to optimise the design and operation of agricultural residue biomass pipelines and facilities. Knowledge of particle size also helps in understanding how feedstock type and pre-processing procedures impact PSD and morphological features, and ultimately the pipeline hydro-transport of biomass in the form of slurry.

PSD analysis is considered a standard procedure to evaluate the dimensional characteristics and morphological features of particulate materials. American Society of Agricultural and Biological Engineers (ASABE) adopted PSD analysis to determine and express the particle size of chopped forage materials by mechanical screening [7]. However, mechanical sieving comes with drawbacks, e.g., number of available standard

[1] Vaezi, M., Pandey. V., Kumar. A., Bhattacharyya. S., ***Biosystems Engineering***, 2013; 114: 97-112.

sieves (56 sieves) is finite, the tests are time consuming and the selection of sieve set involves guesswork. In addition, Igathinathane et al. [8] reported the unbalanced separation of particles on sieves and Womak et al. [9] stated that measured length of particles (compared to their computed length based upon the sieve analysis proposed by ASABE) varies to 5 times for knife-milled ground switchgrass, wheat straw, and corn stover, due to the "fall-through" effect of particles that are fibrous in nature ($X_{gl}/X_{gl,width}>>1$) through smaller sized sieve openings. As a result, the mechanical sieving approach would not appropriately serve the purpose of separation of biomass particles for pipeline hydro-transport of agricultural residue biomass.

In addition to advanced and expensive laser diffraction techniques, computer vision-based digital image processing can be considered as an alternative approach in shape identification and PSD analysis. For example, the technique has been utilised to: determine seed size uniformity of soybean using linear discriminant function models and artificial neural network classifiers [10]; perform leaf area measurement applying a MATLAB (Mathworks Inc., Natick, Massachusetts, U.S.A) algorithm [11]; measure wheat single kernel size directly utilising the java-based ImageJ software [12]; determine the orthogonal dimensions of convex shaped food grains [8]; and simulate mechanical sieve analysis of ground biomass materials using ImageJ [13]. As a result, the applicability of the technique in determination of size and size distribution of agricultural materials has been well established, with advantages comprising of large repeatability, small required quantities of samples, consistency and robustness, and being classified as a non-destructive approach compared to traditional sizing equipment [14, 15].

Requirements for computer vision-based image processing are an image acquisition device and image processing algorithms. Image capturing can be done using either a charge coupled camera [16, 17] or a flatbed scanner [10]. Issues regarding image capturing procedure, including contrast [8] and arrangement of particles [14, 18]; and image processing algorithms such as Visual Basic [19] and Matlab [11], have been well documented and reported in literature. Utilising a flatbed scanner, the present study used ImageJ, a Java-based and platform-independent software by National Institutes of Health (NIH, Bethesda, Maryland USA) [20], and developed a user-coded plugin to measure

particles dimensions, and analyse particles size distribution and corresponding parameters.

The present research aimed to determine how well the nominal sizes represent the real particle dimensions. Size, shape factors, size distribution algorithm, and corresponding parameters of the particles pre-classified (i.e., the output material from a chip classifier) will be later applied to justify the chemical/mechanical behaviour of the slurry [6]. Unlike previous studies by others [11, 12, 16], this research utilised ImageJ to investigate the applicability of an "image processing-based approach" for a practical application. In addition to particle size analysis and the calculation of PSD parameters, the effect of knife mill operating factors on particle dimensions, the suitability of various distribution functions to better describe the PSD algorithm, particles surface roughness, and the particle size reduction effect (degradation) through hydro-pipelining biomass particles were also examined.

3.2. Materials and Methods

3.2.1. Feedstock and Pre-processing

Corn stover and wheat straw are considered as leading candidates for the production of bio-ethanol [21]. As a result, the present research focused on the pipeline hydro-transporta of these specific feedstock. Corn stover (Zea mays ssp. mays L.) and wheat straw (Triticum aestivum L.) were collected from farms in Taber and Township located in Northern and Southern Alberta, Canada, respectively. Whilst dry, the materials were milled using a commercially available knife mill (SM-100; Retsch Inc., Newtown, PA, US). The knife mill utilised a screen with 6 mm squared openings, which was mounted in an arc on the bottom side of rotor. Afterwards, Using a standard [22] chip classifier[2] (BM&M Inc., Surrey, BC, Canada), the knife-milled materials were classified into four nominal sizes of ~19.2 mm, ~6.4 mm, ~3.2 mm, and <~3.2 mm, which were labelled after the size of the classifier sieves openings, as shown in Table 3-1. It is worth mentioning that the chip classifier was set to reduce the wide size range (from less than 3

[2] Due to noticeable amounts of materials required (10 to 29 kg per test), it was not technically appropriate to carry out tests using common sieving machines. A large-scale chip classifier was utilised instead.

mm to more than 19 mm) of the knife-milled particles, not only to more precisely study the effect of particle dimensions on hydro-transport features, but also to better understand the optimum size range of particles to be generated by a full scale mill (grinder) for large-scale hydro-transport purposes.

Finally, 100 g samples from every group of the size-classified materials were representatively taken, from which only a few grams were used for image acquisition. Five sets of images per particle size per feedstock type were captured. As shown later in section 3.3.2.1, a few grams of sample, and five sets of images were fairly sufficient to represent the entire bulk.

Table 3-1: Particle size classification according to classifier sieve sizes

Screen Size	Estimated Average Particle Size
19.2 mm (3/4″)	n/a, discarded
12.8 mm (1/2″)	n/a, discarded
6.4 mm (1/4″)	n/a, discarded
4.0 mm (1/6″)	~19.2 mm
3.2 mm (1/8″)	~6.4 mm
1.28 mm (1/20″)	~3.2 mm
Pan	<~3.2 mm

3.2.2. Image Acquisition and Processing Technique

A flatbed scanner (Epson Stylus NX115, Markham, Ontario, Canada) was used to acquire the 720 dpi colour images of the test materials, while particles were well separated to make the image analysis algorithm simpler and prevent the necessity of using advanced analysis techniques [14]. As all the test sample particles were light in colour, a black background was used to obtain better contrast. To isolate the ImageJ output from input devices and user platforms, the software was calibrated by determining a scale factor, which converted the pixel units of the image to physical units of measurements (e.g., mm) [8]. The scanned image resolution of 720 dpi corresponded to a constant scale factor of 0.0353 mm/pixel.

Using ImageJ and a straight forward procedure, the original colour image was firstly converted to grey-scale (8-bit) image and, secondly, to binary image (Fig. 3-1). Running the plugin, it called the ImageJ "Analyze Particle" routine to measure the basic dimensions. The minimum area to be taken into consideration was set to 500 pixel^2 to

ignore ultra-fine particles (i.e.< 0.8 mm)[3], which technically negligibly affect the characteristics of the two-phase flow of the present research; only increases the viscosity of the carrier liquid [23], which will be further discussed in chapter 4. As shown in Table 3-2, it was calculated that limiting the particle area, although it resulted in ignoring up to 90% of the number of particles, it accounted for only up to 4% of the total particles area. Practically, the ignored particles were mainly minuscule particulates, dusts, and even spots on the scanner screen, which constituted majority of <~3.2 mm particles.

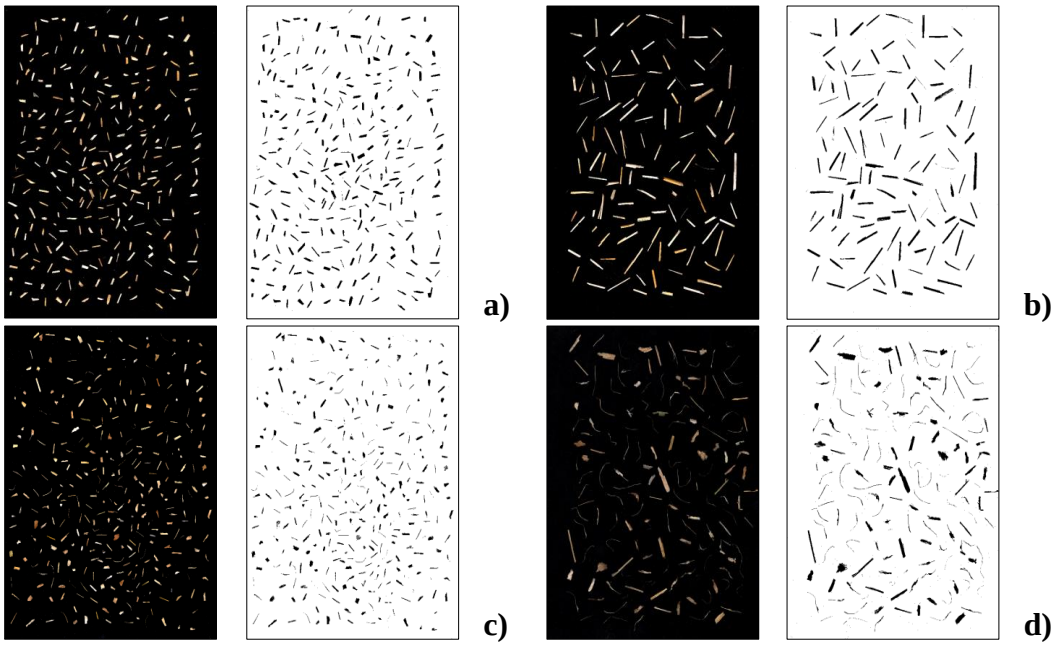

Fig. 3-1: Original colour and ImageJ processed images of a) ~3.2 mm wheat straw, b) ~19.2 mm wheat straw, c) ~3.2 mm corn stover, d) ~19.2 mm corn stover

Table 3-2: Effect of limiting "analyzing threshold" on number/area of processed particles

Nominal Particle Size	Particle Type			
	Wheat Straw		Corn Stover	
	Loss due to increasing minimum particle area of interest from 0 to 500 pixel			
	Area Loss (%)	Count Loss (%)	Area Loss (%)	Count Loss (%)
~19.2 mm	0.43	94.82	1.34	94.62
~6.4 mm	0.57	91.40	0.88	89.22
~3.2 mm	0.45	83.98	1.23	87.81
<~3.2 mm	11.88	90.13	11.21	79.42
Average	3.33	90.08	3.66	87.76

[3] By considering 0.0353 mm/pixel scale factor

The binary image of any particle with a continuous boundary can be modelled as an ellipse having equivalent area and perimeter of the particle. The distribution of the particle boundary coordinates, after equating the second order central moments, produces the best-fitting ellipse [24]. ImageJ follows the same approach. However, overestimation or underestimation of the actual length and width of some basic shapes of the particles has been observed, specifically in the case of polygonal shapes with fewer numbers of sides, such as triangles and rectangles. Igathinathane et al. [25] proposed defining correction factors to rectify the over/underestimation in dimension measurements. Also they developed a shape identification strategy, as the correction factors values depend on the geometric shapes that best represents the particle. The same idea was employed here to develop a Java-based user-coded plugin in ImageJ, to suit the specific requirements of a machine vision approach for this practical application.

Once the particle boundaries were located, the ImageJ analysed the geometry to measure the area, perimeter, and other dimensions of the best fitting ellipse. Upon completion, and for post-processing purposes, the plugin was called in ImageJ to evaluate and output all the user specified measurements. This comprised obtaining the shape parameters to identify the shapes of the particles, utilising the correction factors to produce corrected length, width, and area of the actual non-circular non-elliptical particles, calculating particles geometric and graphic mean lengths with corresponding standard deviations, drawing PSD graphs and evaluating PSD parameters, and determining PSD describing functions (e.g., Rosin-Rammler) and parameters.

To identify the shape, three non-dimensional shape parameters based on ImageJ standard output properties of particles were introduced into the plugin. To correct for the under- and over-estimation in particle diameters, the plugin calculates the area of the best fitting ellipse and assumes the constant aspect ratio for both the ellipse and the corresponding shape of the particle (square, rectangle, circle, and triangle) to obtain the correction factor. Therefore, the constant correction factor, when applied to major and minor axes of ellipse, rectifies the over- and under-estimation and produce correct length and width of the actual shape. More on the details of these procedures can be found elsewhere [25].

3.2.3. Particle Size and Distribution Analysis

Although the standard screening approach [7] employs a limited number of sieves and measures the weight of materials retained on each sieve, image processing technique depends on the number of particles per given length through the entire range of particles, which is considered as a weighting factor in PSD analysis. The measured lengths of whole particles can be categorised into several distinct lengths; a concept which was first introduced by Igathinathane et al. [26], where the majority of particles lengths will match and form unique groups of distinct lengths. The groups of particles, represented by distinct length particles, make up the total particles of the sample. The number of grouped particles can be subsequently subjected to cumulative characteristics, where dimensions of significance based on length can be derived; these dimensions are comprised of d_{95}[4], d_{90}, d_{84}, d_{75}, d_{60}, d_{50} (also known as the median length), d_{30}, d_{25}, d_{16}, d_{10} (known as effective size), and D_5. Also several PSD parameters, such as uniformity index (L_u), size guide number (N_{sg}) [27, 28], graphic skewness (S_{ig}), and graphic kurtosis (K_g) [29] can be calculated accordingly as:

$$I_u = \frac{d_5}{d_{90}} \times 100 \tag{1}$$

$$N_{sg} = d_{50} \times 100 \tag{2}$$

$$S_{ig} = \left[\frac{d_{84} + d_{16} - 2d_{50}}{2(d_{84} - d_{16})}\right] + \left[\frac{d_{95} + d_5 - 2d_{50}}{2(d_{95} - d_5)}\right] \tag{3}$$

$$K_g = \left[\frac{d_{95} - d_5}{2.44(d_{75} - d_{25})}\right] \tag{4}$$

The uniformity index (I_u) characterises the spread in particle size distribution, the size guide number (N_{sg}) is the median (or geometric mean) of the particle sizes; graphic skewness (S_{ig}) indicates the degree of asymmetry compared to a normal distribution of

[4] With 95% of particles larger than this specific diameter

particles versus particle size; and departure from a specific ratio of 2.44 is represented by graphic kurtosis (K_g) [30], as interval between d_5 and d_{95} points on normal probability curve should be exactly 2.44 times the interval between d_{25} and d_{75} points; measuring the width of the central part of the distribution relative to the distance between the tails or extreme values of it.

To determine ranges of lengths of particulate biomass, graphic [31] and geometric [7] means (X_{ig} and X_{gl}, respectively) together with their corresponding standard deviations (σ_{ig} and σ_{gl}) were calculated as:

$$X_{ig} = \frac{d_{16} + d_{50} + d_{84}}{3} \tag{5}$$

$$\sigma_{ig} = \left[\frac{d_{84} - d_{16}}{4}\right] + \left[\frac{d_{95} - d_5}{6.6}\right] \tag{6}$$

$$X_{gl} = ln^{-1}[\frac{\sum(N_i \times lnX_i)}{\sum N_i}] \tag{7}$$

$$\sigma_{gl} = ln^{-1}[\frac{\sum(N_i(lnX_i - lnX_{gl})^2}{\sum N_i}]^{\frac{1}{2}} \tag{8}$$

After obtaining major particle dimensions, it is now possible to calculate particle shape factors, which are of importance in identifying the variation of slurry mechanical behaviour with particles type and size [32-34]. Three shape factors which were considered include aspect ratio, circularity, and roundness, which can be calculated as:

$$Circularity = \frac{4\pi A}{P^2} \tag{9}$$

$$Aspect\ Ratio = \frac{X_{gl}}{X_{gl,width}} \tag{10}$$

$$Roundness = \frac{4A}{\pi X_{gl}^2} \quad (11)$$

As the circularity value approaches from 1.0 (a perfect circle) to 0.0, it indicates an increasingly elongated polygon, aspect ratio represents the ratio between major and minor axis dimensions, and roundness describes the shape of the corners on a particle.

Among PSD parameters, size guide number (N_{sg}) and uniformity index (L_u) are widely used to describe the range of variation in particle sizes [27, 28]. These correspond to the median particle size and the 5th percentile particle size expressed as a percentage of the 95th percentile particle size, respectively. However, this system, usually referred to as size guide number (SGN) model, is of limited value, because it just gives two parameters without a distribution function. Thus, even if two biomass materials posses exactly the same parameters, it does not necessarily mean that those have the same size distribution algorithm. Looking for a better parameterisation system, three common size distribution functions including the log-normal, the Rosin-Rammler, and the Gaudin-Schuhmann equations were investigated. These functions have been previously utilised to describe the particle size distribution of various materials, such as granular mineral fertilisers [35], and soil particles [36]. The accuracy of these approaches in determining PSD was tested to understand which one could potentially be adopted for routine standard use.

The Rosin-Rammler equation was developed [37] to describe broken coal and other comminuted earth materials. The equation is given by:

$$P(X > x) = 100\ exp[-(x/\alpha)^{\beta}] \quad (12)$$

α (intercept) and β (slope) are parameters related to the characteristic size and spread of distribution, respectively, as α represents the particle size corresponding to the 36.78th percentile of the cumulative probability distribution, and β controls the shape of the distribution function [38]. A small β denotes a wide spread of particle size and vice versa [35]. To compare the Rosin–Rammler approach with the SGN model, the size guide number (N_{sg}) and uniformity index (I_u) were estimated using α and β, following Perfect et

al. [35]. The present job compares the theoretical I_u and N_{sg} with those of predicted values (denoted as I'_u and N'_{sg}) to analyse the corresponding variance. The predicted I'_u and N'_{sg} are calculated as:

$$\acute{I_u} = 100\ exp[-3.804/\beta] \tag{13}$$

$$\acute{N_{sg}} = 100\ \alpha\ exp[-0.366/\beta] \tag{14}$$

Epstein [39] showed that the size distribution of fragments resulting from a process of repeated breakage is asymptotically log-normal. The log-normal size distribution function is given by:

$$P(X > x) = 50 - 50\ \text{erf}[\ln(x/X_{gl})/\sqrt{2}\ln(\sigma_{gl})] \tag{15}$$

and finally, when particles of homogeneous solid are repeatedly broken by a series of single fractures, their resulting size distribution is a straight line on a log-log plot [40]. This is the Gaudin-Schuhmann function, which is given by:

$$P(X > x) = 100\ [1 - (x/x_0)^m] \tag{16}$$

3.3. Results and Discussion

3.3.1. Particle Size Analysis of Knife-milled Pre-classified Wheat Straw and Corn Stover

3.3.1.1. Particle Size and PSD Algorithm

The sample images were processed through the developed plugin, and median length (d_{50}), geometric mean length (X_{gl}) [7], and graphic mean length (X_{ig}) [29], besides geometric and graphic standard deviations (σ_{gl} and σ_{ig}) are presented in Table 3-3. The determined ranges of lengths of wheat straw particles were 3.25-15.32 mm for geometric mean, 3.4-15.86 mm for graphic mean, and 4.73-17.47 mm for arithmetic average. These dimensions for corn stover ranged over 2.57-9.11 mm, 2.76-9.7 mm, and 4.26-15.73 mm,

respectively. Generally, the geometric mean length was smaller than the graphic and the arithmetic mean lengths, while the graphic mean length was in between the other two. However, the difference between the three dimensions studied was negligible.

Table 3-3: Nominal and measured particle dimensions of samples

Material Type	Nominal Size (inch)	Median Length (mm)	Geometric Length (mm)	Graphic Length (mm)	Length (mm)			Width (mm)		
		d_{50}	$X_{gl} \pm \sigma_{gl}$	$X_{ig} \pm \sigma_{ig}$	Min.	Max.	Mean ± S.D.	Min.	Max.	Mean ± S.D.
Wheat Straw	19.2 mm	15.09	15.32 ± 1.39	15.86 ± 4.57	1.72	33.23	17.47 ± 9.31	0.3405	3.7	2.02 ± 0.99
	6.4 mm	9.27	9.28 ± 1.27	9.46 ± 2.13	2.61	16.14	9.37 ± 4.00	0.179	3.55	1.86 ± 0.99
	3.2 mm	5.97	5.76 ± 1.33	5.92 ± 1.55	1.71	10.88	6.29 ± 2.71	0.268	2.8	1.53 ± 0.75
	<3.2 mm	3.23	3.25 ± 1.5	3.4 ± 1.39	1.04	8.43	4.73 ± 2.19	0.143	1.788	0.96 ± 0.48
Corn Stover	19.2 mm	9.27	9.11 ± 1.63	9.7 ± 4.74	1.57	29.88	15.73 ± 8.38	0.219	5.997	3.10 ± 1.71
	6.4 mm	6.82	6.64 ± 1.45	6.9 ± 2.43	1.35	16.01	8.68 ± 4.33	0.212	4.558	2.38 ± 1.29
	3.2 mm	4.52	4.44 ± 1.44	4.62 ± 1.67	1.20	9.61	5.4 ± 2.49	0.133	3.372	1.75 ± 0.96
	<3.2 mm	2.56	2.57 ± 1.56	2.76 ± 1.27	0.94	7.58	4.26 ± 1.92	0.18	1.724	0.95 ± 0.45

Particulate material PSD algorithms are generally expressed either as plot of particle frequencies versus particle dimensions, or cumulative number fraction of particles versus particle dimensions. Figure 3-2 represents cumulative PSD and PSD based on the number of samples for 6.4 mm corn stover particles. Here, the image-based particle sizes ranged from 1.4 to 14.8 mm and maximum number of particles occurred in 6.9 mm length. These PSD characteristics provide overall information about the distribution of particle dimensions graphically and also enable several distribution related numerical parameters describing the sample to be derived, e.g., dimensions of significance based on length such as d_{50}. Figure 3-3 shows a curve-fitted PSD algorithm corresponding to four nominal sizes of wheat straw. The observation indicates the increased presence of <~3.2 mm particles, with a consistent, narrow, and thus uniform particle length band. While ~3.2 mm and ~6.4 mm particles were moderate in frequency and length band, the 19.2 mm particles were of about a quarter of the frequency of <~3.2 mm particles and more than fourfold of their length band. It can be observed that various graphs corresponding to

different sizes overlap each other, indicating the limited efficiency of the large-scale classifier with the current number of sieves in separating the particles of various sizes. Also the deviation of the PSD (number of samples vs. particle diameter) is attributed to the small number of samples (5 samples) practiced and the residuals not appropriately converged. Increasing the sample size would fix the problem.

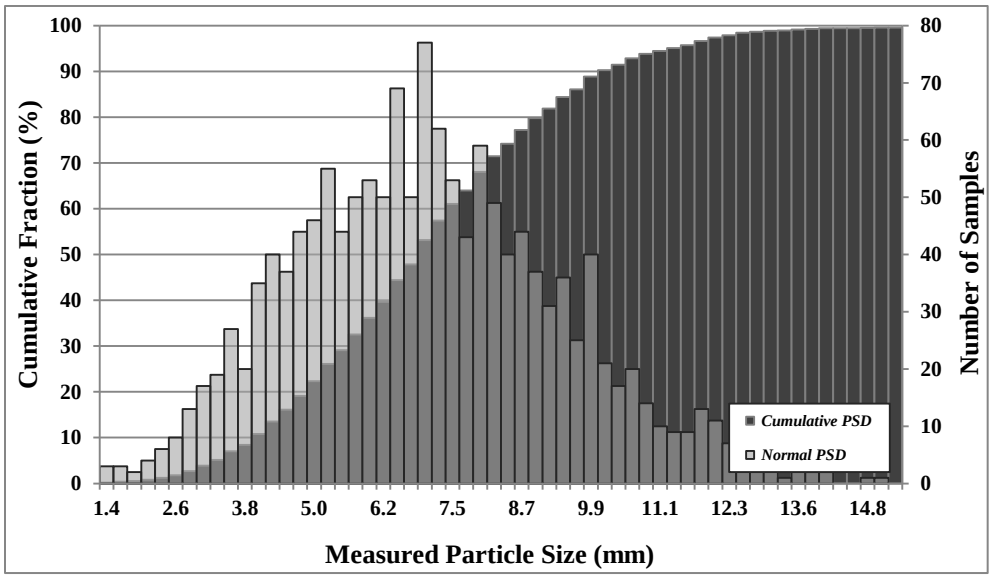

Fig. 3-2: PSD algorithms of ~6.4 mm corn stover

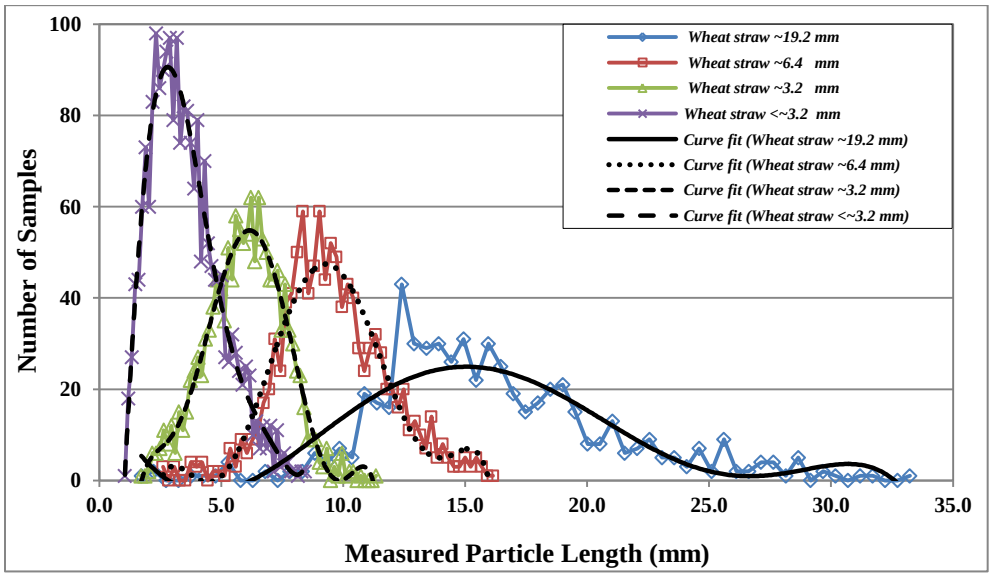

Fig. 3-3: PSD of wheat straw particles (curves best fitted to better distinguish the boundaries of the graphs)

3.3.1.2. Sample Quantity and Accuracy of Approach

In order for the sample to be good representative, there needs to be a minimum sample size for testing. Standard BS812: Part 103 [41] presents the minimum mass of sample required for mechanical sieving analysis. However, there is neither account of similar standard approach for image processing nor it has been reported in any of published papers on image processing of agricultural materials. However, Igathinathane et al. [8] reported that even few grams of sample could consist of thousands of particles. To ensure the amount of materials sampled (out of tens of kgs of knife-milled pre-classified wheat straw and corn stover) were adequate to represent the entire bulk, five sets of samples per particle size per feedstock type were sampled, image-captured, and processed. Each sample was then carefully collected and accurately weighed. The weight of the samples ranged between 0.08 to 0.18 g. Compared to the order of magnitude of samples required for sieving (which ranges from 0.1 kg to 50 kg [41]) the weights of samples used for image processing were significantly small. The number of particles analysed, ranged from 500 for the ~19.2 mm sample to 2,300 for <~3.2 mm sample per five sets of samples per size. However, those numbers were large enough to represent the entire bulk, as shown in Fig. 3-4. This figure presents cumulative number fraction of particles versus the plugin-calculated particle length for corn stover of nominal size of ~3.2 mm. Five sets of samples are graphed together with their corresponding 95% confidence interval lines. It is observed that for the majority of the graph, the corresponding markers fall well between the lines, indicating that both the number and the weight of samples represent reasonably well the entire bulk.

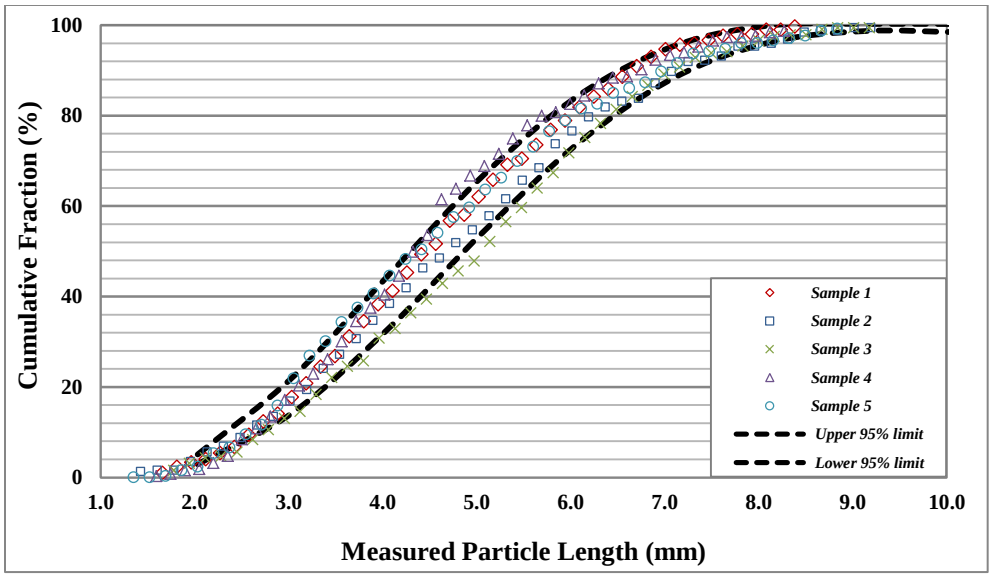

Fig. 3-4: cumulative number fraction of particles vs. particle length for corn stover particles with nominal size of ~3.2 mm

3.3.1.3. Particles Shape Factors

It has been shown that dilute suspensions of specific fibrous particles, exhibit pronounced drag reduction effects [42]. The effectiveness of particulates as drag reducing additives increases as their aspect ratio increases and is appreciable for fibrous additives [43]. This effect arises mainly due to particle-particle interactions of fibrous particles with length scales on the order of millimetres (and larger) and large aspect ratios. As a result, for the specific purpose of the present research; biomass pipeline hydro-transport , aspect ratio is an important piece of information in addition to the particle size. Figure 3-5 shows the aspect ratios of particles in terms of the ratio between geometric mean length and geometric mean width. It can be observed that, aspect ratios ranges between 4.51 to 10.08, and 3.71 to 6.71 for wheat straw and corn stover particles, respectively; confirming the minor importance of "width parameter" for the purpose of this research, and fibrous nature of the test materials. Throughout the rest of the paper, therefore, the focus would be primarily on the "length" parameter as the dominant dimension utilised for particle analysis. However, the choice of appropriate dimension of significance based on length (i.e., median, geometric, or graphic) depends on the corresponding application.

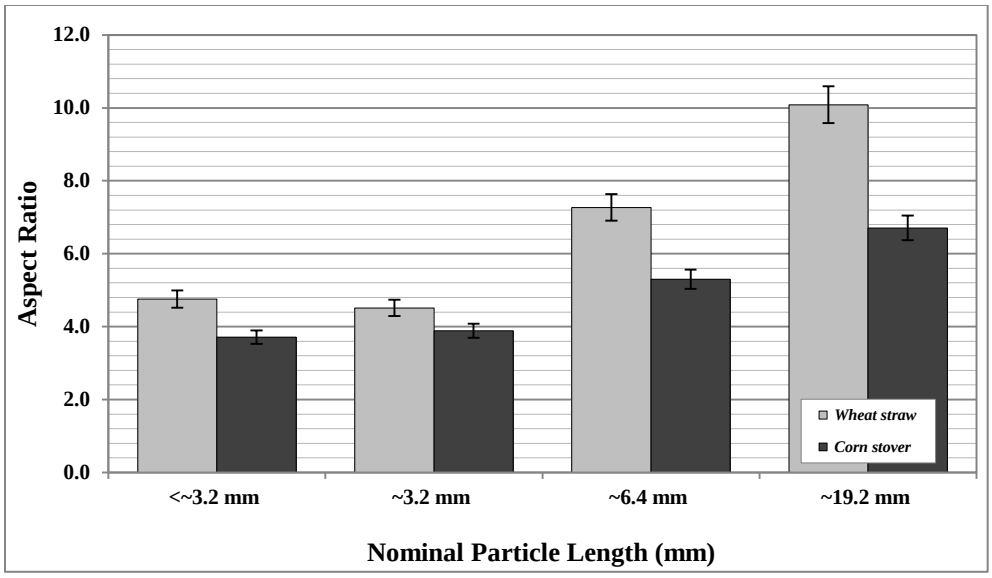

Fig. 3-5: Aspect ratio vs. nominal size of pre-classified particles

Figure 3-6 shows the variation of other shape factors including roundness and circularity versus nominal particle sizes. As the nominal particle size increased, circularity decreased from 0.41 to 0.14, and from 0.36 to 0.18 for corn stover and wheat straw, respectively. The same trend was observed for roundness, where these parameters had a strong negative correlation with aspect ratio. However, there was no surprise, as the larger the size, the less the poligonality, and the sharper particle edges, while fine particles were more or less circular and smooth. Comparing wheat straw and corn stover circularity and roundness at the same size, wheat straw was more circular and had less round particles.

3.3.1.4. Comparison of Nominal and Measured Dimensions

One of the prime purposes of this study was to examine if nominal particle sizes are good representative of real dimensions. Figure 3-7 compares the particle median length (d_{50}) to nominal sizes obtained from the large-scale classifier (see materials and preprocessing section). The wheat straw particles having nominal size of <~3.2 mm come with a median length of <3.23 mm; a nominal size deviation of about +<2%. The deviation for ~3.2 mm, ~6.4 mm, and 19.2 mm were +88%, +46%, and -20%, respectively. The corn stover particles with the same order of nominal sizes include -<20%, +38%, +8%, and -52% deviation, respectively. A specific trend of nominal length deviation was not

obtained with an increase in nominal particle length. As observed, the errors involved in nominal sizes brought about noticeable under- and overestimations of the real dimensions of the particles. Therefore, the nominal sizes, which were numbered according to the classifier sieves openings sizes, were not good criteria to judge the particle dimensions.

3.3.1.5. Knife Mill Operating Factor

To understand how knife mill operating factors, specifically knife mill screen size, affect the PSD of wheat straw and corn stover, two screens with 4 mm and 6 mm squared openings were tested and the median lengths obtained (d_{50}) were compared on Fig. 3-8. Choosing the screen with smaller openings reduced the output length of the particles, as the median size of particles reduced by 0% to 21% for wheat straw and 17% to 31% for corn stover. The entire analysis for the current research was done based upon a screen size with 6 mm openings.

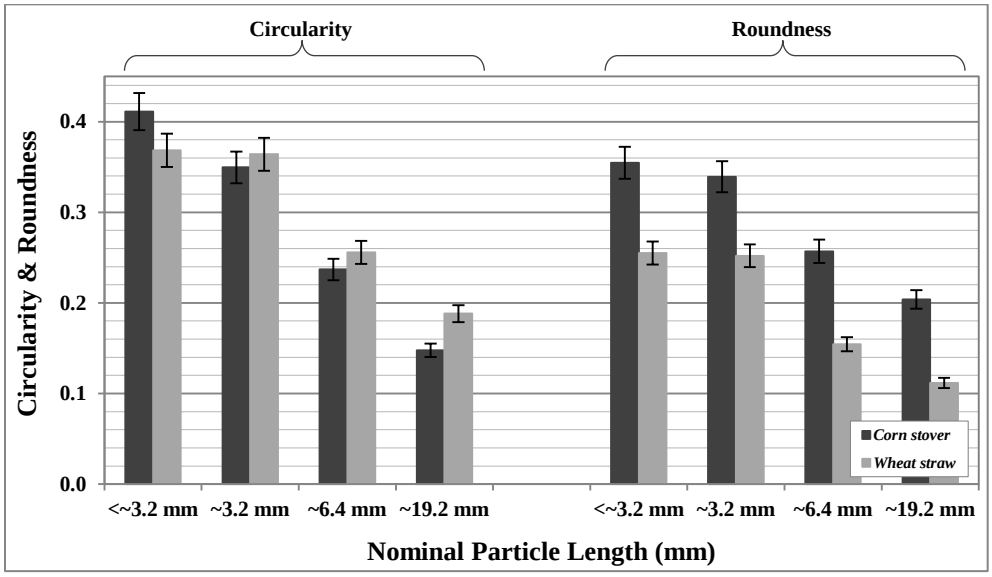

Fig. 3-6: Circularity and roundness vs. nominal size of pre-classified particles

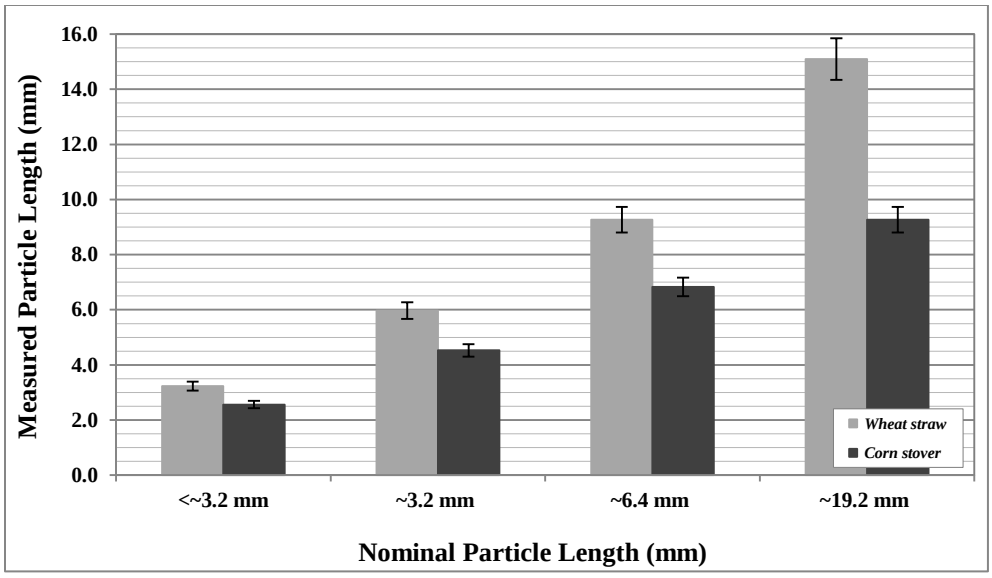

Fig. 3-7: Comparison of particles nominal and measured dimensions (d_{50})

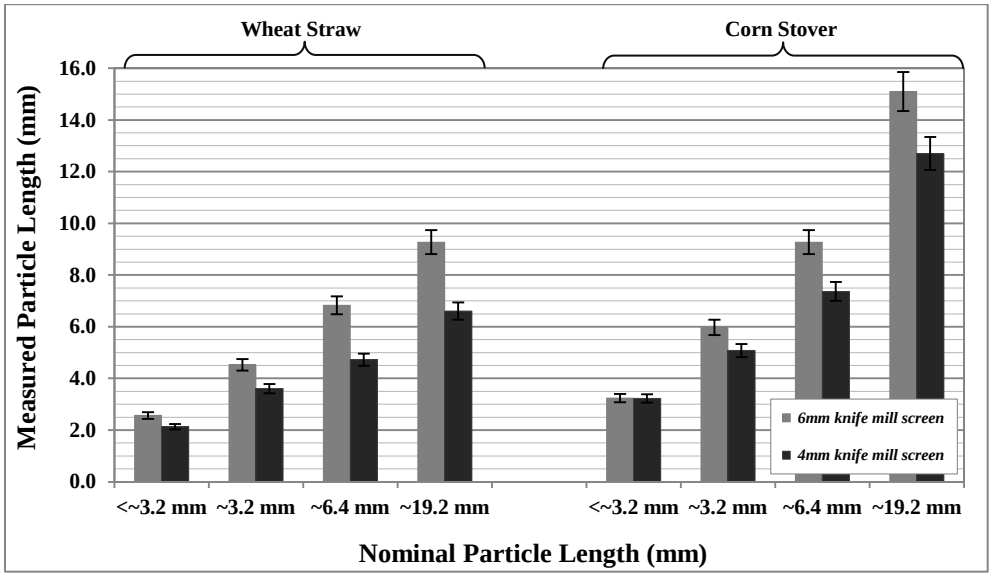

Fig. 3-8: Comparing measured lengths of wheat straw and corn stover knife-milled pre-classified particles for two various knife mill screens with 4 and 6 mm opening sizes

3.3.2. Particle Size Distribution Functions

The three size distribution functions described previously were used to fit the data. Some of square error (SSE) was used as an index for evaluating appropriateness of fit; the smaller this value, the better the fit. To find out which of three PSD equations (Eq.(12), Eq.(15), and Eq.(16)) better fits the distribution of size in a sample, the characterising

parameters of the particles were calculated and the corresponding cumulative faction and number of samples graphs were plotted versus particle length. Figure 3-9 presents these graphs, together with experimental size distribution for ~3.2 mm wheat straw and ~19.2 mm corn stover. As can be seen, the Rosin-Rammler equations were fitted with the least SSE in all scenarios (Fig. 3-10), indicating that particle size distribution of wheat straw and corn stover were well described by the Rosin-Rammler function. This is in good agreement with the published trends for unclassified wheat straw [44]; although the samples were pre-classified, they still followed the same distribution approach as non-classified samples. The Guadin-Schuhmann model had the second best fit, and the log-normal approach had the highest SSE, indicating limited goodness of fit with the experimental results.

The geometric standard deviation took into account only a fraction of the number of particles, disregarding the finest and the largest particles. The finest particles may change the viscosity (depending on slurry solid mass fractino), while coarser particles can cause clogging through pipeline. The advantage of the Rosin–Rammler function is that it takes into account 100% of the particle quantity.

3.3.3. Particle Size Distribution Parameters

Rosin-Rammler size (α) and distribution (β) parameters, the uniformity index (I_u), size guide number (N_{sg}), skewness (S_{ig}), and graphic kurtosis (K_g) were calculated. Figure 3-11 shows Rosin-Rammler parameters for two materials at different nominal sizes. Rosin-Rammler distribution parameter β for wheat straw increased from 3.15 to 4.68 as the nominal particle size increased from <~3.2 mm to ~6.4 mm, and it then slightly decreased to 3.14 as the nominal particle size increased to ~19.2 mm. For corn stover, a similar reduction occurred at ~6.4 mm. Although the smaller β indicates the more spread around the median, the obtained β were adequately large to result in a narrow spread (high uniformity) in the particle size distribution, and a symmetric S-shaped curve, as shown in Fig. 3-3. As the nominal particle size increased, the Rosin-Rammler size parameter α increased from 0.61 to 1.26 for wheat straw, and from 0.54 to 1.09 for corn stover, respectively. Rosin-Rammler size parameter had strong positive correlation with nominal

particle size. Comparing the results with Table 3-3 and Fig. 3-3, it can be observed that the size parameters were always noticeably greater than median, geometric, and graphic mean lengths.

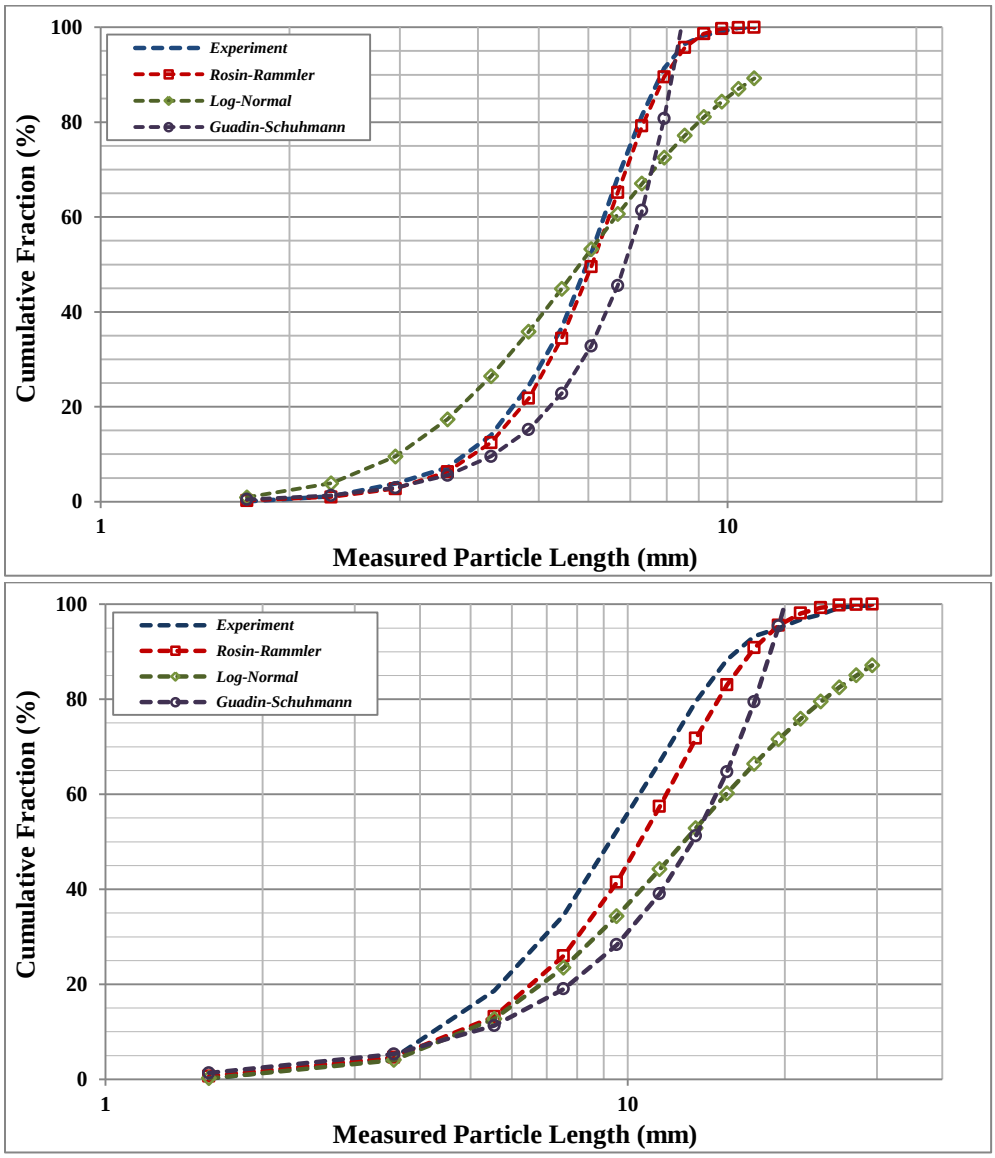

Fig. 3-9: Particles size distributions obtained via three distribution functions and image analysis: (a) ~3.2 mm wheat straw, (b) ~19.2 mm corn stover

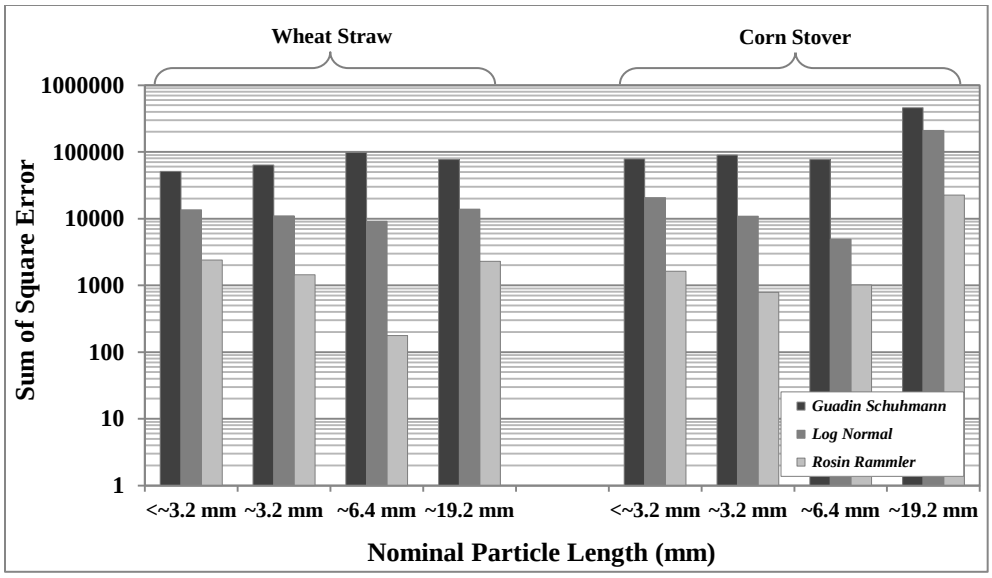

Fig. 3-10: Sum of squares errors (SSE) corresponding with three distribution functions

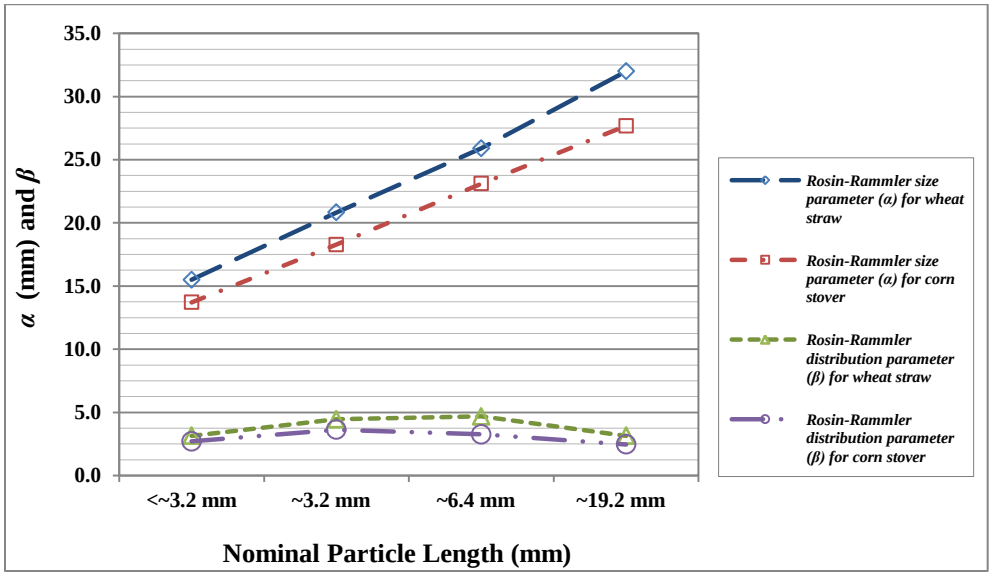

Fig. 3-11: Variation in Rosin-Rammler PSD parameters of wheat straw and corn stover particles for four nominal sizes

The theoretical values of N_{sg} and I_u for each sample were calculated by linear interpolation following the SGN model (Eqs. (1) and (2)). Obtaining α and β, the predicted N'_{sg} and I'_u were also determined (Eqs. (10) and (11)) to compare with theoretical values (Table 3-4). Perfect et al. [35] stated that the uniformity index estimated with SGN model is less accurate than when estimated with the Rosin–Rammler approach, due to the linear interpolation of the uniformity index. In the present study, the

uniformity indices obtained via Rosin–Rammler approach were generally slightly smaller than corresponding SGN model values (Table 3-4). Perfect et al. (1998) also discussed the difference between theoretical and predicted uniformity indices tends to increase with particle size heterogeneity. This difference here was less for corn stover compared with wheat straw, and more for the coarser wheat straw particles compared with finer ones. Consequently, corn stover particles were more homogenous than those of wheat straw, and coarser wheat straw particles were more heterogeneous than those of corn stover. Concerning the SGN, the values obtained via Rosin–Rammler approach were consistently higher than those obtained with the SGN model. This is due to the fact that, while the Rosin–Rammler function provides the most accurate prediction of SGN for spherical granules, it is not suitable for cylindrical shapes, since fragmentation produced fine particles leading to a binomial distribution function, and the Rosin–Rammler function cannot handle this type of distribution [28]. So for the case of fibrous materials, the SGN model may be more reliable than the Rosin–Rammler approach.

Skewness decreased with an increase in wheat straw nominal particle size from <~3.2 mm to ~3.2 mm and then increased with further increase in nominal size to ~19.2 mm (Table 3-4), while for the corn stover, the increase occurred at ~6.4 mm. Positively skewed populations have a tail of excess fine particles (see ~19.2, ~6.4, <~3.2 mm curves on Fig. 3-3) and negatively skew particles have a tail of excess coarse particles (see ~3.2 mm curve on Fig. 3-3) [45]. All the particles were comprised of fine-skewed particles, as almost all the skewness values were within 0.1 to 0.3 [30]. Graphic Kurtosis values for both feedstock and all nominal sizes ranged between 0.9 to 1.1, and corresponding particles were termed as mesokurtic (Table 3-4) [30]. Mesokurtic is a distribution with the same degree of peakedness[5] about the mean as a normal distribution [44]. Hence, knife mill chopping of wheat straw and corn stover resulted in fine-skewed mesokurtic particles. The same result has been reported for unclassified wheat straw by Bitra [44].

[5] Height and steepness of the frequency function near the mode.

Table 3-4: Theoretical and predicted uniformity index and size guide number, skewness, and graphic kurtosis

Material	Particle Nominal Size	I_u (%)	N_{sg} (mm)	I'_u (%)	N'_{sg} (mm)	S_{ig}	K_g
Wheat Straw	<~3.2 mm	28.06	12.73	29.89	54.31	0.22	0.97
	~3.2 mm	41.08	23.50	42.54	75.53	-0.07	0.97
	~6.4 mm	50.20	36.50	44.36	94.33	0.15	1.06
	~19.2 mm	38.83	59.44	29.78	112.14	0.28	1.09
Corn Stover	<~3.2 mm	26.95	10.09	24.44	47.15	0.30	0.91
	~3.2 mm	32.43	17.82	35.07	65.09	0.11	0.90
	~6.4 mm	32.47	26.89	31.13	81.34	0.08	1.00
	~19.2 mm	22.47	36.50	21.30	93.93	0.21	1.03

3.3.4. Post Pumping Image Processing

In a commercial scale biomass pipeline, a series of boosting stations will be installed at intervals along the pipeline to maintain the internal pressure required for a constant flow of slurry. There exists a particle size reduction or degradation effect[6] corresponding with passing through boosting stations centrifugal pumps impellers, also particle-particle interactions, which means effective particle diameters (e.g., d_{50}) will not remain constant during transportation. The same effect could be studied, not by passing particles through a series of pumps, but through one pump a number of times. For this purpose, 3.2% dry-matter solid mass content slurry of ~19.2 mm wheat straw particles was prepared and pumped for 8 hours. Samples were made at 1-hour intervals, surface dried (by spreading wet wheat straw across two layers of high absorbent paper towel, padding down by additional layer, and gently rolling to remove the moisture), oven dried, image captured, and processed to measure particle dimensions. In Table 3-5, it can be seen that initial particle d_{50} of 8.04 mm was reduced by ~29% to 5.74 mm, with 15% within the first hour. Although the same effect could be expected for the smaller size particles, the intensity would be less severe; as the smaller the size of the particles, the less the probability of shredding would be while interacting with other particles or passing through pump impeller. Similarly Kato [46] reported asbestos fibres of <1μm diameter and a few millimetres in length to degrade about 10% during three hours from the start of circulation, and Radin et al. [5] observed the same variation with time, and allowed the

[6] Also referred to as "Shredding Effect".

suspensions of synthetic and natural fibres to circulate for several hours to allow complete dispersion of solids. Proving the existence of such effect through pipeline, it could be later utilised to explain other phenomena while hydraulically transporting biomass particles.

Table 3-5: Nominal and measured particles dimensions of pumped samples

Material Type and Nominal Size	Pumping Time (hrs)	Median Length (mm)	Geometric Length (mm)	Length (mm)			Width (mm)		
		d_{50}	$X_{gl} \pm \sigma_{gl}$	Min.	Max.	Mean ± S.D.	Min.	Max.	Mean ± S.D.
Wheat Straw ~19.2 mm	0.0	8.04	7.85 ± 1.50	1.70	29.29	8.37 ± 3.41	0.23	4.05	1.38 ± 0.54
	0.5	6.92	6.65 ± 1.57	1.05	24.85	7.16 ± 3.06	0.16	7.07	1.20 ± 0.57
	1.0	6.82	6.59 ± 1.55	1.21	20.48	7.06 ± 2.93	0.21	4.72	1.19 ± 0.54
	2.0	6.47	6.26 ± 1.53	0.97	15.98	6.66 ± 2.66	0.14	3.67	1.14 ± 0.51
	3.0	6.43	6.23 ± 1.51	1.14	23.73	6.64 ± 2.61	0.16	4.06	1.23 ± 0.56
	4.0	6.22	6.01 ± 1.52	1.09	16.49	6.45 ± 2.58	0.15	4.36	1.18 ± 0.55
	6.0	5.94	5.84 ± 1.53	1.20	16.87	6.25 ± 2.54	0.18	4.02	1.16 ± 0.53
	8.0	5.74	5.55 ± 1.48	1.40	14.90	5.88 ± 2.22	0.14	3.09	1.10 ± 0.49

3.4. A Different Methodology to Measure a New Quality

Here the micro-scale features of wheat straw and corn stover particles, i.e., the surface roughness of particles, were of interest as well. Although efforts were made to capture high quality images for image processing purposes, scanner was not the appropriate device to detect micro scale surface features. Consequently a confocal scanning microscope (Axio CSM 700; Zeiss, Oberkochen, Germany) was used to acquire defined optical sections of individual particles, combine these to form a three-dimensional topography, and apply a quantitative image analysis to resulting data. Figure 3-12 shows microscope images of ~850,000 µm^2 of wheat straw and corn stover particles surfaces; latter with noticeably coarser surface condition.

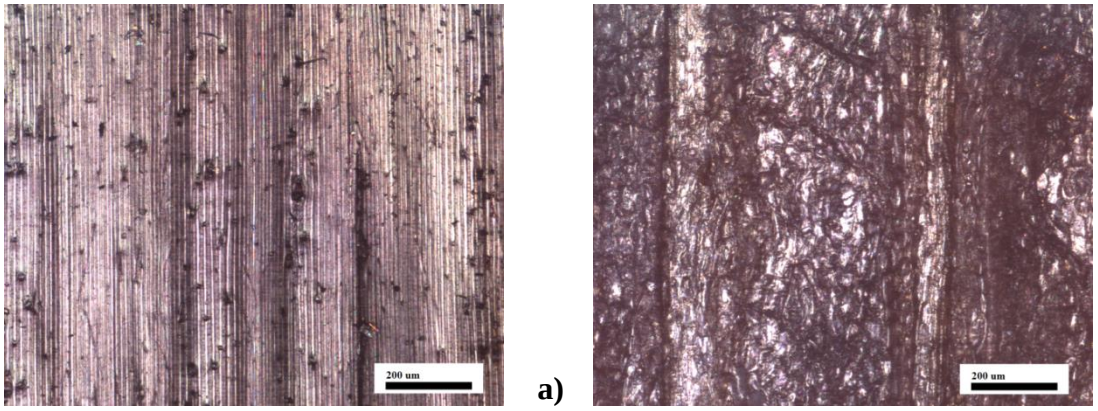

a) **b)**

Fig. 3-12: Confocal scanning microscope images of a) wheat straw b) corn stover particles at 10X magnification

Particles surface roughness parameters, including average roughness (R_a), highest peak (R_p), lowest valley (R_v), maximum peak to valley height (R_t), and kurtosis (R_{ku}) are presented in Table 3-6. These measures of vertical characteristics of the surface may help in better understanding particles surface features. As can be seen in Table 3-6, corn stover particles were more irregular and came with lots of bumps, peaks, and valleys, compared to ribbed wheat straw particles. Data presented in Table 3-6 confirms the above observation, as the absolute value between highest and lowest peaks for corn stover was twice that of wheat straw. Also while a perfectly random surface has a kurtosis value of 3.0 [47], wheat straw particles came with a kurtosis of 9.3, which showed that the wheat straw particles surface was more repetitive and less random in nature , while corn stover particles had a value of 3.3 and a surface with random and sharp peaks. Consequently, considering average roughness values, a corn stover particle surface was almost 7 times rougher than a wheat straw surface.

Table 3-6: Particles surface roughness parameters

Material	Average Roughness (µm)	Highest Peak (µm)	Lowest Valley (µm)	Maximum Peak/Valley Height (µm)	Kurtosis
	R_a	R_p	R_v	R_t	R_{ku}
Wheat Straw	7.9	130.2	149.9	205.1	9.3
Corn Stover	53.1	207.3	250.8	447.4	3.3

3.5. Conclusion

Using ImageJ, a user-coded plugin was developed to process sample images, measure particle dimensions, and analyse PSD of knife-milled wheat straw and corn stover, which were pre-classified into four nominal size groups. Compared to the order of magnitude of samples required for sieving approach, the masses of samples used for image processing were very small. However, it was shown that both the number and the mass of samples used were adequate enough to represent the entire bulk. The particles aspect ratios ranged between 4.51 to 10.08, and 3.71 to 6.71 for wheat straw and corn stover, respectively; confirming the minor importance of a "width parameter" and the fibrous nature of the test materials, which is important in pipelining fibrous materials. The errors involved in nominal sizes brought about noticeable under and overestimations of the real dimensions of the particles. Therefore, the nominal sizes, which were identified with the classifier sieves openings sizes, were not good criteria to judge the real particle dimensions. Reducing the knife mill screen size from 6 mm to 4 mm reduced the output length of the particles by 0% to 21% for wheat straw and 17% to 31% for corn stover. Also of the three distribution functions tested, the Rosin-Rammler equation best fitted the size distribution of the samples, with least SSE in all scenarios. However, when the Rosin-Rammler approach and the size guide number model were compared, for the fibrous materials used here the SGN model was more reliable than the Rosin–Rammler. The particle size reduction (degradation) effect, mainly due to passing through boosting stations centrifugal pumps impellers, was also studied. The d_{50} of 8.04 mm of ~19.2 mm what straw particles reduced by ~29% to 5.74 mm, with 15% within the very first hour after pumping. Finally, while investigating the micro-scale surface features of wheat straw and corn stover particles, corn stover particles were found to be more irregular and came with lots of bumps, peaks, and valleys, compared to ribbed wheat straw particles.

Nomenclature

SSE	sum of squares error
SGN	size guide number
PSD	particle size distribution
Erf	error function
Exp	exponential function
Ln	natural logarithm
A	particles area, mm^2
P	Particles perimeter, mm
M	shape parameter in Gaudin-Schuhmann equation
D_{XX}	corresponding particle lengths in mm at respective *XX* % cumulative number fraction of particles
$P(X > x)$	percentage by number of particles greater than the distinct size *x*
N_i	number of particles of a particular distinct dimension, dimensionless
I_u	uniformity index, %
N_{sg}	size guide number, mm
S_{ig}	graphic skewness, dimensionless
K_g	graphic kurtosis, dimensionless
X_i	distinct length of particle, mm
X_{gl}	geometric mean length, mm
$X_{gl,\ width}$	geometric mean width, mm
X_{ig}	graphic mean length, mm
$X_{ig,\ width}$	graphic mean width, mm
R_a	average roughness or deviation of all points from a plane fit to the test part surface, µm
R_q	root mean square (r.m.s.) roughness, µm
R_p	maximum distance between the mean line and the highest point within the sample surface, µm
R_v	maximum distance between the mean line and the lowest point within the sample, µm
R_t	absolute value between the highest and lowest peaks on the surface, µm
R_{ku}	Kurtosis; a measure of the randomness of heights, and of the sharpness of a surface, dimensionless
x_0	size of the largest particle in the particle size distribution
α	size parameter in Rosin-Rammler equation, mm
β	distribution parameter in Rosin-Rammler equation
σ_{gl}	geometric standard deviation, mm
σ_{ig}	graphic standard deviation, mm

References

[1] Kumar, A., Cameron, J.B., Flynn, P.C. Pipeline transport of biomass. Applied Biochemistry and Biotechnology, 2004; 113: 27-39.

[2] Kumar, A., Flynn, P.C., Cameron, J.B. Large-scale ethanol fermentation through pipeline delivery of biomass. Applied Biochemistry and Biotechnology, 2005; 121: 47-58.

[3] Kumar, A., Flynn, P.C., Cameron, J.B. Pipeline transport and simultaneous saccharification of corn stover. Bioresource Technology, 2005; 96: 819-29.

[4] Bobkowic, A., Gauvin, W.H. Turbulent flow characteristics of model fibre suspensions. Canadian Journal of Chemical Engineering, 1965; 43: 87-91.

[5] Radin, I., Zakin, J.L., Patterson, G.K. Drag reduction in solid-fluid systems. Aiche Journal, 1975; 21: 358-71.

[6] Vaezi, M., Katta, A.K., Kumar, A. Investigation into the mechanisms of pipeline transport of slurries of wheat straw and corn stover to supply a bio-refinery. Biosystems Engineering, 2014; 118: 52-67.

[7] ASABE Standards. Method of determining and expressing particle size of chopped forage materials by screening - ANSI/ASAE S424.1. American Society of Agricultural and Biological Engineers; 2007.

[8] Igathinathane, C., Pordesimo, L.O., Columbus, E.P., Batchelor, W.D., Sokhansanj, S. Sieveless particle size distribution analysis of particulate materials through computer vision. Computers and Electronics in Agriculture, 2009; 66: 147-58.

[9] Womac, A.R., Igathinathane, C., Bitra, P., Miu, P., Yang, T., Sokhansanj, S. Biomass pre-processing size reduction with instrumented mills. ASABE Paper No 076046; 2007.

[10] Shahin, M.A., Symons, S.J., Poysa, V.W. Determining soya bean seed size uniformity with image analysis. Biosystems Engineering, 2006; 94: 191-98.

[11] Li, Z., Hong, T.S., Wu, W.B., Liu, M.J. A novel method of object identification and leaf area calculation in multi-leaf image. ASABE Paper No: 073047, 2007.

[12] Pearson, T.C., Brabec, D.L. Camera attachment for automatic measurement of single-wheat kernel size on a perten SKCS 4100. Applied Engineering in Agriculture, 2006; 22: 927-33.

[13] Igathinathane, C., Pordesimo, L.O., Batchelor, W.D. Ground biomass sieve analysis simulation by image processing and experimental verification of particle size distribution. ASABE Annual International Meeting. Rhode Island Convention Center: ASABE; 2008.

[14] Shahin, M.A., Symons, S.J. Seed sizing from images of non-singulated grain samples CANADIAN BIOSYSTEMS ENGINEERING, 2005; 47: 49-55.

[15] Sun, D.W., Brosnan, T. Inspection and grading of agricultural and food products by computer vision systems - a review. Computers and Electronics in Agriculture, 2002; 36: 193-213.

[16] Kwan, A.K.H., Mora, C.F., Chan, H.C. Particle size distribution analysis of coarse aggregate using digital image processing. Cement and Concrete Research, 1998; 28: 921-32.

[17] Visen, N.S., Paliwal, J., Jayas, D.S., White, N.D.G. Image analysis of bulk grain samples using neural networks. Canadian Agricultural Engineering, 2004; 46: 11-15.

[18] Wang, W., Paliwal, J. Separation and identification of touching kernels and dockage components in digital images. CANADIAN BIOSYSTEMS ENGINEERING, 2006; 48: 1-7.

[19] Igathinathane, C., Prakash, V.S.S., Padma, U., Babu, G.R., Womac, A.R. Interactive computer software development for leaf area measurement. Computers and Electronics in Agriculture, 2006; 51: 1-16.

[20] Rasband, W.S. ImageJ. U.S. National Institutes of Health,; 2008.

[21] Kim, S., Dale, B.E. Global potential bioethanol production from wasted crops and crop residues. Biomass & Bioenergy, 2004; 26: 361-75.

[22] Technical Association of the Pulp and Paper Industry (TAPPI). TAPPI usefull methods NO.21, SCAN CM 40:88 2010.

[23] Shook CA, S.R. Pipeline hydrotransport with application in oilsand industry: SRC publication No. 11508-1E02; 2002.

[24] Rodieck, B. EllipseFitter Class of ImageJ, http://rsb.info.nih.gov/ij/developer/source/ij/process/EllipseFitter.java.html, Accessed September 2011. 2007.

[25] Igathinathane, C., Pordesimo, L.O., Columbus, E.P., Batchelor, W.D., Methuku, S.R. Shape identification and particles size distribution from basic shape parameters using ImageJ. Computers and Electronics in Agriculture, 2008; 63: 168-82.

[26] Igathinathane, C., Melin, S., Sokhansanj, S., Bi, X., Lim, C.J., Pordesimo, L.O., et al. Machine vision based particle size and size distribution determination of airborne dust particles of wood and bark pellets. Powder Technology, 2009; 196: 202-12.

[27] European Blenders Association (EBA). Handbook of Solid Fertilizer Blending, Code of Good Practices for Quality. Le Pontoury, Montviron, France: European Blenders Association 1997.

[28] Allaire, S.E., Parent, L.E. Size guide number and Rosin-Rammler approaches to describe particle size distribution of granular organic-based fertilisers. Biosystems Engineering, 2003; 86: 503-09.

[29] Folk, R.L., Ward, W.C. Brazos River bar: a study in the significance of grain size parameters Journal of sedimentary petrology, 1957; 27: 3-26.

[30] Folk, R.L. Petrology of sedimentary rocks. Austin, Texas: Hemphill Publishing Co; 1974.

[31] Blott, S.J., Pye, K. GRADISTAT: A grain size distribution and statistics package for the analysis of unconsolidated sediments. Earth Surface Processes and Landforms, 2001; 26: 1237-48.

[32] Duffy GG, M.K., Titchener AL. The determination of pipe friction loss. Journal of the Australian and New Zealand pulp and paper industry technical association, 1972; 6: 191-95.

[33] Viamajala, S., McMillan, J.D., Schell, D.J., Elander, R.T. Rheology of corn stover slurries at high solids concentrations - Effects of saccharification and particle size. Bioresource Technology, 2009; 100: 925-34.

[34] I, K. Behaviour of extremely coarse particles in pipe flow. Hydrotransport 4. Banff, Alberta, Canada; 1976.

[35] Perfect, E., Xu, Q., Terry, D.L. Improved parameterization of fertilizer particle size distribution. Journal of Aoac International, 1998; 81: 935-42.

[36] Hwang, S.H., Lee, K.P., Lee, D.S., Powers, S.E. Models for estimating soil particle-size distribution. Soil Science Society of America Journal, 2002; 66: 1143-50.

[37] Rosin, P., Rammler, E. The laws governing the fineness of powdered coal. Journal of the Institute of Fuel, 1933; 7: 26-39.

[38] Gupta, A., Yan, D. Mineral processing design and operation: An introduction. Amsterdam, Netherlans: Elsevier 2006.

[39] Epstein, B. Logarithmico-Normal Distribution in Breakage of Solids. Industrial and Engineering Chemistry, 1948; 40: 2289-91.

[40] Gaudin, A.M., Meloy, T.P. Model and a Comminution Distribution Equation for Single Fracture. Transactions of the Society of Mining Engineers of Aime, 1962; 223: 40-43.

[41] British Standards Institution. Testing aggregates part 103: Methods for determination of particle size distribution, Sec. 103.1: Sieve tests 1985.

[42] Vaseleski, R.C., Metzner, B. Drag reduction in the turbulent flow of fiber suspensions. AlChE, 1974; 20: 301-08.

[43] Lee, P.F.W., Duffy, G.G. Relationships between Velocity Profiles and Drag Reduction in Turbulent Fiber Suspension Flow. Aiche Journal, 1976; 22: 750-53.

[44] Bitra, V.S.P., Womaca, A.R., Yang, Y.T., Miu, P.I., Igathinathane, C., Chevanan, N., et al. Characterization of wheat straw particle size distributions as affected by knife mill operating factors. biomass and bioenergy, 2011; 35: 3674-87.

[45] Flügel, E. Microfacies of Carbonate Rocks: Analysis, Interpretation and Application: Springer; 2004.

[46] Kato, H., Mizunuma, H. Frictional resistance in fiber suspensions (part 1): pipe-flow. Bulletin of the Jsme-Japan Society of Mechanical Engineers, 1983; 26: 231-38.

[47] Al-Kindi, G.A., Shirinzadeh, B. An evaluation of surface roughness parameters measurement using vision-based data. International Journal of Machine Tools & Manufacture, 2007; 47: 697-708.

CHAPTER 4

Investigation into the Mechanisms of Pipeline Transport of Slurries of Wheat Straw and Corn Stover to Supply a Biorefinery[1]

4.1. Introduction

Kumar et al. [1-3] studied various scenarios of pipelining biomass materials and compared the costs of pipeline transport vs. truck delivery. While preliminary economic assessments of biomass pipeline hydro-transport have been carried out via experimental study on wood chip-water mixture (slurry) pipelines, its technical and chemical feasibility has not been studied in detail. Moreover, the pressure drop (frictional loss) correlations that were used to obtain the cost estimates of pipeline hydro-transport of corn stover were originally proposed for pipeline transport of wood chip-water mixtures [4, 5]. Corn stover and wood chips, however, have very different shapes; the former is fibrous in nature with a wide aspect ratio that can give rise to a variety of mechanisms, including drag reduction, during slurry flow [6] that are often not encountered in conventional solid-liquid systems.

Although several hypotheses have been proposed to explain certain aspects of the observed phenomena in slurry flows of woody particles, more complete expressions of the functional relationships between the many variables governing the hydro-transport of woody materials in pipelines have been proposed based upon purely empirical correlations. Luk [7] experimentally studied pipeline hydro-transport of wheat straw particles by measuring longitudinal pressure gradients. The experiment was focused on wheat straw particles and did not include particle characteristics, the rheology of the carrier liquid, or the mechanisms corresponding to drag reduction throughout the pipeline.

[1] Vaezi, M., Katta, A.K., Kumar, A., ***Biosystems Engineering***, 2014; 118: 52-67.

The present research attempts to experimentally investigate pipelining slurries of two types of fibrous agricultural residue biomass, wheat straw and corn stover, and to study the technical limitations, potential advantages, and governing equations. The objectives of the research were to:

- study the technical feasibility of pipelining agricultural residue biomass (corn stover and wheat straw), identify potential difficulties in handling agricultural residue biomass slurry, and propose a standard operating procedure for pipelining irregularly-shaped agricultural residue biomass particles;
- critically examine the applicability of wood chip-water mixtures pressure drop correlations in order to calculate friction losses while hydro-transporting wheat straw and corn stover particles;
- study mechanical behaviour, specifically the change in the pressure drop of agricultural residue biomass (corn stover and wheat straw) slurry for various particles sizes, slurry solid mass contents, and slurry flow rates, and try to obtain optimum operating conditions.

4.2. Methodology

4.2.1. Feedstock Properties and Preparation

The research specifically focused on transporting corn stover (*Zea mays*; leaves and stalks of maize) and wheat straw (*Triticum sativum*; dry stalks of wheat) agricultural residue biomass by pipeline. Corn stover and wheat straw were collected from farms in southern and northern Alberta, Canada. The dry feedstock was firstly milled using a commercially available cutting mill (SM-100; Retsch Inc., Newtown, PA, USA), then classified using a standard [8, 9] chip classifier (BM&M Inc., Surrey, BC, Canada) into four major groups with nominal sizes (i.e., the size of the openings of the classifier sieves) of 19.2 mm, 6.4 mm, 3.2 mm, and <3.2 mm.

The wet-basis moisture content (water mass content - MC) of the samples was measured according to ASABE S358.2 standard [10], wherein a sample of at least 25 g was oven-dried at 103°C for 24 h. Particle density was evaluated according to ASTM standards

[11] by loosely filling a cylinder 150 mm in diameter and 150 mm in height and weighing it in air and water. The difference in weight represented the buoyant force against the material. Consequently, an initial moisture content of 6 ± 0.5% and preliminary particle specific gravities of 1.1 ± 0.01 for wheat straw and 1.2 ± 0.01 for corn stover were calculated for the corn stover and wheat straw samples. The same approach was later followed to monitor the variation in particle moisture content during hydro-transport.

4.2.2. Image Processing and Morphological Studies

Unusual characteristics (e.g., relatively large mean particle size; wide size distribution; extreme shapes; fibrous, pliable, flexible, and asymmetric nature; potential for forming networks) can make agricultural residue biomass particles atypical [12]. While wood pulp fibres (which as largely hydro-transported through pipes over short distances for on-site processing applications) are typically 1-5 mm in length and 15-40 µm width [6, 13-15], the particles studied here come with noticeably larger dimensions that can be visually recognized and classified, a feature that makes transporting agricultural residue biomass by pipeline different from pulp processing.

Understanding particle morphological features is the first step in the study of agricultural residue biomass slurry behaviour, as they influence the deposition velocity, carrier liquid viscosity, slurry apparent viscosity, and slurry friction loss. Using a digital image processing approach and the ImageJ platform [16], a user-coded plugin was developed at the University of Alberta in the Large-Scale Fluids Laboratory to process particle sample images, measure particle dimensions, and analyse particle shape and size distribution (PSD) as well as corresponding parameters of knife-milled pre-classified wheat straw and corn stover [17]. Dimensions of significance based on length, including median length (d_{50}), geometric mean length (X_{gl}) and width (X_{gw}) and corresponding standard deviations (σ_{gl} and σ_{gw}) [18], together with arithmetic mean length and width, are presented in Table 4-1. The results obtained here were later used to justify the behaviour of biomass slurry and corresponding variations.

Table 4-1: Nominal and measured particles dimensions of wheat straw and corn stover samples

Material Type	Nominal Particle Size (mm)	Median Length (mm)	Geometric Length (mm)	Geometric Width (mm)	Length (mm) [c]			Width (mm) [c]			Aspect Ratio
	X_n	d_{50}	X_{gl} [a] ± σ_{gl} [b]	X_{gw} ± σ_{gw}	Min.	Max.	Mean ± S.D.	Min.	Max.	Mean ± S.D.	
Wheat Straw	19.2	8.29	8.42 ± 1.49	1.34 ± 1.54	1.69	27.49	8.92 ± 3.61	0.18	4.31	1.43 ± 0.58	6.28
	6.4	5.00	4.79 ± 1.57	1.07 ± 1.56	0.95	12.79	5.15 ± 2.09	0.19	3.62	1.16 ± 0.51	4.47
	3.2	3.92	3.96 ± 1.41	1.12 ± 1.51	0.98	7.87	4.13 ± 1.34	0.22	3.02	1.19 ± 0.46	3.53
	<3.2	2.42	2.57 ± 1.43	0.74 ± 1.46	0.97	6.94	2.70 ± 0.99	0.18	3.22	0.78 ± 0.30	3.47
Corn Stover	19.2	7.58	7.83 ± 1.46	1.32 ± 1.72	1.86	24.08	8.40 ± 3.30	0.23	4.25	1.48 ± 0.82	5.93
	6.4	4.72	4.66 ± 1.51	1.14 ± 1.70	1.12	12.30	4.98 ± 1.95	0.14	3.67	1.27 ± 0.66	4.08
	3.2	3.32	3.49 ± 1.45	1.21 ± 1.61	1.12	8.53	3.69 ± 1.40	0.24	3.13	1.32 ± 0.56	2.88
	<3.2	1.90	2.11 ± 1.44	0.73 ± 1.42	0.94	6.04	2.22 ± 0.88	0.20	1.68	0.76 ± 0.26	2.89

[a] $\left[X_{gl} = Ln^{-1}[\frac{\sum(N_i \times \ln X_i)}{\sum N_i}]\right]$ [b] $\left[\sigma_{gl} = Ln^{-1}[\frac{\sum(N_i(\ln X_i - \ln X_{gl}))^2}{\sum N_i}]^{\frac{1}{2}}\right]$ [c] Based on samples of 400 to 2000 particles

4.2.3. Experiment Apparatus

A schematic of an experimental pipeline facility is illustrated in Fig. 4-1. The test circuit consisted of 25.5 m of 50 mm diameter Schedule 40 steel pipe with clear acrylic sections for visual observation. The circuit included long radius bends, short radius bends (the latter to ascertain if such standard fittings could be used successfully), and one vertical section. Considering the S, D_{pipe}, R_{pipe}, and R_C to be the distance along the straight pipe section, pipe internal diameter, pipe internal radius, and radius of the curvature of the U-bend section, respectively, the frictional losses were measured along a 7.5 m long test section that was placed 10 m (i.e., 200 times the diameter of the pipeline) downstream of the pump to achieve fully developed turbulent pipe flow and 1.75 m (i.e., 35 times the diameter of the pipeline or $S/D_{pipe} \approx 35$) downstream of the U-bend section (with a curvature, $R_{pipe}/R_C \approx 0.07$) to ensure flow field recovery. Magnitudes of $S/D_{pipe}>18$ [19], $S/D_{pipe}>20$ [20], and $S/D_{pipe}>29$ [21] have been the distances reported to take the viscous dissipation to destroy the extra turbulent energy caused by the curvature of the bend.

A 0.8 m diameter and 455 L capacity mixing tank was agitated by a 0.37 kW centrally placed vertical mixer (EV6P50M; Lightning Inc., Rochester, NY, USA) carrying a motor-boat propeller whose rotation caused the mixture to flow down in the centre of the tank and rise at its periphery, where the centrifugal motion of the suction vortex caused the particles to accumulate. Flow was provided by a 7.45 kW centrifugal slurry pump (CD80M; Godwin Pumps Ltd., Bridgeport, NJ, USA) rated at 10.7 L/s against ~157 kPa at 1765 rpm and ~43% efficiency for clear water, coupled to a 7.45 kW induction electric motor (CC 068A; Madison Industrial Equipment, Vancouver, BC, Canada) and controlled by a 14.91 kW variable frequency drive (VFD) controller (MA7200-2020-N1, TECO-Westinghouse Co., Round Rock, TX, US). Downstream from the pump, a double-tube heat exchanger was installed to partially control the mixture temperature at ~ 15°C. A watt transducer (PC5; Flex-Core, Columbus, OH, USA), an electromagnetic flow meter (FMG-401H; Omega Eng., Stamford, CT, USA) with accuracy of ±0.5% of rate at 1.0 to 10 m/s, and a resistance temperature detector (RTD-E; Omega Eng., Stamford, CT, USA) measured the power consumption of the motor, the mixture bulk velocity, rate of fluid flow, and mixture temperature. The conductivity of fully-saturated agricultural residue biomass particles was measured as well to confirm the applicability of magnetic flow meter to measure the solid particles flow rate. Two 25 mm flush diaphragm low-pressure transmitters (PX42G7; Omega Eng., Stamford, CT, USA) with accuracy of 0.25% of linearity, hysteresis and repeatability combined, measured gauge pressures upstream and downstream of the test section.

Finally, 4-20 mA output signals from the watt transducer, temperature probe, magnetic flow meter, and pressure transmitters were recorded with a frequency of 100 Hz on a data-acquisition system, comprising of a 4-channel current excitation module (NI 9219; National Instrument Corp., Austin, TX, USA) and a data-acquisition program (LabView V.9.0.1f2; National Instrument Corp., Austin, TX, USA).

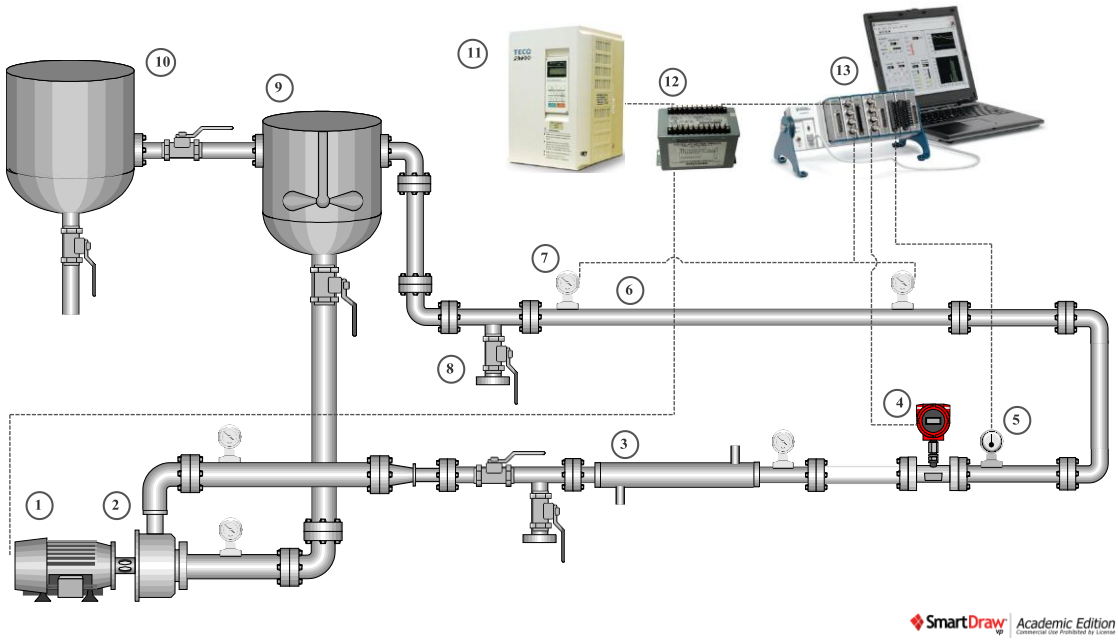

Fig. 4-1: Schematic diagram of experimental set-up consisting of (1) electric motor, (2) centrifugal pump, (3) heat exchanger, (4) magnetic flow meter, (5) temperature sensor, (6) test section, (7) pressure transducer, (8) sampler-discharger, (9) mixing tank, (10) water supply tank, (11) variable frequency drive controller, (12) watt transducer, (13) data logger/analyser

4.2.4. Carrier Liquid Viscosity Measurements

Because the density and viscosity of the carrier liquid (water) is changed by the presence of fine particles, Gillies and Shook [22] suggested that the density and viscosity of the ″fine particles + fluid fraction″ should be measured and taken into account as non-settling homogeneous slurry. The fines fraction was later arbitrarily defined as the fraction of particles of diameters below 40 µm [23], 74 µm [22], and 50 µm [24, 25]. Newitt and Richardson [26] also classified particles of less than 40 to 70 µm to be transported as a homogeneous suspension and continuous media. In the present research, suspension fluid was filtered using 50 µm aluminium woven wire cloth to obtain the fines + fluid fraction, while the remaining particles were too large to contribute to the carrier liquid's rheology. Density was calculated by using the mass of 25 ml filtered liquid phase and its volume. Viscosity was subsequently measured using a rotational viscometer (AR 2000; TA Instrument, New Castle, DE, USA) with a concentric cylinder geometry over a wide

range of shear rates and fluid temperatures (Fig. 4-2). However, this approach is limited to measuring the viscosity of the carrier liquid. The apparent viscosity of the suspension (solid+liquid phase), to be measured experimentally, requires parallel plates geometry which was not available by the time of conducting the experiment. The suspension viscosity was calculated theoretically. The corresponding methodology will be accordingly described in section 4.3.5.1.

a)

b)

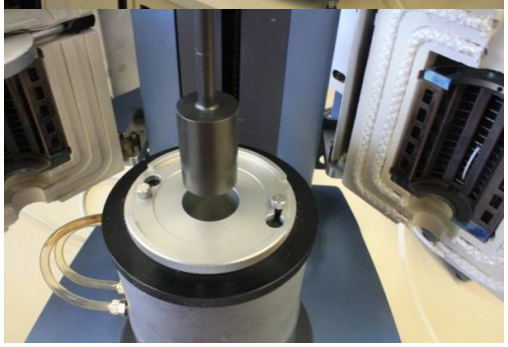

c)

Fig. 4-2: a) Filtering the pumped agricultural residue biomass slurry to separate fine particles (<50 μm) + fluid, b) Rotational viscometer, c) Concentric cylinder geometry chosen for the experiment

4.2.5. Calibration of the Experimental Set-up

Calibration was conducted by blank runs with clear water through the closed-circuit pipeline, in order to validate the experimental measuring techniques and data acquisition system. The plot of the friction factor, *f*, versus the water Reynolds number, Re_f, is presented in Fig. 4-3(a). In this plot friction factor measurements for clear water in this study at 20°C are compared with corresponding values obtained by using Colebrook [27], Churchill [28], Moody [29], and Wood [30] correlations. Friction factor measurements agreed well with the established correlations, except at the lowest flow rates (≤ 1.5 m/s),

where accurate pressure differential measurements were difficult to obtain precisely due to instrument and control limitations. Kazi, Duffy, and Chen [31] reported similar problem.

4.2.6. Slurry Preparation and Friction Loss Measurement

After clear water was circulated for a few minutes to allow for deaereation, pre-measured amounts of feedstock were gradually added to the mixing tank to reach the maximum dry-matter solid mass content achievable for a certain size of material, consisting of 8.8, 7.6, 6.5, and 5.4% achievable for <3.2 mm, 3.2 mm, 6.4 mm, and 19.2 mm, respectively (for example, 5.4% is the maximum slurry solid mass content achievable while hydro-transporting 19.2 mm particles through pipeline). The limited availability of head and relatively large particles were limiting factors towards achieving higher solid mass contents; the latter could increase the possibility of blockage. After achieving a stable slurry, frictional losses corresponding to a range of velocities from 0.5 m/s (minimum measurable value) to 5.0 m/s (maximum achievable value) and solid mass contents from 8.8 to 1.0%, equivalent to 14.7 to 1.8% fully-saturated solid volume content (by diluting the slurry in increments of 1.0%) were measured.

While transporting wood chips by pipeline, Elliott and Montmorency [32] reported an increase in moisture content from 31% to 55% within few minutes and to 70% after several hours. For the current experiment, sampling a 3.2% mixture of 19.2 mm wheat straw particles at 30 min intervals, and following the ASABE S358.2 standard [10] to measure the moisture content, it was shown that this type and size of feedstock can attain more than 95% of its saturation moisture content of ~79% within half an hour, when pumped at about 3.3 m/s velocity and 15 kPa pressure (as shown in Fig. 4-3(b)). Similar results were found for various particle sizes of wheat straw and corn stover. Thus, a general saturation moisture content of 82% and corresponding specific gravity of 1.05 was applied to the entire experiment. Therefore, a relatively dry wheat straw or corn stover particle in a pressurised pipeline system would (through horizontal sections) initially travel at the top of the pipe but would gradually sink towards the bottom.

Accordingly, it was decided to conduct all the experiments with particles fully saturated and with a density slightly greater than the carrier liquid, water.

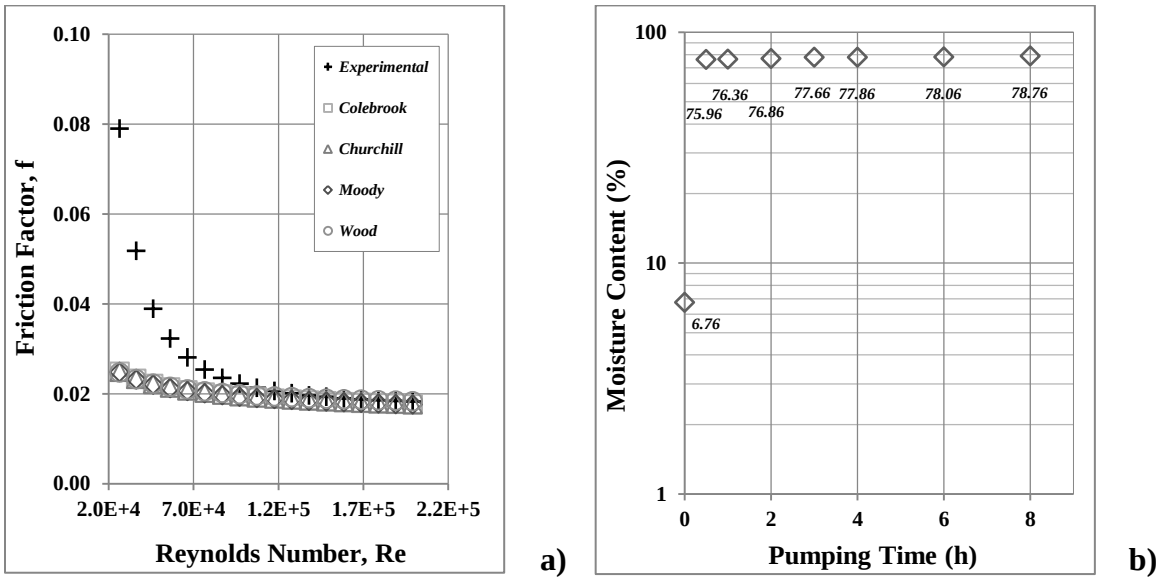

Fig. 4-3: a) Friction factor vs. Reynolds number for clear water through the experimental set-up, b) Moisture content variation of 19.2 mm wheat straw particles in a mixture of 3.2% solid mass content pumped at 3.3 m/s and 15 kPa pressure through the experimental set-up

4.2.7. Uncertainty Analysis

Two sets of experiments were conducted on each particle type (wheat straw and corn stover) and four particle sizes (Table 4-1) to assure repeatability and to investigate the uncertainty of the results. Uncertainty was measured according to the standard uncertainty analysis approach by calculating the precision uncertainty (P_x) of the pressure measurements and the bias uncertainty of the pressure transducers, which eventually give the total uncertainty (U_x). Figure 4-4(a) represents the repeatability of experiments on a 4.3% solid mass content slurry of <3.2 mm corn stover and a 6.5% solid mass content slurry of 6.4 mm wheat straw particles. A good agreement between corresponding tests was observed, with an uncertainty of ±0.015 kPa/m and ±0.068 kPa/m for corn stover and wheat straw experiments, respectively. Generally, a minimum uncertainty of 0.5% and maximum of 10% was obtained through the course of these experiments.

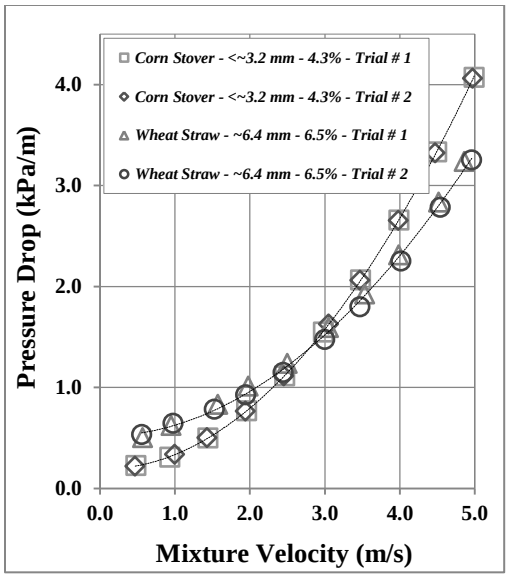

a)

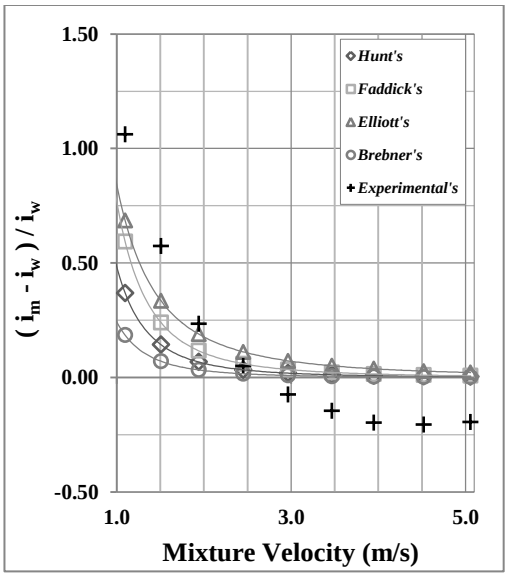

b)

Fig. 4-4: a) The repeatability of two sets of experiments on wheat straw and corn stover slurries based on experimental measurement using the experimental set-up, b) Friction loss parameter vs. mixture velocity for 6.5% mixture of 6.4 mm corn stover particles based on measurement using the experimental set-up

4.3. Experimental Results and Discussion

4.3.1. Investigating the Applicability of Wood Chip Friction Loss Correlations for Agricultural Residue Biomass Particles

Earlier studies investigated the transport of wood chips by pipeline through horizontal sections and proposed correlations to predict friction loss values through pipelines 75 to 300 mm in diameter. Later, Kumar et al. [2, 3] used the friction loss equation by Hunt [4] originally proposed for wood chips while investigating the feasibility of pipelining corn stover for large-scale ethanol fermentation. Figure 4-4(b) compares friction loss values obtained via wood chip correlations provided by Brebner [33], Elliot and Montmorency [32], Faddick [34], and Hunt [4] with those obtained experimentally in the present research for a 6.5% slurry of 6.4 mm corn stover particles through a 50 mm diameter pipeline. While the correlations estimated friction loss values above those of clear water, the corn stover slurry friction loss exhibited a unique trend and dropped below that of water (water corresponds to $(i_m\text{-}i_w)/i_w = 0.0$, where i_m is hydraulic gradient of the mixture and i_w is hydraulic gradient of the clear water), although it appeared to be the case above

a specific velocity. Moreover, correlations studied here were found to be not capable of predicting wood chips friction loss behaviour at velocities below 1.0 m/s. Thus, the pressure drop correlations proposed for a wood chip slurry are not appropriate for agricultural residue biomass slurries.

4.3.2. Fibre Suspension Flow Regimes

The distribution of particles over the cross section of a horizontal pipe is often described in terms of flow regimes. In terms of flow features, slurries can be classified as either a non-settling slurry (in which case the solid phase shows little or no tendency to settle under conditions of no-flow and can often be treated as a single-phase system) or classified as settling slurry. Durand and Condolios [23] used a different approach to classify solid-liquid mixtures in horizontal pipes. This classification was later refined by Newitt and Richardson [26] and others to show four flow regimes: (1) flow with a stationary bed or flow with a moving bed and saltation (with or without suspension; transferred by continuous or sporadic inter-granular contacts), (2) a heterogeneous mixture with some particles present in the form of a bed and others supported by fluid turbulence, (3) pseudo-homogeneous at very high flow rates where solids may approach an even distribution, and (4) homogeneous mixtures with all the solids in suspension (particles between 40 to 70 μm are transported by the fluid), a characteristic typical of non-settling slurries [35].

Considering the minimum particle diameter (d_{50} = 1.9 mm, see Table 4-1), flow rates range, and visual observations, the flow regime in the present experiment can be classified as being a settling heterogeneous slurry through the entire range of particle sizes and pumping velocities, where a gradient of solid mass contents exists in the vertical plane. Therefore, the solid and liquid phases remain identifiable; there is no increase in the viscosity of the liquid phase on account of its association with the solid particles. This was experimentally observed here using viscometry wherein carrier liquids of 19.2 mm, 6.4 mm, and 3.2 mm particle suspensions were filtered to contain particles < 50 μm only (as described on section 2.4). As an example, Fig. 4-5(a) represents the viscosity of the filtered carrier liquid corresponding to 2.0 to 7.6% suspensions of 3.2 mm

wheat straw particles. As observed, the carrier liquids represent the feature of Newtonian fluids with viscosities equal to the viscosity of clear water. In addition, although the fluids might look like a Bingham fluid, a minimum yield stress of 0.01 Pa is required for a fluid to be considered as Bingham [36], a requirement which is not met here. However, it is worth mentioning that if the solid mass content of particles is increased (beyond 8.8% for most slurries), the mixture is expected to become more viscous and develop non-Newtonian properties [36].

A heterogeneous/homogeneous (or heterogeneous/pseudo-homogeneous) flow regime is a complex compound regime in which the fine particles move as a homogeneous mixture while the remaining coarse particles move as a heterogeneous mixture [36]. In these flows, the carrier liquid can no longer be regarded as clear water, and calculations should be adjusted based on the assumption that the remaining solids (i.e., those conveyed in the heterogeneous flow) are supported by the new carrier liquid, the density and viscosity of which have to be determined [37]. For the case of the <3.2 mm particle suspensions here, however, the fraction of fine particles (< 50 μm) was reasonably small so that fine particles increased the viscosity of the carrier liquid but did not cause it to become non-Newtonian. This can be observed on Fig. 4-5(b), where the viscosity increases proportionally with increasing mixture solid mass content, while the carrier liquid retains its original Newtonian features. It is worth mentioning that, since the agricultural residue biomass practiced here were cut/baled by machines and stored long in the farm before being transferred into the lab, there were dirt and soil coming with biomass as well, which would constitute a portion of fine particles.

The modified carrier liquid density and viscosity were accordingly used to calculate the mixture density and the Reynolds number. As it will be seen in the next sections, the increased buoyancy of the solid phase, due to the increased density of the liquid phase assisted in reducing the pipeline pressure drop.

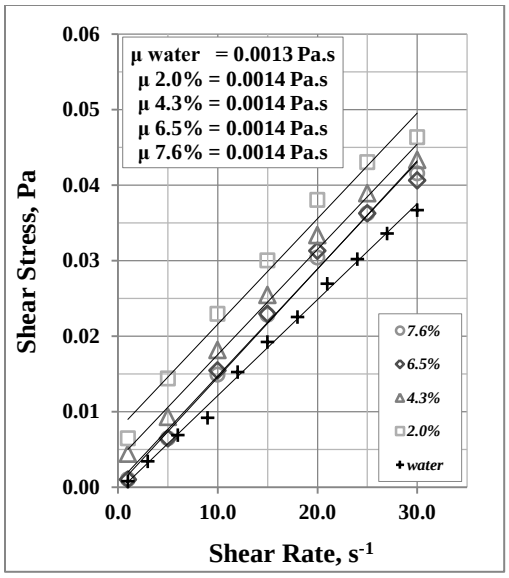

a)

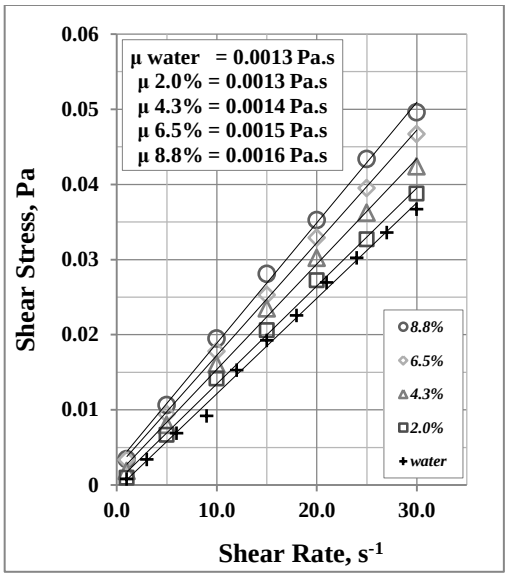

b)

Fig. 4-5: a) Viscosity of the filtered carrier liquid of 2.0 to 7.6% suspensions of 3.2 mm wheat straw particles at 15°C, b) Viscosity of the filtered carrier liquid of 2.2 to 8.8% suspensions of <3.2 mm wheat straw particles at 15°C, based on the experimental measurement using the experimental set-up

4.3.3. Drag-reducing Characteristics

A reduced pumping requirement is a direct benefit of the drag-reducing ability of fibre suspensions. Understanding feedstock specifications and operating conditions, where such an advantage can be achieved, helps select and improve the design procedure of the feedstock, pump size, material-preparing equipment, pipeline facility, and operating conditions. To better understand this purpose, drag reduction in wood pulp fibre suspensions is briefly reviewed before drag reduction in slurries of agricultural residue biomass and the corresponding similarities and/or differences are analysed.

4.3.3.1. Drag Reduction in Wood Pulp Fibre Suspension Flows

Typical flow resistance data obtained for wood pulp fibre suspensions are presented on Fig. 4-6 as plots of logarithms of friction loss, $\Delta P/L$ (Fig. 4-6(a)), and pressure drop friction factor, ø (as a function of longitudinal friction loss ($\Delta P/L$), carrier liquid or mixture density ($\rho_{f\,or\,m}$), mixture velocity (V_m), and pipe internal diameter (D_{pipe}) – see Eq. 1) - (Fig. 4-6(b)) versus logarithms of mixture velocity. Because of the near-wall effects

in the flow of fibre suspensions [38], three regimes of flow take place with increasing velocity: plug flow, transition flow, and turbulent flow, respectively. These flow regimes form the unique S-shaped friction loss curve (see Fig. 4-6(a)) and can be explained by the formation and breakage of fibre structures.

$$\Phi = \frac{\Delta P}{L} \frac{2D_{pipe}}{\rho_{fluid\ or\ mixture} V_m^2} \tag{1}$$

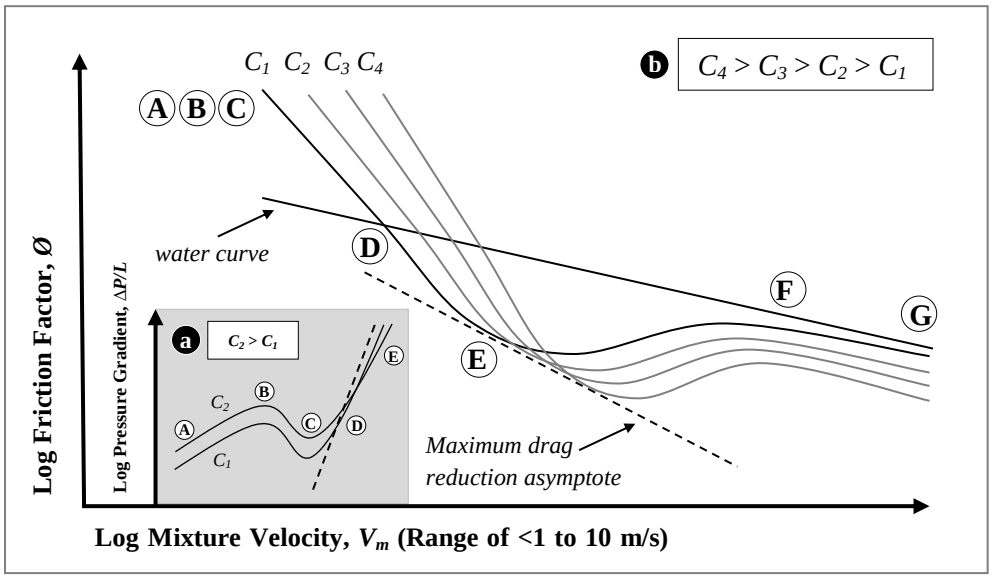

Fig. 4-6: Typical friction - velocity curve for fibre suspensions in pipes, adopted from Duffy and Lee [6] and Moller [39], a) logarithm of friction loss versus logarithm of mixture velocity, b) logarithm of friction factor versus logarithm of mixture velocity

The three flow regimes, together with the corresponding changes in flow specifications, can be observed with increasing velocity from A to G marked on Fig. 4-6, as follows: flow of fibre suspension as a central unsheared or plug flow up to a point well beyond the minimum (from A to D) [40, 41]; some interaction between the plug and the pipe wall prior to the maximum (at B); flow without any plug-wall interaction (from B to D) with a progressive increase in the size of the annulus and a decrease in friction loss (from B to C); a change in the nature of the annulus from laminar to turbulent (about C) [39] and rapid growth in annulus thickness (from C to D) [42]; a change in flow regime from plug flow to transition flow and dropping friction loss further below the water alone (beyond

D); reaching the maximum value of drag reduction in transition flow regime (at E); developing a region of approximately constant friction factor (from E to F); and eventually attaining a fully turbulent flow over the whole diameter [13, 15, 39, 43] (from F to G).

4.3.3.2. Drag Reduction in Agricultural Residue Biomass Particles Slurry Flow

Representing drag-reducing characteristics reported in the literature is limited to natural and synthetic fibres of several μm to 5.0 mm in length and aspect ratios of 25 to several hundred. Duffy and Lee [6] and Radin et al. [44] stated the drag reduction to be achievable only with fibrous additives with aspect ratios > ~ 30. The results obtained through the present research, however, not only questioned the above general understanding but also set new boundaries for the type and size of the materials that can be used to achieve pressure drops below that of the carrier liquid alone. In this work, uncommon fibrous agricultural residue biomass particles with noticeably large dimensions of 2.0 to 9.0 mm in length and considerably small aspect ratios of 2 to 7 (see Table 4-1) exhibited drag-reducing behaviour.

While Fig. 4-7(a) represents the pressure drop per unit length of 50 mm diameter horizontal pipeline in the experimental set-up over a velocity range of 0.5 to 5.0 m/s, Fig. 4-7(b) illustrates corresponding friction factors (see Eq. 1) versus the generalised Reynolds number over the drag reduction region only. The generalised Reynolds number (see Eq. 3) was calculated based upon the mixture density (ρ_m as a function of slurry solid volume content (C_v), solid particle density (ρ_s), and carrier liquid density (ρ_f) - see Eq. 2), carrier liquid viscosity (μ_f), mixture velocity (V_m), and pipe internal diameter (D_{pipe}) as discussed in the previous section.

$$\rho_m = C_v \rho_s + (1 - C_v)\rho_f \tag{2}$$

$$\mathrm{Re}_g = \frac{\rho_m V_m D_{pipe}}{\mu_f} \tag{3}$$

The flow mechanism of agricultural residue biomass slurry (presented in Figs. 4-6 and 4-7) appeared to be predominantly similar to that for a chemical wood pulp slurry. In a chemical wood pulp slurry, various flow regimes, including an unsheared plug flow with a turbulent annulus (from C to D), transition flow (from D to E), and a fully turbulent flow with a nearly constant friction factor (Beyond E), were detected for various solid mass content slurries of wheat straw and corn stover particles of diverse dimensions (labels adopted from Fig. 4-6). The only difference observed between the two slurries was the absence of the points corresponding to the maximum and minimum friction losses at low velocities (points B and C). The same phenomenon was reported for the ground wood pulps (also neutral sulphite semi chemical pulp) [42], where the friction loss curve first rose sharply (plug flow with rolling friction – at extremely low velocities – not observed here), then levelled off (undisturbed plug structure surrounded by a sheared annulus with individual fibres and fibre fragments moving at a lower velocity than the plug, which accordingly increased the effective viscosity of the annulus fluid) until near the point where it crossed the clear water curve (onset of drag reduction and transition regime). Understanding the similarity of the slurry of agricultural residue biomass particles to that of the synthetic and natural fibres is major achievement, since the governing rules and developed correlations for such fibres, e.g., ground wood and chemical pulp suspensions, could be well adopted for the purpose of the present research on pipelining agricultural residue biomass.

To better represent the changes in the drag reduction potential of biomass slurry, the drag ratio (the pressure drop of the fibre suspension divided by the pressure drop of the carrier liquid at the same pumping velocity) vs. the mixture velocity is presented on Fig. 4-8 for various wheat straw particle dimensions and mixture solid mass contents. The transition flow regime (from D to E), the maximum drag reduction asymptote (at E), and fully turbulent flow regime (from E to F where drag reduction reduces in magnitude because of a simultaneous decrease of the carrier liquid pressure drop) can be clearly recognized on all the graphs and are correspondingly labelled on Fig. 4-8(a).

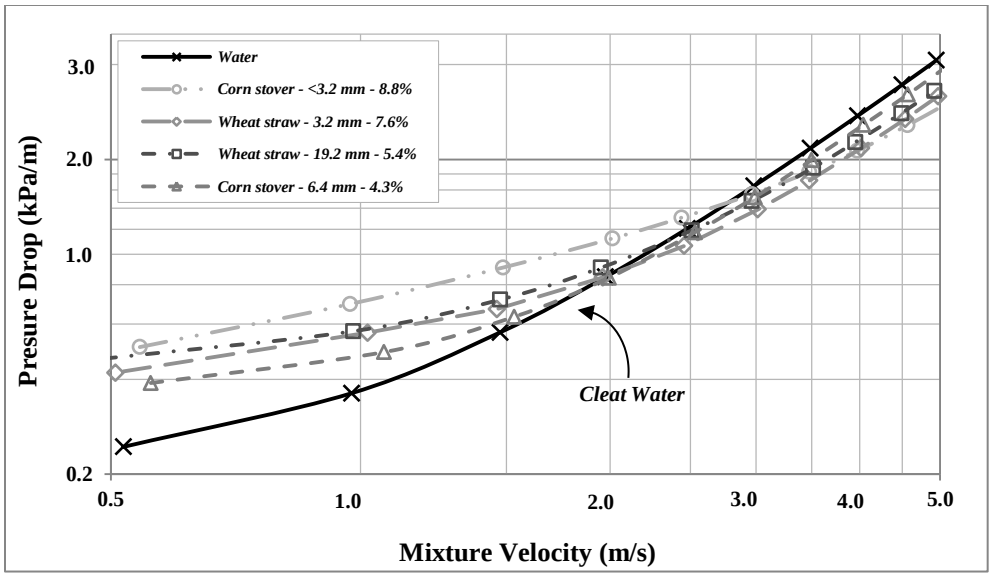

(a)

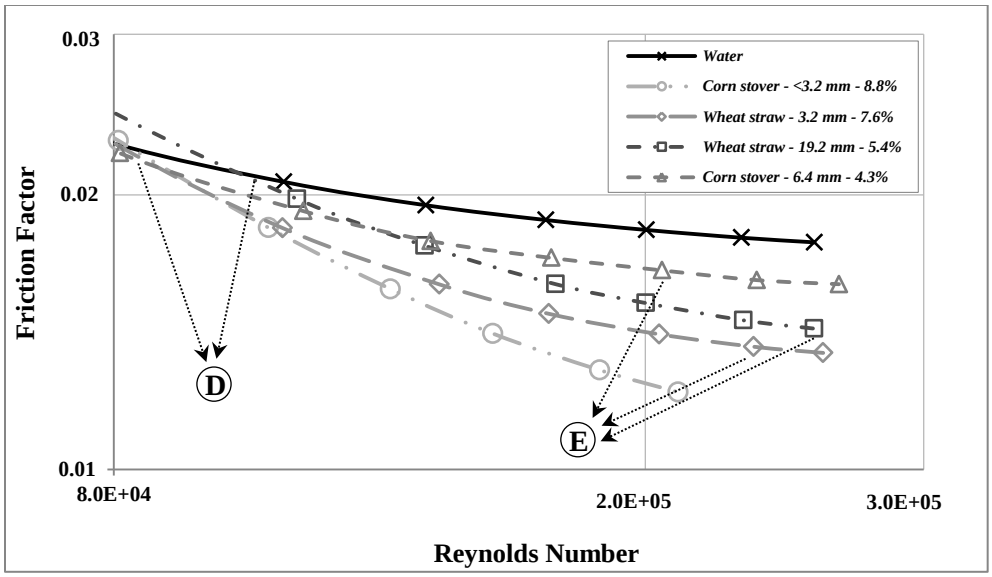

(b)

Fig. 4-7: a) Pressure drop vs. mixture velocity over the entire velocity range, b) friction factor vs. generalised Reynolds number for velocities above 2.0 m/s, for various slurries of wheat straw and corn stover particles measured using the experimental set-up (the points D and E on Fig. 4-7(b) adopted from Fig. 4-6)

For a given particle size, an increase in slurry solid mass content increased the maximum drag reduction (decreased the minimum drag ratio) and the corresponding onset velocity (cross-section with a drag ratio of 1.0), presumably because the fibre network strength increased [15]. However, at a constant solid mass content, increasing the particle size resulted in an increase in the maximum drag reduction, as well as an increase in the

corresponding onset velocity. Consequently, above certain flow rates, larger-sized particles at lower solid mass contents produced the same drag ratio and, therefore, lower pump power requirements than smaller size particles at higher solid mass contents.

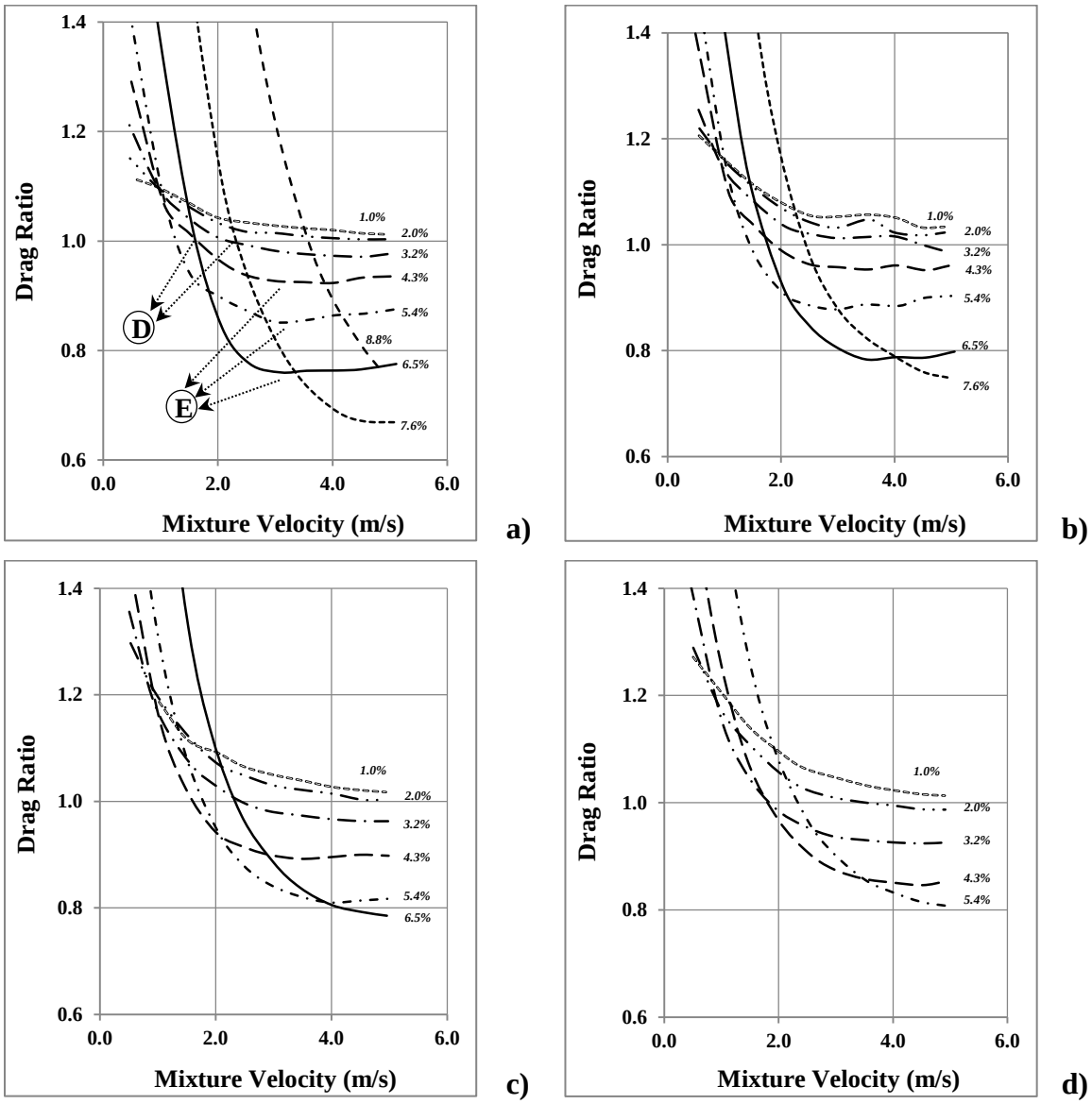

Fig. 4-8: Drag ratio vs. mixture velocity for various mixture solid mass contents of wheat straw particles of a) <3.2 mm, b) 3.2 mm, c) 6.4 mm, d) 19.2 mm through the laboratory-scale pipeline (the points D and E on Fig. 4-8(a) adopted from Fig. 4-6)

Figure 4-9 compares the maximum achievable drag reductions (% reduction in friction loss with respect to water at the same velocity) for wheat straw and corn stover particles at equal solid mass contents and approximately equal fibre diameters and aspect ratios.

Although the fibres studied here do not yet produce drag reductions similar to those investigated by Radin [44] and Duffy and Lee [6] who reported up to 50% drag reduction for synthetic and natural fibres with aspect ratios of 25 to several hundred, the slurries here achieved a 33% drag reduction with an 8.8% slurry of <3.2 mm corn stover particles with low aspect ratios of about 3. As can be observed on Fig. 4-9, corn stover fibres were generally more effective at reducing drag than wheat straw particles. This was attributed to distinct morphological features, e.g., irregular surface (in another study by the present authors [17], it was shown that corn stover particles are more irregularly shaped and also almost 7 times rougher than ribbed wheat straw fibres. Also the greater longitudinal flexibility of corn stover particles leads to a greater tendency to entangle and allows stronger fibre networks to form than with wheat straw particles).

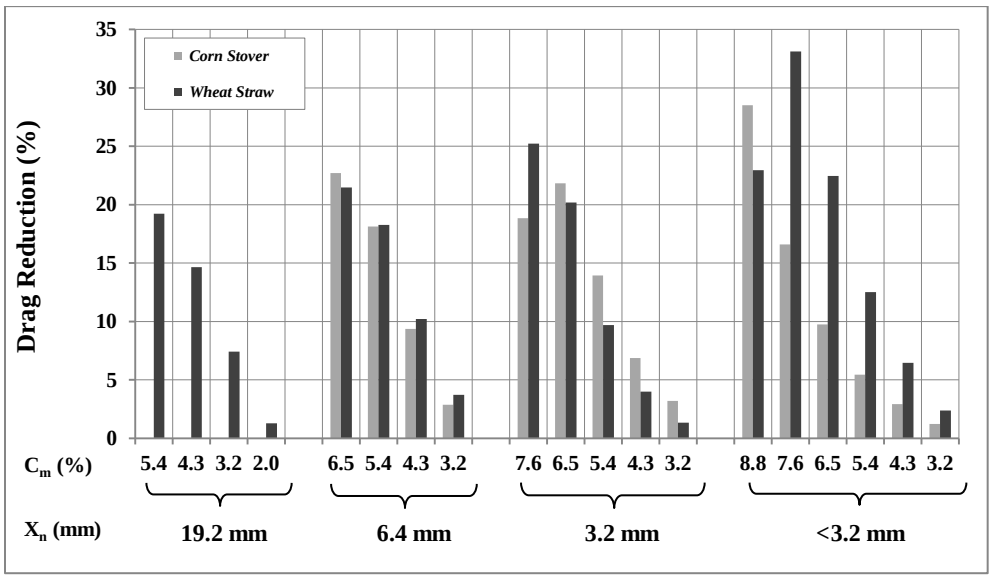

Fig. 4-9: Drag reduction as a function of slurry solid mass contents measured using the experimental set-up (data not available for 19.2 mm corn stover particles)

4.3.4. Effect of Slurry Solid Mass Content

Particle-particle interaction, which predominantly governs slurry friction loss behaviour and suspension viscosity, is a function of slurry solid mass content as well as pumping velocity and particle dimensions. Slurry solid mass content influences the pressure drop behaviour of heterogeneous suspensions of agricultural residue biomass totally differently than conventional solid-liquid systems. While typical solid-liquid mixtures,

such as coal, ash, or sand, as well as wood chip forest biomass [33], present increasing pressure gradients with increasing solid mass content [35-37, 45] (various carrier liquids and particle features produce only minor differences), slurries of wheat straw and corn stover particles studied here showed a decreasing trend even lower than the friction loss of the carrier liquid flowing alone, for more concentrated suspensions though. Figure 4-10 presents the above distinction between suspensions of typical coarse solids (i.e., greater than 1.5 mm) [37] and 6.4 mm wheat straw fibres at various solid mass contents. This phenomenon occurs because of the change in the viscous nature and physical structure of the fibre suspensions at solid mass contents above approximately 1.0% [38], i.e., the formation of flocs and the subsequent increase in floc coherence, mean floc size, and more plug-like characteristics of the slurry. In addition, in conventional solid-liquid systems, the excess pressure gradient (the difference between slurry and water pressure drop per unit length of pipe at the same velocity) due to the presence of the solids is always positive and directly proportional to the solid mass content of the mixture (Fig. 4-11(a)). However, in fibre-water slurries the excess pressure gradient becomes negative at solid mass contents above ~1.0% and velocities above ~1.5 m/s, and is described by a third order polynomial function of the mixture solid mass content. This makes it difficult to model its behaviour (Fig. 4-11(b)).

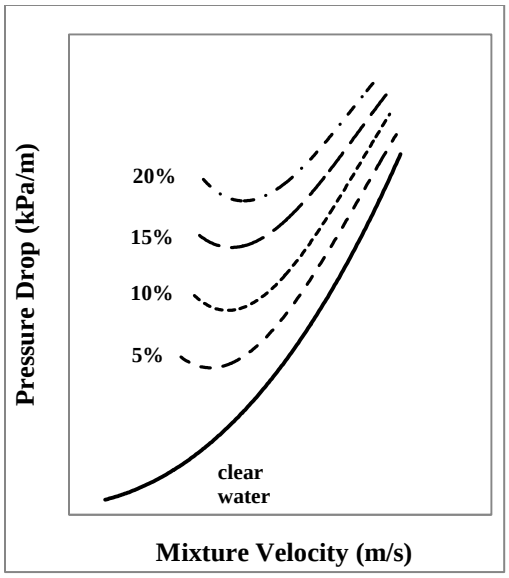

a)

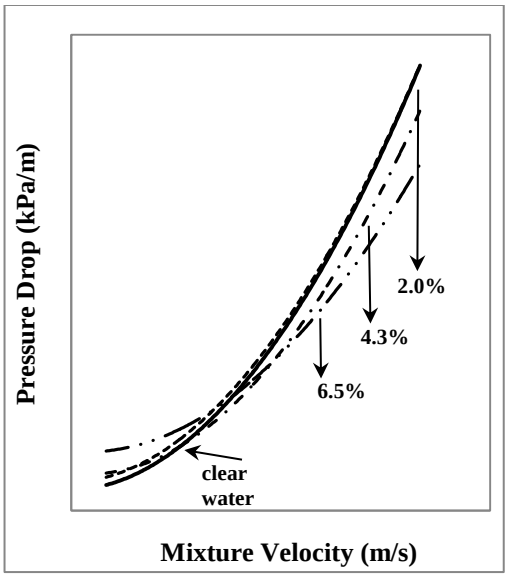

b)

Fig. 4-10: Pressure drop vs. velocity for a) <1.5 mm typical solid particles (i.e., coal, sand, etc.) in 230 mm diameter pipeline as a function of slurry solid volume content) [37], b) 6.4 mm wheat straw particles as a function of solid mass content measured using the experimental set-up

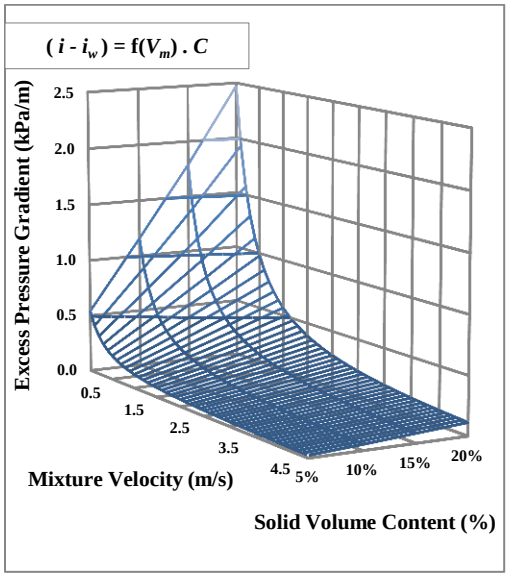

a)

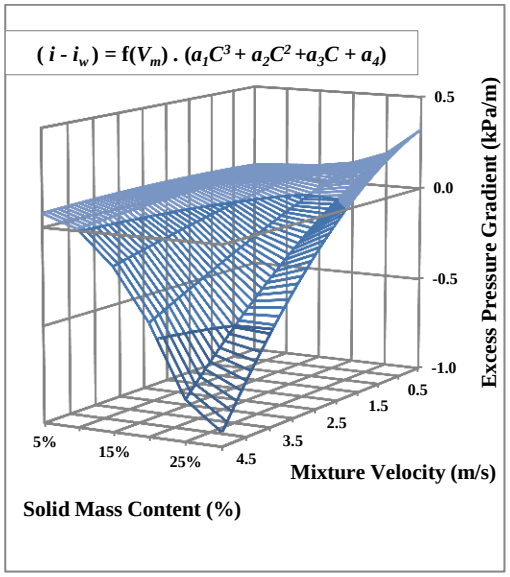

b)

Fig. 4-11: Excess pressure gradient as a function of mixture velocity and solid mass content for a) <1.5 mm typical solid particles in 230 mm diameter pipeline [37], b) 6.4 mm wheat straw particles measured using the experimental set-up

The pressure drop data at particular flow rates for slurries of various particle type and size and over a range of solid mass contents are presented on Fig. 4-12. Broadly

speaking, for any given velocity, as solid mass content and, therefore, particle-particle interactions increased, drag reduction increased significantly up to relatively high solid mass contents, where with further increase in solid mass content pressure drops rose rapidly. A similar trend was observed by Kerekes and Douglas [46] for suspensions of nylon fibres at their lowest velocity.

At a constant velocity of 0.5 m/s, where turbulent plug flow could be observed through the entire range of solid mass contents, the slurry pressure drop, although close to that of the carrier liquid, was almost independent of slurry solid mass content up to 5.4%. For a given size, however, friction loss changed rapidly at solid mass contents above 5.4% due to the change in the viscous nature of the suspension. Apparent (or relative) suspension viscosity, which takes into account the rheology of the entire suspension, has been reported as being a function of fibre dimension and slurry solid mass content. Apparent suspension viscosity has been shown to increase with decreasing fibre size [47], change linearly with lower solid mass contents, and be proportional to the cube of higher solid mass contents [48]. Therefore, for a given particle size and at a low velocity of 0.5 m/s, the apparent suspension viscosity increased dramatically at solid mass contents above 5.4%, which consequently resulted in a rapid rise in corresponding pressure drops. However, these high solid mass content suspensions showed significant drag-reducing abilities at higher flow rates (see Fig. 4-12 at above 3.5 m/s velocity).

The effect of particle diameter on apparent suspension viscosity could be clearly observed at velocities above of 1.0 m/s, where in addition to the slurry solid mass content, particle dimension influenced the slurry mechanical features. At a velocity of 1.5 m/s and a slurry of 3.2% solid mass content, particle sizes of 19.2 mm, compared to 6.4 mm, 3.2 mm, and <3.2 mm, had lower apparent suspension viscosity with stronger flocs and produced little drag reduction. However, increasing the solid mass content at the same flow rate increased the pressure drop rapidly for slurries of all particle sizes. The same trend could be observed for velocities of 2.5 m/s and 3.5 m/s.

At velocities above 2.5 m/s, along with the change in the nature of the flow from turbulent plug flow to transition (caused by the disruption of the fibre network) and fully

turbulent flow, the slurry pressure gradient dropped below that of the carrier liquid pressure drop at lower solid mass contents. However, for a few of the slurries tested, the increased viscous nature, even at the maximum solid mass content of 8.8%, was not sufficient to lessen the drag-reducing ability even at the highest velocity studied here (5.0 m/s). A further increase in solid mass content would presumably give predominantly plug flow behaviour even at higher velocities.

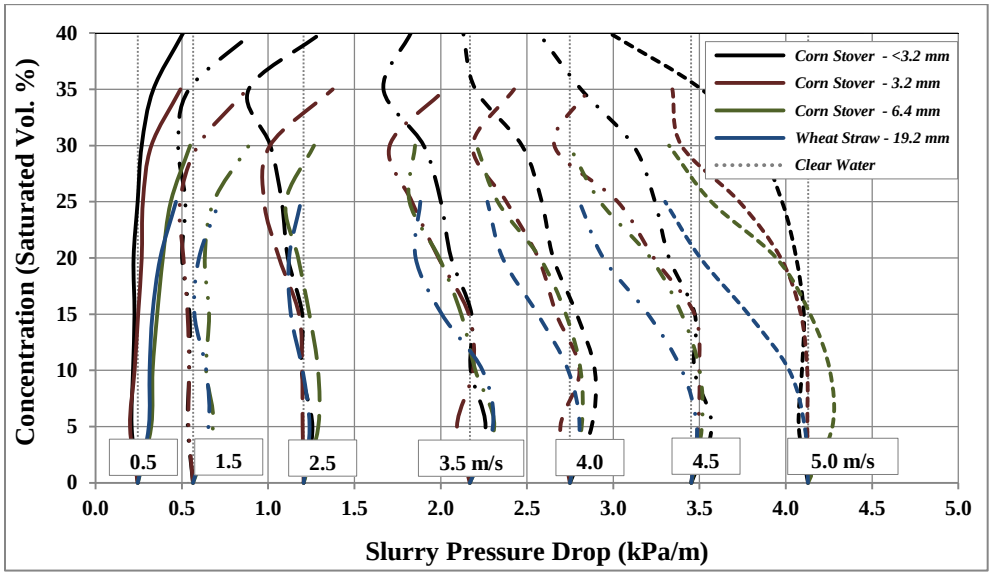

Fig. 4-12: Slurry solid mass content vs. pressure drop at constant velocities for slurries of <3.2 mm, 3.2 mm, and 6.4 mm corn stover particles, and a slurry of 19.2 mm wheat straw particles measured using experimental set-up

4.3.5. The Effect of Solid Particle Properties

The interactive characteristics of the agricultural residue biomass particles (e.g., wide size range, extreme shapes, large fibre length and aspect ratio, etc.) appear to give rise to a variety of mechanisms that are often not encountered in conventional solid-liquid slurry systems, which lack the internal particulate structure or the ability of the particles to flex, absorb energy, and absorb the carrier liquid. Understanding how such features impact on the mechanical behaviour of the slurry helps not only in modifying the feedstock preparation processes (see section 2.1), but also helps optimising the design and operation of agricultural residue biomass pipeline facilities.

The impact of particle size distribution has been recognised in all types of slurry flows, with broad size distributions producing lower friction losses at high flow rates [6, 49]. Figure 4-13(a) presents the size distributions (PSDs) of wheat straw and corn stover particles obtained through the particle image processing course of the present research, and Fig. 4-13(b) and 4-13(c) shows the change in pressure drop for the 5.4% slurries of wheat straw and 6.5% slurries of corn stover particles, respectively. A similar conclusion could be reached here, where 19.2 mm wheat straw particles, which come with a wide size range of 18.4 mm, reduced the pressure drop more noticeably (at velocities above 2.5 m/s) compared to <3.2 mm particles with narrow size range of 5.2 mm, and also 8.59 mm size range of the 6.4 mm corn stover particles at 5.0 m/s resulted in a pressure differential that was 13% less than <3.2 mm fibres. However, for small differences in size ranges, the state of the suspension (e.g., suspension viscosity) and morphological factors (e.g., fibre shape) may dominate the effects of particle size distribution resulting in comparable pressure drop gradients. It is noteworthy that it was not possible to transport a 3.2% slurry of 19.2 mm corn stover particles along a 50 mm diameter pipeline, whereas experiments at a 5.4% solid mass content could be successfully conducted with the same size wheat straw particles. Since the PSD of 19.2 mm corn stover particles was not noticeably narrower than for the 19.2 mm wheat straw fibres, the difference in the solid mass content that could be transported without forming a blockage was probably due to particle shape and the longitudinal flexibility of the corn stover particles.

As well as PSD, the effect of absolute particle dimension was investigated. While the particles widths were of the same order of magnitude (see Table 4-1), the differences in particle length could have influenced fluid mechanics of the fibre suspension by altering the rheology and momentum transfer mechanisms; both of which will be discussed here in detail. Broadly speaking, for the same flow rates and solid mass contents, the larger the fibre length (more accurately, the greater the aspect ratio) the less the frictional pressure drop and the more the potential to show drag-reducing behaviour (see Figs. 4-13(b) and 4-13(c)). Bobkowic and Gauvin [50] and Radin et al. [44] reported the same trend for nylon and rayon fibres.

4.3.5.1. The Effects of Solid Particle Dimension on Slurry Rheology

As discussed earlier, while keeping the suspension solid volume content ($C_v = \pi n X_{gl} X_{gw}^2 / 4$) and particle aspect ratio ($\alpha = X_{gl} / X_{gw}$) constant, increasing the fibre length resulted in a decrease in suspension viscosity, which was caused not only by hydrodynamic interactions but also by some attractive forces dependent on an average inter-fibre distance, as follows:

$$h_{av} = (nX_{gl})^{-\frac{1}{2}} \tag{4}$$

where h_{av} is the average inter-fibre distance.

A low average fibre distance promotes adhesive forces and flocculation and results in an increased suspension viscosity [47]. As can be observed on Fig. 4-13(b), at constant solid mass content of 5.4%, the suspension of 19.2 mm wheat straw particles with X_{gl} = 8.42 mm and α = 6.28, compared to the suspension of <3.2 mm fibres with X_{gl} = 2.57 mm and α = 3.47, had a tenfold lower fibre number fraction and consequently an approximately double inter-fibre distance. This resulted in a decrease in the apparent suspension viscosity and pressure drop. The same was true for corn stover particles on Fig. 4-13(c), where 6.5% slurries of 6.4 mm corn stover fibres came with 1.5 times greater inter-fibre distance compared to <3.2 mm particles and a reduced apparent suspension viscosity with correspondingly reduced friction loss.

4.3.5.2. The Effect of Solid Particle Dimension on Slurry Flow Momentum Transfer Mechanisms

According to Kerekes and Schell [51], the longer the fibre length, the larger the floc size. However, the way that fibre length and subsequently fibre floc size influence pressure drop behaviour depends on the suspension flow rate and corresponding momentum transfer mechanisms. Immediately after the drag-reducing regime develops (point D on Fig. 4-6 and 4-13(c)), fibre flocs can affect momentum transfer in two opposing ways: lowering the small-scale momentum transfer by damping the turbulence of the

suspending phase and increasing the momentum transfer by providing solid links between adjacent layers in suspension. The relative influence of these two effects on momentum transfer depends on the average floc size. A large average floc size favours the formation of solid links between adjacent layers. At the point of maximum drag reduction (point E on Fig. 4-6 and 4-13(c)) in the transition flow regime, where a fibre plug with the size approximately 20% of the pipe diameter still exists, the competing mechanisms are at equilibrium. From this point forward, the effect of flocs in suppressing radial turbulence dominates and the friction loss curve moves closer to the water curve with increasing velocity [6, 15, 52, 53]. This can be seen on Fig. 4-13(c) for the curve of <3.2 mm corn stover fibres and on Fig. 4-8(a) for below 7.6% slurries of <3.2 mm wheat straw particles where drag ratio curves slope upward (the corresponding labels are adopted from Fig. 4-6). For conditions corresponding to a low intensity of turbulence (between D and E), the effect of large flocs near the pipe axis (central plug) in providing solid links between adjacent fluid layers dominates. Under these conditions, increasing the intensity of turbulence by increasing the flow rate decreases the average floc size in the turbulent annulus. Consequently momentum transfer decreases, local mean velocity gradients increase, and drag reduction continues to increase. This can be observed on Fig. 4-13(c) at velocities below ~3.5 m/s, where 6.4 mm corn stover particles present pressure drops greater than 3.2 mm corn stover fibres at high velocities.

The momentum transfer concept introduced here could also be used to explain the instability in velocity and pressure drop measurements in early stages of the experiment, when it took 12 -14 h at a pumping velocity of 4.0 to 5.0 m/s before a stable mixture condition was reached and pressure and velocity fluctuations were reduced to less than 1.0% per hour (see Fig. 4-13(d)). Radin et al. [44] observed a similar variation in pressure and velocity with time in their experiments and allowed the suspensions of synthetic and natural fibres to circulate for several hours to allow complete dispersion of solids. As it was previously stated, the larger the fibre flocs, the more the formation of solid links between adjacent layers for conditions corresponding to low intensity turbulence in the drag-reducing regime (D to E on Fig. 4-6) and the greater the momentum transfer in the slurry. In the present experiment, an increase in the bulk flow rate over a period of eight hours was detected (see Fig. 4-13(d)), at the expense of an increase in local mean velocity

gradients and a decrease in momentum transfer, which indicates reduced formation of solid links and decreasing floc sizes over time. Decreasing floc size could be a result of physical breakdown or the degradation of feedstock particles caused by the mixer impellers and centrifugal pump, as well as particle-particle interactions. Degradation brought about the effective diameter of the particles (e.g., d_{50}) not remaining constant during transportation. The degradation effect was studied here with a 3.2% solid mass content mixture of 19.2 mm wheat straw particles. It was observed that the initial particle d_{50} of 8.04 mm was reduced by ~29% to 5.74 mm in 8 h. Degradation was even observed to take place for small particles of <3.2 mm. Similarly, Kato and Mizunuma [54] reported that asbestos fibres <1 μm diameter and a few mm long degraded by about 10% during three hours of circulation. Elliot [55] also reported that wood chips < 12.7 mm degraded by 39% as compared to 10% in control chips from the original batch after four hours circulation. According to Elliot [55], most of this reduction in size is caused by the pump, a small amount by the mixer, and none by passage through the pipe alone. A lower reduction in size would be expected from improved equipment design at normal commercial practice than was experienced in this laboratory-scale facility.

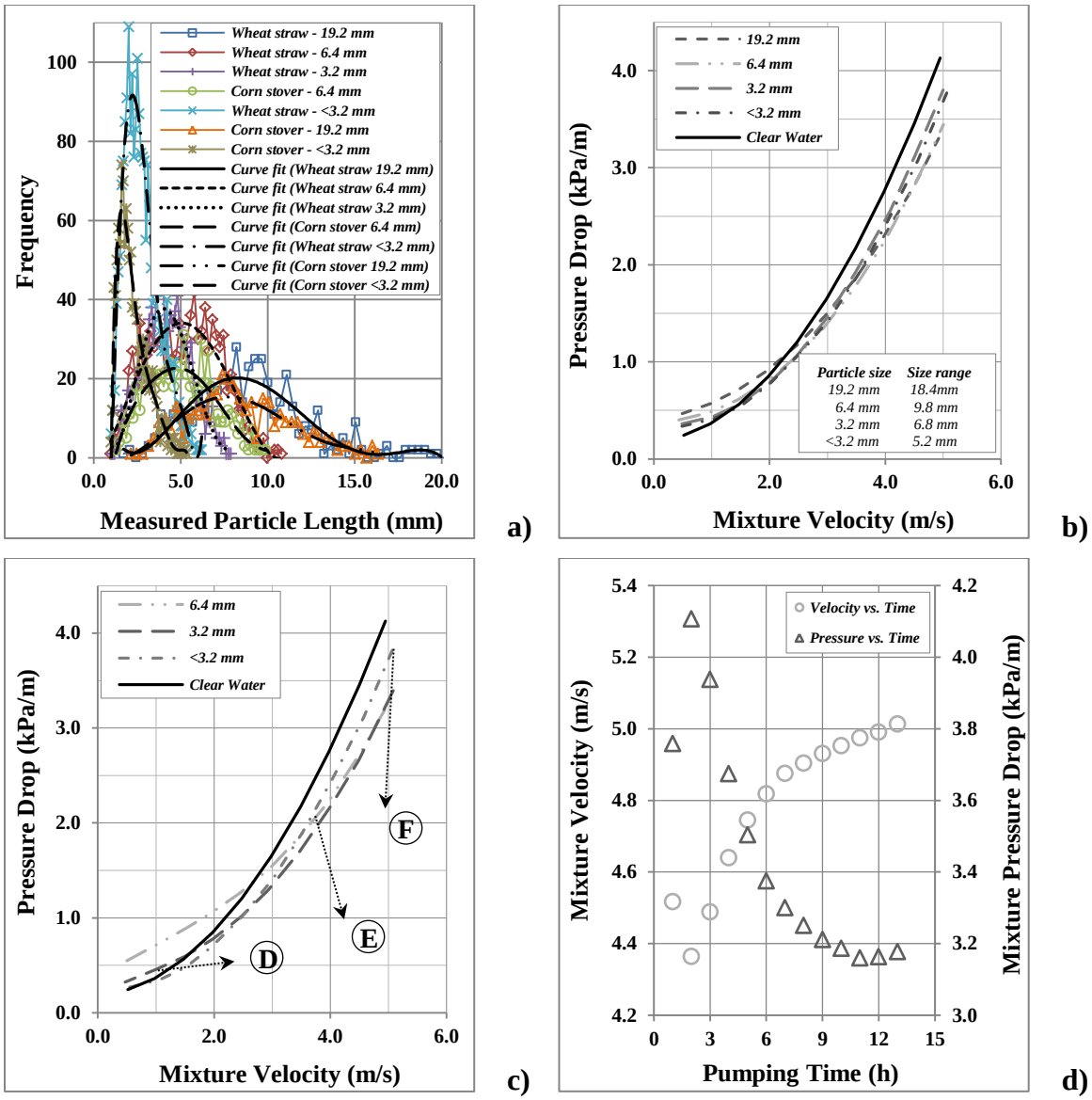

Fig. 4-13: a) Particle size distribution of wheat straw and corn stover particles, b) Pressure drop vs. pumping velocity for 5.4% slurries of various size wheat straw particles, c) Pressure drop vs. pumping velocity for 6.5% slurries of various size corn stover particles, d) Average mixture bulk velocity and pressure drop variation of a 7.6% solid mass content mixture of 3.2 mm wheat straw particles at first 15 h of pumping (the points D, E, and F on Fig. 4-13(c) adopted from Fig. 4-6) – all the results obtained from the experimental set-up

4.3.5.3. The Effects of Solid Particle Dimension on Drag-reduction Onset Velocity

Concerning the effects of fibre length on the onset velocity of drag reduction, it can be concluded that (see Fig. 4-13) for certain particle types and suspension solid mass contents, increasing the particle length increases the onset velocity. This increase can be attributed to an increase in floc size, more formation of solid links, and a subsequent increase in momentum transfer, which results in a decrease in drag-reducing ability. Also, it is thought that increasing fibre length not only increases floc size but also floc strength and plug-like characteristics, which requires a higher intensity of turbulence to cause disruption.

4.4. Conclusions

Pipeline hydro-transportation of wheat straw and corn stover agricultural residue biomass was experimentally studied. While no similarity was observed between friction loss behaviour of the slurries of wood chips and corn stover particles, the slurry of fibrous agricultural residue biomass particles exhibited drag-reduction characteristics at high flow rates. A maximum drag reduction of 33% could be achieved with an 8.8% slurry of <3.2 mm corn stover particles at a slurry flow rate of 5.0 m/s. In addition, the dependency of the rheological behaviour of the slurry and the longitudinal pressure gradient on feedstock type, particle dimension, slurry solid mass content, and slurry flow rate were experimentally investigated. Solid mass content was found to impact the slurry friction loss behaviour differently compared to conventional solid-liquid systems, and to decrease pressure gradient with increasing solid mass content. The impact of particle size distribution was recognised with broad size distributions producing lower friction losses at high flow rates where 19.2 mm wheat straw particles, which come with a wide size range of 18.4 mm, reduced the pressure drop more noticeably at velocities above 2.5 m/s compared to <3.2 mm particles with a narrow size range of 5.2 mm. Friction loss variations were also well explained based on two different momentum transfer mechanisms, where an increase in flow rate and a corresponding increase in the intensity of turbulence, and a decrease in average floc size in the turbulent annulus with a decrease in momentum transfer were both found to increase drag reduction in the transition flow

regime before reaching the maximum drag-reduction asymptote. Also, it was concluded that for certain particle types and slurry solid mass content, increasing particle length increases the drag-reduction onset velocity. The results presented here could be help optimise the design and operation of agricultural residue biomass hydro-transport pipelines.

Nomenclature

Exp	exponential function
PSD	particle size distribution
MC	moisture content, % (wet basis)
S	distance along the straight pipe section downstream U-bend section, m
S_x	standard deviation of the measurements, corresponding unit
P_x	precision uncertainty ($P_x = t_{\frac{\propto}{2},\nu}\frac{S_x}{\sqrt{n}}$), corresponding unit
B_x	bias uncertainty, corresponding unit
U_x	total uncertainty ($U_x = \sqrt{\sum B_x^2 + P_x^2}$), corresponding unit
N_i	number of particles of a particular distinct dimension, dimensionless
X_n	nominal length of particle, mm
X_i	distinct length of particle, mm
X_{gl}	geometric mean length, mm
X_{gw}	geometric mean width, mm
d_{XX}	corresponding particle lengths in mm at respective XX % cumulative number fraction of particles
V_m	solid-liquid mixture (slurry) velocity, m/s
V_f	carrier liquid velocity, m/s
D_{pipe}	pipe internal diameter, m
R_{pipe}	pipe internal radius, m
R_C	radius of curvature of U-bend section, m
C_v	slurry solid volume content, %
C_m	slurry solid mass content, %
Re_f	carrier fluid Reynolds number ($Re_f = \frac{\rho_f V_f D_{pipe}}{\mu_f}$), dimensionless
Re_g	generalised Reynolds number ($Re_g = \frac{\rho_m V_m D_{pipe}}{\mu_f}$),dimensionless
$\Delta P/L$	longitudinal pressure gradient in the pipe, kPa/m
k	ratio of particle dimensions to diameter of pipe
n	fibre number fraction
f	friction factor
g	gravitational acceleration, m/s^2
x_0	size of the largest particle in the particle size distribution
h	pumping time, h
h_{av}	average inter-fibre distance, µm

Nomenclature – Cont'd

i_m	hydraulic gradient of mixture, m[water]/m[pipe]
i_w	hydraulic gradient of clear water, m[water]/m[pipe]
σ_{gl}	geometric length standard deviation, mm
σ_{gw}	geometric width standard deviation, mm
v	kinematic viscosity of carrier liquid, m^2/s
μ_f	dynamic viscosity of carrier liquid, Pa.s
ρ_m	density of mixture, kg/m^3
ρ_f	density of carrier liquid, kg/m^3
n'	number of measurements taken
$t_{\frac{\propto}{2},v}$	t-distribution with $\alpha = 1 - 95\%$ confidence and $v = n' - 1$

References

[1] Kumar, A., Cameron, J.B., Flynn, P.C. Pipeline transport of biomass. Applied Biochemistry and Biotechnology, 2004; 113: 27-39.

[2] Kumar, A., Cameron, J.B., Flynn, P.C. Large-scale ethanol fermentation through pipeline delivery of biomass. Applied Biochemistry and Biotechnology, 2005 (a); 121: 47-58.

[3] Kumar, A., Cameron, J.B., Flynn, P.C. Pipeline transport and simultaneous saccharification of corn stover. Bioresource Technology, 2005 (b); 96: 819-29.

[4] Hunt, W.A. Friction factors for mixtures of wood chips and water flowing in pipelines. 4th International Conference on the Hydraulic Transport of Solids in Pipes. Alberta, Canada; 1976, p. 1-18.

[5] Wasp, E.J., Aude, T.C., Thompson, T.L., Bailey, C.D. Economics of chip pipelining. Tappi, 1967; 50: 313-18.

[6] Duffy, G.G., Lee, P.F.W. Drag reduction in turbulent flow of wood pulp suspensions. Appita, 1978; 31: 280-86.

[7] Luk, J. Pipeline transport of wheat straw slurry [dissertation]. University of Alberta; 2010.

[8] Institution, S.-T. SCAN CM 40:88. Scandinavian Pulp, Paper and Board Testing Committee.

[9] TAPPI. Technical Association of the Pulp and Paper Industry (TAPPI),. TAPPI usefull methods NO21; 2010.

[10] ASABE. Moisture measurement for forages. Standard S3582 American Society of Agricultural and Biological Engineers, St. Joseph, MI, US; 2008.

[11] ASTM. Standard test method for density, relative density, and absorption of coarse aggregate. ASTM, Designation C127; 2012.

[12] McKendry, P. Energy production from biomass (part 1): overview of biomass. Bioresource Technology, 2002; 83: 37-46.

[13] Duffy, G.G. The optimum design of pipelines for transporting wood pulp fiber suspensions. Appita Journal, 1989; 42: 358-61.

[14] Duffy, G.G., Kazi, S.N., Chen, X.D. Monitoring pulp fibre quality by frictional pressure drop measurement. Proceeding of 56th Appita Annual Conference, 2002: 119-26.

[15] Paul, T., Duffy, G., Chen, D. New insights into the flow of pulp suspensions. Tappi Solutions, 2001; 1.

[16] Rasband, W.S. http://rsb.info.nih.gov/ij/index.html, U.S. National Institutes of Health, Accessed September 2011. 2008.

[17] Vaezi, M., Pandey, V., Kumar, A., Bhattacharyya, S. Lignocellulosic biomass particle shape and size distribution analysis using digital image processing for pipeline hydro-transportation. Biosystems Engineering, 2013; 114: 97-112.

[18] ASABE. Method of determining and expressing particle size of chopped forage materials by screening. Standard ANSI/ASAE S4241. St. Joseph, MI, US: American Society of Agricultural and Biological Engineers, St. Joseph, MI, US; 2007.

[19] Anwer, M., So, R.M.C., Lai, Y.G. Perturbation by and recovery from bend curvature of a fully-developed turbulent pipe-flow. Physics of Fluids, 1989; 1: 1387-97.

[20] Hellstrom, L.H.O., Smits, A.J. Turbulent pipe flow through a 90 degree bend. Fluid Mechanics Meeting. 1000 Islands, Ontario, Canada; 2012.

[21] Rowe, M. Measurements and computations of flow in pipe bends. Journal of Fluid Mechanics, 1970; 43: 771-83.

[22] Gillies, R.G., Shook, C.A. A deposition velocity correlation for water slurries. Canadian Journal of Chemical Engineering, 1991; 69: 1225-28.

[23] Durand, R., Condolios, E. Experimental investigation of the transport of solids in pipes France Hydrolic Society Conference. Paris; 1952, p. 29-55.

[24] Fangary, Y.S., Ghani, A.S.A., ElHaggar, S.M., Williams, R.A. The effect of fine particles on slurry transport processes. Minerals Engineering, 1997; 10: 427-39.

[25] Weir. Slurry pump handbook. Fifth ed; 2009.

[26] Newitt, D.M., Richardson, J.F. Hydraulic Conveying of Solids. Nature, 1955; 175: 800-01.

[27] Colebrook, C.F. Turbulent flow in pipes, with particular reference to the transition region between the smooth and rough pipe laws. Journal of the Institution of Civil Engineers, 1939; 11: 133-56.

[28] Churchill, S.W. Friction factor equation spans all fluid regimes. Chemical Engineering, 1977; 84: 91-92.

[29] Moody, L.F. An approximate formula for pipe friction factors. Transactions of the ASME, 1947; 69: 1005-06.

[30] Wood, D.J. An explicit friction factor relationship. Civil Engineering, 1966; 36: 60-61.

[31] Kazi, S.N., Duffy, G.G., Chen, X.D. Heat transfer in the drag reducing regime of wood pulp fibre suspensions. Chemical Engineering Journal, 1999; 73: 247-53.

[32] Elliott, D.R., Montmorency, W.H. The transportation of pulpwood chips in pipelines,. Pulp and Paper Research Institute of Canada (PPRIC) Technical Report; 1963.

[33] Brebner, A. On pumping of wood chips through 4-Inch Aluminum pipeline. Canadian Journal of Chemical Engineering, 1964; 42: 139-42.

[34] Faddick, R.R. Head loss studies of transport of woodchips in pielines. [dissertation]. Queen's University; 1963.

[35] Brown, N.P., Heywood, N.I. Surry handling - Design of solid liquid systems. New York: Elsevier; 1991.

[36] Abulnaga, B.E. Slurry systems handbook. New York: McGraw-Hill; 2002.

[37] Bain, A.G., Bonnington, S.T. The hydraulic transport of solids by pipeline. 1st ed. Oxford ; New York: Pergamon Press; 1970.

[38] Fock, H., Claesson, J., Rasmuson, A., Wikstrom, T. Near wall effects in the plug flow of pulp suspensions. Canadian Journal of Chemical Engineering, 2011; 89: 1207-16.

[39] Moller, K. Correlation of pipe friction data for paper pulp suspensions. Industrial & Engineering Chemistry Process Design and Development, 1976; 15: 16-19.

[40] Meyer, H. An analytical treatment of the laminar flow of annulus forming fibrous suspensions in vertical pipes. Tappi, 1964; 47: 78-84.

[41] Moller, K., Duffy, G.G., A., T. Laminar plug flow regime of paper pulp suspensions in pipes. Svensk Papperstidning-Nordisk Cellulosa, 1971; 74: 829-34.

[42] Duffy, G.G., Titchener, A.L., Lee, P.F.W., Moller, K. The mechanism of flow of pulp suspensions in pipes. Appita, 1976; 29: 363-70.

[43] Duffy, G.G., Abdullah, L. Fibre suspension flow in small diameter pipes. Appita Journal, 2003; 56: 290-95.

[44] Radin, I., Zakin, J.L., Patterson, G.K. Drag reduction in solid-fluid systems. Aiche Journal, 1975; 21: 358-71.

[45] Shook, C.A., Gillies, R.G., Sanders, R.S. Pipeline hydrotransport with applications in the oil sand industry. Saskatoon, SK: SRC Publicatin; 2002.

[46] Kerekes, R.J.E., Douglas, W.J.M. Viscosity properties of suspensions at limiting conditions for turbulent drag reduction. Canadian Journal of Chemical Engineering, 1972; 50: 228-31.

[47] Djalili-Moghaddam, M., Toll, S. Fibre suspension rheology: effect of concentration, aspect ratio and fibre size. Rheologica Acta, 2006; 45: 315-20.

[48] Powell, R.L., Morrison, T.G., Milliken, W.J. Apparent viscosity of suspensions of rods using falling ball rheometry. Physics of Fluids, 2001; 13: 588-93.

[49] Schaan, J., Sumner, R.J., Gillies, R.G., Shook, C.A. The effect of particle shape on pipeline friction for Newtonian slurries of fine particles. Canadian Journal of Chemical Engineering, 2000; 78: 717-25.

[50] Bobkowic, A., Gauvin, W.H. Turbulent flow characteristics of model fibre suspensions. Canadian Journal of Chemical Engineering, 1965; 43: 87-91.

[51] Kerekes, R.J., Schell, C.J. Effects of fiber length and coarseness on pulp flocculation. Tappi Journal, 1995; 78: 133-39.

[52] Lee, P.F.W., Duffy, G.G. Analysis of drag reducing regime of pulp suspension flow. Tappi, 1976 (a); 59: 119-22.

[53] Lee, P.F.W., Duffy, G.G. Velocity profiles in drag reducing regime of pulp suspension flow. Appita, 1976 (b); 30: 219-26.

[54] Kato, H., Mizunuma, H. Frictional resistance in fiber suspensions (part 1): pipe-flow. Bulletin of the Jsme-Japan Society of Mechanical Engineers, 1983; 26: 231-38.

[55] Elliott, D.R. The transportation of pulpwood chips in pipelines,. Pulp and Paper Magazine of Canada, 1960; 61: 170-75.

CHAPTER 5

The Flow of Wheat Straw Suspensions in an Open-impeller Centrifugal Pump[1]

5.1. Introduction

Following a series of techno-economic analyses of pipeline hydro-transport of wood chips and corn stover biomass materials [1], a lab-scale closed-circuit pipeline facility was designed and fabricated. Slurries of agricultural residue biomass particles (wheat straw and corn stover) were first prepared over a wide range of particle sizes and dry matter solid mass contents. The slurry was then pumped through the closed-circuit pipeline using a centrifugal slurry pump to investigate the feasibility of biomass pipeline hydro-transport and measure the mechanical parameters of slurry flow, e.g., friction loss and pump performance characteristics.

The performance of centrifugal slurry pumps has been the subject of several studies. Conventional Newtonian and non-Newtonian solid-liquid mixtures have been used to investigate the effects of solid particles' specifications (i.e., size, specific gravity (density of particle relative to density of water), drag coefficient), slurry specifications (i.e., rheological property, solid mass content), and pump features (i.e., impeller size and operating conditions) on the power consumed, the head produced, and the efficiency achieved by the centrifugal slurry pump [2-6]. In general, lower head and efficiency were reported for the pumps handling slurries of medium- and coarse-size particles in comparison to the pumps handling pure water only, which has been attributed to the difference in the velocity of liquid and solids leaving the impeller [7], as well as to the additional friction loss in the flow passages due to suspended solids [8]. Gandhi [2] studied the performance characteristics of a couple of small and large centrifugal slurry pumps handling slurries of fly ash, bed ash, and zinc tailings, where a decrease in head and efficiency of the pump was observed with increase in solid mass content, particle

[1] Vaezi, M., Kumar, A., ***Biomass and Bioenergy***, 2014; 69: 106-123

size, and slurry viscosity. Using 19 various basic pump designs, Horo [5, 8] experimentally investigated pumping of groundwood pulp (natural fibre used for pulp and paper production) through centrifugal pump and studied the effect of fibres on suction and pumping capacity, and the effect of air on the pump operation. They reported that the same, or higher than, the head height produced with pure water could be achieved with groundwood pulp at solid volume contents up to 7.0% provided a centrifugal pump specifically designed for pumping pulp was used.

Several attempts have been made to correlate the experimental data with solid particle properties, solid mass content, and pump specifications [9-14]. These correlations are dependent on pump size, properties of the slurries, and solid particles specifications, and are not universally applicable. The majority of the literature published on the performance characteristics of centrifugal slurry pumps used conventional solid particles with median lengths of 0.042 mm [2] for fly ash to 2.2 mm for sand [5] and density of 1480 kg/m^3 for coal [13] to 6240 kg/m^3 for mild steel [15]. The agricultural residue biomass particles studied here were noticeably larger (from 1.9 to 8.3 mm) compared to fly ash particles and had much smaller density (saturated) of 1050 kg/m^3. Such particle specifications, together with several unusual particle characteristics (e.g., wide size distribution; extreme shapes; fibrous, pliable, flexible, and asymmetric nature; potential for forming networks; ability to take up the carrier liquid) [16] give rise to a variety of mechanisms in slurry flow, e.g., drag reduction [17] which are often not encountered in classical solid-liquid systems. Typical fibrous particles slurry flows (e.g., slurry of natural and synthetic fibres of several micrometers to 5.0 mm in length and aspect ratios of 25 to several hundred) with progressively increasing fibre populations (i.e., slurry solid mass content) exhibit similar phenomena as well, i.e., drag reduction, particularly when fibres in suspension are subject to high shear rates and there is insufficient volume for the fibres to move freely. The details of corresponding mechanisms have been extensively discussed in literature [18-27]. Unusual physical and morphological particle characteristics, together with special slurry properties including unique friction loss behavior and ability to form fibre boundles, make pumping agricultural residue biomass difficult and impact the centrifugal slurry pump performance unconventionally. The researchers are, therefore, limited in seeking solutions to the problems involved with

pumping agricultural residue biomass slurries, and using previously proposed correlations might result in over-sizing of the pumps.

Following a previous study on the feasibility of biomass pipeline hydro-transport concept, as well as the biomass slurry flow mechanical and rheological behavior [17, 28], the authors attempt to experimentally establish the effect of concentrated slurries of fibrous agricultural residue biomass particles with non-conventional properties on performance characteristics of centrifugal slurry pumps. The main objectives were to study the effects of particle size and slurry solid mass content on head, efficiency, and power consumption of the centrifugal slurry pump, also develop an empirical correlation to predict the performance of the centrifugal pump when handling the slurry of agricultural residue biomass. The results could be used in selecting appropriate slurry pumps and in the design and operation of hydraulic pipelines to transport wheat straw and corn stover fibrous particles.

5.2. Experimental Measurements

5.2.1. Agricultural Residue Biomass Material Preparation and Properties

Wheat straw (*Triticum sativum*; dry stalks of wheat) and corn stover (*Zea mays*; leaves and stalks of corn) were used to prepare the slurry in the present study. Wheat straw and corn stover were collected from farms in Northern (54°03'57.8"N, 113°34'11.3"W) and Southern (49°47'20.9"N, 112°09'00.9"W) Alberta, Canada, in fall 2012, with heights of cut of 0.25 m for wheat straw and 0.4 m for corn stover. The square bales of wheat straw and round bales of corn stover were stored in open shelters in the farms for a minimum of two months before being deliverd to Large-scale Fluids Lab at University of Alberta. The materials, as received in the lab, were first milled using a commercially available cutting mill (SM-100; Retsch Inc., Newton, PA, USA), then classified using a standard [29, 30] chip classifier (BM&M Inc., Surrey, BC, Canada) with seven sieves 19.2 mm, 12.8 mm, 6.4 mm, 4.0 mm, 3.2 mm, and 1.28 mm in size, and pan. The material retained on four bottom trays were collected and classified into four groups with nominal sizes of 19.2 mm, 6.4 mm, 3.2 mm, and <3.2 mm. These nominal sizes were chosen to represent the particles dimensions throughout the chapter.

The initial wet-basis water mass content (moisture content or MC) of wheat straw and corn stover particles were measured according to ASABE S358.2 standard [31] to be 6 ± 0.5%. Particle density of wheat straw and corn stover were also measured according to ASTM C127 standards [32] to be 1026 ± 10 kg/m^3 and 1169 ± 10 kg/m^3, respectively.

5.2.1.1. Image Processing and Morphological Studies

Digital image processing was subsequently used to study the detailed characteristics (e.g., the relatively large mean particle size; wide size distribution; extreme shapes; fibrous, pliable, flexible, and asymmetric nature; potential for forming networks) and the morphological features of atypical agricultural residue biomass particles. ImageJ platform, a Java-based and platform-independent software by the National Institutes of Health (NIH, Bethesda, Maryland USA) [33], together with a user-coded plugin developed by the authors [16], was used to process particle sample images, measure particle dimensions, and analyze particle shapes, particle size distribution (PSD), size distribution algorithms, and corresponding parameters of knife-milled pre-classified wheat straw and corn stover. Dimensions of significance based on length, including median length (d_{50}; the particle size value in case-cumulative distribution percentage reaches 50%) and geometric mean length (X_{gl}; central tendency or typical value of particles' sizes), together with corresponding standard deviation (σ_{gl}), are presented in Table 5-1. Comparing nominal, median, and geometric particle lengths uncovers the 20 to 130% under- and over estimation of real dimensions of particles involved in nominal sizes. A comparison of the agricultural residue biomass particles' dimensions with those of conventional solid particles (see Table 5-6) showed that biomass particles come with diverse shapes (morphological features), surface features, and dimensions [16] that distinguish the slurry of agricultural residue biomass from classical solid-liquid systems. This unique feature was validated by comparing mechanical features of a water-sand mixture with the slurry of wheat straw biomass and is described later in this chapter. Normal PSD algorithms for <3.2 mm corn stover particles and for <3.2 mm, 3.2 mm, 6.4 mm, and 19.2 mm wheat straw fibres are shown in Fig. 5-1(a).

Table 5-1: Physical properties of particles and slurries of agricultural residue biomass

Solid Biomass	Particle Properties									Slurry Properties	
	Particle Size				Particle Aspect Ratio	Density		Wet-basis Water Mass Content		Dry matter Solid Mass Content, %	Density, kg/m^3
	Nominal Length, mm	Median Length (d_{50}), mm	Geometric Length ($X_{gl} \pm \sigma_{gl}$), mm	Shape Factor		Initial, kg/m^3	Saturated, kg/m^3	Initial, %	Saturated, %		
Wheat Straw	19.2	8.29	8.42 ± 1.49	0.105	6.28	1026 ± 10	1050 ± 10	6.0 ± 0.5	82.0 ± 0.5	1.0 – 5.4	1000.94–1004.7
	6.4	5.00	4.79 ± 1.57	0.156	4.47					1.0 – 6.5	1000.94-1005.7
	3.2	3.29	3.96 ± 1.41	0.266	3.53					1.0 – 7.6	10009.4-1006.6
	<3.2	2.42	2.57 ± 1.43	0.777	3.47						
Corn Stover	<3.2	1.90	2.11 ± 1.44	0.529	2.89	1169 ± 10				1.0 – 8.8	1000.94-1007.6

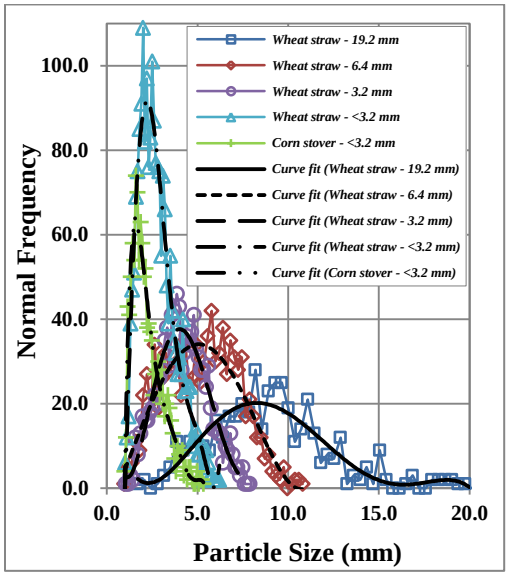

a)

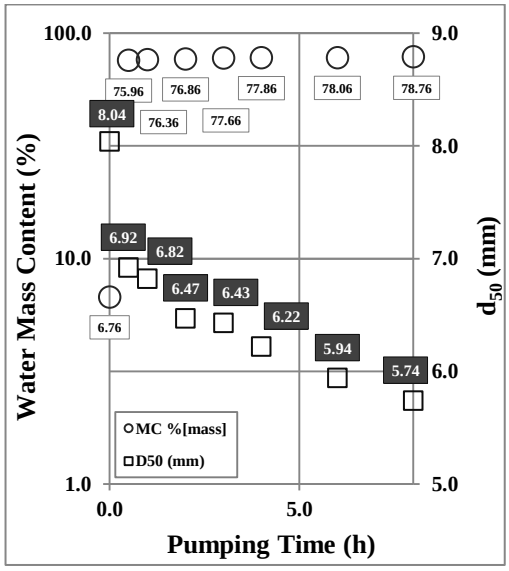

b)

Figure 5-1: a) Particle size distribution (PSD) of wheat straw and corn stover particles used during the course of present research, b) Water mass content and median length (d_{50}) variation of 19.2 mm wheat straw particles in a mixture of 3.2% dry matter solid mass content pumped at 3.3 m/s and 15.0 kPa pressure measured in this study

5.2.1.2. Particle Shape Factor

In order to extend the specific results and conclusions obtained here for wheat straw and corn stover particles to other sorts of fibrous particles, a shape factor was defined that takes into account the particle's physical properties (particle density) and shape characteristics (thickness, width, length) (Eqs. 1-2, Table 5-2). Although fibrous particles are structurally diverse, here the fibers are defined on the basis of their size and shape as particles with aspect ratio (X_{gl}:$X_{gl,width}$) ≥ 3:1, length ≥ 2 mm, and width ≤ 1.5 mm.

$$\lambda = \frac{M_s}{\rho_s \times \sum_{i=1}^{n} (X_{gl,width,i} \times A_{s,i})} \quad (1)$$

$$\text{Shape factor} = \lambda \times \sqrt{\frac{X_{gl,width}}{X_{gl}}} \quad (2)$$

Based on the assumption that particles similar in nature should have more or less the same shape characteristics [34], common agricultural residue biomass (e.g., wheat straw, corn stover, rice straw) and energy crops (e.g., switch grass, miscanthus), are all fibrous in nature and the shape factor could be used as a parameter to compare the ground particles' physical properties and shape characteristics (Table 5-1). Solid particles with similar shape factors with agricultural residue biomass particles studied here are expected to come with similar mechanical behavior when mixed with water and pumped into pipeline. However, particle degradation, the structure of the fibre suspensions, particle-particle interactins, quantity and nature of the fine particles, and flexibility of particles could change with different material, different situations like once-through pumping, and different pump designs and sizes. Therefore, care must be taken when trying to extend the results obtained here to other sorts of biomass materials.

Table 5-2: Physical properties and shape specifications of wheat straw particles

Particle Size	Nominal Length (mm)	19.2	6.4	3.2	<3.2
	Geometric Length (mm)	8.42	4.79	3.96	2.57
	Geometric Width (mm)	1.34	1.07	1.12	0.74
	Geometric Thickness (mm)	0.534	0.563	0.744	1.237
Density of Particles, kg/m^3		1026.57			
Number of Particles in Sample		572	1082	1403	2159
Weight of particles in Sample, g		7.112	7.039	6.924	6.591
Thickness Factor (λ)		0.335	0.415	0.561	1.692
Shape Factor		0.133	0.196	0.298	0.908

5.2.2. Experimental Apparatus

A schematic of the experimental pipeline facility used in the present study is illustrated in Fig. 5-2. The test circuit consisted of a 455 dm^3 slurry mixing tank with a 0.37 kW centrally placed vertical mixer, 25.5 m of 50 mm diameter Schedule 40 steel pipe, and a double-tube heat exchanger to partially maintain the slurry temperature at 15±2°C. An electromagnetic flow meter (FMG-401H; Omega Eng., Stamford, CT, US) and a resistance temperature detector (RTD-E; Omega Eng., Stamford, CT, US) is included to measure the rate of slurry flow and the mixture temperature, respectively. In addition, a couple of 25 mm flush diaphragm low-pressure transmitters (PX42G7; Omega Eng., Stamford, CT, US) is included to measure the slurry flow gauge pressures upstream and downstream of a 7.5 m horizontal test section.

Slurry flow was provided by a specifically designed 7.45 kW centrifugal pump (CD80M; Godwin Pumps Ltd., Bridgeport, NJ, US) [35] coupled with a 7.45 kW induction electric motor (CC 068A; Madison Industrial Equipment, Vancouver, BC, Canada) and controlled by a 14.9 kW variable frequency drive (VFD) controller (MA7200-2020-N1, TECO-Westinghouse Co.). The dimension and performance parameters of the centrifugal slurry pump, together with the performance characteristics of the electric motor and VFD controller, are shown in Tables 5-3 and 5-4.

An optical electronic tachometer (DT-2236; Elma Instruments, Farum, Denmark) measured the rotational speed of the pump. A watt transducer (PC5; Flex-Core, Columbus, OH, US) was connected to the input supply via a couple of current

transformers (189-060; Flex-Core, Columbus, OH, US) and was calibrated using a power quality analyzer (43B; Fluke Corp., Mississauga, ON, Canada). The watt transducer measured the pump input power indirectly by the measurement of the input power to the electric motor with an accuracy of ±5.5%, using the electric motor's known efficiency.

The suction and discharge pressures were measured using 100 kPa and 200 kPa Bourdon tube pressure gauges (21X.53, WIKA Instruments Ltd., Edmonton, AB, Canada), respectively, which came with an uncertainty of ±1.5%, and were calibrated using a portable pressure calibrator (DPI 610/615, GE Druck, Leicester, United Kingdom) once every six months during experimentation. The pressure gauges, pipe layout, and measurements were set up, configured, and operated in accordance with the acceptance tests and standard test procedures for centrifugal pumps [36, 37].

The 4-20 mA output signals from the watt transducer, temperature probe, magnetic flow meter, and pressure transmitters were recorded with a sampling rate of 100 Hz. on a data acquisition system comprised of a 4-channel current excitation module (NI 9219; National Instrument Corp., Austin, TX, US) and a data acquisition program (LabView V.9.0.1f2; National Instrument Corp., Austin, TX, US).

5.2.3. Experimental Procedure

5.2.3.1. Agricultural Residue Biomass Slurry Preparation

The performance characteristics of the centrifugal pump were evaluated using pure water before and periodically during the solid-water experiments. The measured amount of feedstock was afterwards mixed with water and pumped through the closed-circuit pipeline. It took 12 to 14 hours at a pumping velocity of 4.0 to 5.0 m/s before a stable mixture condition was reached and pressure and velocity fluctuations, caused by particle degradation and decrease in momentum transfer, damped down to less than 1.0% per hour. Meanwhile, biomass solid particles absorbed 96% of their saturated water mass content in one hour and became fully saturated after six hours, as observed in Fig. 5-1(b). The friction loss of the slurry through a 7.5 m horizontal test section, together with the performance of the centrifugal pump, i.e., head, efficiency, and input power, was

measured afterwards (after 12 to 14 hours) with two types of biomass materials (wheat straw and corn stover) over a wide range of dry matter (oven-dried) solid mass contents (2.0 to 8.8% for <3.2 mm, 2.0 to 6.5% for 3.2 mm and 6.4 mm, and 2.0 to 4.3% for 19.2 mm particles), slurry bulk velocities (0.5 to 5.0 m/s), and pump rotational speeds (185, 167, 146, and 125 rad/s). In this chapter, dry matter solid mass content (from this point forward simply referred to as solid mass content) is the preferred unit to report the fraction of agricultural residue biomass particles in the slurry. However, equivalent saturated mass and volume contents have been presented in Table 5-5 for comparing/converting purposes. The values in Table 5-5 were calculated based on the mass of the feedstock, initial moisture content, saturated moisture content, density of dry and saturated particles, and volume of the loop. Initial and saturated moisture contents, together with density of dry and saturated solid particles were measured experimentally. Volume of the loop was fixed and mass of the required feedstock changed with the change in saturated solid mass content.

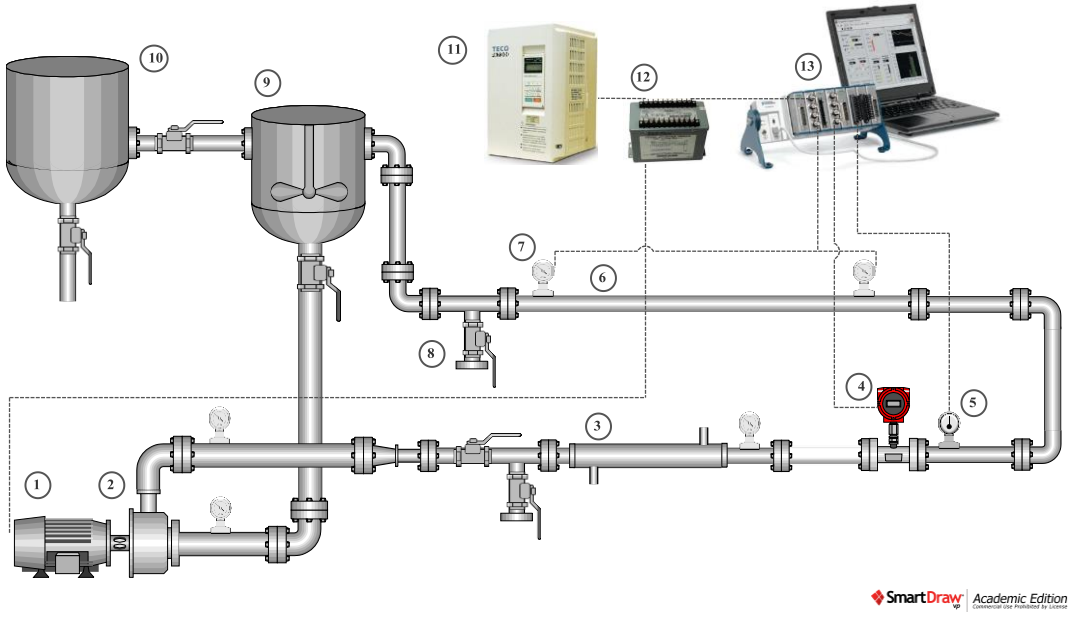

Figure 5-2: Schematic diagram of the pipeline facility [(1) electric motor, (2) centrifugal pump, (3) heat exchanger, (4) magnetic flow meter, (5) temperature sensor, (6) test section, (7) pressure transducer, (8) sampler-discharger, (9) mixing tank, (10) water supply tank, (11) variable frequency drive controller, (12) watt transducer, (13) data logger/analyzer]

Table 5-3: Dimensions and performance parameters (as per manufacturer) of the centrifugal slurry pump used in this study

Centrifugal Pump		
Type	Brand	Godwin
	Model	CD80M
Impeller	Type	Open
	Material	Cast chromium steel to minimum Brinell hardness, 341 HB
	Diameter	190 mm
	No. of vanes	3
	Impeller inlet cane angle	19°
	Impeller outlet cane angle	25°
Casing	Type	Single volute
	Material	ASTM-A48 30B
	Throat area	502.65 mm^2
Suction/Delivery Flange	Size	80 mm
Performance Characteristics	Power	7.45 kW (10.0 hp)
	Maximum operating speed	230 rad/s (2200 rpm)
	Maximum operating temperature	100°C
	Maximum working pressure	280 kPa (41.0 psi)
	Maximum suction pressure	200 kPa (29.0 psi)
	Maximum casing pressure	420 kPa (61.0 psi)
	Pipe connections	75mm
	Solids handling	Up to 40 mm diameter
	Maximum capacity	0.0284 m^3/s (28.4 L/s)
	Total dynamic heads	28.3 m
	Best efficiency point specifications at 188 rad/s (1800 rpm)	
	- Total developed head	134.3 kPa (13.7 meter of head)
	- Discharge capacity	0.0151 m^3/s (15.1 L/s)
	- Pump efficiency	40%
	- Pump input power	5.0 kW

At constant pump rotational speed, the bulk velocity of the slurry was adjusted using a ball valve downstream of the centrifugal pump (as shown in Fig. 5-2). During the experiments, samples were frequently collected to monitor the variation in wet-basis water mass content and physical breakdown (degradation) of the particles (Fig. 5-1(b)) [16]. The same approach as for dry particles (section 2.1) was followed to measure the wet-basis water mass content and density of saturated particles, whose properties were calculated to be 82 ± 0.5% and 1050 ± 10 kg/m^3, respectively (Table 5-1), independent of the type and size of the particles.

Table 5-4: Performance data of the electric motor and variable frequency drive controller (VFD) used in this study

Electric Induction Motor		
Type	Brand	Ultraline PE
	Model	CC 068A
Performance Data (***Provided by Madison Industrial Equipment, Vancouver, BC, Canada***)	Power	7.45 kW (10.0 hp)
	Phase	3
	Volts	208-230/460 V
	Amps	26.6-24.0/12.0 A
	rad/s (rpm) at 60 Hz	185 (1765)
	Power factor - (% of full load)	85.0 - (100.0)
		84.5 - (75.0)
		76.8 - (50.0)
	Nominal efficiency - (% of full load)	91.7 - (100.0)
		91.8 - (75.0)
		91.6 - (50.0)
		81.8 - (12.5)
		78.9 - (10.0)
Variable Frequency Drive Controller		
Type	Brand	TECO Westinghouse
	Model	MA 7200-2020-N1
Specifications	Power	14.9 kW (20.0 hp)
	Phase	3
	Volts	200-240 V
	Amps	64.0 A
	VFD Efficiency - (% of full load) [38]	97.0 - (100.0)
		96.0 - (75.0)
		95.0 - (50.0)
		94.0 - (42.0)
		93.0 - (25.0)
		86.0 - (12.5)
		47.0 - (1.6)

5.2.3.2. Sand Slurry Preparation

To understand how agricultural residue biomass slurries behave mechanically differently from conventional solid-liquid mixtures, a slurry of a common type of sand (play sand) [39] particles with known specifications (Table 5-6) was prepared and pumped through the same closed-circuit pipeline. Since the influences of circulation on friction loss results were not observed, friction loss measurements were made immediately after making the

slurry through 7.5 m test section of the pipeline over a wide range of solid mass contents of 5 to 20% and pumping velocities (0.5 to 5.0 m/s). The results were compared with those in the literature, as well as with pressure drop measurements of agricultural residue biomass slurries at identical properties and operating conditions.

Table 5-5: Saturated and dry matter (oven-dried) solid volume and mass contents of wheat straw slurries

Saturated Solid Mass Content, %	Saturated Solid Volume Content[1], %	Dry matter Solid Mass Content, %	Dry matter Solid Volume Content, %
40	14.7	8.8	8.6
35	12.8	7.6	7.4
30	11.0	6.5	6.3
25	9.2	5.4	5.2
20	7.4	4.3	4.1
15	5.5	3.2	3.1
10	3.7	2.0	2.0
5	1.8	1.0	1.0

[1] The solid volume content was calculated based on the volume of the solid materials (mass of saturated feedstock divided by density of saturated particles) divided by total volume of the loop

Table 5-6: Physical properties of particles and slurries of play sand and other conventional solids

Reference	Particle Properties					Slurry Properties	
	Solid Particle	Particle Size			Density, kg/m^3	Solid Mass Fraction, %	Density, kg/m^3
		Median Length (d_{50}), mm	Effective Size (d_{10}), mm	Geometric Length ($X_{gl} \pm \sigma_{gl}$), mm			
Sand particles used in the course of the present experiment							
[40]	**Play Sand (Quartz)**	0.446	0.579	0.366 ± 0.0012	2650	5.0 – 20.0	1030-1140
Conventional solids reported in literature							
[41]	**Medium sand**	0.37	0.24	-	-	0.12 – 0.43	-
[2]	**Fly Ash**	0.042	-	-	2080	13.27 – 60.52	
[42]	**Glass Bead**	0.090			2420	10.0 - 50.0	
[15]	**Mild Steel**	0.230			6240	5.2 - 23.2	
[11]	**River Sand**	1.29			2640	13.5 - 56.1	
[13]	**Coal**	0.9			1480	0.0 – 60.0	
[12]	**Iron Ore**	1.8			4150	40 - 60	

5.2.4. Electrical Efficiency Calculations

A VFD controller was used in conjunction with the electric motor in an attempt to improve control in the pipeline. However, analysis of the pump performance with various particle sizes and slurry solid mass contents over a range of pump rotational speeds (rad/s) and flow rates requires knowledge of how the efficiencies of the pump, electric motor, and VFD controller change with pump rotational speed and flow rate.

Full-load motor efficiency standards, at maximum rotational speed, for polyphase induction motors of various sizes were specified by the U.S. Energy Policy Act of 1992 [43] and the NEMA Premium™ efficiency electric motor program [44]. However, at a constant rotational speed, motor efficiency changes as the load changes. The electric motor manufacturer (Madison Industrial Equipment, Vancouver, BC, Canada) provided limited efficiency-load data, which are shown in Fig. 5-3(a) together with the data published by Natural Resources Canada (NRC) [45] and Facility Dynamic Engineering [46]. When reasonable agreement was observed between manufacturer and NRC efficiencies, manufacturer efficiency-load fitted curve and corresponding correlation were used to approximate the motor efficiency at loads smaller than 100%.

The introduction of the VFD controller, however, changes the efficiencies shown on Fig. 5-3(a) and makes it necessary to take into account the efficiency of the VFD controller, as well as losses generated in the motor at lower-than-rated frequencies by the VFD and losses in the motor due to the motor duty-point movement. Although the VFD controller partly-loaded efficiencies for various VFD controllers over a range of power ratings have been published [38], there have been difficulties in accurately measuring the efficiency of a motor controlled by a VFD. For instance, in the 1980s an IEEE working group [47] made an unsuccessful attempt to write a standard procedure for determining the efficiency of induction motors in VFD systems, and the computations at the Industrial Assessment Center of the University of Massachusetts [48] assumed a full-load motor efficiency at all speeds and loads. Wallbom-Carlson [49], however, proposed a VFD efficiency factor as a function of relative frequency (Fig. 5-3(b) - the effect of motor

duty-point movement is ignored) to estimate the overall efficiency of the electric motor at various rotational speeds, as follows:

Overall electric efficiency = (VFD efficiency factor) ×

(Motor efficiency at 100% speed at specific load) (3)

This approach was followed here to calculate the electric motor efficiency as a function of load and rotational speed.

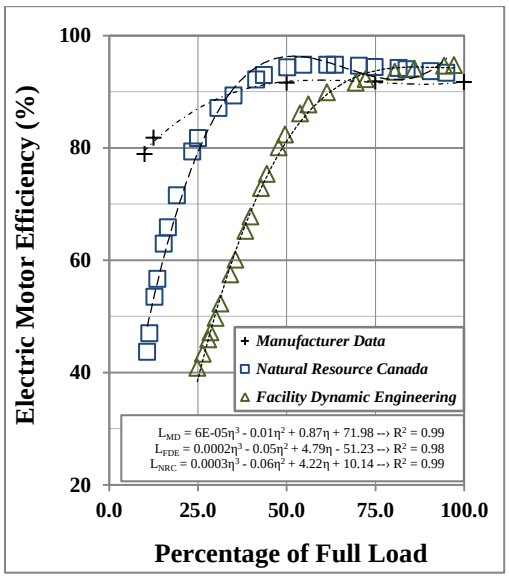

a)

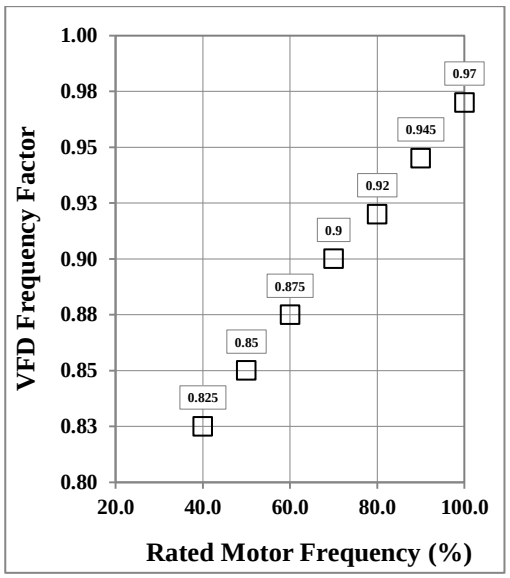

b)

Figure 5-3: a) Electric motor efficiency vs. load at 188 rad/s (1800 rpm), b) VFD controller efficiency factor

5.2.5. Uncertainty Analysis

Two individual sets of experiments were conducted on wheat straw particles of four different sizes (Table 5-1) to assure reproducibility (i.e., reproduce a measurement whenever a pre-defined set of conditions is recreated) and to investigate the uncertainty involved in the results. Uncertainty was measured according to the ISO uncertainty analysis guideline [50] by calculating the precision (repeatability) uncertainty (P_x) of the pressure measurements and the bias (systematic) uncertainty (B_x) of the suction and discharge pressure gauges, which eventually give the total uncertainty (U_x). Table 5-7

reports the uncertainty involved in the centrifugal pump suction/discharge pressure measurements for 2.0 to 6.5% solid mass content slurries of 6.4 mm wheat straw particles at 167 rad/s (1600 rpm) and 2.0 to 8.8% solid mass content slurries of <3.2 mm wheat straw particles at 185 rad/s (1765 rpm), with a maximum precision uncertainty of ±0.12 m_{slurry} and a total uncertainty of ±0.5 m_{slurry} for the entire measurements. Generally, a minimum uncertainty of 3.9% and a maximum uncertainty of 4.4% were obtained through the course of the present experiment. Fig. 5-4 presents the variation of the total head height versus the pump flow rate for various solid mass contents and rotational speeds for two individual trials, together with 95% confidence level lines for trial No. 1. As observed, the measurements corresponding to trial No. 2 fall well within the 95% confidence level lines of trial No. 1, indicating the good agreement and acceptable level of reproducibility of the results.

Table 5-7: Repeatability and systematic uncertainty in suction/discharge pressure measurements

Nominal Particle Size, mm	Rotational Speed, rad/s (rpm)	Slurry Dry matter Solid Mass Content, %	Standard Deviation, kPa	Precision Uncertainty (P_X), kPa	Bias Uncertainty (B_X), kPa	Total Uncertainty (U_X), kPa
6.4	167 (1600)	2.0	1.96	0.91	5.18	5.26
		4.3	2.07	0.96		5.26
		6.5	2.53	1.18		5.30
<3.2	185 (1765)	2.0	1.41	0.66		5.22
		4.3	1.43	0.67		5.21
		6.5	1.74	0.81		5.22
		8.8	2.28	1.06		5.26

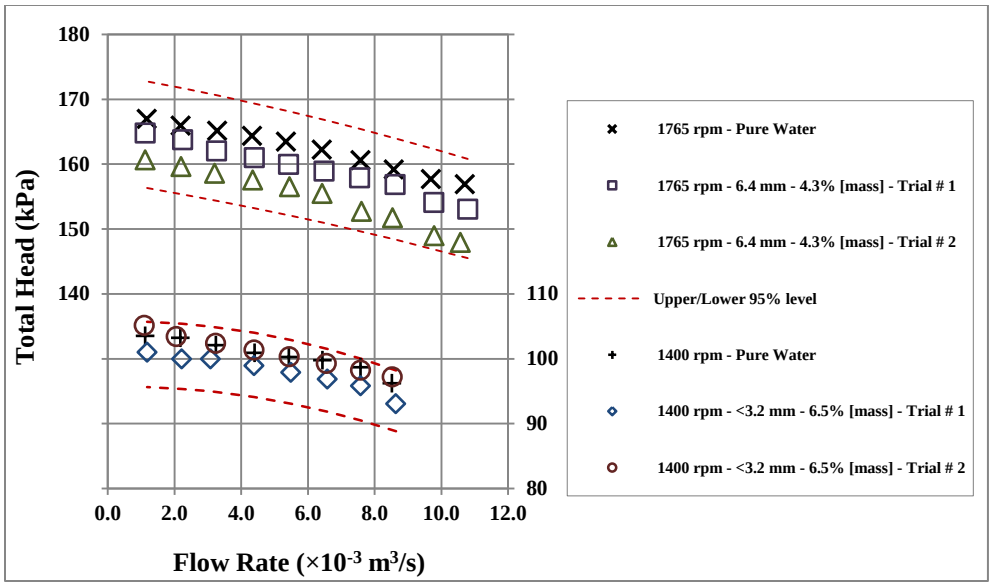

Figure 5-4: The reproducibility of two sets of pump performance evaluation experiments using 6.4 mm and <3.2 mm wheat straw particles at 185 rad/s (1765 rpm) and 146 rad/s (1400 rpm)

5.3. Experimental Result and Discussion

5.3.1. Characterizing the Slurry Flow of Agricultural Residue Biomass

Fig. 5-5(a) represents the friction factor versus slurry bulk velocity in the flow of wheat straw and corn stover particles slurry per unit length, measured through a 7.5 m horizontal test section of 50 mm diameter and 22.5 m long closed-circuit pipeline over a velocity range of 2.0 to 5.0 m/s (drag reduction region only). The friction loss behaviors of the flow of agricultural residue biomass slurry appeared to be predominantly similar to those for natural and synthetic fibres [18-27] as discussed in introduction section. Non-common fibrous particles of agricultural residue biomass with noticeably large dimensions of 2.0 to 9.0 mm in size and considerably small aspect ratios of 2 to 7 resulted in the friction factor of the slurry being smaller than that for water (exhibited drag reducing behavior) at high solid mass contents and elevated pumping velocities. This is a unique feature of which the detailed mechanisms, together with the impact of particle morphological features, slurry properties, and pumping velocity on friction loss behavior of agricultural residue biomass slurry through pipelines, have been discussed in a previously published papers [17, 28].

The friction factors for the slurry of a common type of sand (play sand) with known specifications (Table 5-6) obtained is shown on Fig. 5-5(b). In a clear contrast with the slurry of agricultural residue, the friction factor in the water-sand mixture is greater than that for water at the same slurry bulk velocity by an amount that is proportional to the volume content of the solid. Furthermore, while the agricultural residue biomass-water mixtures present decreasing pressure gradients with increasing solid mass contents, more concentrated sand-water mixtures studied here showed an increasing trend producing of higher friction losses than the carrier liquid flowing alone. The same effect has been reported for typical solid-liquid mixtures such as coal, ash, etc. [41, 51-54].

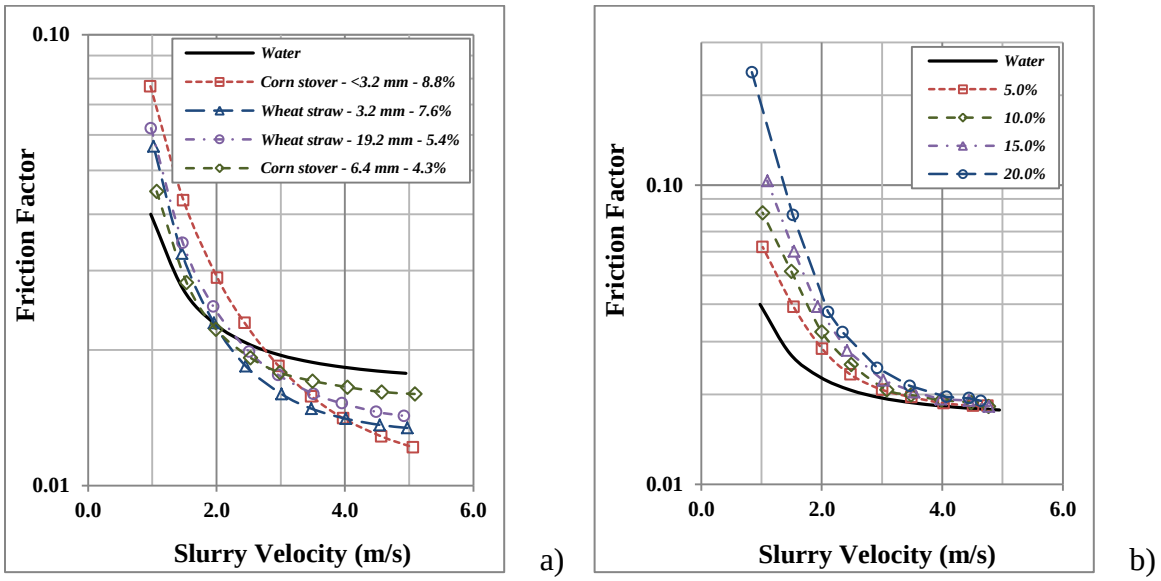

Figure 5-5: Friction factor vs. slurry bulk velocity for velocities above 1.0 m/s in a 50 mm diameter pipeline for various dry matter solid mass content slurries of a) wheat straw and corn stover particles and b) play sand particles

5.3.2. Evaluating the Performance of the Pump Handling Pure Water

The performance curve of the centrifugal slurry pump handling pure water only was precisely developed and is presented on Fig. 5-6. The maximum centrifugal pump efficiency achievable was about 41%. The corresponding values of produced head, discharge rate, and input power were 157.16 kPa (16.03 meter of head), 0.01078 m^3/s (10.78 L/s), and 3.9 kW, respectively, which showed reasonable agreement with the data given by the manufacturer in the range of operation [35]. However, it is not appropriate

to evaluate the performance of the pump handling slurries based on the performance of the pump when pumping water only, because a satisfactory performance with water does not necessarily imply good efficiency when pumping slurries.

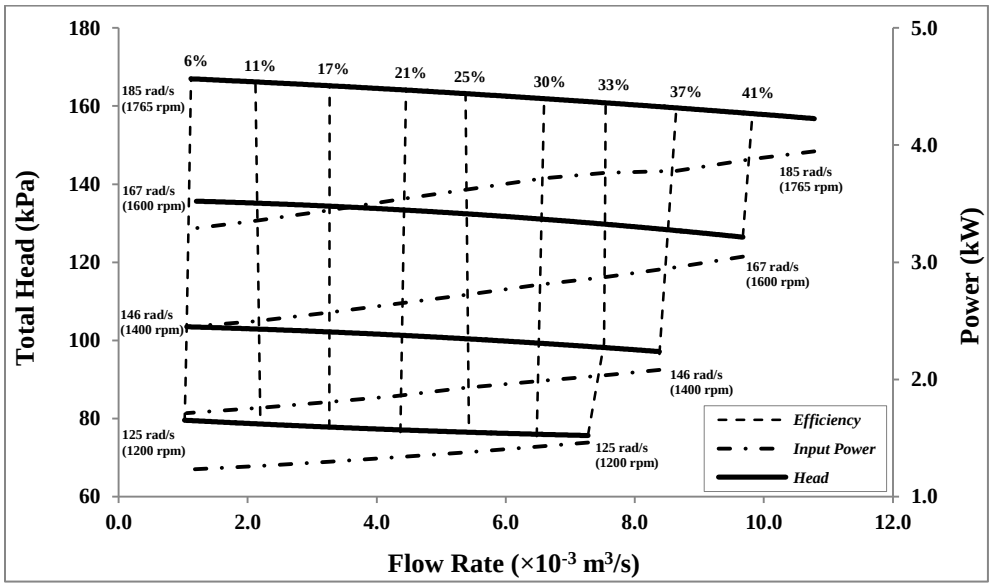

Figure 5-6: Performance curve developed for the centrifugal slurry pump while handling pure water

5.3.3. Evaluating the Performance of the Pump Handling Wheat Straw Slurries

The results of the experiments conducted here on a centrifugal slurry pump for various slurry solid mass contents of agricultural residue biomass differ considerably from those commonly presented in the literature [11-13, 15]. The performance of the centrifugal pump handling slurry of 6.4 mm wheat straw particles was qualitatively similar to the performance of the pump handling 3.2 and 19.2 mm particles, and different from its performance while pumping <3.2 mm particles. Therefore, the pump performance graphs corresponding to 6.4 mm wheat straw particles were chosen to represent particles ≥3.2 mm in size and were compared with the performance graphs of <3.2 mm particles on Fig. 5-7, over the entire range of applied flow rates of 0.001 to 0.011 m^3/s (1.0 to 11.0 L/s) and solid mass contents of 0.0 to 8.8% at 185 rad/s (1765 rpm). In this section, the effect of slurry solid mass content and particle size on head, efficiency, and power of the centrifugal slurry pump has been investigated.

5.3.3.1. Analyzing the Head Height of the Centrifugal Slurry Pump

The curves corresponding to the total head height, shown in Figs. 5-7(a) and 5-7(b), illustrate (1) expected behavour (i.e., decreasing head with increase in flow rate) similar to pure water, (2) decreasing head with increase in particle size, and (3) the total head always less than, or equal to, pure water.

The centrifugal pump handling slurry of 4.3% solid mass content of 6.4 mm wheat straw particles produced 152.9 kPa (15.6 meter of head) head at 0.0108 m^3/s (10.8 L/s) and 185 rad/s (1765 rpm), and the pump handling slurry of 4.3% solid mass content of 19.2 mm wheat straw particles produced 150 kPa (15.3 meter of head) head at similar operating conditions. This small difference can be explained according to the difference in particle motion mechanisms, as the head loss is higher for larger particles due to the extra energy required to keep the particles in motion.

However, in a clear contrast to the centrifugal pump performance curves of conventional solid-liquid systems [2, 5, 51], the head height increases with an increase in solid mass content, as for <3.2 mm particles slurry at a flow rate of 0.0085 m^3/s (8.5 L/s) (Fig. 5-7(a)), the head height is 154.9 kPa (15.8 meter of head) at 2.0% solid mass content, compared to 158.8 kPa (16.2 meter of head) with pure water, and 157.8 kPa (16.1 meter of head) at 8.8% solid mass content, all at 185 rad/s (1765 rpm). This phenomenon could be attributed to the drag reducing feature of the slurry of fibrous wheat straw particles (section 3.1 and [17]) in the pump [52] similar to what was observed throughout the pipeline (Fig. 5-9 - where at sufficiently high velocities the friction loss of the slurries of <3.2 mm and 6.4 mm particles are less than, or equal to, the pressure drop of pure water at the same flow rate, caused by the drag reducing effect of the fibrous wheat straw particles), change in slippage, or damping of turbulence. Furthermore, increased slurry solid mass content results in decreased friction loss due to the change in physical structure of the fibre suspension [17]. This could potentially be the reason the head height increases with an increase in slurry solid mass content in the centrifugal pump. Understanding the true reason behind such behavior requires further study of the behavior of the flow at the pump.

Horo [6] reported similar results while pumping 4.8% solid volume content slurry of paper stock (groundwood fibre-water mixture) using a specifically designed centrifugal pump (discharge opening diameter = 150 mm, outlet diameter of impeller = 450 mm) at 155 rad/s (1480 rpm). Horo reported an even higher head height (666.6 kPa or 68 meter of head) than the pumping water (637.2 kPa or 65 meter of head), where efficiency remained almost unchanged at 25%. Lowering the pump solid content effect (i.e., effect of solid particles on the pump performance) due to addition/presence of fine particles has also been reported for conventional solid-liquid pumping systems [2, 5, 53] as early as 1974 when Vocadlo [53] reported a slurry head higher than the water head when centrifugally pumping a polythene bead-water mixture.

5.3.3.2. Analyzing the Power Consumption of the Centrifugal Slurry Pump

Figs. 5-7(c) and 5-7(d) show the variation of the pump input power with flow rate. The input power of 6.4 mm-particle slurry (as shown on Fig. 5-7(d)), as well as 3.2 mm- and 19.2 mm-particle mixtures, (a) is behaviorally compatible with typical pump input power of conventional solid-liquid systems, (b) is noticeably greater than corresponding values for pure water, and (c) increases with an increase in solid mass content. In contrast, the input power for <3.2 mm-particle slurry is 83% to 96% smaller than that of water throughout the entire range of flow rates and solid mass contents. For instance, the centrifugal pump studied here requires a minimum of 4.5 kW to pump a 2.0% solid mass content slurry of 6.4 mm wheat straw particles at 185 rad/s (1765 rpm) and 0.0011 m^3/s (1.1 L/s). Keeping the operating conditions constant, the power consumption value reduces to 3.2 kW for pure water and to 2.7 kW for 2.0% solid mass content slurry of <3.2 mm wheat straw particles (a 40% reduction). The power consumed in centrifugally pumping the slurry of <3.2 mm particles of corn stover was measured to compare with that of <3.2 mm wheat straw particles, where the input power values were all smaller than corresponding values for pure water too.

While the pump input power is generally proportional to the density of the slurry (Table 5-1), the difference observed for small and large particles is attributed to the various particle sizes, PSDs, and the rheological behavior of the carrier liquid and the slurry. As

previously mentioned, extra energy is required to keep the larger solid particles in motion. In addition, <3.2 mm wheat straw particles come with a narrow length band (Fig. 5-1(a)) with more than 90% of the particles smaller than 0.4 mm, which, together with a fraction of fine (<0.05 mm) partiulates (whose presence has already been proven by increasing density and viscosity of the carrier liquid [17]), help in suspending larger particles; therefore, at the same slurry solid mass content, the energy spent is lower for smaller particles.

At fixed particle size, the energy required increased with an increase in slurry solid mass content [2]. This is attributed to the apparent suspension viscosity, which takes into account the rheology of the entire suspension and is a function of fibre dimension and slurry solid mass content, in order that increases with decreasing fibre size (at similar aspect ratio) changes linearly with lower solid mass contents and is proportional to the cube of higher solid mass contents [17, 54]. Consequently, increasing the slurry solid mass content resulted in an increased suspension viscosity and, subsequently, increased power consumption to pump the correspondingly more viscous slurry.

5.3.3.3. Analyzing the Efficiency of the Centrifugal Slurry Pump

Variation in pump efficiency versus flow rates is shown on Figs. 5-7(e) and 5-7(f). As with power consumption, the efficiency of the pump handling the slurry of <3.2 mm particles varied differently with respect to water compared to the efficiency while pumping slurries of larger wheat straw fibres. The former came with an efficiency of 2 to 20% greater than the efficiency of the pump handling pure water at the same operating conditions, and the latter had a lower efficiency than that of the pump handling pure water; an effect which has been reported for conventional solid-liquid systems [2, 5, 51]. The efficiency of both, however, decreased with an increase in slurry solid mass content, as the corresponding head decrease (discussed in section 5.3.3.1) did not lower the power consumption. The deviation in efficiency at lower flow rates is lowest compared to higher flow rates. The maximum increase in efficiency, with respect to the efficiency of the pump handling pure water, was 18.4% at 2.0% solid mass content slurry of <3.2 mm particles at 0.0022 m^3/s (2.2 L/s), where a considerable saving in energy was achieved

and the maximum drop in efficiency was 38% measured while pumping 6.5% solid mass content slurry of 6.4 mm particles at 0.00108 m^3/s (1.08 L/s).

Figure 5-8 presents the head height and efficiency produced by the same pump handling 2.0 to 6.5% slurries of 3.2 mm and 19.2 mm wheat straw particles at 125 rad/s (1200 rpm). Although decreased pump rotational speed limiteded the pump flow rate, the performance of the pump followed the same trend as obtained for 6.4 mm particles.

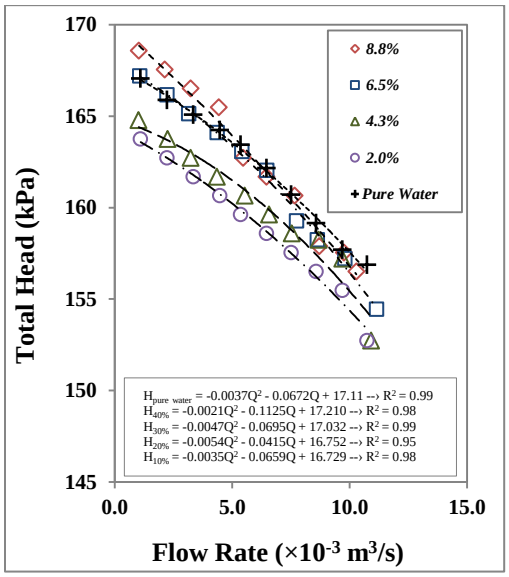

a)

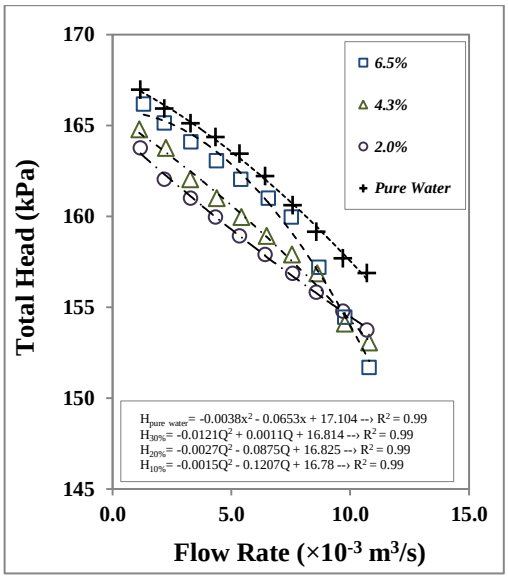

b)

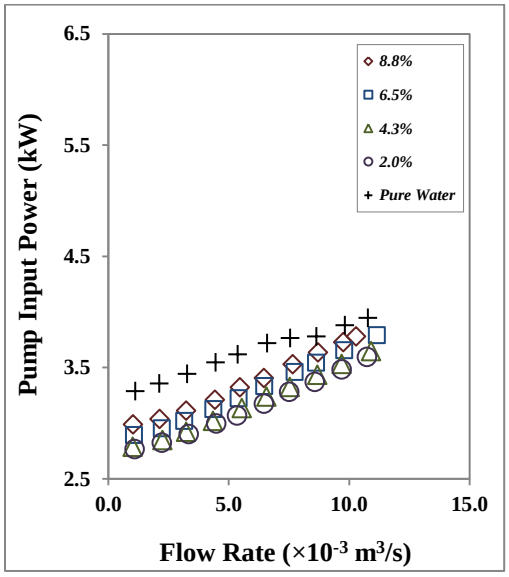

c)

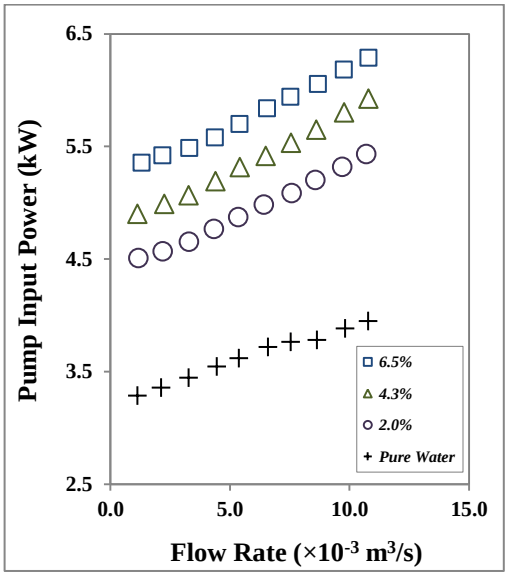

d)

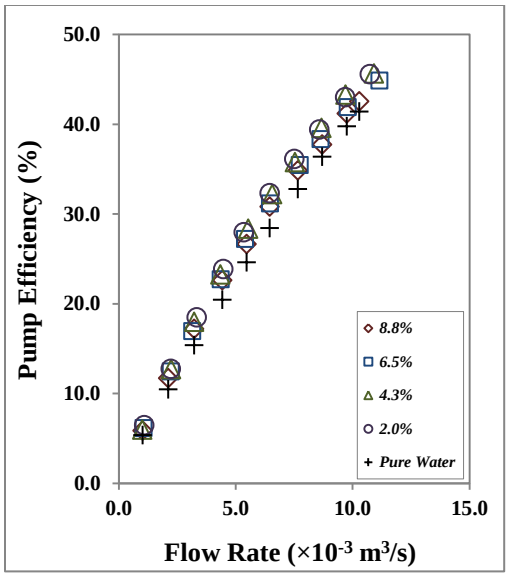

e)

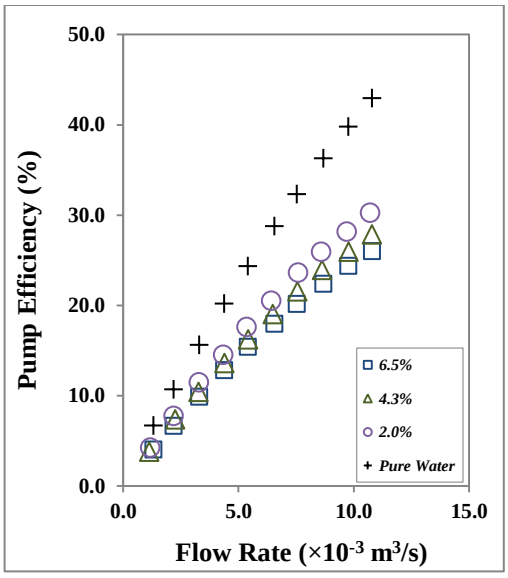

f)

Figure 5-7: Centrifugal slurry pump performance characteristics (pump head, input power, and efficiency) over a range of flow rates (0.5 to 5.0 m/s) and dry matter solid mass contents (2.0 to 8.8%) at 185 rad/s (1765 rpm). a), c), and e) show characteristics for <3.2 mm wheat straw particle slurries; b), d), and f) show characteristics for 6.4 mm wheat straw particle slurries

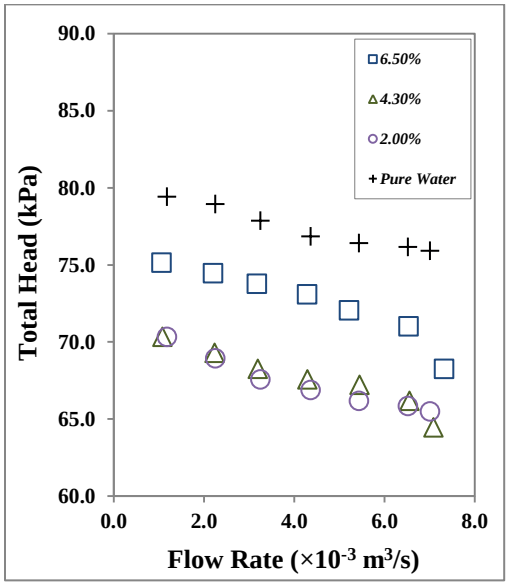

a)

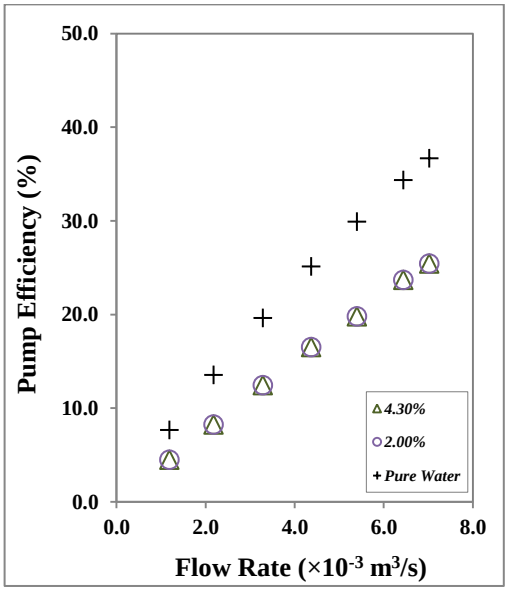

b)

Figure 5-8: Centrifugal slurry pump performance characteristics over a range of flow rates (0.5 to 3.5 m/s) and dry matter solid mass contents (2.0 to 6.5%) at 125 rad/s (1200 rpm). a) shows pump head for 3.2 mm wheat straw particle slurries; b) shows efficiency for 19.2 mm wheat straw particle slurries

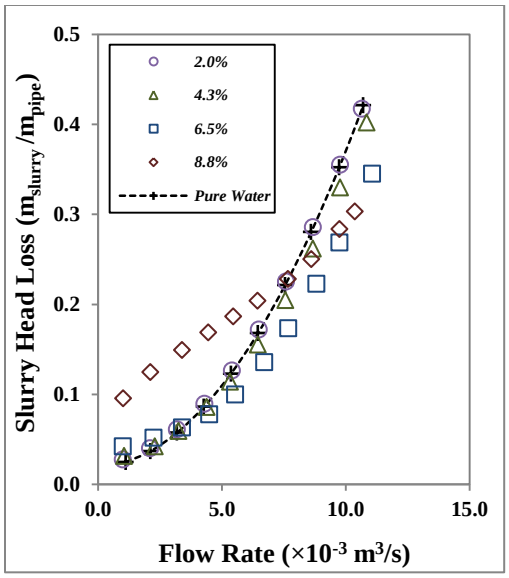

a)

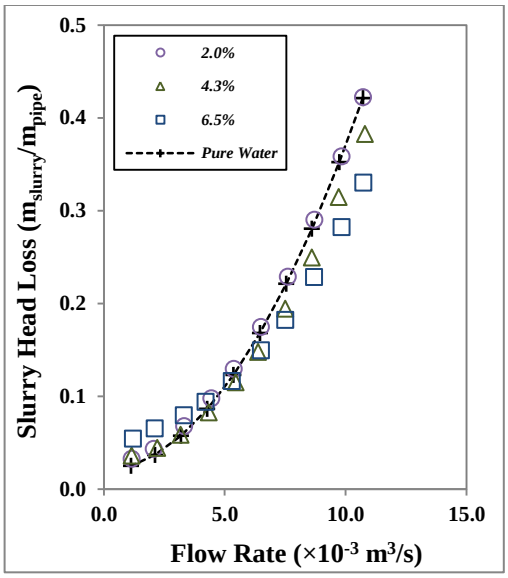

b)

Figure 5-9: Pressure drop per unit length of the pipeline vs. flow rate for slurries of a) <3.2 mm and b) 6.4 mm wheat straw particles through a 50 mm diameter pipeline.

5.3.3.4. Head Ratio, Power Ratio, and Efficiency Ratio

To compare the performance of the pump handling slurries of various particles sizes with the pump handling pure water only over the entire range of flow rates and solid mass contents, the measured data were expressed in terms of head ratio (H_r), efficiency ratio (E_r) and power ratio (P_r), as the developed head, efficiency, and the input power drawn by the pump handling slurry with respect to the pump handling pure water only (Fig. 5-10). The head ratio, efficiency ratio, and power ratio did not vary significantly with flow rate, and the variation is within ±1.8% throughout the entire range of velocity (0.5 to 5.0 m/s) tested for given solid mass contents (Fig. 5-11). Consequently, it can be reasonably concluded that these ratios are independent of the flow rate. Similar conclusions have been made by others while pumping conventional solid particles [2, 5, 14, 51]. The slurry solid mass content parameter, however, impacted the ratios more noticeably, e.g., a reduction of 6.6% in head ratio was measured while diluting a slurry of 3.2 mm wheat straw fibres from 6.5 to 2.0% solid mass content at 125 rad/s (1200 rpm). The head ratio (and the total head produced) was reduced linearly with a decrease in slurry solid mass content due to a change in slurry mechanical features and corresponding reduction in drag-reducing ability (section 3.1 and [17]). Mez [55] reported the opposite trend while

pumping a slurry of coal and gravel particles. With regards to efficiency, an increase of 10.0% in efficiency ratio was observed while diluting the slurry of 6.4 mm wheat straw particles from 4.3 to 2.0% solid mass content at 146 rad/s (1400 rpm), because less power is required to pump the less viscous slurry.

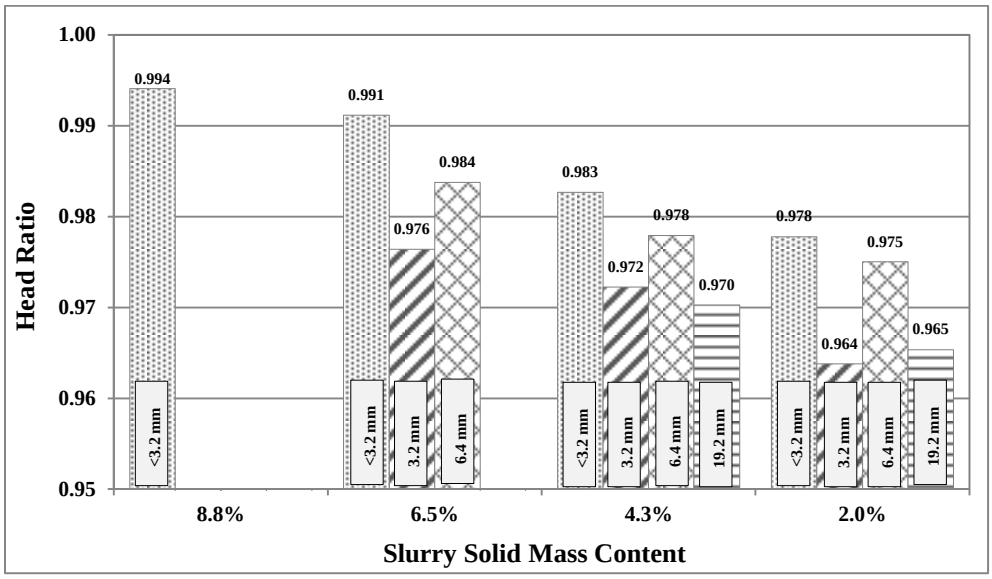

a)

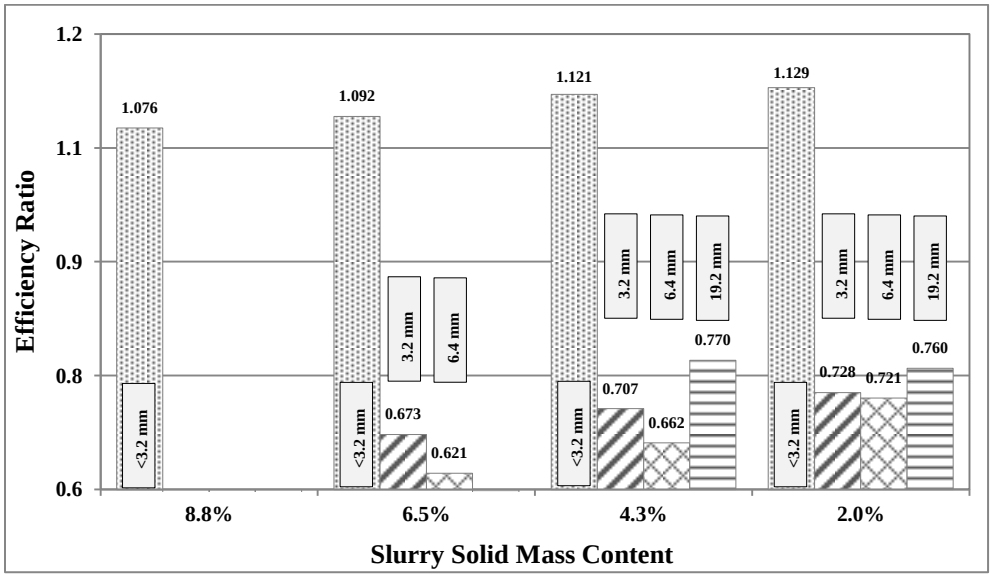

b)

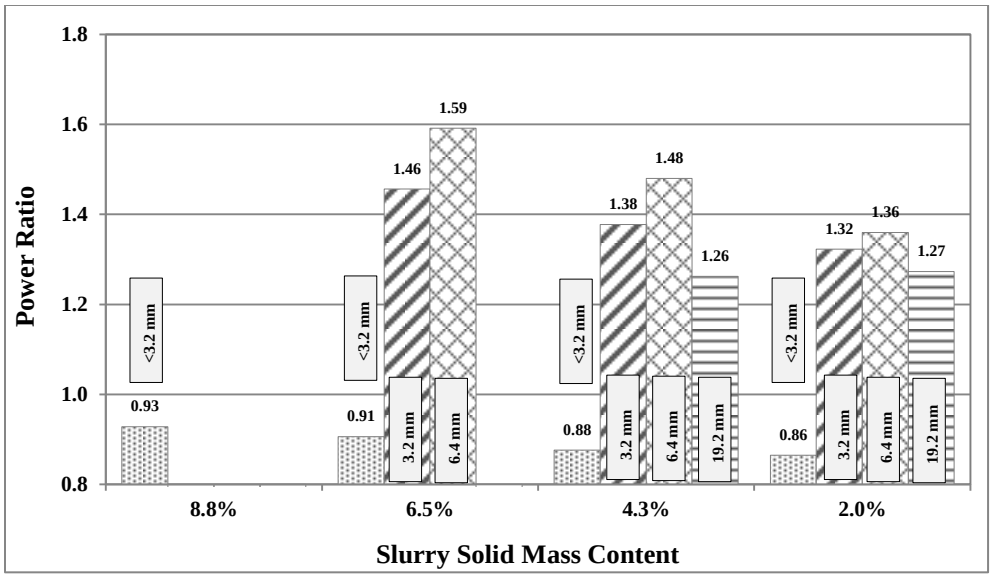

c)

Figure 5-10: Variation of a) head ratio, b) efficiency ratio, and c) power ratio with particle diameters and slurry dry matter solid mass contents at 185 rad/s (1765 rpm)

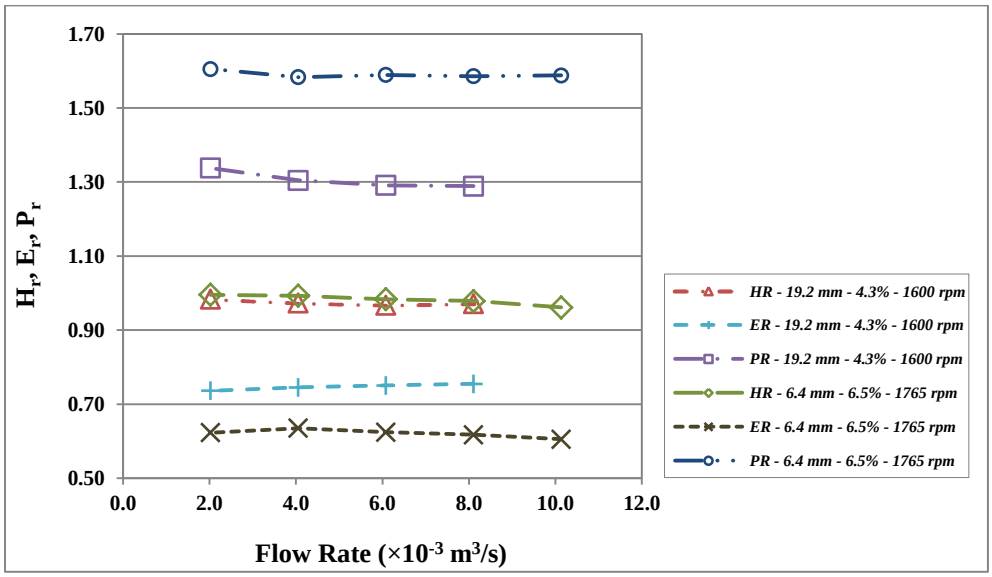

Figure 5-11: The variation of head, efficiency, and power ratios with slurry flow rate

5.4. Empirical Correlation

The effect of agricultural residue biomass particles on centrifugal slurry pump performance is a major consideration in the pump selection procedure and slurry handling facility design. Designing the system based on the performance of the pump handling

pure water only may lead to an inefficient use of the system and even the failure of the equipment. The knowledge of how the presence of solid particles affects the performance of the pump was developed in the previous section. However, there is no correlation reported in the literature to predict the change in the head while pumping agricultural residue biomass particles. In this section, the applicability of pump performance correlations previously developed for common solid particles is investigated for agricultural residue biomass particles studied here. An improved correlation is proposed to predict the head reduction of centrifugal slurry pumps and, finally changes in the efficiency of the centrifugal slurry pumps.

5.4.1. Existing Correlations vs. Experimental Measurements

Among several investigators, Cave [10], Kazim et al. [14], and Engin and Gur [9, 56] proposed general empirical correlations that predict the effect of solid particles on the head ratio of centrifugal slurry pumps (Eqs. 4-7). Cave's correlation estimates a head ratio within ±10% of measured values for particle sizes up to 1.29 mm and solid volume contents up to 20%. Kazim's equation comes with a ±10% error in predicting the head reduction factor (K_H) over a wide range of density of 1480 to 6230 kg/m^3, particle sizes (d_{50}) of 0.105 to 26.7 mm, and slurry solid mass content up to 62.75%. Finally Engin's expression error band in predicting the head reduction factor lies within the range of ±15% covering a wide range of density from 1480 kg/m^3 to 6240 kg/m^3, representative particle sizes from 0.030 to 26.7 mm, slurry solid mass content up to 65.742%, and impeller exit diameters from 210 to 850 mm.

[10] $$Cave: H_r = 1 - K_H = 1 - [0.0385(S_p - 1)(1 + 4/S_p)C_w \ln(d_{50}/22.7)] \quad (4)$$

[9] $$Engin\ I: H_r = 1 - [0.11C_w(S_p - 1)^{0.64} \ln(d_{50}/22.7)] \quad (5)$$

[56] $$Engin\ II: H_r = 1 - [2.705C_w(S_p - 1)^{0.64}(d_{50}/D_{imp})^{0.313}] \quad (6)$$

[14] $$Kazim: H_r = 1 - [0.13C_w\sqrt{S_p - 1} \ln(d_{50}/20)] \quad (7)$$

In order to examine the applicability of the proposed correlations for slurries of agricultural residue biomass particles, physical properties of <3.2 mm wheat straw particles and solid mass contents of corresponding solid-water mixtures (2.0 to 8.8% solid mass content) were substituted in correlations (4) to (7) and the head ratios predicted were compared with the head ratios experimentally measured. As observed on Fig. 5-12, while mathematically predicted and experimentally measured head ratios are all of the same order of magnitude, the trends are opposite; the head ratio increases with increasing solid mass contents of agricultural residue biomass slurries, in contrast with common conventional solid-liquid mixtures. This shows that the head ratio correlations proposed for conventional solid-liquid mixtures are not applicable to agricultural biomass slurries.

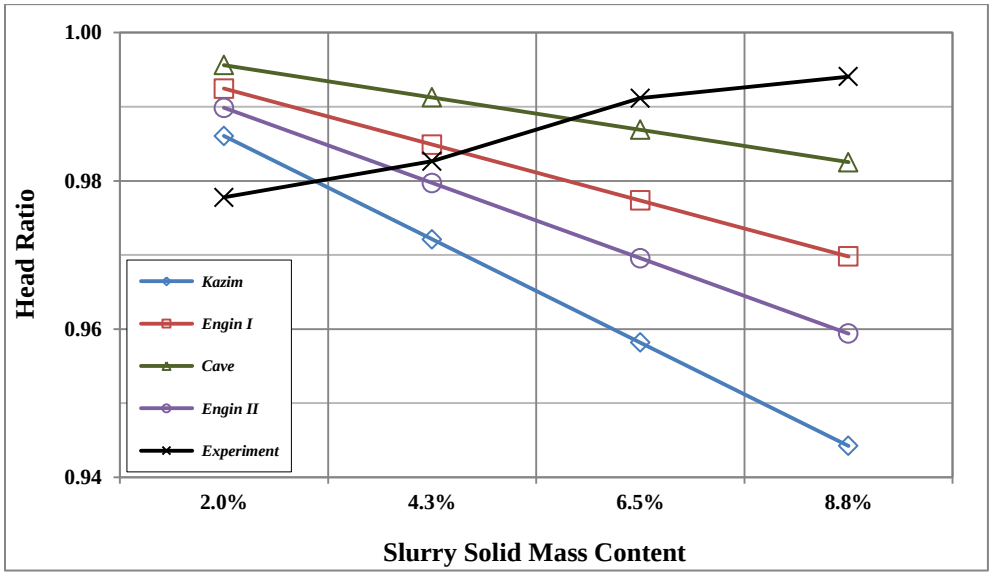

Figure 5-12: Accuracy of proposed correlations in the literature for prediction of head ratio of slurries of <3.2 mm wheat straw particles

5.4.2. A modified Empirical Correlation

Centrifugal slurry pump performance data were collected from the literature [9, 10, 13, 15] for a wide variety of conventional solid particles (e.g., sand, coal, iron ore, fly ash) over a wide range of physical properties of solids, e.g., density (1480 to 6240 kg/m^3), particle size (0.030 to 26.7 mm), and solid mass content (up to 65% solid mass content). Pump flow rate was not taken into account because, as it was previously concluded, the

change in the pump head and efficiency is independent of the pump flow rate (Fig. 5-11). The correlation proposed by Engin and Gur [56] (Eq. 5) was used to predict the head ratio of corresponding slurries over a corresponding range of solid mass contents. Since the head ratio of the slurry of common solid particles was (1) of the same order of magnitude as the slurry of agricultural residue biomass and (2) decreased with increasing solid mass content in contrast to the slurry of agricultural residue biomass, the order of the results for the head ratio with respect to the slurry solid mass content was reversed to provide a database of head ratio of the slurries that mechanically behave similarly to the slurry of agricultural residue biomass particles. The least squares (e.g., non-linear least squares (NLS) and auto regressive moving average (ARMA)) regression analysis method was used to model the variation of newly calculated head ratios with particle specific gravity (particle density with respect to water at the same temperature), particle dimension, and slurry solid mass content, as follows:

$$H_r = 1 - [(0.4C_w - 0.3)(0.1d_{50}^2 + 28)(-0.0016S_p^{1.7})] \quad (8)$$

The model consisted of a R^2 equal by 0.88 which confirmed the acceptable overall fit of the estimated regression line to the input data. The proposed model was then used to predict the head ratio while pumping the slurry of agricultural residue biomass particles over a range of median particle sizes (d_{50}) of 2.42 to 8.29 mm (Table 5-1) and solid mass contents of 2.0 to 8.8% and the results were compared with experimental measurements (Fig. 5-13). A good agreement was observed between measured and predicted head ratios with a negligible uncertainty of ±1.0%. This model can be used to predict the performance of centrifugal pumps while handling slurries of fibrous agricultural residue biomass particles with large aspect ratios (X_{gl}:$X_{gl,width}$>>1) and similar shape factors (as discussed in section 2.1.2). However, cautious should be taken while applying the model to other sorts of fibrous particles.

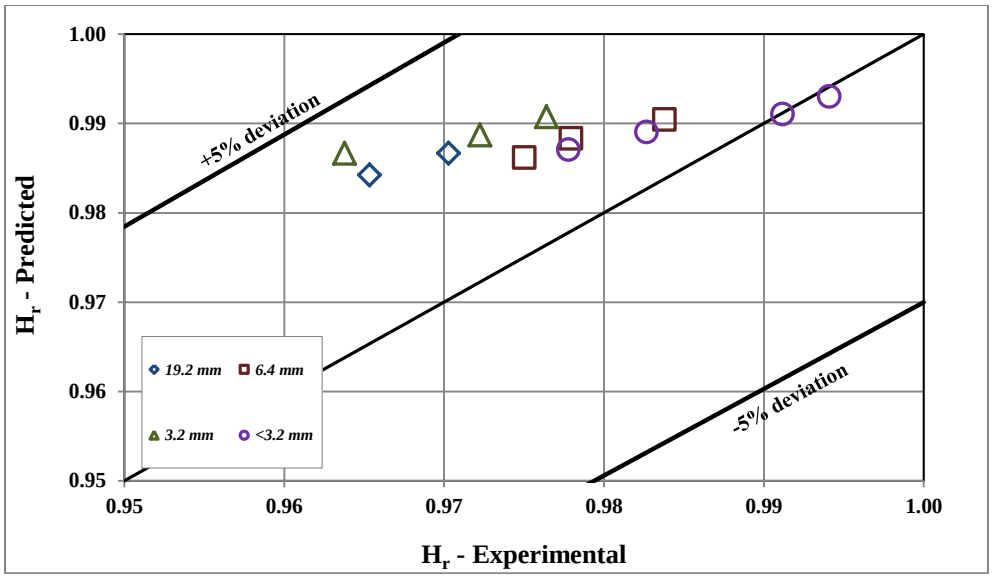

Figure 5-13: Accuracy of modified correlation for prediction of head ratio of the slurry of agricultural residue biomass particles

5.4.3. Comparison Between Head and Efficiency Ratios

Several investigators reported the power ratio to be approximately equal to the specific gravity of the homogenous (conventional) solid-liquid mixtures at a fixed flow rate, which means the efficiency ratio could be considered equal to the corresponding head ratio for practical applications [10, 53, 57], more specifically in small pumps [58]. Although a deviation of 2 to 10% between head ratio and efficiency ratio has been reported in the literature [2, 13, 15], the modified correlation proposed here to predict the head ratio of the slurry of agricultural residue biomass, if applied to predict the efficiency ratio, results in about ±20% under- and overestimations (Fig. 5-14(a)). While applying the correlations proposed in the literature to predict the efficiency ratio of the centrifugal pump handling slurries of agricultural residue biomass particles resulted in efficiency ratios between 0.94 and 0.98 (Fig. 5-11), the experimentally measured efficiency ratio of the pump varied between 0.6 and 0.8 for coarse wheat straw particles (3.2, 6.4, and 19.2 mm) and rose to above 1.0 for fine particles (<3.2 mm) (Fig. 5-14(b)). Consequently, the modified correlation proposed here should be used with caution when applied to predict the efficiency ratio of fibrous particles and, depending on the size of the particles, a deviation from -20% to +10% should be considered.

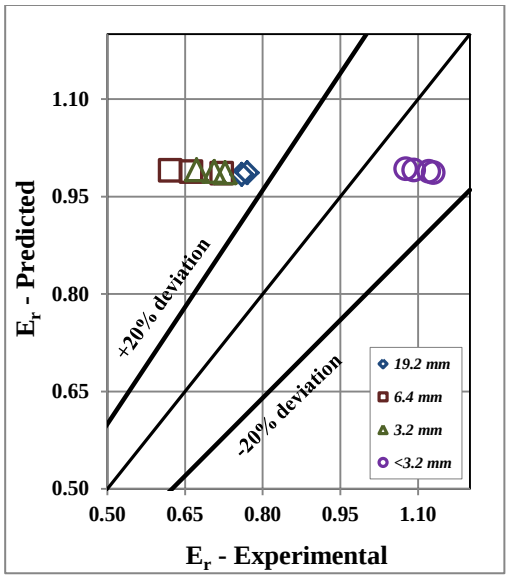

a)

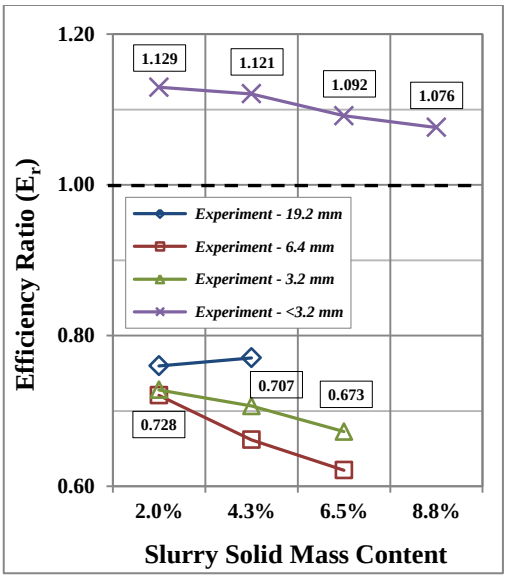

b)

Figure 5-14: a) Accuracy of modified correlation for predicting the efficiency ratio of the slurry of agricultural residue biomass particles, b) Variation of efficiency ratios with wheat straw particle diameter and slurry dry matter solid mass content at 185 rad/s (1765 rpm)

5.5. Effect of Pump Size

The results discussed in the previous section were obtained from a medium size pump (Table 5-3) and needed to be extended to large size pumps. Sellgren and Addie [59] proposed a correlation to correlate variation in head with individual pump design factors (Eq. 9), when it was clearly demonstrated that the effect of solid particles are much smaller in large pumps.

$$\frac{1-H_{r,2}}{1-H_{r,1}} = \left(\frac{D_{imp,2}}{D_{imp,1}}\right)^{-0.9} \tag{9}$$

The results obtained here for fibrous agricultural residue biomass could be well scaled up using Eq. 9, as Wilson [60] demonstrated the applicability of scale-up techniques for turbulent flows to solutions exhibiting drag reduction, similar to the mixtures studied here.

5.6. Conclusion

The effect of wheat straw fibrous agricultural residue biomass slurry on the performance characteristics of centrifugal slurry pumps was experimentally investigated using a lab-scale pipeline facility. Pumping a play sand-water mixture through the same closed-circuit pipeline under similar operating conditions and comparing corresponding friction loss behavior with that of agricultural residue biomass slurry demonstrated the unique mechanical behavior of wheat straw-water mixtures. In contrast to all conventional solid-liquid mixtures, the head increased with an increase in slurry solid mass content for agricultural biomass slurry. It was observed that by using small size wheat straw fibrous particles (< 3.2 mm) under known slurry solid mass contents and pump operating conditions, it is possible to keep the total head and efficiency at the same level as the pump handling pure water and to reduce the power consumption to below that required for pumping pure water alone. Finally, a correlation was developed to predict the reduction in head of the centrifugal slurry pumps while handling agricultural residue biomass slurries, with respect to the head produced while handling pure water. The results obtained here could be used in the design and handling of pumps and pipelines in the hydro-transport of fibrous agricultural residue biomass and similar solid particles.

Nomenclature

PSD	Particle size distribution
MC	Wet-basis water mass content (moisture content), %
NLS	Non-linear least squares
ARMA	Autoregressive moving average
$\mathbf{L_{MD}}$	Electric motor load – data provided by manufacturer
$\mathbf{L_{FDE}}$	Electric motor load – data provided by Facility Dynamic Engineering
$\mathbf{L_{NRC}}$	Electric motor load – data provided by Natural Resource Canada
$\boldsymbol{H}$	Electric motor efficiency, %
$\boldsymbol{Q}$	Flow rate, m^3/s
$\boldsymbol{A_s}$	Solid particle area, mm^2
$\boldsymbol{S_x}$	Standard deviation of the measurements ($S_x = \sqrt{\sum(x_i - \bar{x})^2/n-1}$), corresponding unit
$\boldsymbol{P_x}$	Precision uncertainty ($P_x = t_{\frac{\propto}{2},v}\frac{S_x}{\sqrt{n}}$), corresponding unit
$\boldsymbol{B_x}$	Bias uncertainty, corresponding unit
$\boldsymbol{U_x}$	Total uncertainty ($U_x = \sqrt{\sum B_x^2 + P_x^2}$), corresponding unit
$\boldsymbol{V_m}$	Solid-liquid mixture velocity, m/s
$\boldsymbol{M_s}$	Mass of solid particle sample, g
$\boldsymbol{X_{gl}}$	Geometric mean length, mm
$\boldsymbol{X_{gl,width}}$	Geometric mean width, mm
$\boldsymbol{D_{pipe}}$	Pipe internal diameter, m
$\boldsymbol{Re_g}$	Generalized Reynolds number, ($Re_g = \rho_m V_m D_{pipe}/\mu_f$)
$\boldsymbol{C_w}$	Saturated solid mass content, %
$\boldsymbol{C_v}$	Saturated solid volume content, %
$\boldsymbol{H_{C\%}}$	Head height produced by the centrifugal pump for C_w% solid mass content slurry, kPa
$\boldsymbol{H_r}$	Head ratio: $\frac{\text{head developed with slurry at any flow rate}}{\text{head developed with water at the same flow rate}}$
$\boldsymbol{E_r}$	Efficiency ratio: $\frac{\text{efficiency of the pump for slurry at any flow rate}}{\text{efficiency of the pump for water at the same flow rate}}$
$\boldsymbol{K_H}$	Head reduction factor
$\boldsymbol{S_p}$	Specific gravity of saturated solid particles
$\boldsymbol{D_{imp}}$	Pump impeller exit diameter, mm
$\boldsymbol{n}$	Number of measurements
$\boldsymbol{d_{50}}$	Median length, mm
$\boldsymbol{\lambda}$	Thickness factor
$\boldsymbol{\rho_s}$	Solid particle density, kg/m^3
$\boldsymbol{\rho_m}$	Density of mixture, kg/m^3
$\boldsymbol{\sigma_{gl}}$	Geometric mean length standard deviation, mm
$\boldsymbol{\sigma_{gl,width}}$	Geometric mean width standard deviation, mm
$\boldsymbol{\mu_f}$	Dynamic viscosity of carrier liquid, Pa s
$\boldsymbol{t_{\frac{\propto}{2},v}}$	t-distribution with $\alpha = 1 - 95$ % confidence and $v = n - 1$

References

[1] Kumar, A., Cameron, J.B., Flynn, P.C. Large-scale ethanol fermentation through pipeline delivery of biomass. Applied Biochemistry and Biotechnology, 2005; 121: 47-58.

[2] Gandhi, B.K., Singh, S.N., Seshadri, V. Performance characteristics of centrifugal slurry pumps. Journal of Fluids Engineering-Transactions of the Asme, 2001; 123: 271-80.

[3] Horo, K., Niskanen, T. Centrifugal Pumps - Research on Pumping Paper Stock. Tappi, 1978; 61: 67-70.

[4] Kazim, K.A., Maiti, B., Chand, P. Effect of drag reducing polymers on the performance characteristics of centrifugal pumps handling slurries. Journal of Polymer Materials, 1997; 14: 245-50.

[5] Sellgren, A., Addie, G., Scott, S. The effect of sand-clay slurries on the performance of centrifugal pumps. Canadian Journal of Chemical Engineering, 2000; 78: 764-69.

[6] Horo, K., Niskanen, T. Pumping paper stock efficiently. Pumps-Pompes-Pumpen, 1979; 156: 427-29.

[7] Fairbank, L.C. Effect on the characteristics of centrifugal pumps. Solids in Suspension Symposium; 1942.

[8] Wiedenroth, W. The influence of sand and gravel on the characteristics of centrifugal pumps, some aspects of wear in hydraulic transportation installations. 1st International Conference on the Hydraulic Transport of Solids in Pipes; 1970.

[9] Engin, T., Gur, M. Comparative evaluation of some existing correlations to predict head degradation of centrifugal slurry pumps. Journal of Fluids Engineering-Transactions of the Asme, 2003; 125: 149-57.

[10] Cave, I. Effects of suspended solids on the performance of centrifugal pumps. Hydrotransport 4: BHRA Fluid Engineering 1976, p. 35-52.

[11] Burgess, K.E., Reizes, J.A. Effect of sizing, specific gravity, and concentration on the performance of the centrifugal slurry pump. Institution of Mechanical Engineers (London), 1976; 190: 391-99.

[12] Sellgren, A. Performance of a centrifugal pump when pumping ores and industrial minerals Hydrotransport, 1979; 1: 291-304.

[13] Gahlot, V.K., Seshadri, V., Malhotra, R.C. Effect of Density, Size Distribution, and Concentration of Solid on the Characteristics of Centrifugal Pumps. Journal of Fluids Engineering-Transactions of the Asme, 1992; 114: 386-89.

[14] Kazim, K.A., Maiti, B., Chand, P. A correlation to predict the performance characteristics of centrifugal pumps handling slurries. Proceedings of the Institution of Mechanical Engineers Part a-Journal of Power and Energy, 1997; 211: 147-57.

[15] Kazim, K.A., Maiti, B., Chand, P. Effect of particle size, particle size distribution, specific gravity and solids concentration on centrifugal pump performance. Powder Handling and Processing, 1997; 9: 27-32.

[16] Vaezi, M., Pandey, V., Kumar, A., Bhattacharyya, S. Lignocellulosic biomass particle shape and size distribution analysis using digital image processing for pipeline hydro-transportation. Biosystems Engineering, 2013; 114: 97-112.

[17] Vaezi, M., Katta, A.K., Kumar, A. Investigation into the mechanisms of pipeline transport of slurries of wheat straw and corn stover to supply a bio-refinery. Biosystems Engineering, 2014; 118: 52-67.

[18] Duffy, G.G. measurement, mechanisms, and models: some important insights into the mechanisms of flow of fibre suspensions. Annula Transaction of Nordic Rheology Society, 2006; 14: 19-31.

[19] Duffy, G.G., Titchener, A.L., Lee, P.F.W., Moller, K. The mechanism of flow of pulp suspensions in pipes. Appita, 1976; 29: 363-70.

[20] Paul, T., Duffy, G., Chen, D. New insights into the flow of pulp suspensions. Tappi Solutions, 2001; 1.

[21] Duffy, G.G., Lee, P.F.W. Drag reduction in turbulent flow of wood pulp suspensions. Appita, 1978; 31: 280-86.

[22] Lee, P.F.W., Duffy, G.G. Analysis of drag reducing regime of pulp suspension flow. Tappi, 1976 (a); 59: 119-22.

[23] Bobkowic, A., Gauvin, W.H. Turbulent flow characteristics of model fibre suspensions. Canadian Journal of Chemical Engineering, 1965; 43: 87-91.

[24] Duffy, G.G., Moller, K., Titchene.Al. Determination of Pipe Friction Loss. Appita, 1972; 26: 191-95.

[25] Fock, H., Claesson, J., Rasmuson, A., Wikstrom, T. Near wall effects in the plug flow of pulp suspensions. Canadian Journal of Chemical Engineering, 2011; 89: 1207-16.

[26] Lee, P.F.W., Duffy, G.G. Velocity profiles in drag reducing regime of pulp suspension flow. Appita, 1976 (b); 30: 219-26.

[27] Moller, K., Duffy, G.G., A., T. Laminar plug flow regime of paper pulp suspensions in pipes. Svensk Papperstidning-Nordisk Cellulosa, 1971; 74: 829-34.

[28] Luk, J., Mohammadabadi, H.S., Kumar, A. Pipeline transport of biomass: Experimental development of wheat straw slurry pressure loss gradients Biomass and Bioenergy, 2014.

[29] Scandinavian Pulp, Paper and Board Testing Committee. SCAN CM 40:88. Stockholm, Sweden.

[30] Technical Association of the Pulp and Paper Industry (TAPPI). Usefull methods No. 21. 2010.

[31] American Society of Agricultural and Biological Engineers (ASABE). Moisture measurement for forages. Standard S3582 St. Joseph, MI, US; 2008.

[32] American Society for Testing and Materials (ASTM). Standard test method for density, relative density, and absorption of coarse aggregate. ASTM, Designation C127; 2012.

[33] Rasband, W.S. http://rsb.info.nih.gov/ij/index.html, U.S. National Institutes of Health, Accessed September 2011. 2008.

[34] Kwan, A.K.H., Mora, C.F., Chan, H.C. Particle shape analysis of coarse aggregate using digital image processing. Cement and Concrete Research, 1999; 29: 1403-10.

[35] Godwin Pumps, http://www.godwinpumps.com/en/index.php/godwin-products/cd-range/cd80m/, Accessed Feb. 2014.

[36] Sulzer Pumps - Chapter three - Acceptance tests with centrifugal pumps. Centrifugal Pump Handbook (Third Edition). Oxford: Butterworth-Heinemann; 2010, p. 69-88.

[37] Bureau of Indian Standards (BIS). Technical requirements for rotodynamic special purpose pumps, IS: 5120. Government of India; 1977.

[38] U.S. Department of Energy, Advanced Manufacturing Office. Adjustable speed drive part-load efficiency Motor systems tip sheet#11. Washington, DC; 2012.

[39] SIL Industrial Minerals Inc., http://www.sil.ab.ca/images/stories/pdf/Products/playsand.pdf, Accessed: Jan, 2014.

[40] Lee, P.F.W., Duffy, G.G. Relationships between Velocity Profiles and Drag Reduction in Turbulent Fiber Suspension Flow. Aiche Journal, 1976; 22: 750-53.

[41] Matousek, V. Pressure drops and flow patterns in sand-mixture pipes. Experimental Thermal and Fluid Science, 2002; 26: 693-702.

[42] Sheth, K.K., Morrison, G.L., Peng, W.W. Slip factors of centrifugal slurry pumps. Journal of Fluids Engineering-Transactions of the Asme, 1987; 109: 313-18.

[43] United States Department of Energy. Energy Policy Act of 1992, https://www1.eere.energy.gov/femp/regulations/epact1992.html, Accessed: May, 2013. 1992.

[44] National Electrical Manufacturer Association (NEMA). The NEMA Premium™ efficiency electric motor program. The NEMA Premium™ efficiency levels MG 1-2003, Tables 12-12 and 12-13: NEMA Standards Publication; 2003.

[45] Natural Resources Canada (NRC). Technical fact sheet, Premium efficiency motors, Catalog No. M144-21/2003E. Office of Energy Efficiency, NRC; 2004.

[46] Sellers, D. Variable Frequency Drive System Efficiency – Part 1, Facility Dynamic Engineering, http://av8rdas.wordpress.com/2010/12/18/variable-frequence-drive-system-efficiency, Accessed: May, 2013. 2013.

[47] Nailen, R.L. Just how important is drive motor efficiency? Chicago: Barker Publications, Inc.; 2002.

[48] Center for Energy Efficiency and Renewable Energy (CEERE). Electric Motor Systems. Industrial Assessment Center (IAC): University of Massachusetts, Amherst; 2006.

[49] Wallbom-Carlson, A. Energy comparison. VFD vs. on-off controlled pumping stations. Scientific impeller, ITT Flygt AB, 1998: 29-32.

[50] Internatinal Standards Organization (ISO), Guidance for the use of repeatability, reproducibility and trueness estimates in measurement uncertainty estimation, ISO 21748:2010(E). 2010.

[51] Wilson, K.C., Addie, G.R., Sellgren, A., Clift, R. Slurry transport using centrifugal pumps Third ed. New York, NY, USA: Springer; 2006.

[52] Yadeta, R., Durst, R.E. The behavior of gas-water-fiber systems in centrifugal pumps. Hydrotransport 1. Coventry, UK; 1970.

[53] Vocadlo, J.J., Koo, J.K., Prang, A.J. Performance of centrifugal pumps in slurry service. Hydrotransport 3: BHRA Fluid Engineering 1974, p. MAY 15-7, 1974.

[54] Djalili-Moghaddam, M., Toll, S. Fibre suspension rheology: effect of concentration, aspect ratio and fibre size. Rheologica Acta, 2006; 45: 315-20.

[55] Mez, W. The influence of solids concentration, solids density and grain size distribution on the working behaviour of centrifugal pumps. Hydrotransport 9: BHRA Fluid Engineering; 1984, p. 345-58.

[56] Engin, T., Gur, M. Performance characteristics of a centrifugal pump impeller with running tip clearance pumping solid-liquid mixtures. Journal of Fluids Engineering-Transactions of the Asme, 2001; 123: 532-38.

[57] Wilson, G. Effect of slurries on centrifugal pump performance Fourth International Pump Symposium. Houston, TX, USA; 1987, p. 19-25.

[58] Sellgren, A., Addie, G.R. Solid effects on characteristics of centrifugal slurry pumps Hydrotransport 12. Belgium; 1993, p. 3-18.

[59] Sellgren, A., Addie, G. Effect of solids on large centrifugal pump head and efficiency. CEDA Dredging Day. Netherlands; 1989.

[60] Wilson, K.C. Two mechanisms for drag reduction. Drag reduction in fluid flows : techniques for friction control. Ed. Sellin H.R.J. and Moses, R.T.,. New York, NY, USA: Chichester 1989.

CHAPTER 6

Development of Correlations for the Flow of Agricultural Residue Biomass Slurries in Pipes[1]

6.1. Introduction

There have been few studies conducted on techno-economic analysis of pipelining lignocellulosic biomass which have compared the cost of pipeline hydro-transport with truck delivery [1-3]. However, these studies were based on the assumption that the pressure drop in the pipeline transport of agricultural residues slurries (i.e., chopped agricultural residue biomass-water mixture) was same as the pipeline transport of wood chip-water mixtures. At that time there was no information available, either in terms of experimental results or empirical correlations, on the pipeline hydro-transport of agricultural residue biomass. Recently Luk et al. [4] and Vaezi et al. [5-7] experimentally investigated pipeline hydro-transport of wheat straw and corn stover in a 25 m long and 50 mm diameter closed-circuit lab-scale pipeline facility. They studied wheat straw and corn stover morphology and its impact on mechanical behavior and frictional pressure gradients of corresponding solid-water mixtures (slurries) in pipeline [5], studied the mechanical feasibility of agricultural residue biomass pipeline hydro-transport, investigated friction loss behavior of wheat straw and corn stover slurries through pipelines [6], and evaluated the performance of centrifugal slurry pumps while handling agricultural residue biomass slurries [7].

To design an industrial scale pipeline for hydro-transport of agricultural residue biomass, it is necessary to understand how the slurry pressure gradient changes with slurry specifications (i.e., biomass type, particle size, slurry solid mass content (concentration), and slurry temperature) and operating conditions (i.e., pumping velocity, pipe diameter, and pipe roughness). This knowledge is essential to size the slurry pumps, determine the number of booster stations, and estimate the capital and operational costs of the slurry

[1] Paper submitted to the Journal of Biosystems Engineering, 2014

pipeline and hence the overall cost of pipeline hydro-transport of agricultural residue biomass. Therefore, the experimental measurements and governing rules obtained in the lab-scale pipeline facility need to be modeled and corresponding correlations accordingly developed before these can be applied to a large-scale pipeline. Since the mechanisms of the flow of agricultural residue biomass slurries in pipes were found to be unique, different from wood chips slurries, and predominantly similar to those of the synthetic and natural fibres, e.g., wood pulp fibre suspensions[2] [6, 7], the empirical models, theoretical correlations, and scale-up methods proposed for the flow of synthetic and natural fibres in pipes (mainly wood pulp suspensions) were considered here to help develop correlations for the flow of agricultural residue biomass slurry in pipes.

Unlike agricultural residue biomass slurry flows, the flow of wood chips and wood pulp fibre suspensions have been extensively studied, and several empirical and theoretical models have been developed to predict the corresponding pressure gradients through pipelines. Following an experimental study on pipeline hydro-transport of spruce and balsam fir wood chips over a 160 m long and 200 mm diameter aluminum pipeline, Elliott and de Montmorency [8, 9] modified the Durand universal equation (a general correlation presented to estimate the friction loss in solid-liquid pipelines) [10] and presented an empirical correlation for estimating friction loss in wood chip-water mixtures in pipes. Hunt [11] experimentally studied hydro-transport of plate shape wood chips of lodgepole pine in 200 and 300 mm diameters and 91 m and 183 m long steel pipes and proposed a correlation to predict the mixture friction loss as a function of four dimensionless parameters including mixture solid volume content and particle-to-pipe size ratio. Moller et al. [12] proposed a design correlation to predict the friction loss of chemically prepared wood pulp suspensions as a function of suspension velocity, suspension solid mass content, and pipe diameter for several kraft pulps in 50, 75, and 100 mm diameter pipes. Duffy et al. [13] obtained pressure gradient correlations for groundwood, semi-chemical, and refiner pulps as a function of suspension solid mass content, suspension velocity, and pipe diameter. They also investigated the effect of suspension temperature, fibre aspect ratio, and pipe roughness on suspension pressure

[2] The terms slurry, mixture, and suspension are used interchangeably

gradient, where the pressure gradient was found to decrease by an average of 1.0% for each degree Celsius increase in temperature. Moller [14] proposed a new dimensionless representation of pipe friction data to correlate accurately the flow data for a given chemical pulp on a single diagram with respect to pipe roughness and irrespective of variables such as suspension velocity, solid mass content, and pipe diameter. Duffy [15] presented two design methods for determining the pipe pressure gradient components for the pulp suspension flows together with the basic design correlations. Correlations were derived to obtain optimum fibre mass content for an existing piping system and the optimum pipe diameter for a new pipeline system. Finally, the Technical Association of the Pulp and Paper Industry (TAPPI) issued a Technical Information Paper (TIP) in 1981, which was revised in 2007 [16], to provide friction loss correlations for pulp suspension flows obtained based upon laboratory experiments, pulp mill piping systems, and the research work done by Duffy et al. [12, 13, 17, 18].

Several researchers specifically studied the techniques to scale up slurry pressure gradients obtained in small pipe diameters to larger pipe diameters. Among those, Bowen [19] presented a complete design procedure for scaling up the results of a solid-liquid mixture flow at a particular solid mass content in small diameter pipes to large diameter pipes in both laminar and turbulent regimes, Sauermann and Webster [20] at the National Mechanical Engineering Research Institute in Pretoria proposed a method that requires only experimental results for one pipe diameter to predict the pressure gradient in pipes with smaller or larger diameters, Thomas [21, 22] discussed a scale-up technique that requires the experimental results in more than one pipe diameter to predict the pressure gradient in pipes with larger diameters only, and Lokon et al. [23] modified Bowen's correlation by including the effect of a change in slurry solid mass content on pressure gradients in iron ore slurry pipe flows.

The present research attempts to achieve two objectives: (1) to develop an empirical correlation (based on experimental measurements taken in the laboratory scale pipeline) to predict longitudinal pressure gradients of the flow of the slurry of agricultural residue biomass (of any fibrous agricultural residue biomass type, biomass particle diameter, and slurry solid mass content over commercial slurry velocity ranges) in a 50 mm diameter

pipeline and (2) to scale up the pressure gradient correlation to account for pipe diameters larger than 50 mm. Finally, a comprehensive model will be developed that is capable of predicting longitudinal pressure gradients of various agricultural residue biomass slurries at a variety of slurry specifications, operating conditions, and pipe diameters.

6.2. Experimental Methodology

6.2.1. Feedstock Properties and Preparation

Through the course of experimental investigation, agricultural residue biomass of wheat straw (*Triticum sativum*; dry stalks of wheat) and corn stover (*Zea mays*; leaves and stalks of corn) were collected, knife-milled, and classified into four size groups with nominal diameters of 19.2 mm (0.75″), 6.4 mm (0.25″), 3.2 mm (0.125″), and <3.2 mm (<0.125″). The initial wet-basis water mass content (moisture content or MC) and specific gravity of wheat straw and corn stover particles were measured according to ASABE S358.2 [24] and ASTM C127 [25] standards to be 6 ± 0.5% and 0.9 ± 0.01, respectively.

6.2.2. Image Processing and Morphological Studies

Unusual characteristics (e.g., relatively large mean particle size; wide size distribution; fibrous, pliable, flexible, and asymmetric nature; potential for forming networks) make agricultural residue biomass particles atypical [26] and distinguish their corresponding slurry from classical solid-liquid systems [6]. The ImageJ digital image processing platform [27], together with a user-coded plugin developed by the authors [5], was used to study unusual characteristics and morphological features (particle shapes, particle dimensions, particle size distribution (PSD), size distribution algorithms, particle surface features, etc.) of knife-milled pre-classified wheat straw and corn stover particles [5]. Figure 6-1 compares normal size distribution of wheat straw and corn stover particles. Standard dimensions of significance [28] – median length (d_{50}); geometric mean length (X_{gl}), width (X_{gw}), and thickness (X_{gth}); and corresponding standard deviations (σ_{gl}, σ_{gw}, σ_{gth}) – are presented in Table 6-1, together with a few characteristics of common classical solid particles for comparison.

The particle shape factor (S) was also accordingly defined to take into account the particle's physical properties and shape characteristics (Eqs. 1-2, Table 6-1) and extend the specific results obtained here to other sorts of (non-wood) fibrous[3] particles.

$$\lambda = \frac{M_s}{\rho_p \times \sum_{j=1}^{n} (X_{gw,j} \times A_{s,j})} \tag{1}$$

$$\text{Shape factor } (S) \ = \lambda \times \sqrt{\frac{X_{gw}}{X_{gl}}} \tag{2}$$

Table 6-1: Physical properties and shape specifications of wheat straw and corn stover particles, together with classical solid particles

Reference	Particle Properties									Slurry Properties		
	Solid Particle	Nominal Particle Size (mm)	Median Length (mm)	Geometric Length (mm)	Geometric Width (mm)	Geometric Thickness (mm)	Particle Aspect Ratio	Particle Specific Gravity	Particle Shape Factor	Slurry Solid Mass Content		Slurry Specific Gravity
		X_n	d_{50}	X_{gl} [a] ± σ_{gl} [b]	X_{gw} ± σ_{gw}	X_{gth} ± σ_{gth}		ρ_p / ρ_f	S	C_s	C_d	ρ_s / ρ_f
Present Study	Wheat Straw	19.2	8.29	8.42 ± 1.49	1.34 ± 1.54	0.45 ± 0.51	6.28	1.026	0.133	5-25	1-5.4	1.00094–1.0047
		6.4	5.00	4.79 ± 1.57	1.07 ± 1.56	0.44 ± 0.64	4.47		0.196	5-30	1-6.5	1.00094-1.0057
		3.2	3.92	3.96 ± 1.41	1.12 ± 1.51	0.63 ± 0.84	3.53		0.298	5-35	1-7.6	1.00094-1.0066
		<3.2	2.42	2.57 ± 1.43	0.74 ± 1.46	1.25 ± 2.47	3.47		0.908	5-40	1-8.8	1.00094-1.0076
	Corn Stover	19.2	7.58	7.83 ± 1.46	1.32 ± 1.72	0.36 ± 0.47	5.93	1.169	0.113	-	-	-
		6.4	4.72	4.66 ± 1.51	1.14 ± 1.70	0.39 ± 0.58	4.08		0.169	5-30	1-6.5	1.00094-1.0057
		3.2	3.32	3.49 ± 1.45	1.21 ± 1.61	0.72 ± 0.96	2.88		0.351	5-35	1-7.6	1.00094-1.0066
		<3.2	1.90	2.11 ± 1.44	0.73 ± 1.42	0.75 ± 1.47	2.89		0.610	5-40	1-8.8	1.00094-1.0076
[29]	Play Sand	-	0.446	0.366 ± 0.0012	-	-	-	2.650	-	-		1.03-1.14 [c]
[30]	Glass Bead		0.090					2.420				
[31]	Coal		0.9	-				1.480				-
[32]	Iron Ore		1.8					4.150				

[3] Although fibrous particles are structurally diverse, here the fibers are defined on the basis of their size and shape as particles with an aspect ratio (X_{gl}:X_{gw}) ≥ 3:1, length ≥ 2 mm, and width ≤ 1.5 mm.

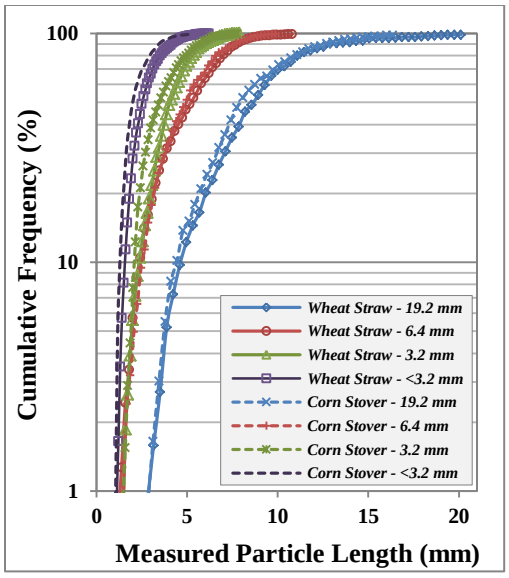

a)

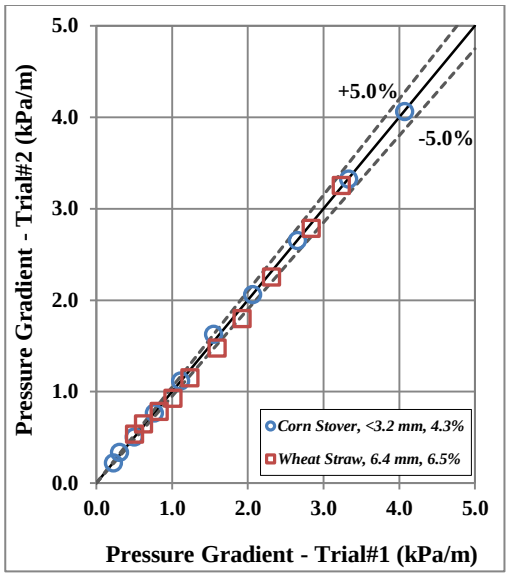

b)

Fig. 6-1: a) Cumulative particle size distribution of wheat straw and corn stover particles, b) Repeatability of two sets of pressure gradient measurements of the flows of wheat straw and corn stover slurries in 50 mm diameter and 25 m length pipeline

6.2.3. Experimental Set-up

The test circuit (Fig. 6-2) consisted of a 0.455 m^3 slurry mixing tank with a 0.37 kW centrally placed vertical mixer, 25.5 m of 50 mm diameter Schedule 40 steel pipe, and a double-tube heat exchanger to partially maintain the slurry temperature at 15±2°C. An electromagnetic flow meter (FMG-401H; Omega Eng., Stamford, CT, US) and a resistance temperature detector (RTD-E; Omega Eng., Stamford, CT, US) were included to measure the rate of the slurry flow and the mixture temperature, respectively. In addition, a couple of 25 mm flush diaphragm low-pressure transmitters (PX42G7; Omega Eng., Stamford, CT, US) were used to measure the slurry flow gauge pressures upstream and downstream of a 7.5 m horizontal test section. Slurry flow was provided by a specifically designed 7.45 kW centrifugal pump (CD80M; Godwin Pumps Ltd., Bridgeport, NJ, US) coupled with a 7.45 kW induction electric motor (CC 068A; Madison Industrial Equipment, Vancouver, BC, Canada) and controlled by a 14.9 kW variable frequency drive (VFD) controller (MA7200-2020-N1, TECO-Westinghouse Co.). The 4-20 mA output signals from the temperature probe, magnetic flow meter, and pressure transmitters were recorded on a "one hundred data per second" basis on a data

acquisition system comprised of a 4-channel current excitation module (NI 9219; National Instrument Corp., Austin, TX, US) and a data acquisition program (LabView V.9.0.1f2; National Instrument Corp., Austin, TX, US).

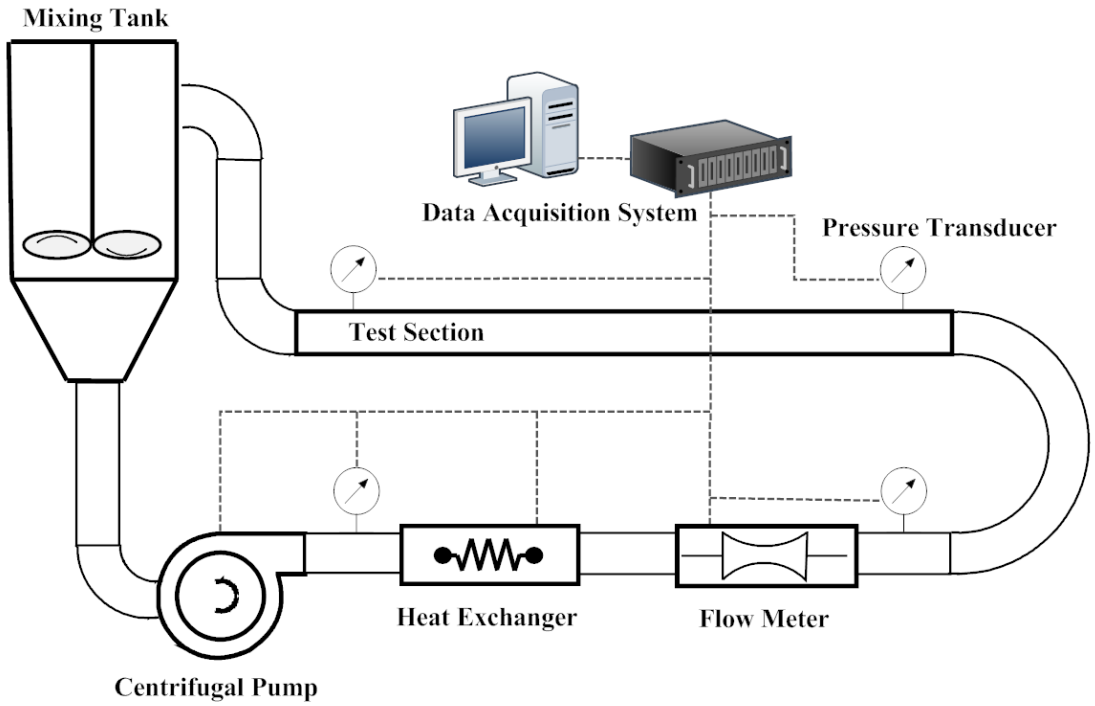

Fig. 6-2: Schematic diagram of the experimental set-up

6.2.4. Slurry Preparation and Frictional Pressure Gradient Measurement

The pre-measured amount of feedstock was initially mixed with pure water and pumped through the closed-circuit pipeline. It took 12 to 14 hours at a pumping velocity of 4.0 to 5.0 m/s before a stable mixture condition was reached, and pressure and velocity fluctuations were damped down to less than 1.0% per hour. This is caused by particle deterioration during pipeline transportation and its impact on momentum transfer mechanisms [6]. Meanwhile, biomass solid particles absorbed 96% of their saturated water mass content (MC) in one hour and became fully saturated (82% MC for wheat straw and corn stover particles) after six hours [6]. Generally speaking, increasing the water mass fraction would increase the flexibility of fibrous particles and, accordingly, increase the potential to form a fibre network and decrease the friction loss. No impact due to change in the moisture content was found on carrier liquid or slurry viscosity [6].

The friction loss of the slurry through a 7.5 m horizontal test section was measured afterwards with two types of biomass materials (wheat straw and corn stover) and four sizes of biomass particles (19.2 mm, 6.4 mm, 3.2 mm, and <3.2 mm) over a wide range of saturated (pumped for a minimum of six hours) solid mass contents (C_s=5 to 40% for <3.2 mm, C_s=5 to 35% for 3.2 mm, C_s=5 to 30% for 6.4 mm, and C_s=5 to 25% for 19.2 mm particles) and slurry bulk velocities (0.5 to 5.0 m/s). In this paper, the equivalent dry matter (oven-dried) solid mass content (C_d=1 to 8.8% for <3.2 mm, C_d=1 to 7.6% for 3.2 mm, C_d=1 to 6.5% for 6.4 mm, and C_d=1 to 5.4% for 19.2 mm particles) is chosen for simplicity and comparability purposes.

6.2.5. Uncertainty Analysis

Two sets of experiments were conducted on every particle type and size to assure the repeatability and investigate the uncertainty of the results. For instance, a good agreement was found, as observed on Fig. 6-1(b), between successive trials of a 4.3% solid mass content slurry of <3.2 mm corn stover and a 6.5% solid mass content slurry of 6.4 mm wheat straw particles with uncertainties of ±0.015 kPa/m and ±0.068 kPa/m, respectively.

Uncertainties in experimental measurements, carrier liquid viscosity measurement, calibration of the experimental set-up, and evaluating the performance of the centrifugal pumps handling agricultural residue biomass slurries have been extensively discussed by the authors elsewhere [6, 7].

6.3. Experimental Results

Although the pipeline hydro-transport of woodchip biomass has been previously experimentally investigated and numerically modeled [33-36], the authors of this paper demonstrated that the pressure drop correlations proposed for woodchip-water mixtures are not appropriate choices to apply to agricultural residue biomass slurries [6]. Furthermore, the authors of this paper compared the similarity in the mechanical behavior of agricultural residue biomass slurries and classical solid-liquid mixtures (play sand-water mixture – see the sand specifications in Table 6-1) and found that in a clear contrast with agricultural residue biomass slurry, the friction factor in a water-sand mixture is

greater than the friction factor for pure water at the same generalized Reynolds number (calculated based upon the slurry density (ρ_s), carrier liquid viscosity (μ_f), slurry bulk velocity (V), and pipe internal diameter (D)). Moreover, the sand-water mixtures showed a trend of increasing pressure gradients with an increasing solid mass content (Fig. 6-3), while in the slurry of agricultural residue biomass, the pressure gradient decreases with an increase in the solid mass content.

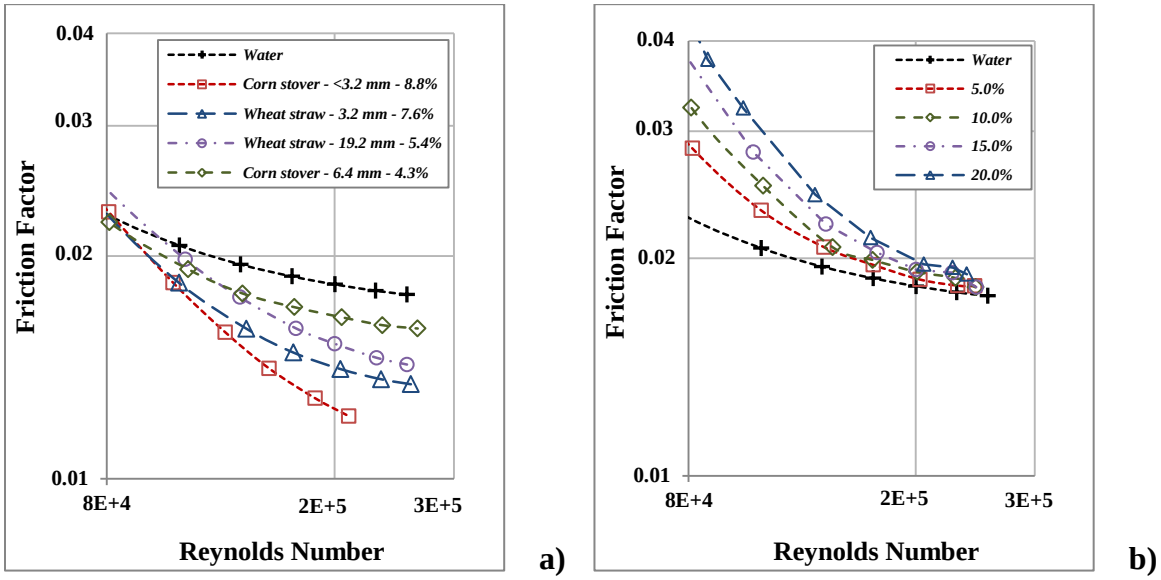

Fig. 6-3: Friction factor vs. generalized Reynolds number for velocities above 2.0 m/s in a 50 mm diameter pipeline for various solid mass content slurries of a) wheat straw and corn stover particles and b) play sand particles

The friction loss behaviors of the flow of agricultural residue biomass slurry appeared to be predominantly similar to those for natural and synthetic fibre suspensions, e.g., wood pulp fibre suspensions, where with increasing velocity from zero the pressure gradient passes successively through maximum and minimum values and, eventually, becomes less than the pressure gradient for pure water; i.e., the suspension exhibits drag-reduction features [37, 38]. Although drag-reducing characteristics reported in the literature are limited to natural and synthetic fibres of several micrometers to 5.0 mm in length and aspect ratios of 25 to several hundred, non-common fibrous particles of agricultural residue biomass with noticeably large dimensions of 2.0 to 9.0 mm in diameter and considerably small aspect ratios of 2 to 7 (Table 6-1) resulted in the friction factor of the

slurry being smaller than that for water at high solid mass contents and elevated pumping velocities (Fig. 6-3). This is a unique feature often not encountered in classical solid-liquid systems, which lack the internal particulate structure or the ability of the particles to flex, absorb energy, and take up the carrier liquid [6]. The detailed mechanisms of such features, together with the impact of particle morphological features, slurry properties, and pumping velocity on friction loss behavior of agricultural residue biomass slurry through pipelines, are beyond the scope of the present paper and have been discussed by authors in previously published papers [5-7].

Figure 6-4(a) presents variations of pressure gradient vs. slurry bulk velocity for various particle diameters and slurry solid mass contents. A drag-reduction effect can be clearly observed for more concentrated slurries at elevated velocities. Figure 6-4(b) shows the percentage drag reduction (slurry pressure gradient with respect to pure water pressure gradient at the same velocity) produced by the same slurries as Fig 6-4(a). Achieving a 22% drag reduction with a 6.5% slurry of <3.2 mm wheat straw particles was outstanding.

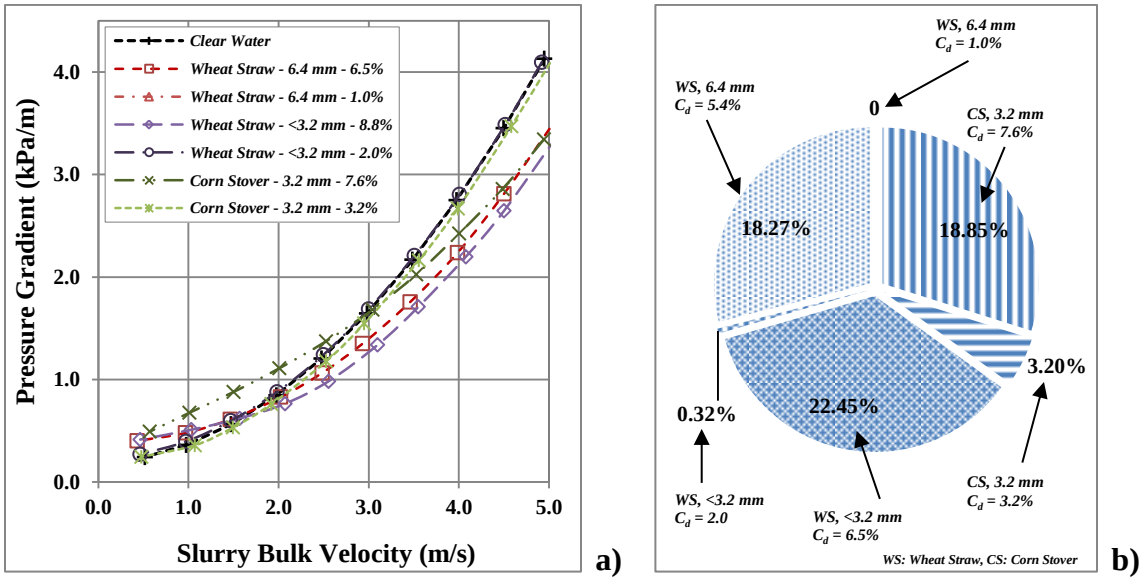

Fig. 6-4: a) Pressure gradient vs. slurry bulk velocity of various particle types, particle diameters, and solid mass contents**,** b) Drag reduction produced by the slurries shown on Fig. 6-4(a) at 5.0 m/s slurry bulk velocity

6.4. Empirical Correlation Development

6.4.1. Numerical Modeling

The core purpose of the present study was to develop an empirical model based on measurements on a 50 mm diameter and 25 m length experimental facility, capable of predicting the dependent variable of the pressure gradient (kPa/m) as a function of independent variables of slurry bulk velocity (m/s), slurry dry solid mass content (%), and solid particle size representative (particle shape factor). Therefore, EViews 7.1 [39] econometric software was used to analyze 837 experimental measurements from the experiments with wheat straw and corn stover. A fourth-order polynomial equation with all of the possible interactions of independent variables (36 variables and interactions) was introduced, and the nonlinear least square (NLS) regression analysis model was used to estimate the regression coefficients (α, β, γ, and δ) as well as the statistics associated with each coefficient. The model was later re-specified to correct for moving average (MA) errors that could result in the residuals being correlated with their own lagged values (serial correlation). Finally, the estimation of the coefficients based on experimental measurements resulted in Eq. 3, where the coefficients of α, β, γ, and δ are defined according to Table 6-2.

$$\frac{\Delta H}{L} = \sum_{m=1}^{3} (\alpha_m S^m + \beta_m V^m + \gamma_m C_d^m + \delta_m V^m C_d^m) \quad (3)$$

Table 6-2: Coefficients for empirical correlations 3 and 6

Coefficient	Dummy					
	m = 1	***m = 2***	***m = 3***	***n = 1***	***n = 2***	***n = 3***
α	1.26444	-2.06961	0.71200	1.22465	-1.97098	0.64855
β	0.00000	0.16413	0.00000	0.00000	0.16389	0.00000
γ	0.00000	0.00000	0.00066	0.00000	0.00000	0.00066
δ	0.00000	-0.00104	0.00000	0.00000	-0.00104	0.00000
D_0	0.0508 m					

Estimated regression coefficients, statistics associated with each coefficient, and statistics associated with the entire regression analysis are presented in Table 6-3. Standard errors associated with each regression coefficient (Std. Error), t-statistics (for the hypothesis

that the coefficient in the same row equals zero), and probabilities (Prob.) prove all the variables to be ″strongly significant.″ Furthermore, the R^2 and adjusted R^2 equal to 0.99 confirm the perfect overall fit of the estimated regression line to the experimental points, an outcome that can be seen on Fig. 6-5. The ″Durbin-Watson″ statistic [40] was increased, after correcting for moving average errors, from 0.2 to close to 2.0, which is consistent with no serial correlation. Finally, the standard deviation of the dependent variable (S.D. Dependent Var.) is about 20 times larger than the standard error of the regression (S.E. of Regression), which is an indication that the regression has explained most of the variance in volume; the same conclusion was made based on R^2.

6.4.2. Model Validation

Figure 6-6(a) compares the pressure gradients for the slurry of 3.2 mm wheat straw particles experimentally measured and numerically predicted. As shown, the experimental measurements are in compliance with numerical results that were obtained by substituting the values of 0.298 for *S*, 1.0, 3.2, 5.4, and 7.6% for C_d, and 0.5 to 5.0 m/s for *V* in Eq. 3 and solving these for $\Delta H/L$, with an average error of 5.99 ± 3.52%. Figure 6-6(b) compares experimentally measured and numerically predicted results for all 837 pressure gradient measurements. 70% of the entire numerical results fall between ±10% of the corresponding experimental measurements. A total average error of 9.91 ± 2.89% reconfirms the accuracy of the model in predicting friction loss of wheat straw and corn stover agricultural residue biomass slurries through a 50 mm diameter pipeline.

Table 6-3: Estimated regression coefficients and statistics for experimental data

Variable	Coefficient	Std. Error	t-Statistics	Prob.
S	1.264440	0.128644	9.828952	0.0000
S^2	-2.069609	0.446193	-4.638376	0.0000
V^2	0.164128	0.000625	262.5910	0.0000
$V^2C_d^2$	-0.001039	0.000025	-41.19837	0.0000
S^3	0.711997	0.363653	1.957904	0.0506
C_d^3	0.000662	0.000064	10.24157	0.0000

R-squared	0.996674	Durbin-Watson Stat.	1.901867	
Adjusted R-squared	0.996638	Mean Dependent Var.	1.645276	
S.E. of Regression	0.068049	S.D. Dependent Var.	1.173636	

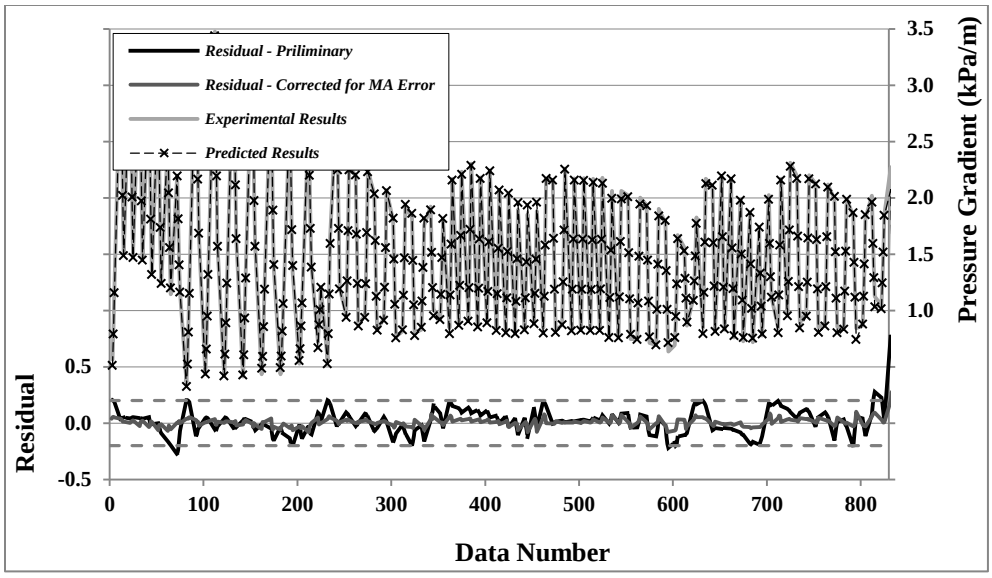

Fig. 6-5: Residuals of the model, together with a sample of experimental and predicted results

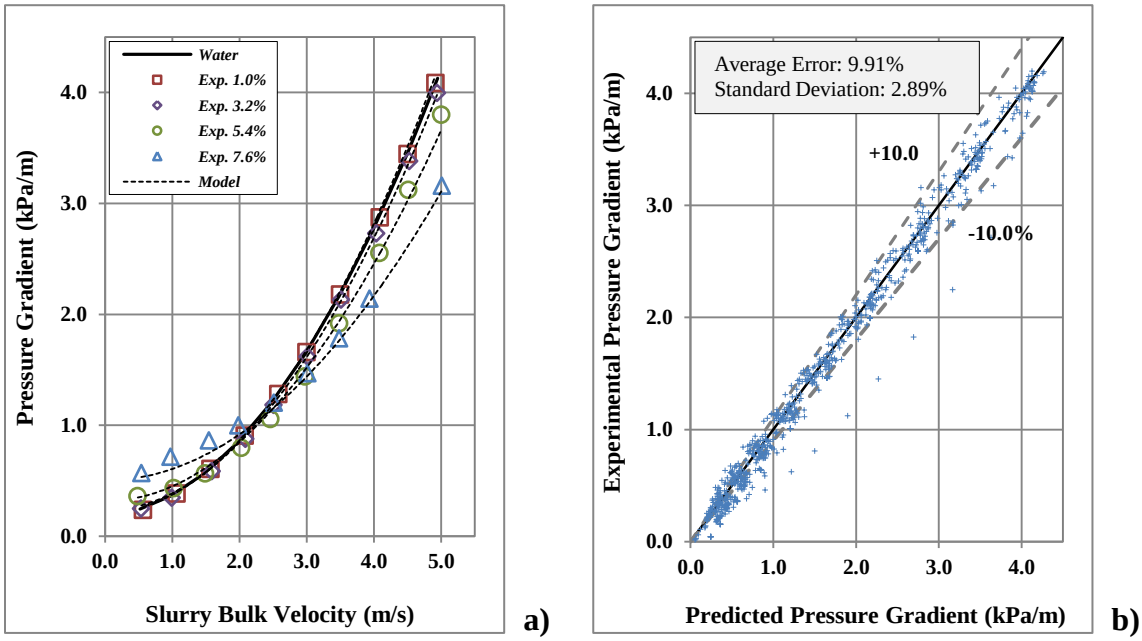

Fig. 6-6: a) A comparison of experimentally measured and numerically predicted pressure gradients for a slurry of 3.2 mm wheat straw particles, b) Accuracy of the numerical model in predicting pressure gradients for the entire 837 experimental measurements

6.4.3. Model Applications

As previously discussed, the model is not limited to the agricultural residue biomass studied here. Based on the assumption that particles similar in nature should have more or less the same shape characteristics [41], common agricultural residue biomass or, generally, non-wood fibres (e.g., wheat straw, corn stover, rice straw, bagasse) and energy crops (e.g., switch grass, miscanthus), if ground, would be fibrous in nature (see section 6.2.2) [42-44] and are expected to show similar mechanical behavior when mixed with water and pumped into the pipeline. Therefore, the corresponding shape factors, if accordingly substituted in Eq. 3, together with the appropriate solid mass content and slurry bulk velocity, will result in the pressure gradient of corresponding slurry through a 50 mm pipeline.

Although the range of slurry velocity (0.5 to 5.0 m/s) and slurry solid mass content (1.0 to 8.8%) of experimental measurements are pretty wide and easily cover the industrial and commercial range of operations, the authors are not able to confirm the accuracy of the proposed correlation at operating conditions outside the above ranges.

6.5. Scale-up Approach

A large-scale long-distance pipeline, in order to be economically viable, uses large diameter pipes, e.g., the 440 km long 457 mm diameter Black Mesa coal pipeline, the 150 km long 250 mm diameter Chevron phosphate slurry pipeline, and the 35 km long 324 mm diameter MacKay River bitumen pipeline [45]. Therefore, before planning a large-scale long-distance agricultural residue biomass slurry pipeline, it is necessary to understand how the slurry mechanical behavior changes with pipeline specifications, i.e., pipeline diameter; or, more specifically, is the pressure gradient correlation developed for a 50 mm diameter pipeline valid for larger diameters?

According to Duffy and Lee [37] and Radin et al. [46], who studied flow and drag-reduction features of various fibre suspensions (e.g., wood pulp, nylon, and rayon), there is an increase in drag reduction (and corresponding onset velocity[4]) with increasing pipe

[4] The velocity at which the slurry pressure gradient becomes less than the pressure gradient for pure water, V_w.

diameter. Since a larger pipe has an appreciable percentage of its flow in a non-shear condition, and it has been shown that drag reduction is caused by modification of the turbulence structure in the core and not in the boundary layer (i.e., it is not a wall effect) [38, 47], it might be expected that a pipe with a larger diameter will bring about more drag reduction than a pipe with a smaller diameter. Rao [48] also confirms that the friction loss is higher for smaller pipe diameters under similar conditions of fibre suspension (pulp) flows. Consequently, the pressure gradient predicted for a slurry of agricultural residue biomass in a 50 mm diameter pipe would be conservatively valid for a larger diameter pipe as well. However, it will obviously result in overestimating the slurry friction loss and oversizing the pump facilities, which will accordingly increase capital investment and operating costs. Therefore, it is necessary to modify the correlation to account for the pipe diameter as well.

6.5.1. Scale-up Approaches for the Pulp Fibre Suspension Flows in Pipes

The mechanisms of flow of fibre suspensions have been previously described in the literature [6, 18, 48-54]. The models reviewed here specifically discuss the approaches that have been taken to account for the effect of increasing pipe diameter on corresponding friction loss in pulp fibre suspension flows. Since the similarity between flow of agricultural residue biomass slurry and natural and synthetic fibre suspensions, e.g., wood pulp fibre suspensions, have been previously demonstrated [6], the results obtained here would be used for scaling up the agricultural residue biomass slurry pipelines.

The earliest data used for the purpose of designing a fibre suspension flow pipeline were obtained by Trimbey in 1907 for groundwood pulp in spiral riveted steel pipes and were later published as the Cameron Hydraulic Data [55]. Forrest and Grierson in 1931 [56] published data for sulphite and groundwood pulps over a wide range of velocities, stock solid mass contents, and pipe diameters. Brecht and Heller [57] also reported extensive data for unbleached sulphite pulp for stock solid mass contents up to 5.0% over various copper pipe diameters. Later, Durst et al. [58] analyzed the experimental data in the Cameron Hydraulic Data Book as reported by Forrest and Grierson and Brecht and Heller

on the flow of various pulp fibre suspensions in pipes. Using Brecht and Heller's data on unbleached sulphite pulp as a basis, they proposed a correlation using a plot of friction factor versus a pseudo-Reynolds number on logarithmic co-ordinates, known as the University of Maine Correlation of Brecht and Heller Data. Riegel [59] reduced the Brecht and Heller correlation to a single expression of the form

$$\frac{\Delta H}{L} = kV^p D^q C_d^r \tag{4}$$

Correlations in the form of Eq. 4 have been developed by several investigators for various pulps between 1966 and 2003, as summarized in Table 6-4.

Table 6-4: Values proposed for the exponents *p*, *q*, and *r* in equation 4

Source	Year	Constant	Exponents		
		k	***p***	***q***	***r***
Riegel [59]	1966	12.68	0.36	-1.33	1.87
Aktiebolaget Pumpindustri (API) [60]	1966	$5.53+\frac{D}{19.69+D}$	$0.15+\frac{D}{19.69+D}$	-1.00	2.20
Bodenheimer [61]	1969	5.40	0.15	-1.00	2.50
Moller, Duffy, Titchener [62]	1971	3.63	0.33	-1.33	n.a.
Duffy [50]	2003	11.75	0.31	-1.34	1.81
Moller, Duffy, Titchener [12]	1973-1976	143	0.18	-1.09	2.34
Duffy and Titchener [17]		87	0.32	-1.16	2.19
Duffy, Moller, Lee, Milne [13]		369	0.43	-1.20	2.31
Duffy [18]					
Average				-1.18	

As seen in the results in Table 6-4, the velocity exponent *p* is not a strong function of pipe diameter but the fibre suspension type (pulp) itself. Moller et al. [62]; however, expected the pipe roughness to influence the value of the exponent *p* to some extent. Exponent *q*, which indicates the variation of pressure gradient with the pipe diameter, has an average value of -1.18.

As mentioned in the introduction, the Technical Association of the Pulp and Paper Industry (TAPPI) issued a Technical Information Paper (TIP) in 1981, which was revised in 2007 [16], to provide friction loss correlations for pulp suspension flows obtained based upon laboratory experiments, pulp mill piping systems, and research work

done by Duffy et al. [12, 13, 17, 18]. The technical paper proposed Eq. 4 to calculate pipe friction loss by substituting the appropriate values for stock parameters, i.e., *K*, *p*, *q*, and *r*, pipe diameter, oven-dried solid mass content, and corresponding values for slurry bulk velocity. However, for bulk velocities greater than the velocities corresponding to the onset of drag reduction (V_w) the technical paper recommends calculating the friction loss for pure water flowing alone under the same conditions using accepted correlations, e.g., Blasius or Colebrook [63]. It is obvious that such an approach would noticeably overestimate the pressure gradient at velocities above V_w (see Fig. 6-4(a)) and make the design of the piping system unnecessarily conservative. This is due the fact that the TAPPI paper simply ignores the drag reduction by fibre suspension flows at elevated velocities that can be as noticeable as 50% [37, 46].

6.5.2. Scale-up Approaches for the Flow of Classical Solid-Liquid Mixtures in Pipes

To compare the scale-up approaches for fibre suspension flows and classical solid-liquid mixtures in pipes, a well-known correlation for scaling up common solid-particle (e.g., sand, coal, iron ore, clay, phosphate) slurry pipelines is reviewed here to compare the variation of pressure gradient with diameter to that obtained for natural and synthetic fibre suspensions.

According to the solid-liquid mixtures classification by Thomas [21], the slurry of agricultural residue biomass studied here can be classified as homogeneous settling slurries for which, according to Bowen's procedure for scaling up small-scale classical solid-liquid mixture (with a Newtonian carrier liquid) pipelines [19], the longitudinal pressure gradient can be obtained as follows:

$$\frac{\Delta H}{L} = 2kV^{2-x}D^{-1-x}\rho^{1-x}\mu_f^x \tag{5}$$

Bowen proposed an *x* value of 0.25 for smooth and 0.20 for rough pipes. However, he indicated that, although the actual value of *x* must be obtained experimentally, substituting 0.2 for *x* in Eq. 5 will result in errors of, at most, only a few percent, because of the narrow velocity range of slurry flow. Lokon et al. [23] developed an empirical

model to predict the longitudinal pressure gradients in iron ore slurry pipe flows that was based on the model by Bowen [19]. Consequently, the proposed exponent for *D* in Eq. 5 would be -1.2, which fits the value averaged from Table 6-4.

6.5.3. Scale-up Approaches for the Flow of Agricultural Residue Biomass Slurries in Pipes

Webster et al. [22] discussed two various pressure gradient scale-up approaches for slurry pipelines. First, the CSIR (the Council for Scientific and Industrial Research, Pretoria, South Africa) approach [20], also referred to as the i_s method, which requires the results for one pipe diameter only. Second, the Thomas method [21], which needs the results in more than one pipe diameter to predict the pressure gradient in larger pipe diameters. Based upon the CSIR approach, by plotting on a log-log graph of pressure gradients (i) versus pipe diameter (D), plotting the value for the slurry pressure gradient (i_{exp}) experimentally obtained in a fixed-diameter experimental pipe (D_0) at the design velocity of a commercial pipe, and drawing a straight line through this point parallel to the straight line for the pure water pressure gradient (i_w), pressure gradients predicted by the CSIR method (i_s) for any D can be obtained.

In Fig. 6-7 the results for i_{exp} versus D_0 = 50 mm are plotted on a log-log scale, together with i_w and i_s versus D lines for the pipes with diameters from 75 to 250 mm, all at 1.5, 3.0, and 4.5 m/s slurry bulk velocity. i_s lines of the CSIR approach demonstrate a power relationship between the pressure gradient and the pipe diameter with an average power of -1.201±0.005. This is identical to the average value obtained from the literature reviewed in Table 6-4 for pulp fibre suspension flows and section 6.5.2 for classical solid-liquid systems. Consequently, a value of -1.2 is selected as the exponent for the pipe diameter in the agricultural residue biomass slurry pressure gradient correlation, which indicates that in the scale-up procedure, the pressure gradient changes with the diameter proportional to the pipe diameter to the power of -1.2.

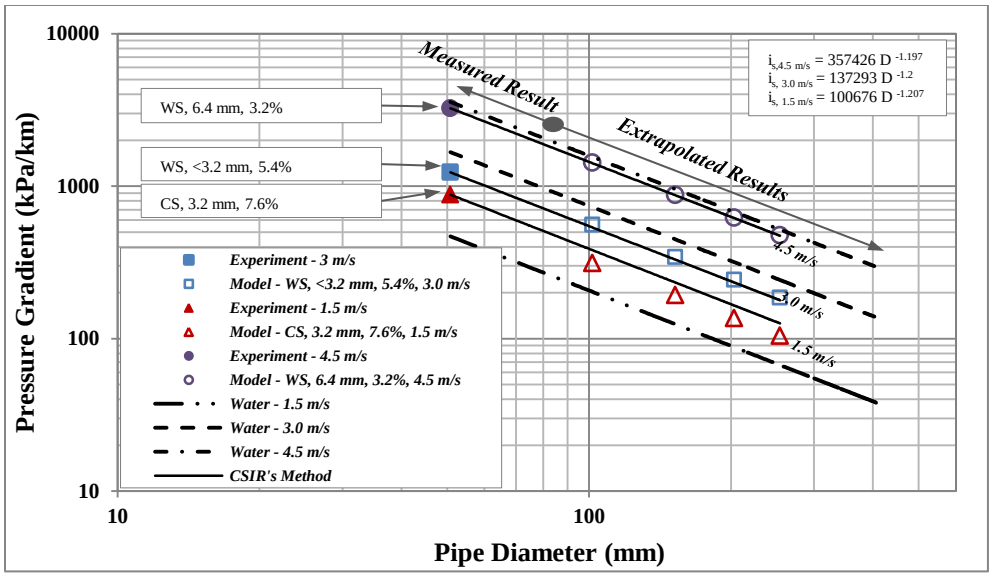

Fig. 6-7: The CSIR pressure gradient scale-up approach applied to the agricultural residue biomass slurry flows in pipelines

6.5.4. Numerical Modeling

As per previous discussion, the exponents *p* and r in Eq. 4 are not functions of pipe diameter but of the fibre suspension type itself. Therefore, by increasing the scale (i.e., diameter) of the pipe, the pressure gradient will be modified proportional only to $D^{-1.2}$. During the scale-up procedure, while the slurry bulk velocity (from 0.5 to 5.0 m/s) and dry solid mass content (from 1.0 to 8.8%) remained unchanged, the model database was extended to account for the pipe diameters of 50 to 250 mm and corresponding scaled-up pressure gradients.

EViews 7.1 [39] econometric software was used one more time to analyze the extended database with 7533 pressure values (of which 837 are experimental measurements and the rest were comprised of the pressure gradient values predicted by taking into account the effect of pipe diameter, $(D/D_0)^{-1.2}$), a fourth-order polynomial equation with all the possible interactions of independent variables (64 variables and interactions) was introduced, a nonlinear least square (NLS) regression analysis method was used to estimate the regression coefficients and associated statistics, and the model was re-specified to correct for MA errors. The estimation of coefficients based on experimental and scaled-up data resulted in Eq. 6, where the coefficients of α, β, γ, δ, and D_0 are

defined according to Table 6-2. Equation 7 is a reproduction of Eq. 6 with values substituted for coefficients.

$$\frac{\Delta H}{L} = [\sum_{n=1}^{3}(\alpha_n S^n + \beta_n V^n + \gamma_n C_d^n + \delta_n V^n C_d^n)](\frac{D}{D_0})^{-1.2} \quad (6)$$

$$\frac{\Delta H}{L} = (1.22S - 1.97S^2 + 0.16V^2 - 0.001V^2C_d^2 + 0.64S^3 + 0.0006C_d^3)(\frac{D}{0.05}) \quad (7)$$

Estimated regression coefficients, statistics associated with each coefficient, and statistics associated with the entire regression are presented in Table 6-5. Standard errors, t-statistics, and probabilities associated with each regression coefficient prove all the variables to be ″strongly significant,″ R^2 and adjusted R^2 equal by 0.99 confirm the perfect overall fit of the estimated regression line to the experimental and scaled-up points, and the Durbin-Watson statistic of 1.93 confirms no inter-correlation between residuals.

Table 6-5: Estimated regression coefficients and statistics associated with coefficients and regression analysis of scaled-up data

Variable	Coefficient	Std. Error	t-Statistics	Prob.
S	1.224649	0.045545	26.88872	0.0000
S^2	-1.970975	0.158711	-12.41864	0.0000
V^2	0.163890	0.000204	802.5681	0.0000
$V^2C_d^2$	-0.001035	0.000008	-125.1320	0.0000
S^3	0.648550	0.129462	5.009583	0.0506
C_d^3	0.000663	0.000022	30.10296	0.0000
R-squared	0.998050	Durbin-Watson Stat.	1.936826	
Adjusted R-squared	0.998047	Mean Dependent Var.	0.616415	
S.E. of Regression	0.030436	S.D. Dependent Var.	0.688783	

The results for the pressure gradients predicted by Eq. 6 (i_n) versus specific pipe diameters of 100, 150, 200, and 250 mm, *D*, at 1.5, 3.0, and 4.5 m/s slurry bulk velocity are plotted on the log-log graph of Fig. 6-7. For the velocities of 4.5 m/s and 3.0 m/s, the numerical model, compared to the CSIR approach, comes with negligible average errors of 0.82% and 4.18%, respectively. In the case of a 7.6% solid mass content slurry of 3.2

mm corn stover particles at 1.5 m/s, where the i_n line converges towards the i_w line, the numerical model yields conservative values for i_n. The error will be small since the convergence between i_n and the i_w curve was found to be within the scatter of the test data in all cases investigated.

Figure 6-8(a) compares experimentally measured and numerically predicted pressure gradients for 5.4% slurries of various types and particle diameters on a 50 mm diameter pipeline. Experimental results were obtained on the 50 mm diameter lab scale pipeline facility and numerical results were predicted using Eq. 6 for the same size pipe. The majority of uncertainties occur in velocities of 1.0 m/s and lower, a velocity range which is out of the range of accepted commercial slurry velocities. However, at velocities above 1.0 m/s, the average errors measured are as low as 4, 8, 5, and 5% for wheat straw slurries of 3.2 and 19.2 mm particles and corn stover slurries of <3.2 and 6.4 mm particles, respectively.

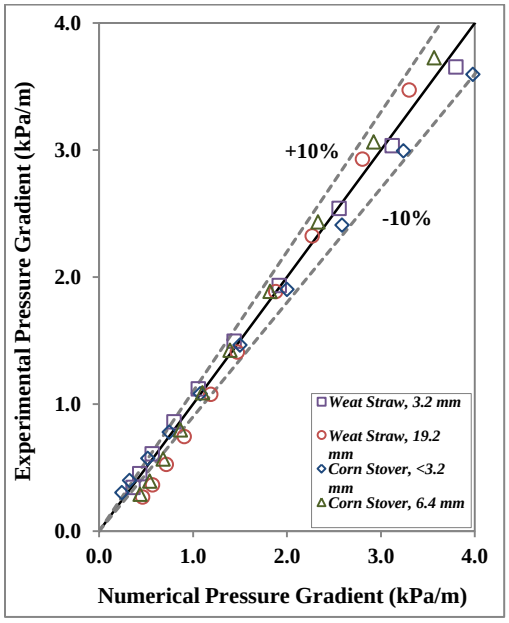

a)

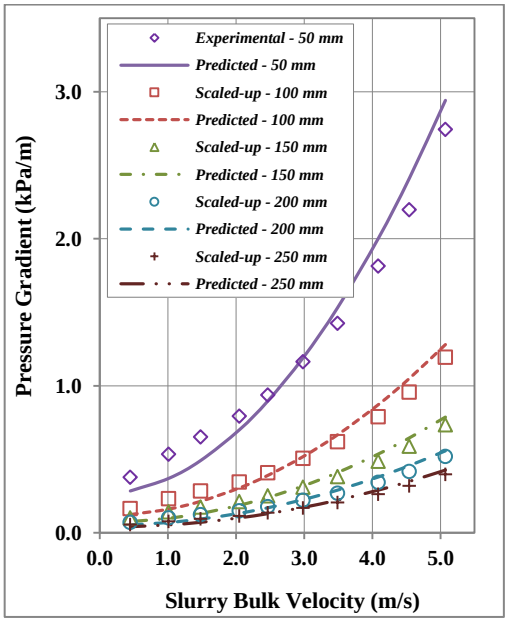

b)

Fig. 6-8: a) Comparing the pressure gradients experimentally measured and numerically predicted by Eq. 6 for 5.4% slurries of various types and particle diameters in a 50 mm diameter pipeline, b) Comparing pressure gradients scaled up proportional to $D^{-1.2}$ and numerically predicted by Eq. 6 for a 7.6% slurry of <3.2 mm wheat straw particles in 50, 100, 150, 200, and 250 mm diameter pipelines

6.5. Conclusion

Slurries of wheat straw and corn stover agricultural residue biomass were prepared in a wide range of solid particle dimensions and slurry solid mass contents and were then pumped over a broad range of slurry velocities (0.5 to 5.0 m/s) through a 50 mm diameter 25 m length closed-circuit pipeline facility to measure the longitudinal pressure gradient of corresponding slurries. With EViews 7.1 econometric software and the nonlinear least square regression analysis method, the experimentally measured pressure gradients were analyzed and an empirical correlation was consequently proposed to predict the slurry pressure gradient as a function of agricultural residue biomass particle type and dimension, slurry solid mass content, and slurry velocity. Considering the similarity between friction loss behavior of the flow of wood pulp fibre suspensions and the flow of agricultural residue biomass slurries and using the CSIR (i_s) scale-up method, the proposed correlation was then modified to take into account the effect of pipe diameter as well. The pressure gradient was found to be proportional to the pipe diameter to the power of -1.2. The final empirical correlation can, with less than 10% uncertainty, predict the longitudinal pressure gradient of the flows of slurries of agricultural residue (non-wood fibrous) biomass in pipes within wide ranges of slurry specifications, operating conditions, and pipe diameters. The majority of uncertainties occur in velocities of 1.0 $m.s^{-1}$ and lower, a velocity range which is out of the range of accepted commercial slurry velocities. However, at velocities above 1.0 $m.s^{-1}$, the average errors measured are as low as 4, 8, 5, and 5% for wheat straw slurries of 3.2 and 19.2 mm particles and corn stover slurries of <3.2 and 6.4 mm particles, respectively. The proposed correlation can be applied to estimate the pressure gradient of the flow of agricultural residue biomass slurry through large-scale pipelines; this knowledge is necessary to estimate the capital and operational costs of commercial pipelines.

Nomenclature

MC	Moisture content or water mass content, %
S	Solid particle shape factor, dimensionless
V	slurry bulk velocity, m/s
D	Pipe internal diameter, m
L	Pipe length, m
$\Delta H/L$	Longitudinal pressure gradient in the pipe, kPa/m
V_w	slurry bulk velocity at the onset of drag reduction, m/s
A_s	Solid particle area, mm^2
M_s	Mass of solid particle sample, kg
D_0	Experimental setup pipe diameter, 0.0508 m
C_d	Dry matter solid mass content, %
C_s	Saturated solid mass content, %
N_i	Number of particles of a particular distinct dimension, dimensionless
X_i	Distinct length of particle, mm
X_n	Nominal particle length, mm
X_{gl}	Geometric mean length, mm
X_{gw}	Geometric mean width, mm
p, q, r, k	Constants
m, n, j	Dummy variables
x	Experimental exponent for flow in smooth/rough pipes, dimensionless
i	Pressure gradient, kPa/m
i_w	Pressure gradient of the pure water, kPa/m
i_n	Pressure gradient predicted by the numerical model, kPa/m
i_{exp}	Pressure gradient experimentally measured, kPa/m
i_s	Pressure gradient predicted by the CSIR method, kPa/m
d_{50}	Particle median length, mm
α, β, γ, δ	Constants
λ	Parameter dependent of the flakiness of the particle, dimensionless
ρ_f	Density of career fluid, kg/m^3
ρ_s	Density of slurry, kg/m^3
ρ_p	Density of solid particle, kg/m^3
μ_f	Viscosity of career fluid, Pa.s
σ_{gl}	Geometric mean length standard deviation, mm
σ_{gw}	Geometric mean width standard deviation, mm
σ_{gth}	Geometric mean thickness standard deviation, mm

References

[1] Kumar, A., Cameron, J.B., Flynn, P.C. Pipeline transport of biomass. Applied Biochemistry and Biotechnology, 2004; 113: 27-39.

[2] Kumar, A., Cameron, J.B., Flynn, P.C. Large-scale ethanol fermentation through pipeline delivery of biomass. Applied Biochemistry and Biotechnology, 2005 (a); 121: 47-58.

[3] Kumar, A., Cameron, J.B., Flynn, P.C. Pipeline transport and simultaneous saccharification of corn stover. Bioresource Technology, 2005 (b); 96: 819-29.

[4] Luk, J., Mohammadabadi, H.S., Kumar, A. Pipeline transport of biomass: Experimental development of wheat straw slurry pressure loss gradients Biomass and Bioenergy, 2014; 64: 329-36.

[5] Vaezi, M., Pandey, V., Kumar, A., Bhattacharyya, S. Lignocellulosic biomass particle shape and size distribution analysis using digital image processing for pipeline hydro-transportation. Biosystems Engineering, 2013; 114: 97-112.

[6] Vaezi, M., Katta, A.K., Kumar, A. Investigation into the mechanisms of pipeline transport of slurries of wheat straw and corn stover to supply a bio-refinery. Biosystems Engineering, 2014; 118: 52-67.

[7] Vaezi, M., Kumar, A. The Effect of Agricultural Waste Biomass Slurries on Performance Characteristics of Centrifugal Pumps. Biomass and Bioenergy, 2014; XX: XX.

[8] Elliott, D.R., de Montmorency, W.H. The transportation of pulpwood chips in pipelines. Report of an exploratory study. Montreal: Pulp and Paper Institute of Canada; 1963.

[9] Elliott, D.R. The transportation of pulpwood chips in pipelines. Pulp and Paper Magazine of Canada, 1960; 61: 170-75.

[10] Durand, R., Condolios, G. The hydraulic trasnport of coal and solids in pipes. Hydraulic Transport of Coal Conference London; 1952.

[11] Hunt, W.A. Friction factors for mixtures of wood chips and water flowing in pipelines. 4th Hydrotransport Internatinoal Conference. Banff, AB, Canada; 1976.

[12] Moller, K., Duffy, G.G., A.L., T. Design Correlation for Flow of Pulp Suspensions in Pipes. Appita, 1973; 26: 278-82.

[13] Duffy, G.G., Moller, K., Lee, P.F.W., Milne, S.W.A. Design Correlations for Groundwood Pulps and Effects of Minor Variables on Pulp Suspension Flow. Appita, 1974; 27: 327-33.

[14] Moller, K. General correlations of pipe friction data for pulp suspensions. Tappi, 1976; 59: 111-14.

[15] Duffy, G.G. The optimum design of pipelines for transporting wood pulp fiber suspensions. Appita Journal, 1989; 42: 358-61.

[16] TAPPI. The Technical Association of the Pulp and Paper Industry (TAPPI). Generalized method for determining the pipe friction loss of flowing pulp suspensions. TIP 0410-14. Atlanta, GA, USA; 2007.

[17] Duffy, G.G., Titchene.Al. Design Procedures for Obtaining Pipe Friction Loss for Chemical Pulps. Tappi, 1974; 57: 162-66.

[18] Duffy, G.G. Review and Evaluation of Design Methods for Calculating Friction Loss in Stock Piping Systems. Tappi, 1976; 59: 124-27.

[19] Bowen, R.L. Series of articles. Chemical Engineering, 1961.

[20] Sauermann, H.B., Webster, I.W. Scaling-up slurry pressure gradients from test loop data. CSIR Report No ME 1415. Pretoria, Australia 1975.

[21] Thomas, A.D. Scale-up methods for pipeline transport of slurries. International Journal of Mineral Processing, 1976; 3: 51-69.

[22] Webster, I.W., Sauermann, H.B. Pressure gradient scale-up methods for slurry pipelines. The South African Mechanical Engineer, 1978; 28: 312-17.

[23] Lokon, H.B., Johnson, P.W., Horsley, R.R. A scale-up model for predicting head loss gradients in iron ore slurry pipelines Hydrotransport 8. Johannesburg, South Africa; 1982.

[24] American Society of Agricultural and Biological Engineers (ASABE). Moisture measurement for forages. Standard S3582 St. Joseph, MI, US; 2008.

[25] American Society for Testing and Materials (ASTM). Standard test method for density, relative density, and absorption of coarse aggregate. ASTM, Designation C127; 2012.

[26] McKendry, P. Energy production from biomass (part 1): overview of biomass. Bioresource Technology, 2002; 83: 37-46.

[27] Rasband, W.S. http://rsb.info.nih.gov/ij/index.html, U.S. National Institutes of Health, Accessed September 2011. 2008.

[28] ASABE. Method of determining and expressing particle size of chopped forage materials by screening. Standard ANSI/ASAE S4241. St. Joseph, MI, US: American Society of Agricultural and Biological Engineers, St. Joseph, MI, US; 2007.

[29] SIL Industrial Minerals Inc., http://www.sil.ab.ca/images/stories/pdf/Products/playsand.pdf, Accessed: Jan, 2014.

[30] Sheth, K.K., Morrison, G.L., Peng, W.W. Slip factors of centrifugal slurry pumps. Journal of Fluids Engineering-Transactions of the Asme, 1987; 109: 313-18.

[31] Gahlot, V.K., Seshadri, V., Malhotra, R.C. Effect of Density, Size Distribution, and Concentration of Solid on the Characteristics of Centrifugal Pumps. Journal of Fluids Engineering-Transactions of the Asme, 1992; 114: 386-89.

[32] Sellgren, A. Performance of a centrifugal pump when pumping ores and industrial minerals Hydrotransport, 1979; 1: 291-304.

[33] Elliott, D.R. The transportation of pulpwood chips in pipelines,. Pulp and Paper Magazine of Canada, 1960; 61: 170-75.

[34] Faddick, R.R. Hydraulic transportation of solids in pipelines [dissertation]. Montana State University; 1970.

[35] Hunt, W.A. Friction factors for mixtures of wood chips and water flowing in pipelines. 4th International Conference on the Hydraulic Transport of Solids in Pipes. Alberta, Canada; 1976, p. 1-18.

[36] Brebner, A. On pumping of wood chips through 4-Inch Aluminum pipeline. Canadian Journal of Chemical Engineering, 1964; 42: 139-42.

[37] Duffy, G.G., Lee, P.F.W. Drag reduction in turbulent flow of wood pulp suspensions. Appita, 1978; 31: 280-86.

[38] Lee, P.F.W., Duffy, G.G. Analysis of drag reducing regime of pulp suspension flow. Tappi, 1976 (a); 59: 119-22.

[39] Quantitative Micro Software (QMS), EViews 7.1. IHS Global Inc., Irvine, CA, USA; 2010.

[40] Chatterjee, S., Simonoff, J.S. Handbook of Regression Analysis. Hoboken, New Jersey: Wiley; 2013.

[41] Kwan, A.K.H., Mora, C.F., Chan, H.C. Particle shape analysis of coarse aggregate using digital image processing. Cement and Concrete Research, 1999; 29: 1403-10.

[42] Adapa, P., Tabil, L., Schoenau, G. Grinding performance and physical properties of non-treated and steam exploded barley, canola, oat and wheat straw. Biomass & Bioenergy, 2011; 35: 549-61.

[43] Bitra, V.S.P., Womac, A.R., Yang, Y.C.T., Miu, P.I., Igathinathane, C., Chevanan, N., et al. Characterization of wheat straw particle size distributions as affected by knife mill operating factors. Biomass & Bioenergy, 2011; 35: 3674-86.

[44] Chevanan, N., Womac, A.R., Bitra, V.S.P., Igathinathane, C., Yang, Y.T., Miu, P.I., et al. Bulk density and compaction behavior of knife mill chopped switchgrass, wheat straw, and corn stover. Bioresource Technology, 2010; 101: 207-14.

[45] Vaezi, M., Kumar, A. Pipeline hydraulic transport of biomass materials: A review. Biomass & Bioenergy, 2014; XX.

[46] Radin, I., Zakin, J.L., Patterson, G.K. Drag reduction in solid-fluid systems. Aiche Journal, 1975; 21: 358-71.

[47] Lee, P.F.W., Duffy, G.G. Velocity profiles in drag reducing regime of pulp suspension flow. Appita, 1976 (b); 30: 219-26.

[48] Rao, N.J. Process piping design for pulp suspensions IPPTA, 1985; 22: 27-35.

[49] Duffy, G.G., Titchener, A.L., Lee, P.F.W., Moller, K. Mechanisms of Flow of Pulp Suspensions in Pipes. Appita, 1976; 29: 363-70.

[50] Duffy, G.G. The significance of mechanistic-based models in fibre suspension flow. Nordic Pulp & Paper Research Journal, 2003; 18: 74-80.

[51] Lee, P.F.W., Duffy, G.G. Velocity Profiles in Drag Reducing Regime of Pulp Suspension Flow. Appita, 1976; 30: 219-26.

[52] Lee, P.F.W., Duffy, G.G. Analysis of Drag Reducing Regime of Pulp Suspension Flow. Tappi, 1976; 59: 119-22.

[53] Luthi, O. The flow of MC fibre suspensions TAPPI Engineering Conference. Atlanta; 1987, p. 347.

[54] Pande, H., Rao, N.J., Kapoor, S.K., Roy, D.N. Hydrodynamic behavior of nonwood fiber suspensions. Tappi, 1999; 82: 140-45.

[55] Ingersoll-Rand Co. Cameron Hydraulic Data. 11 ed. New York, NY.

[56] Forrest, F., Grierson, G.H.A. Friction losses in cast iron pipe carrying paper stock Paper Trade, 1931; 92: 39-41.

[57] Brecht, W., Heller, H. A Study of the Friction Losses of Paper Stock. Suspensions. Tappi, 1950; 33.

[58] Durst, R.E., Chase, A.J., Jenness, L.C. An analysis of data on material flow in pipes. Tappi, 1952; 35: 529.

[59] Riegel, P.S. XXX. Tappi, 1966; 49: 32A.

[60] Aktiebolaget Pumpindustri. (1966). Friction losses in piping systems for paper stock suspensions. Goteborg, Sweden.

[61] Bodenheimer, V.B. Channeling in bleach towers and friction losses in pulp stock lines. Southern Pulp and Paper Manufacture, 1969; 32: 42.

[62] Moller, K., Duffy, G.G., A.L., T. Laminar Plug Flow Regime of Paper Pulp Suspensions in Pipes. Svensk Papperstidning-Nordisk Cellulosa, 1971; 74: 829-&.

[63] Genić, S., Arandjelović, I., Kolendić, P., Jarić, M., Budimir, N., Genić, V. A review of explicit approximations of Colebrook's equation. FME Transactions, 2011; 39: 67-71.

CHAPTER 7

Is the Pipeline Hydro-transport of Wheat Straw and Corn Stover to a Biorefinery Realistic?[1]

7.1. Introduction

The United Nations [1] reports biomass as the most significant type of fuel in terms of the quantities used worldwide. Globally people depend on biomass more than any other fuel for energy production. While the residential sector is the largest consumer of biomass for small-scale applications, the industrial sector uses relatively small amount of biomass for electricity generation and fuel/chemical production globally. Trucks are used as the main mode of transporting biomass, and biomass materials come with low bulk density (kg/m^3) and low energy density (GJ/m^3) compared to fossil fuels. These factors result in high delivered cost of biomass, increasing frequency of delivery with increasing scale, and subsequent traffic congestion concerns. Consequently, the desire for short distance truck delivery with fewer congestion issues has favored small-scale biomass-based (bio-based) energy facilities. The challenge with small-scale development is that the capital cost per unit output of conversion facilities are high, resulting in high cost of product (i.e., heat, electricity or liquid fuels) [2, 3]. Earlier work has suggested that biomass conversion facilities have an economic optimum size at which the cost of production is minimum [4]. Such economic optimum size is a trade-off between the transportation cost of biomass (a function of yield of biomass, dry t/ha) and the capital cost per unit output of the plant. The studies have estimated the optimum sizes for a number of biomass-based products as well [5]. At economic optimum sizes the requirement of biomass is large but even these sizes of biomass-based facilities are very small compared to a fossil fuel based plants. For example, the production of ethanol from corn stover exemplifies the issues around large-scale industrial applications of biomass: a plant requires approximately 15 standard highway trucks per hour to receive 2 M dry t/yr of corn stover and produces only 960

[1] Paper submitted to the Journal of Biofuels, Bioproducts, and Biorefining, 2014

ML/yr of ethanol [6, 7];a very small production capacity compared to the 25 GL/yr capacity of a typical oil refinery [8, 9].

Traffic congestion is not the only issue raised with increased scale. The transport and logistics arrangements of biomass from its point of availability, i.e., farm or forest, to its point of use, e.g., bio-based energy facility, contribute significantly to the total delivered cost of biomass. This cost is directly proportional to the number and frequency of trucks required and the distance over which the fuel has to be moved. These factors increase with increasing scale, i.e., economies of scale do not apply to truck delivery [5, 10, 11]. Allen and Browne [12] reported the cost of transporting biomass to be 29%, 22%, 17%, and 12% of the total delivered cost of straw, forest biomass, coppice, and miscanthus, respectively. Epplin [13] estimated the cost to transport switchgrass to a conversion facility to be 8.8 $/dry t or 24% of the total delivered cost. Morey et al. [14] found the truck transport of round bales of corn stover to contribute 24.9% to the total cost. Aden et al. [15] showed the contribution of corn stover delivery to the total delivered cost to be 24%. Kumar and Sokhansanj [16] also reported the cost of truck transport to contribute between 40 to 80% of total cost of transportation, including loading, unloading, stacking, and processing (size reduction) before or after transportation of biomass. Here there is an obvious need to develop an alternative biomass delivery system which is cost effective and can significantly reduce the delivered cost to a large-scale biomass-based facility, also reduce the traffic congestion issue.

Pipeline hydro-transport of biomass (i.e., transporting biomass solid particle-water mixtures in pipes) is an alternative mode of transport which can potentially reduce the cost of biomass transportation compared to trucks, benefit from economy of scale, and minimize the traffic congestion issues of overland transportation. Although such an approach comes with limitations for applications involving combustion [17], there is no penalty in pipeline hydro-transport of biomass in the form of a solid-liquid mixture (slurry) for conversion processes such as ethanol production via fermentation [8], hydrothermal hydrolysis [18], and hydrothermal liquefaction [19] since such conversion processes are all aqueous. In this case, most of the equipment at the pipeline inlet facility replaces those at the bio-refinery that would otherwise be required if biomass were

directly delivered to the plant, e.g., washing, shredding, sizing, and slurrying machines [8]. Biomass slurry would contain almost the required amount of process water, and the slurry would enter the facility directly with or without adjustments in the biomass-water ratio, depending on the concentration at which the slurry is pipelined [20].

Kumar et al. [8, 17, 21] conducted a series of techno-economic analyses on pipeline hydro-transport of wood chips and corn stover. They investigated one-way and two-way pipeline scenarios wherein a one-way pipe would discharge/use the carrier liquid at the receiving facility and a two-way pipe would return all or a portion of the carrier liquid to the inlet facility. They found the cost of transport of wood chips by pipeline at a solid volume content of 30% to be less than the cost of truck delivery at capacities above 0.5 M dry t/yr for one-way pipeline and 1.25 M dry t/yr for two-way pipeline. They also studied the cost of pipeline hydro-transport of corn stover at a 20% solids volume content, compared it with the cost of truck delivery, and found that pipeline hydro-transport costs less than truck delivery at capacities above 1.4 M dry t/yr for one-way pipeline and 4.4 M dry t/yr for two-way pipeline. However, the pressure drop correlation used to obtain corn stover pipeline cost estimates had been originally proposed for transporting wood chips-water mixtures through a pipeline [22, 23]. Luk et al. [24] experimentally studied the technical feasibility of pipelining wheat straw slurries in order to understand the pressure drop behavior of corn stover and other agricultural residue (lignocellulosic) biomass slurries, and Vaezi et al. [20, 25] investigated the friction loss behavior of the slurries of knife-milled and size-classified wheat straw and corn stover particles in pipes as a function of biomass particle type and size, slurry solid mass content, and slurry velocity. They also proposed an empirical correlation to predict the pressure drop of the flow of agricultural residue biomass slurries in pipes which were significantly different than the correlations presented for wood chip-water mixtures.

In this work, the technical parameters and constraints as well as the empirical correlations obtained through the course of experimental study by Vaezi et al. [20, 25-27], together with the pipeline economic structure proposed by Kumar et al. [8, 17, 21], were used to develop a data-intensive techno-economic model to estimate the cost of pipeline hydro-

transport of wheat straw and corn stover agricultural residue biomass to biorefinery. The specific objectives of the present study are:

- Estimating the cost of pipeline hydro-transport of agricultural feedstocks using the pressure drop correlations specifically proposed for agricultural residue biomass [25];
- Comparing the total cost of delivery with the total cost obtained using wood chip pressure drop correlations;
- Estimation of the optimum slurry solid mass content and velocity to obtain the highest throughput at the lowest transport cost;
- Investigating the effect of pipeline capacity and transport distance on the total cost of delivery.

7.2. Techno-economic Modeling

Techno-economic models are powerful tools that combine the technical and financial parameters of a system and help in decision making. In this study, a data-intensive techno-economic model for the transport of wheat straw and corn stover agricultural residue biomass via pipeline was developed. All the costs reported here, even those cited from literature, are based on the 2014 U.S. dollar.

7.2.1. Truck Delivery

The truck transportation cost of biomass consists of two components: distance variable cost (DVC) and distance fixed cost (DFC). The DVC includes equipment, labor, and fuel associated with delivery of biomass and DFC is comprised of equipment and labor associated with loading and unloading of biomass. Further details on this can be found in literature elsewhere [15, 28-32]. The techno-economic model developed in this study includes both DVC and DFC for truck delivery of biomass (Table 7-1). There is a significant variation in the DVC reported earlier, as it is dependent on the type of biomass feedstocks and the methodologies applied in estimation [8]. Figure 7-4 shows the total truck delivery costs (DVC plus DFC for known distance). This figure indicates the independency of truck delivery costs from capacity of transportation where no saving occurs with larger throughputs.

Table 7-1: Distance variable and fixed cost of biomass transportation by truck in North America

Biomass[1]	**Distance Fixed Cost** ($/dry t)	**Distance Variable Cost**[2] ($/dry t.km)	**Total Cost Over A Distance of 150 km** ($/dry t)
Wheat straw [28]	6.66	0.27	47.16
Corn stover [15] (NREL[3])	9.45	0.24	45.45
Switchgrass [29]	10.77	0.15	33.27
Hay and forage [30]	9.20	0.16	33.2
Hay (less than 100 km)[Personal Communication [32]]	9.02[4]	0.40	69.02
Wheat straw [31] (less than 100 km)	-	0.37	-
Wheat straw [31] (more than 200 km)	-	0.25	-

[1] All the costs in the tables are for transportation of biomass in the form of large round bales
[2] The distance accounts for the one-way trip, but the cost includes the return trip
[3] U.S. National Renewable Energy Laboratory
[4] Not available - average of all the distance fixed costs

7.2.2. Pipeline Hydro-transport

The techno-economic model of pipeline hydro-transport was based on economic principles also empirical correlations obtained through previous course of experimental measurements by the authors [20, 24, 27]. The technical model included parameters associated with all the unit operations at inlet, receiving, and booster station facilities involved in pipeline hydro-transport of wheat straw and corn stover. It also characterized operating conditions (e.g., density and viscosity of the biomass slurry, biomass slurry flow rate, etc.), process equipment (e.g., size of water/mixing tanks, diameter of the pipeline, power required for the main and booster pumps, etc.), and unit operations' inputs (water, electricity, biomass feedstock, etc.). The economic parameters in the model were comprised of capital, operating, and maintenance costs of unit operations. Similar to the model by Kumar et al. [8, 17, 21], one- and two-way pipeline scenarios were modeled here, where the two-way pipeline would be required in the case of the scarcity of water upstream or a downstream water discharge prohibition [8, 17]. The techno-economic model was capable of estimating the total cost of pipeline hydro-transport as well as the cost per unit input of feedstock as a function of biomass particle type and size, distance of transport, capacity of pipeline, slurry solid mass content, and pumping velocity.

Kumar et al. [8] reviewed several pressure drop correlations proposed for wood chip-water mixtures in pipes, including correlations by Hunt [33], Brebner [34], Elliot [35], and Faddick [36]. They used the correlation by Hunt [33] to predict the pressure drop of

slurries of corn stover particles in pipes. Vaezi et al. [20] experimentally investigated the applicability of wood chip-water mixture correlations to estimate the pressure drop of slurries of knife-milled and size-classified wheat straw and corn stover particles through a 25 m long, 50 mm diameter closed-circuit pipeline . As observed in Fig. 7-1(a), while the woodchip correlations estimated pressure drop values above those of pure water, the pressure drop of the slurries of both wheat straw and corn stover particles exhibited a unique trend and dropped below that of water at velocities above 2 m/s due to the diverse nature and unusual characteristics of agricultural residue biomass particles, e.g., their relatively large mean particle size; wide size distribution; extreme shapes; fibrous, pliable, flexible, and asymmetric nature; and potential for forming networks (see Table 7-2) [26]. Also, unlike wood chip-water mixtures and all other traditional solid-liquid systems (e.g., sand, coal, clay, iron ore), the pressure drop of the slurry of agricultural residue biomass particles decreases with increasing solid mass content and proved the inapplicability of wood chip-water mixture correlations for the slurries of agricultural residue biomass particles. Figure 7-1(a) illustrates why applying appropriate pressure loss correlations is so critical. Calculating the pressure loss of slurries of agricultural residue biomass particles using correlations proposed for wood chip-water mixtures results in a noticeable overestimation of the pressure losses and, accordingly, the size of the pumps and the total power required. Based on experimental measurements, Vaezi and Kumar [25] later proposed an empirical correlation to predict the pressure drop of the slurries of agricultural residue biomass particles. The same correlation was then applied in this techno-economic model. The ranges of the variables were also adopted from the ranges tried while experimentally pipelining agricultural residue biomass particles [20]. For simplicity, minor losses due to bends, fittings, etc., as well as the change in elevation were ignored, since those are highly localized and specific to a given pipeline project. Table 7-3 shows the technical features of the model and Table 7-4 lists the general economic parameters of the pipeline.

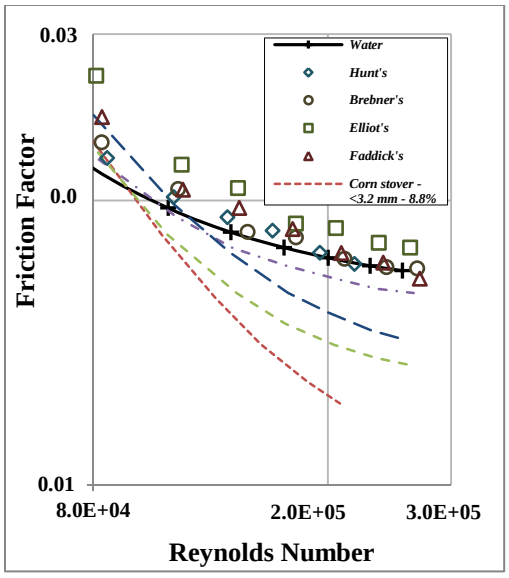

a)

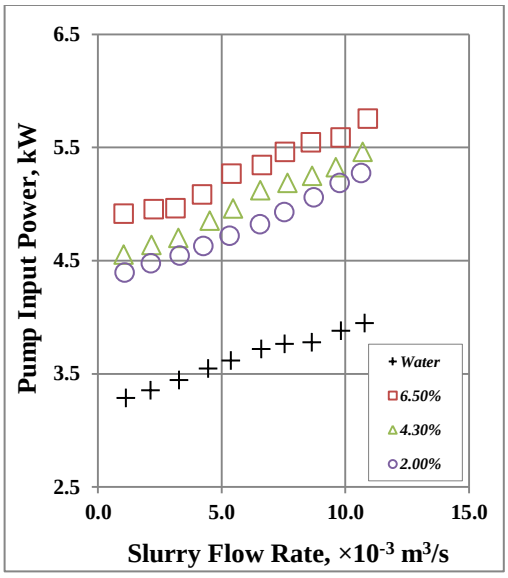

b)

Fig. 7-1: a) Friction factor of the wood chip-water mixtures and slurries of wheat straw and corn stover particles vs. slurry flow Reynolds number, b) Input power to the centrifugal slurry pump handling slurries of 3.2 mm wheat straw particles at 1800 rpm

Table 7-2: Physical properties and shape specifications of wheat straw and corn stover knife-milled and size-classified particles

Solid Particle	Nominal Particle Size (mm)	Median Length (mm)	Particle Aspect Ratio	Particle Specific Gravity	Particle Shape Factor	Slurry Solid Mass Content
	X_n	d_{50}		ρ_p/ρ_f	S	C_d
Wheat Straw	19.2	8.29	6.28	1.026	0.133	1-5.4
	6.4	5.00	4.47		0.196	1-6.5
	3.2	3.92	3.53		0.298	1-7.6
	<3.2	2.42	3.47		0.908	1-8.8
Corn Stover	19.2	7.58	5.93	1.169	0.113	-
	6.4	4.72	4.08		0.169	1-6.5
	3.2	3.32	2.88		0.351	1-7.6
	<3.2	1.90	2.89		0.610	1-8.8

Table 7-3: Input parameters for techno-economic model

Item	Description/Value
Pipeline capacity[*]	250,000 to 4,000,000 M dry t/yr
Average transportation distance[*]	50 to 300 km
Slurry and water pipe material	commercial steel pipe
Slurry and water pipe roughness [37]	0.06096 mm
Biomass particle type[*]	wheat straw and corn stover
Biomass particle size [26][*]	Nominal: <3.2, 3.2, 6.4, and 19.2 mm d_{50}: 1.9 to 8.29 mm
Particle shape factor correlation [25, 27]	$\lambda = \frac{M_s}{\rho_p \times \sum_{j=1}^{n}(X_{gw,j} \times A_{s,j})}$ $shape\ factor = \lambda \times \sqrt{\frac{X_{gw}}{X_{gl}}}$ **Item** / **Description**: λ — Parameter dependent of the flakiness of the particle; dimensionless; M_s — Mass of solid particle sample, kg; ρ_p — Density of solid particle, kg/m^3; X_{gw} — Geometric mean width, mm; X_{gl} — Geometric mean length, mm; A_s — Solid particle area, mm^2
Particle saturated moisture content [20]	82%
Saturated biomass particle density [20]	1050 kg/m^3
Dry matter solid mass content[*]	2 to 8.8%
Slurry velocity[*]	1.5 to 4.5 m/s
Velocity of water in water return pipeline	2 m/s
Slurry pressure drop correlation [25] **Note***: The model is not limited to the agricultural residue biomass studied here. Common agricultural residue biomass or, generally, non-wood fibers and energy crops, if ground, would be fibrous in nature [38-40] and are expected to come with similar mechanical behavior when mixed with water and pumped into pipeline.*	$\frac{\Delta H}{L} = [\sum_{n=1}^{3}(\alpha_n S^n + \beta_n V^n + \gamma_n C_d^n + \delta_n V^n C_d^n)](\frac{D}{D_0})^{-1.2}$ **Item** / **Description**: $\Delta H/L$ — Longitudinal pressure gradient in the pipe, kPa/m; S — Solid particle shape factor; dimensionless; V — slurry bulk velocity, m/s; C_d — Dry solid mass content, %; D — Pipe internal diameter, m; $\alpha, \beta, \gamma, \delta$ — Constants **n = 1** / **n = 2** / **n = 3**: α: 1.2246 / -1.9709 / 0.6485; β: 0.0000 / 0.16389 / 0.0000; γ: 0.0000 / 0.00000 / 0.0006; δ: 0.0000 / -0.0010 / 0.0000; D_0: 0.0508 m
Slurry and water pump efficiency [41]	80%
Maximum pressure of the pump	3100 kPa

[*] Model initial and operating variables

Table 7-4: General economic parameters of the techno-economic model

Item	Values
Inflation rate	2.1%
Discount rate	10%
Life of pipeline	30 yr
Life of pump	20 yr
Capacity factor of pipeline	0.85
Maintenance cost of	
- equipment	3% of capital cost
- pipeline	0.5% of capital cost
Power cost	50 $/MWh
Engineering cost	10% of total capital cost
Contingency cost	5% of total cost
Scale factor	0.75

A contingency cost equal by 5% of the total capital and engineering cost of pipeline was calculated in the model, versus 20% contingency applied by Kumar et al. [17]. A sensitivity analysis on contingency cost revealed increasing the contingency from 5% to 20% will increase the cost of pipeline hydro-transport of biomass ($/dry t/km) between 7 to 11%.

Table 7-5 summarizes the major unit operations at inlet, booster stations, and receiving facilities together with the capital and operating/maintenance costs of the units. The unit operations' capital cost estimates were made according to correlations proposed in earlier studies [17, 41-43]. The capital, operating, and maintenance costs were calculated here in Table 7-5 for a sample case of pipeline hydro-transport of biomass: a 1.16 m diameter one-way pipeline transporting 2,000,000 dry t/yr slurry of <3.2 mm (d_{50} = 2.42 mm) wheat straw particles at 8.8% dry matter solid mass content and 2.5 m/s velocity over a distance of 200 km. All the initial and operating variables were chosen from corresponding ranges presented on Tables 7-2 and 7-3. The pipeline diameter was calculated based on the pipeline transport capacity and slurry velocity, and the number of booster stations was obtained by dividing the total pressure drop throughout the pipeline by the total head produced by the main and booster pumps.

Pipeline hydro-transport has a cost structure similar to that of truck delivery with costs either fixed or variable with distance. The fixed (distance-independent) cost is associated with the equipment at inlet and receiving facilities, and variable (distance-dependent) costs come from operating and maintenance costs, recovery of the capital investment in the pipeline and booster stations, and associated infrastructures such as road access. Fixed capital costs at inlet and receiving facilities are typically lower than the total capital costs of the pipeline system. It can be observed on the same example as of Table 7-5 that, in a pipeline with a capacity of 2 M dry t/yr that hydraulically transports an 8.8% slurry of <3.2 mm wheat straw particles at a velocity of 2.5 m/s over a distance of 200 km, the investment in inlet and receiving facilities comprises only 5.6% of the pipeline costs (material, construction, etc.) and 5.2% of the total capital cost of the one-way pipeline system.

Table 7-5: Capital, operating, and maintenance costs of inlet, booster stations, and receiving facilities

Item	Cost	Description*
Note: *The results are for a 1.16 m diameter one-way pipeline transporting 2 M dry t/yr slurry of <3.2 mm (d_{50} = 2.42 mm) wheat straw particles at an 8.8% dry matter solid mass content and 2.5 m/s velocity over a distance of 200 km with one booster station in the middle*		
Inlet Facility		
Capital Costs		
Land, $	51,513	- 30 hectare - Includes truck unloading area, weight scale, dead storage area, tank space, and pump space - Estimated by Kumar et al. [17] at 2000 and inflated to 2014 USD with a rate of 7.1%
Intake piping for water, $	708,316	- 100 m long and 0.6 m diameter pipeline to transport 0.6 m^3/s of water - Includes piping from mixing tank to the water storage tank - Calculated using the formula by Liu et al. [41]
Mixing tank, $	80,949	- 27 m^3 with a slurry residence time of 45 s - Calculated using the formula by Peter et al. [43]
Storage tank for water, $	1,015,535	- 790 m^3 - 30 min storage - Calculated using the formula by Peter et al. [43]
Power supply lines, $	528,000	- 4.5 MW - Estimated by Epcor Utilities Inc.
Building, $	312,631	- 300 m^2 - Includes control room for pump, site monitoring, maintenance area, warehouse, communication and pipeline control room - Estimated by Kumar et al. [17]
Slurry pipeline, $	225,777,903	- Calculated using the formula by Liu et al. [41] as a function of pipe diameter
Main pump (with one redundant pump), $	5,538,211	- Calculated using formula by Liu et al. [41] as a function of total pump power required - Total power required is the product of flow rate (m^3/s), head loss (m), and efficiency of the pump
Total capital cost at inlet facility, $	235,325,298	
Amortized capital cost at inlet facility, $/yr	25,034,571	
O/M Costs		
Main pump power, $/yr	2,737,079	- Based on 60 $/MWh electricity cost and 0.85 pipeline capacity factor
Salary and wages, $/yr	1,080,000	- Based on 4 staffs, 2000 hr/yr, 27 $/hr,
Maintenance cost, $/yr	1,359,657	- Based on 3 and 0.5% of capital costs for equipment and pipeline, respectively
Total operating cost at inlet facility, $/yr	5,493,731	

Table 7-5 (Cont'd): Capital, operating, and maintenance costs of inlet, booster stations, and receiving facilities

Booster Station Facility		
Capital Costs		
Booster pump, $	2,783,718	- Calculated using formula by Liu et al. [41] as a function of extra pump power required in addition to the initial power provided by the main pump
Substation, $	528,000	- 4MW - Estimated by Epcor Utilities Inc.
Total capital cost at booster station, $	3,476,760	
Amortized capital cost at booster station, $/yr	525,691	
O/M Costs		
Booster pump, $/yr	2,755,020	- Based on 60 $/MWh electricity cost and 0.85 pipeline capacity factor
Maintenance cost, $/yr	83,511	- Based on 3% of capital cost for equipment
Total operating cost at booster station, $/yr	2,866,081	
Receiving Facility		
Capital Costs		
Buildings, $	312,631	- 300 m^2 - It includes control room for pump and pipeline, site monitoring, and communication - Estimated by Kumar et al. [17]
Water intake tank, $	1,015,535	- 790 m^3 - Heated and insulated - Calculated using the formula by Peter et al. [43]
Total capital cost at receiving facility, $	2,337,895	
Amortized capital cost at receiving facility, $/yr	279,877	
O/M Costs		
Salary and wages, $/yr	540,000	- Based on 2 staffs, 2000 hr/yr, 27 $/hr
Maintenance cost, $/yr	70,897	- Based on 3, 0.5, and 5% of capital costs for equipment, pipeline, and conveyer belts, respectively
Total operating cost at receiving facility, $/yr	678,087	
Total capital cost of pipeline hydro-transport system, $	241,139,955	
Total operating cost of pipeline hydro-transport system, $/yr	9,037,901	
Fixed cost of pipeline hydro-transport, $/dry t	1.23	
Variable cost of pipeline hydro-transport, $/dry t.km	0.10	

* The unit operations capital cost estimates were made according to correlations proposed by Liu et al. [41], Chandler et al. [42], Peters and Timmerhaus [43], and Kumar et al. [17]

7.3. Results and Discussion

7.3.1. Sensitivity Analysis

Every single parameter studied here, if changed, could change the total cost of pipeline hydro-transport independently of the other parameters. Of all the variables (biomass particle type and size, pipeline capacity, pipeline length, and slurry solid mass content and velocity), the slurry solid mass content and slurry velocity were optimized first, as the former defines the material/water ratio at the inlet facility and the latter determines the diameter of the pipe. In addition, the two variables impact the pressure drop throughout the pipeline and contribute to the total power required. Therefore, the effect of these parameters on the cost of pipeline hydro-transport was investigated first to obtain the optimum (with respect to the cost) velocity and solid mass content.

Vaezi et al. [20] found that the slurry pressure drop decreased with increasing velocity and solid mass content (Fig. 7-1(a)). In another study [27], it was observed that the pump input power increased with an increase in slurry velocity and solid mass content (Fig. 7-1(b)). Therefore, although increasing the slurry velocity and solid mass content decreased the pressure drop, it increased the power required to run the centrifugal pumps. The authors first tried to find an optimum slurry velocity and solid mass content where the cost of pipeline hydro-transport was the lowest. Figure 7-2 presents the cost of hydro-transport of <3.2 mm wheat straw particles using a commercial scale pipeline with a capacity of 2 M dry t/yr over a long distance of 200 km as a function of slurry velocity and solid mass content. Considering the variation of the cost of pipeline hydro-transport with respect to the slurry solid mass content only, it was noted that the cost continuously decreased with increasing solid mass content. This was because an increase in slurry solid mass content decreased the slurry volumetric flow rate, which subsequently, at fixed slurry velocity, decreased the pipe diameter and hence the corresponding capital costs. However, at fixed slurry solid mass content, fluctuations in the cost were observed with continuous increase in slurry velocity. The total cost first decreased with an increasing velocity from 1.5 to 2.5 m/s and then increased with increasing velocity from 2.5 to 4.5 m/s. The reason is that although the diameter of the pipe and the total capital cost continuously decreased with increasing velocity, the pressure drop and, consequently, the number of booster stations and total operating cost increased with increasing velocity more noticeably at elevated velocities.

Consequently, at a velocity of 2.5 m/s and a solid mass content of 8.8%, the variable cost of pipeline hydro-transport was found to be at its lowest in both one-way and two-way pipeline systems. This was true for all the pipeline lengths, capacities, biomass particles types and sizes. The optimum velocity was, in fact, within the range of velocity of commercial pipelines, 1.5 to 3 m/s.

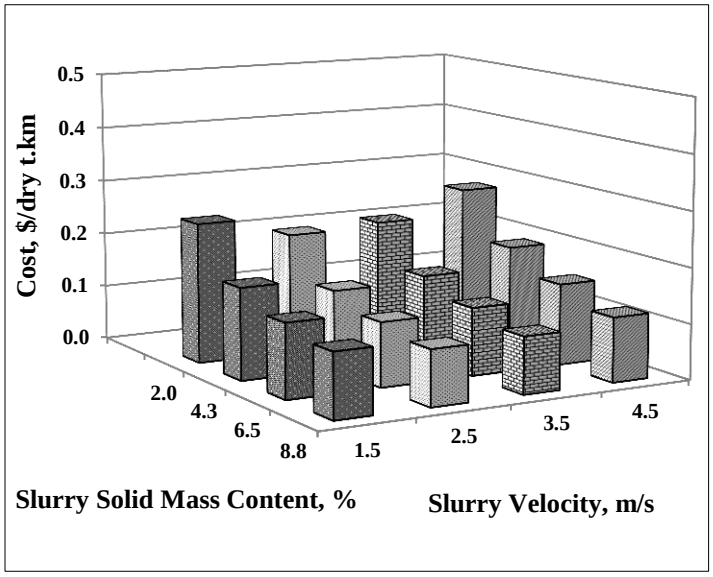

a) Distance variable cost of one-way pipeline hydro-transport of 2,000,000 dry t/yr of<3.2 mm wheat straw particles over a 200 km distance as a function of slurry velocity and solid mass content

% / m/s	2	4.3	6.5	8.8
1.5	0.254	0.166	0.134	0.116
2.5	0.218	0.143	0.116	**0.100**
3.5	0.226	0.152	0.122	0.102
4.5	0.273	0.188	0.147	0.116

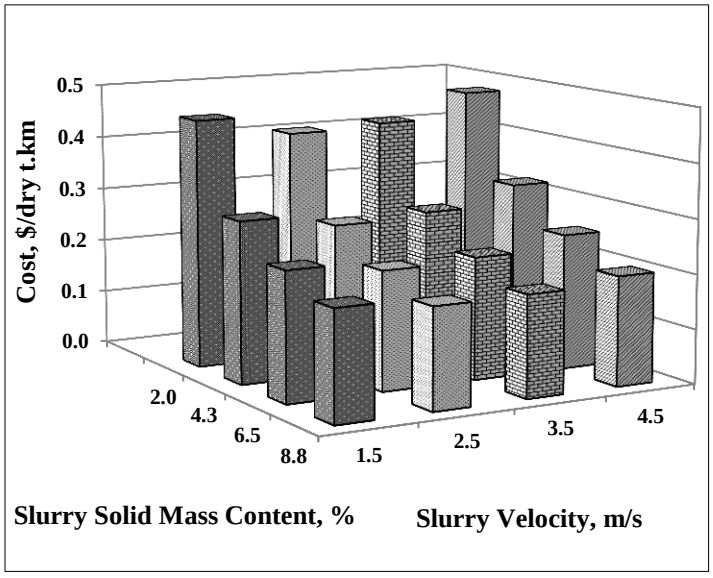

b) Distance variable cost of two-way pipeline hydro-transport of 2,000,000 dry t/yr of <3.2 mm wheat straw particles over a 200 km distance as a function of slurry velocity and solid mass content

% / m/s	2	4.3	6.5	8.8
1.5	0.458	0.297	0.237	0.201
2.5	0.422	0.274	0.219	**0.185**
3.5	0.430	0.283	0.225	0.187
4.5	0.477	0.319	0.249	0.201

Fig. 7-2: Distance variable cost of pipeline hydro-transport of wheat straw particles as a function of slurry velocity and solid mass content

Other variables whose impacts on the cost of pipeline hydro-transport were investigated were biomass particle type and size. As observed on Table 7-2, two types of agricultural residue biomass of wheat straw and corn stover were chosen for this study. In an earlier study, Vaezi et al. [26] investigated the particle size, particle size distribution, and morphological features of wheat straw and corn stover and found that the knife-milled pre-classified wheat straw and corn stover particles had nominal sizes of <3.2, 3.2, 6.4, and 19.2 mm with corresponding median lengths (d_{50}) between 1.9 mm and 8.29 mm (Table 7-2).The nominal sizes were chosen in this work as the common dimensions of significance to refer to the biomass particles throughout the paper. It was found that, although slurry pressure drop throughout the pipe is a function of biomass particle type and size, or more specifically biomass shape factor (see Table 7-3), the effect of biomass shape factor on the cost of pipeline hydro-transport was negligible. Figure 7-3 compares various particle types and sizes, where for a certain type a change in the size of the particles resulted in an average change of only1.4% in the pipeline hydro-transport cost. However, the authors are not able to validate the same effect on the particles that are out of the range of the dimensions studied here. For simplicity, <3.2 mm wheat straw particles were chosen for which, together with a slurry velocity of 2.5 m/s and solid mass content of 8.8% (fixed when needed), all the costs of pipeline hydro-transport were calculated and reported.

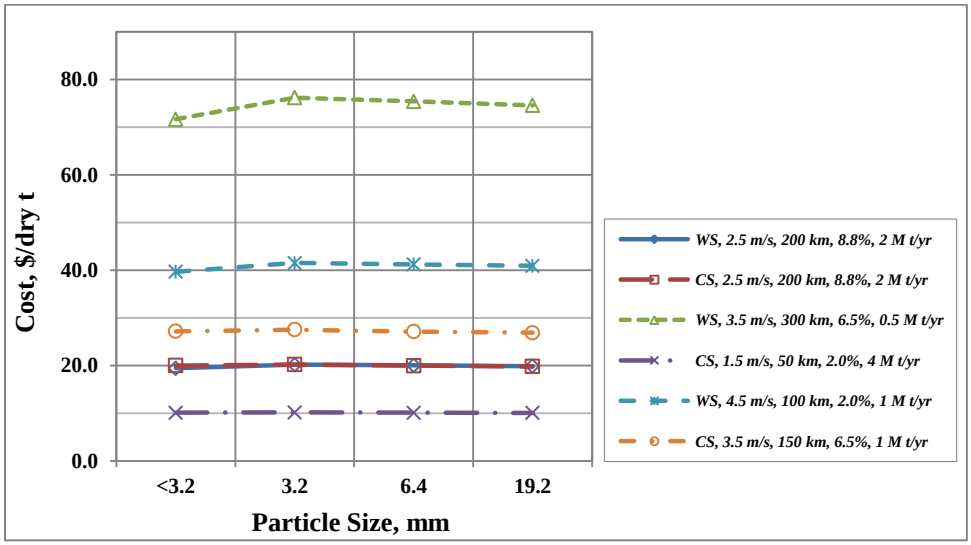

Fig. 7-3: Cost of pipeline transport of various biomass particle sizes

7.3.2. Truck Delivery vs. Pipeline Hydro-transport of Biomass

In light of the sensitivity analyses conducted on biomass particle type and size, as well as slurry velocity and solid mass content, results were calculated for slurries of <3.2 mm wheat straw particles at a velocity of 2.5 m/s. When needed, the solid mass content was fixed at the optimum value of 8.8% dry matter, and the cost of pipeline hydro-transport was compared with the total cost of truck delivery from four sources (Kumar et al. [28], Aden et al. [15], and Duffy [29], and personal communication with a local transport company [32]) and is shown in Table 7-1.

Figure 7-4 shows the cost of one-way and two-way pipeline hydro-transport of <3.2 mm wheat straw particles at 2.5 m/s over 150 km as a function of pipeline capacity and slurry solid mass content. As observed, unlike with truck delivery, there are strong economies of scale in pipeline hydro-transport of agricultural residue biomass. The economies of scale benefits are associated with the cost of pipeline and its construction, also the cost of equipment at inlet and receiving facilities. Increasing the pipe diameter also decreases the slurry pressure drop [17] which cause saving in the total pumping power required. For instance, on a 200 km one-way pipeline transporting 8.8% solid mass content slurry of <3.2 mm wheat straw particles at 2.5 m/s, doubling the pipeline capacity from 2 M dry t/yr to 4 M dry t/yr, increased the capital cost, operating cost, and total cost by 49%, 27%, and 44%, respectively. This resulted in a decrease in the total cost per unit mass delivered ($/dry t) by 28%. Liu et al. [41] suggested a capital cost scale factor of 0.59-0.62 for a pipeline systems. However, a more conservative scale factor of 0.75 was applied here to inlet, receiving, and booster station facilities, excluding pumps and pipes. Figure 7-4 also reveals the significant cost of a two-way pipeline with the return of the carrier liquid, as compared with a one-way pipeline.

For a given distance, pipeline hydro-transport costs decreased with increasing solid mass content (as discussed in section 3.1) and pipeline capacity. The point at which pipeline hydro-transport costs drop below truck delivery costs depends strongly on the total truck delivery cost for a given distance. Based on an 8.8% slurry solid mass content, 2.5 m/s slurry velocity, and the lowest estimate of the total truck delivery costs reported [29] (i.e.,

0.22 $/dry t.km), pipeline hydro-transport becomes economically more viable than truck delivery at capacities of 0.45 M dry t/yr or more for a one-way pipeline and 1.4 M dry t/yr or more for a two-way pipeline. However, the highest estimate of truck delivery costs (i.e., 0.46 $/dry t) [32] would always cost more than pipeline hydro-transport for one-way pipelines. It would also cost more for two-way pipelines with capacities above 0.35 M dry t/yr.

For this specific case of study (<3.2 mm wheat straw particles at 2.5 m/s over 150 km), at a typical pipeline capacity of 2 M dry t/yr and slurry solid mass content of 8.8%, 76% of the total costs of a one-way pipeline system is due to its capital cost (22.6 M $/yr) and 24% are operating costs (7.3 M $/yr). Among the operating costs, the largest component, 56%, is electrical power for pumping (4.1 M $/yr). Corresponding numbers for two-way pipelines are 80%, 20%, and 64%, respectively.

Figure 7-5 compares the DFC and DVC of pipeline hydro-transport and truck delivery of biomass. The costs for pipeline hydro-transport of biomass are calculated for a slurry of <3.2 mm wheat straw particles at the optimum slurry and operating conditions of 8.8% solid mass content and 2.5 m/s velocity (section 3.1). The distance fixed and variable costs for truck delivery are taken from Table 7-1. As observed in Fig. 7-4(a), all one-way pipelines with transport capacities of 1 M dry t/yr and higher, always have DFC and DVC lower than those for hauling by truck. For a one-way pipeline with a capacity of 0.5 M dry t/yr, pipeline hydro-transport of biomass can compete with truck delivery only up to a distance of 228 km, based on the lowest estimate of reported truck delivery costs [29]. For a one-way pipeline with a capacity of 0.25 M dry t/yr, the viability of the pipeline hydro-transport of biomass depends strongly on DVC and DFC of truck delivery, as considering the reported lowest estimate of the cost of truck delivery [29] makes the pipeline competitive only up to a distance of 30 km, and choosing the highest cost estimate of truck delivery [32] makes the pipeline hydro-transport cost always less than truck delivery.

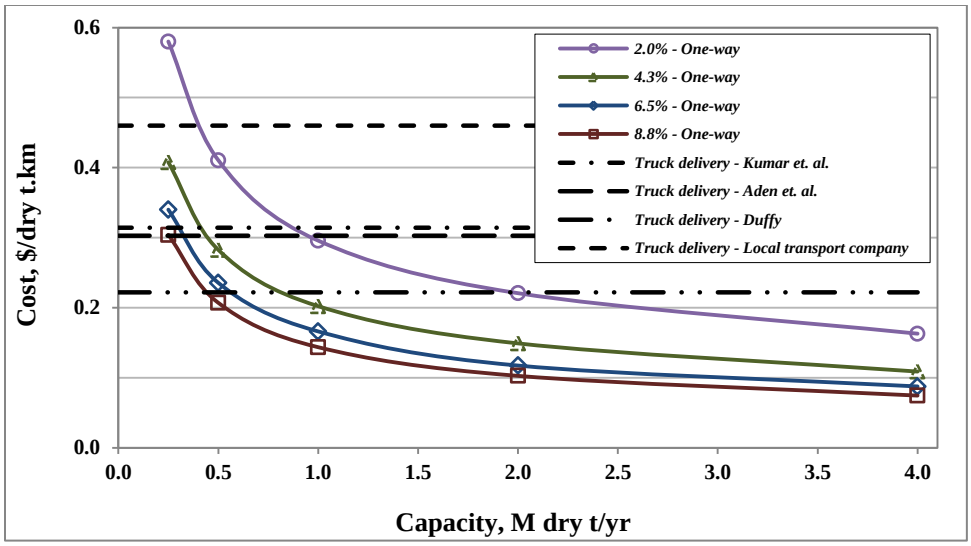

a)

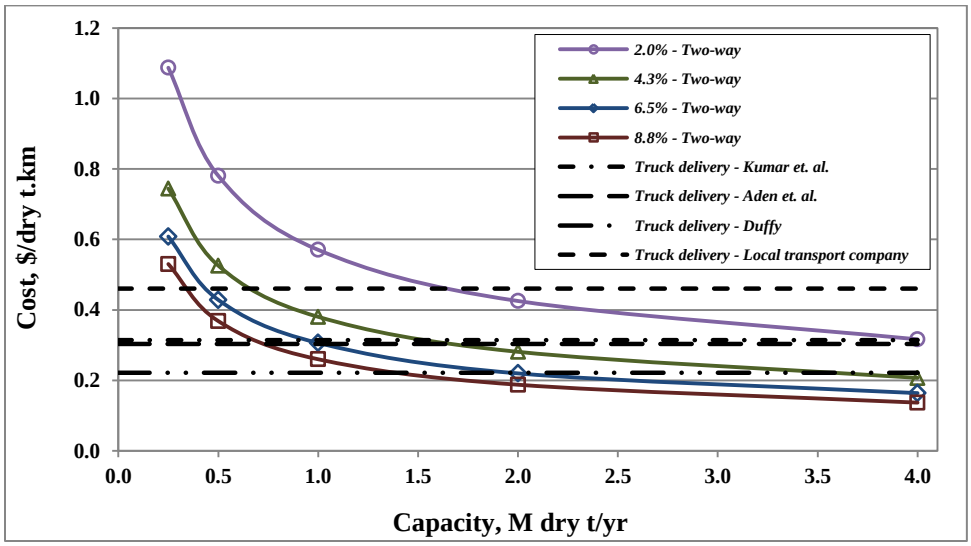

b)

Fig. 7-4: Costs of a) one-way and b) two-way pipeline hydro-transport of <3.2 mm wheat straw particles at 2.5 m/s over 150 km as a function of pipeline capacity and slurry solid mass content

Figure 7-5(b) compares the costs of two-way pipeline hydro-transport of biomass and truck delivery for similar slurry and operating conditions. For two-way pipelines with capacities of 2 M dry t/yr and more, pipeline hydro-transport would always cost less than truck transport.

Technically, every extra booster station required for extra distances would slightly increase the total cost and would shape the pipeline hydro-transport cost curve like a sawtooth. However, in practice, the cost of an incremental booster station is negligible

compared to the total cost of the pipeline system, and so the sawtooth effect can be ignored [17]. For instance, for a pipeline system with a capacity of 2 M dry t/yr pumping 8.8% solid mass content slurry of <3.2 mm wheat straw particles at 2.5 m/s, every extra booster stations adds only 1.8% to the total cost of pipeline system.

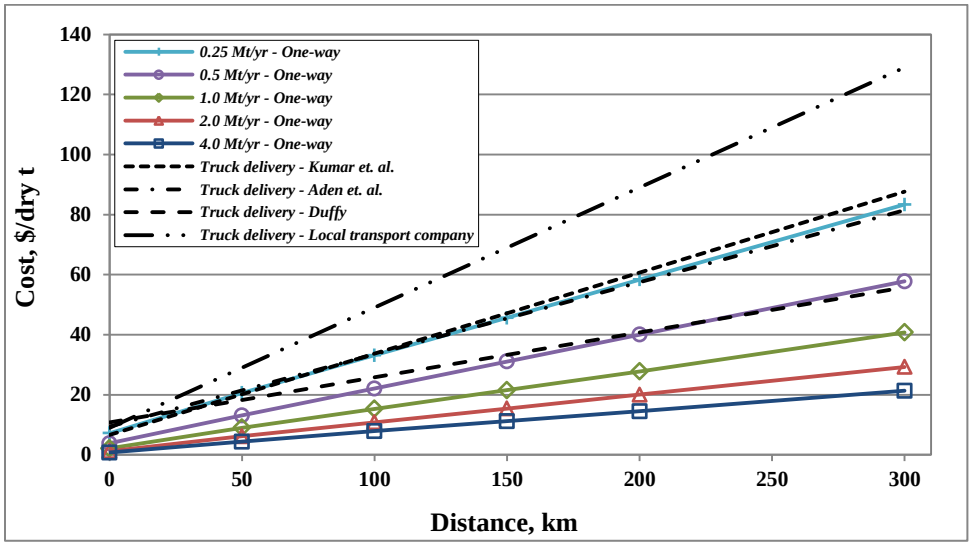

a)

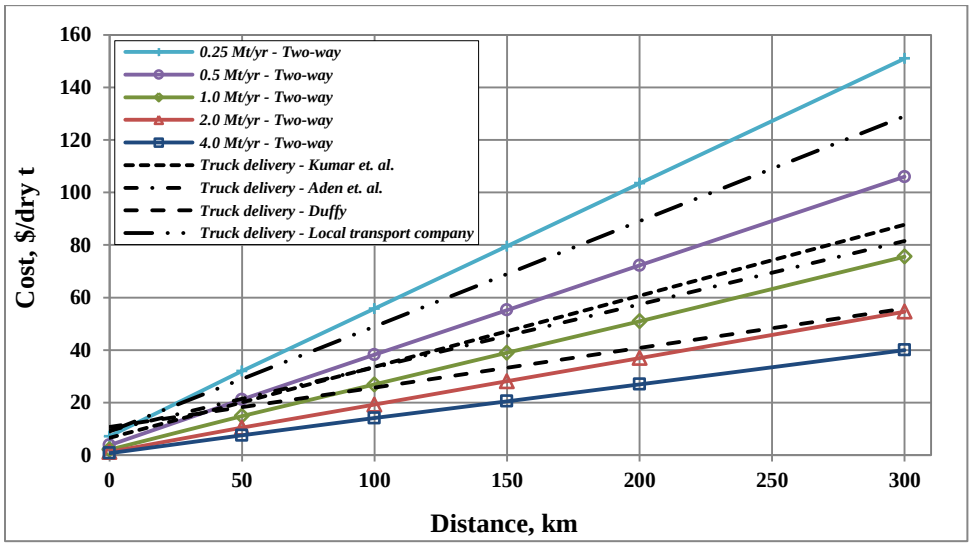

b)

Fig. 7-5: Cost of a) one-way and b) two-way pipeline transport of 8.8% solid mass content slurry of <3.2 mm wheat straw particles at 2.5 m/s as a function of pipeline length and capacity

7.3.3. Integrated Truck/Pipeline ransport of Biomass

Kumar et al. [17] pointed out that pipeline hydro-transport of biomass normally requires an initial truck delivery of biomass to the pipeline inlet, where the fixed costs of both truck delivery and hydro-transport are incurred. In this study, considering an average yield of 0.39 dry t/ha for straw [28], the initial distance of truck delivery to collect and transport 0.5 M dry t/yr (minimum economic capacity for one-way pipeline as per Fig. 7-4(a)) and 1.4 M dry t/yr (minimum economic capacity for two-way pipeline as per Fig. 7-4(b)) of wheat straw was calculated [44] to be 59 and 96 km, respectively. The corresponding costs of truck delivery to a pipeline inlet facility were afterwards included into the model, with further transport of wheat straw by one- and two-way pipeline in the form of 8.8% solid mass content slurry at 2.5 m/s velocity. Figure 7-6 shows the cost curves of integrated truck/pipeline systems together with truck-only transport. As it is observed, pipeline transport always cost more than truck delivery at capacities of 0.5 M dry t/yr for one-way and 1.4 M dry t/yr for two-way pipelines thus cannot compete with truck delivery over the extra distance. This occurs because DVC of truck delivery is smaller than DVC of truck plus either one- or two-way pipeline at these minimum economic capacities. However, there will be intersection between truck and integrated truck/pipeline DVC lines at higher capacities, where integrating will cost less than truck-only delivery. For instance, at a capacity of 2 M dry t/yr, the minimum pipeline distance to recover the fixed costs of the pipeline and the initial 115 km truck delivery to the pipeline inlet is 141 km for a one-way pipeline. Pipelines shorter than 141 km are less economical than truck-only delivery.

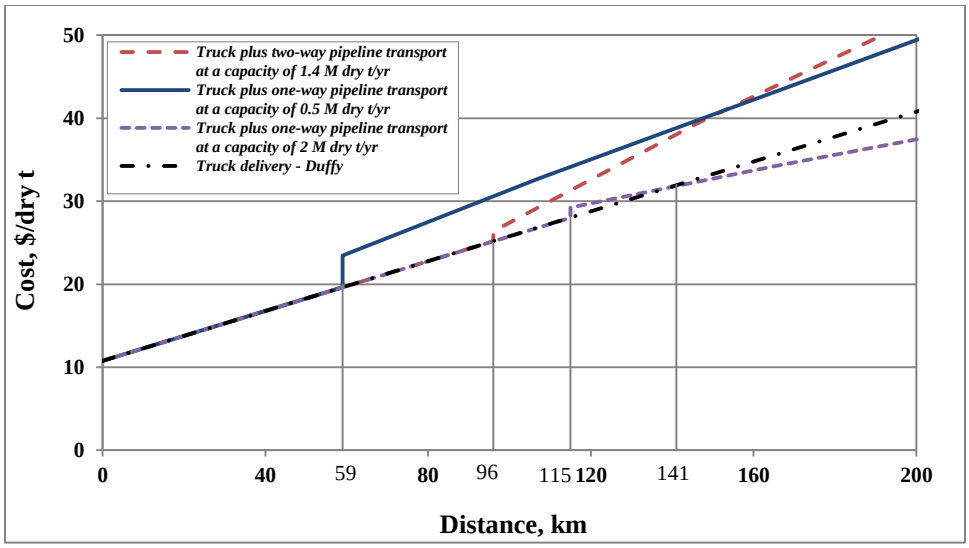

Fig. 7-6: Comparison of integrated truck/pipeline transport with truck-only delivery of <3.2 mm wheat straw particles at one-way pipeline capacities of 0.5 and 2 M dry t/yr and two-way pipeline capacity of 1.4 M dry t/yr, slurry solid mass content of 8.8%, and pipeline slurry velocity of 2.5 m/s

7.4. Conclusions

Pipeline hydro-transport can economically compete with truck delivery of agricultural residue biomass at medium to large capacities over long distances. Based on 8.8% slurry solid mass content, 2.5 m/s slurry velocity, 150 km medium-range distance, and the lowest estimate of the total cost of truck delivery reported (0.22 $/dry t.km), pipeline hydro-transport is economically more viable than truck delivery at capacities of 0.5 M dry t/yr or more for one-way pipelines and 1.4 M dry t/yr or more for two-way pipelines. Considering the highest estimate of the total cost of truck delivery reported ($0.46/dry t), pipeline hydro-transport of the same slurry would always cost less than truck delivery for one-way pipeline, also it would cost less than truck delivery at capacities above 0.35 M dry t/yr for two-way pipelines. Integrated truck/pipeline transport of agricultural residue biomass at minimum economic capacities of 0.5 and 1.4 M dry t/yr for one- and two-way pipeline with initial truck delivery of 59 and 96 km was also studied. For these scenarios, pipeline transport was found economically not capable of competing with truck delivery over the extra distance. However, benefits were found at higher capacities to integrate truck and pipeline, where truck plus pipeline transport of biomass would cost less than

truck-only delivery. Understanding the structure of the cost of the pipelines transporting agricultural residue biomass helps to identify and optimize critical variables to reduce the total cost of delivery and enable bio-based energy facilities to achieve higher capacities.

References

[1] UN. Green energy: biomass fuels and the evironment. Geneva, Switzerland United Nations; 1991.

[2] Miller, P., Kumar, A. Techno-economic assessment of hydrogenation-derived renewable diesel production from canola and camelina. Sustainable Energy Technologies and Assessments, 2014; 6: 105-15.

[3] Sarkar, S., Kumar, A., Sultana, A. Biofuels and biochemicals production from forest biomass in Western Canada. Energy, 2011; 36: 6251-62.

[4] Ruth, M. Large scale ethanol facilities and short cut for changing facility size. Internal Report, National Renewable Energy Laboratory (NREL); 1999.

[5] Sultana, A., Kumar, A. Optimal configuration and combination of multiple lignocellulosic biomass feedstocks delivery to a biorefinery. Bioresource Technology, 2011; 102: 9947-56.

[6] Kadam, K.L., McMillan, J.D. Availability of corn stover as a sustainable feedstock for bioethanol production. Bioresource Technology, 2003; 88: 17-25.

[7] Sokhansanj, S., Turhollow, A., Cushman, J., Cundiff, J. Engineering aspects of collecting corn stover for bioenergy. Biomass & Bioenergy, 2002; 23: 347-55.

[8] Kumar, A., Cameron, J.B., Flynn, P.C. Pipeline transport and simultaneous saccharification of corn stover. Bioresource Technology, 2005 (b); 96: 819-29.

[9] Wallace, B., Yancey, M., Easterly, J. Bioethanol co-location with a coal-fired power plant. 25th Symposium on Biotechnology for Fuels and Chemicals Breckenridge, CO; 2003.

[10] Sarkar, S., Kumar, A. Biohydrogen production from forest and agricultural residues for upgrading of bitumen from oil sands. Energy, 2010; 35: 582-91.

[11] Sultana, A., Kumar, A., Harfield, D. Development of agri-pellet production cost and optimum size. Bioresource Technology, 2010; 101: 5609-21.

[12] Allen, J., Browne, M. Logistics management and costs of biomass fuel supply. International Journal of Physical Distribution & Logistics Management, 1998; 28: 463-77.

[13] Epplin, F.M. Cost to produce and deliver switchgrass biomass to an ethanol-conversion facility in the Southern Plains of the United States. Biomass & Bioenergy, 1996; 11: 459-67.

[14] Morey, R.V., Kaliyan, N., Tiffany, D.G., Schmidt, D.R. A biomass supply logistics system. 2009, p. 4802-14.

[15] Aden, A., Ruth, M., Ibsen, K., Jechura, J., Neeves, K., Sheehan, J., et al. Lignocellulosic biomass to ethanol process design and economics utilizing co-current dilute acid prehydrolysis and enzymatic hydrolysis for corn stover (Report No TP-510-32438). National Renewable Energy Laboratory (NREL); 2002.

[16] Kumar, A., Sokhansanj, S. Switchgrass (Panicum vigratum, L.) delivery to a biorefinery using integrated biomass supply analysis and logistics (IBSAL) model. Bioresource Technology, 2007; 98: 1033-44.

[17] Kumar, A., Cameron, J.B., Flynn, P.C. Pipeline transport of biomass. Applied Biochemistry and Biotechnology, 2004; 113: 27-39.

[18] Thangavelu, S.K., Ahmed, A.S., Ani, F.N. Bioethanol production from sago pith waste using microwave hydrothermal hydrolysis accelerated by carbon dioxide. Applied Energy, 2014; 128: 277-83.

[19] Zhu, Y., Biddy, M.J., Jones, S.B., Elliott, D.C., Schmidt, A.J. Techno-economic analysis of liquid fuel production from woody biomass via hydrothermal liquefaction (HTL) and upgrading. Applied Energy, 2014; 129: 384-94.

[20] Vaezi, M., Katta, A.K., Kumar, A. Investigation into the mechanisms of pipeline transport of slurries of wheat straw and corn stover to supply a bio-refinery. Biosystems Engineering, 2014; 118: 52-67.

[21] Kumar, A., Cameron, J.B., Flynn, P.C. Large-scale ethanol fermentation through pipeline delivery of biomass. Applied Biochemistry and Biotechnology, 2005 (a); 121: 47-58.

[22] Hunt, W.A. Friction factors for mixtures of wood chips and water flowing in pipelines,. 4th International Conference on the Hydraulic Transport of Solids in Pipes. Alberta, Canada; 1976., p. 1-18.

[23] Wasp, E.J., Aude, T.C., Thompson, T.L., Bailey, C.D. Economics of chip pipelining. Tappi, 1967; 50: 313-18.

[24] Luk, J., Mohammadabadi, H.S., Kumar, A. Pipeline transport of biomass: Experimental development of wheat straw slurry pressure loss gradients Biomass and Bioenergy, 2014; 64: 329-36.

[25] Vaezi, M., Kumar, A. A design correlation for the flow of agricultural waste biomass slurries in pipes Biosystems Engineering, 2014; XX.

[26] Vaezi, M., Pandey, V., Kumar, A., Bhattacharyya, S. Lignocellulosic biomass particle shape and size distribution analysis using digital image processing for pipeline hydro-transportation. Biosystems Engineering, 2013; 114: 97-112.

[27] Vaezi, M., Kumar, A. The flow of wheat straw suspensions in an open impeller centrifugal pump. Biomass and Bioenergy, 2014; XX: XX.

[28] Kumar, A., Cameron, J.B., Flynn, P.C. Biomass power cost and optimum plant size in western Canada. Biomass & Bioenergy, 2003; 24: 445-64.

[29] Duffy, M. Estimated costs for production, storage and transportation of switchgrass. Ag Decision Maker: An agricultural economics and business; 2008.

[30] Dhuyvetter, K.C. 2014 projected custom rates for Kansas. Kansas State University, Department of Agricultural Economics 2014.

[31] DeSmet, O. Bales R Us Co.; 2014.

[32] Personal communication with local truck transport company In: Schmuecker, B., editor. Sherwood Park, Alberta, +1 403 795 7997; May 7th, 2014.

[33] Hunt, W.A. Friction factors for mixtures of wood chips and water flowing in pipelines. 4th International Conference on the Hydraulic Transport of Solids in Pipes. Alberta, Canada; 1976, p. 1-18.

[34] Brebner, A. On pumping of wood chips through 4-Inch Aluminum pipeline. Canadian Journal of Chemical Engineering, 1964; 42: 139-42.

[35] Elliott, D.R. The transportation of pulpwood chips in pipelines,. Pulp and Paper Magazine of Canada, 1960; 61: 170-75.

[36] Faddick, R.R. Head loss studies of transport of woodchips in pielines. [dissertation]. Queen's University; 1963.

[37] White, F.M. Fluid mechanics 7th ed. New York, N.Y. : McGraw Hill; 2011.

[38] Adapa, P., Tabil, L., Schoenau, G. Grinding performance and physical properties of non-treated and steam exploded barley, canola, oat and wheat straw. Biomass & Bioenergy, 2011; 35: 549-61.

[39] Bitra, V.S.P., Womac, A.R., Yang, Y.C.T., Miu, P.I., Igathinathane, C., Chevanan, N., et al. Characterization of wheat straw particle size distributions as affected by knife mill operating factors. Biomass & Bioenergy, 2011; 35: 3674-86.

[40] Chevanan, N., Womac, A.R., Bitra, V.S.P., Igathinathane, C., Yang, Y.T., Miu, P.I., et al. Bulk density and compaction behavior of knife mill chopped switchgrass, wheat straw, and corn stover. Bioresource Technology, 2010; 101: 207-14.

[41] Liu, H., Noble, J., Zuniga, R., Wu, J. Economic analysis of coal log pipeline transportation of coal. Report No 95-1. Capsule Pipeline Research Center (CPRC), University of Missouri, Columbia, USA; 1995.

[42] Chandler, H.M. RS Means Company - Heavy construction data, 14th annual edition Kingston, USA; 2000.

[43] Peter, M.S., Timmerhaus, K.D. Plant design and economics for chemical engineers 4th ed. New York, NY, USA: McGraw-Hill; 1991.

[44] Overend, R.P. The average haul distance and transportation work factors for biomass delivered to a central plant. Biomass, 1982; 2: 75-79.

CHAPTER 8

Conclusion and Recommendations for Future Research

8.1. Conclusion

Pipeline hydro-transport of agricultural residue biomass (wheat straw and corn stover) was experimentally studied in a 50 mm diameter and 25.5 m long closed-circuit pipeline facility. Several technical, modeling, and economic issues were investigated to understand the feasibility of pipeline hydro-transport of agricultural residue, as well as the technical limitations, equipment performance, governing formulas, and economic viability of such a pipeline system.

A review was first performed on the literature published on pipeline hydro-transport of biomass materials. A series of experiments was conducted on pipeline transport of wood chip-water mixtures over a wide range of pipeline materials, pipeline lengths, pipeline diameters, wood chips moisture contents, wood chip diameters, and wood chip-water mixture concentrations and velocities. It was found that mounting the pipeline horizontally, increasing the pipe diameter, and decreasing mixture solid volume content give the optimum pipeline conditions and reduce the probability of wood chips blockade throughout the pipe. Several investigators also proposed correlations to predict the friction loss of laminar and turbulent wood chip-water mixture flows of various regimes in pipes. A deviation of 30% between estimated values of the friction loss of the same mixture using various correlations and a deviation of 300% between estimated values and experimental measurements were reported in literature, which pointed out the need for additional experimental work. Finally, based on experimental measurements and empirical correlation reported in literature, a few researchers studied the economic feasibility of pipelining wood chip-water mixtures to processing plants. The concept of economy of scale was found to be highly applicable to these biomass pipeline systems. It was shown that the power required and, accordingly, the operating costs of the pipeline system would decrease and the capital costs of the pipeline system would increase with

an increase in solid volume content, decrease in mixture velocity, and increase in pipeline length. Furthermore, capital charges were reported to account for more than 70% of the total transportation cost. Some investigators used friction loss correlations originally proposed for wood chip-water mixtures to estimate pressure drop and associated costs of water mixtures of other sorts of biomass (e.g, corn stover) in pipes. It was found that more research needed to be conducted in this field to develop specific empirical friction loss correlations for specific biomass particles and to understand how the mechanical and economic features would change with the change of biomass type and size.

Apart from several factors affecting initial and operating parameters, biomass particle size/size distribution (PSD) and morphological features are critical in biomass slurry pipeline transport. Therefore, using ImageJ image processing platform, a user-coded plugin was developed in this research to process biomass sample images, measure biomass particle dimensions, and analyse the PSD of knife-milled wheat straw and corn stover, which were pre-classified into four nominal size groups. The particles aspect ratios ranged between 4.51 to 10.08, and 3.71 to 6.71 for wheat straw and corn stover, respectively. Of the three distribution functions tested, the Rosin-Rammler equation best fitted the size distribution of the samples, with least some-of-square error in all scenarios. The particle size reduction (degradation) effect, mainly due to passing through boosting stations' centrifugal pumps impellers, was also studied. The d_{50} of 8.04 mm of 19.2 mm wheat straw particles were reduced by ~29% to 5.74 mm, with 15% within the first hour after pumping. Finally, the micro-scale surface features of wheat straw and corn stover particles were investigated and the corn stover particles were found to be more irregular and to come with many bumps, peaks, and valleys, compared to ribbed wheat straw fibres.

To understand the mechanical specifications of the flow of slurry of agricultural residue biomass, pipeline hydro-transport of wheat straw and corn stover was experimentally investigated in a 50 mm diameter and 25.5 long closed-circuit pipeline facility. While no similarity was observed between friction loss behaviour of the slurries of wood chips and corn stover particles, the slurry of fibrous agricultural residue biomass particles exhibited drag-reducing feature at high flow rates. A maximum drag reduction of 33% could be

achieved with an 8.8% slurry of <3.2 mm corn stover particles at a slurry flow rate of 5.0 m/s. In addition, the dependency of the rheological behaviour of the slurry and the longitudinal pressure gradient on feedstock type, particle dimension, slurry solid mass content, and slurry flow rate were investigated. The solid mass content affected the slurry friction loss behaviour differently than the conventional solid-liquid systems did, and the pressure gradient decreased with increasing solid mass content. The impact of particle size distribution was recognised with broad size distributions producing lower friction losses at high flow rates where 19.2 mm wheat straw particles (which come with a wide size range of 18.4 mm) reduced the pressure drop more noticeably at velocities above 2.5 m/s compared to <3.2 mm particles with a narrow size range of 5.2 mm. Friction loss variations were also well explained based on two different momentum transfer mechanisms, where an increase in flow rate and a corresponding increase in the intensity of turbulence and a decrease in average floc size in the turbulent annulus with a decrease in momentum transfer were both found to increase drag reduction in the transition flow regime before reaching the maximum drag-reduction asymptote. Also, it was concluded that for given particle types and slurry solid mass content, increasing the particle length increases the drag reduction onset velocity.

In the next step, efforts were made to understand how the agricultural residue biomass slurry properties impact the performance of the mechanical equipment throughout the pipeline. The effect of wheat straw fibrous agricultural residue biomass slurry on the performance characteristics of centrifugal slurry pumps was, therefore, experimentally investigated. Pumping a play sand-water mixture through the same closed-circuit pipeline under similar operating conditions and comparing corresponding friction loss behavior with that of agricultural residue biomass slurry demonstrated the unique mechanical behavior of wheat straw-water mixtures. In contrast to all conventional solid-liquid mixtures, the pump head increased with an increase in slurry solid mass content for agricultural residue biomass slurry. It was observed that by using small, fibrous wheat straw particles (< 3.2 mm) under known slurry solid mass contents and pump operating conditions, it is possible to keep the total head and efficiency at the same level as the pump handling pure water and to reduce the power consumption to below that required for pumping pure water alone. Finally, a correlation was developed to predict the

reduction in head of the centrifugal slurry pumps while handling agricultural residue biomass slurries, with respect to the head produced while handling pure water.

With EViews 7.1 econometric software and the nonlinear least square regression analysis method, the experimentally measured pressure gradients were analyzed and an empirical correlation was proposed to predict the slurry pressure gradient as a function of agricultural residue biomass particle type and dimension, slurry solid mass content, and pumping velocity. Considering the similarity between friction loss behavior of the flow of wood pulp fibre suspensions and the flow of agricultural residue biomass slurries and using the CSIR (i_s) scale-up method, the proposed correlation was then modified to take into account the effect of pipe diameter as well.

Finally, the technical parameters and constraints, also the empirical correlations obtained through this course of experimental study, together with the pipeline economic structure proposed by Kumar et al. [1-3], were used to develop a data-intensive techno-economic model to estimate the cost of pipeline hydro-transport of wheat straw and corn stover agricultural residue biomass to a bio-ethanol refinery. This study calculated the delivered costs of feedstock using the pressure drop correlation proposed here specifically for agricultural residue biomass, compared the total cost of delivery with the total cost obtained using wood chip pressure drop correlations, identified the relative advantages of pipeline transport over truck delivery, proposed optimum slurry solid mass content and velocity to obtain the highest throughput at the lowest transport cost, and investigated the effect of pipeline capacity and transport distance on the total cost of delivery. Based on an 8.8% slurry solid mass content, 2.5 m/s slurry velocity, 150 km medium-range distance, and the lowest estimate of the total cost of truck delivery reported (0.22 $/dry t.km), pipeline hydro-transport was found to be economically more viable than truck delivery at capacities of 0.45 M dry t/yr or more for one-way pipelines (without the return of the carrier liquid) and 1.4 M dry t/yr or more for two-way pipelines (with the return of the carrier liquid). Considering the highest estimate of the total cost of truck delivery reported (0.46 $/dry t), pipeline hydro-transport of the same slurry would always cost less than truck delivery for one-way pipelines and would cost less than truck delivery at capacities above 0.35 M dry t/yr for two-way pipelines. All one-way pipelines with

transport capacities of 1.0 M dry t/yr and greater always had fixed and distance variable costs lower than those for hauling by truck. The corresponding capacity for two-way pipelines was 2.0 M dry t/yr.

Investigating the morphological features of agricultural residue biomass revealed their atypical characteristic, specifically their fibrous nature, which helped to understand the unique features of agricultural residue-water mixture flows in pipes, e.g., drag reducing feature, and pumps. The developed empirical correlation also helped to conduct a techno-economic analysis on the pipeline hydro-transport of agricultural residue biomass. By the end of the study, a comprehensive understanding of agricultural residue biomass pipelines was obtained which included the feasibility of the concept, equipment performance, technical limitations, undergoing phenomena, governing rules, and economic parameters. This study was the first major step towards large-scale long-distance agricultural residue biomass pipelines, and results obtained here could be used to design and operate the pipeline and associated equipment.

8.2. Recommendations for Future Research

To understand the mechanical behavior of the slurry of agricultural residue biomass, the effects of operating parameters (e.g., biomass particle type and size, slurry solid mass content, pumping velocity) on slurry friction loss were investigated. All the measurements were made on a 7.5 m long and 50 mm diameter horizontal test section after pumping the slurry for a minimum of 12 hours until the pressure and velocity fluctuations and changes in particle and slurry specifications were damped down to below 1% per hour. However, such design and operating conditions is difficult to maintain in a large-scale long-distance commercial pipes. Although efforts were made to scale up the results obtained here, they were limited to large-scale horizontal pipelines and to slurries pumped for a minimum of 12 hours. To understand how changes in the diameter and orientation of the pipe and the duration of pumping change the slurry mechanical behavior, further research is required, as proposed below:

8.2.1. Investigating the Effect of Pipe Diameter on Slurry Mechanical Behavior

A study should experimentally examine the effect of large pipe diameters on slurry mechanical behavior, specifically slurry pressure drop. Pipes with large diameters (e.g., 100 mm, 200 mm) should be installed parallel to the current 50 mm diameter pipe to investigate:

- the effect of increasing pipe diameter on slurry friction loss
- the effect of pipe diameter on centrifugal pump performance

8.2.2. Studying the Slurry Flow Mechanical Behavior over Vertical, Inclined, and Bent Sections throughout the Pipeline

The purpose of this proposed research is to measure the slurry pressure drop over vertical, inclined, and bent sections throughout the pipeline to understand:

- how the slurry behaves mechanically differently through a vertical test section
- how the slurry behaves mechanically differently through an inclined test section
- how the angle of inclination impacts the slurry mechanical behavior
- how the pressure drop correlations developed for the horizontal section could be adjusted to predict the mechanical behavior over vertical and inclined sections
- how the change in pipe diameter changes the slurry mechanical behavior over the inclined and vertical sections
- how a bent section changes the solid mass content distribution across the cross section
- how much distance the slurry should travel downstream in a bent section before the extra turbulent energy caused by the curvature of the bend is destroyed and the flow field is fully recovered
- how a bent section increases the probability of pipeline blockage

8.2.3. Investigating the Transient Biomass Slurry Behavior

The proposed research is aimed at investigating the slurry mechanical behavior within the first hours the slurry is pumped into the pipeline. The proposed study should:

- model the particle degradation throughout the first few hours
- model the particle moisture content and density variations during the first few hours
- model the carrier liquid and slurry viscosity variations during the first few hours
- understand how the boosting stations and pipeline specifications should be adjusted accordingly in first few kilometers of the pipe
- develop a new model to predict the slurry pressure drop during the first few hours as a function of particle properties and slurry conditions

8.2.4. Measuring Slurry Deposition Velocity

The minimum velocity at which the slurry was successfully pumped for the present study was 0.5 m/s. However, this was the minimum velocity technically achievable and was obtained for a steady slurry flow after 12 hours of pumping. The proposed research should measure the minimum velocity below which the particles will deposit and form a stationary bed. Measurements should be made during the transition period and on the steady slurry flow. More precise pressure transducers should replace the current ones to accurately measure the velocities below 0.5 m/s. To capture the deposition at the early stage, image capturing or tomography techniques should replace visual observations. The proposed research should measure the minimum pumping velocity as a function of material type, particle size, slurry solid mass/volume content, and pumping time.

8.2.5. Using Flow Imaging Techniques to Study Slurry Flow Patterns

Currently, research is being conducted in a laboratory using the Electric Resistance Tomography (ERT) technique. ERT is based on the difference in conductivity of liquid and solid phases. The variation in conductivity across the cross section of the pipe is recorded and analyzed in order to reconstruct the image of the solid-liquid flow passing through the ERT device. Besides the ERT approach, other flow imaging techniques such as MRI and PIV can be also applied to obtain a better understanding of the slurry flow pattern throughout the straight, vertical, and bent sections of the pipeline as a function of particle size, slurry solid mass/volume content, and pumping velocity.

References

[1] Kumar, A., Cameron, J.B., Flynn, P.C. Pipeline transport of biomass. Applied Biochemistry and Biotechnology, 2004; 113: 27-39.

[2] Kumar, A., Flynn, P.C., Cameron, J.B. Large-scale ethanol fermentation through pipeline delivery of biomass. Applied Biochemistry and Biotechnology, 2005; 121: 47-58.

[3] Kumar, A., Flynn, P.C., Cameron, J.B. Pipeline transport and simultaneous saccharification of corn stover. Bioresource Technology, 2005; 96: 819-29.

References

Abulnaga, B.E. (2002). ***Slurry systems handbook***. New York, McGraw-Hill.

Adapa, P., Tabil, L. and Schoenau, G. (2011). "***Grinding performance and physical properties of non-treated and steam exploded barley, canola, oat and wheat straw***." Biomass and Bioenergy, 35 (1): 549-561.

Aden, A., Ruth, M., Ibsen, K., Jechura, J., Neeves, K., Sheehan, J., Wallace, B., Montague, L., Slayton, A. and Lukas, J. (2002). ***Lignocellulosic biomass to ethanol process design and economics utilizing co-current dilute acid prehydrolysis and enzymatic hydrolysis for corn stover***, Report no. NREL/TP-510-32438, National Renewable Energy Laboratory.

Aktiebolaget Pumpindustri. (1966). ***Friction losses in piping systems for paper stock suspensions***. Goteborg, Sweden.

Al-Kindi, G.A. and Shirinzadeh, B. (2007). "***An evaluation of surface roughness parameters measurement using vision-based data***." International Journal of Machine Tools and Manufacture, 47 (3-4): 697-708.

Allaire, S.E. and Parent, L.E. (2003). "***Size guide number and Rosin-Rammler approaches to describe particle size distribution of granular organic-based fertilisers***." Biosystems Engineering, 86 (4): 503-509.

Allen, J. and Browne, M. (1998). "***Logistics management and costs of biomass fuel supply.***" International Journal of Physical Distribution and Logistics Management, 28 (6): 463-477.

Anwer, M., So, R.M.C. and Lai, Y.G. (1989). "***Perturbation by and recovery from bend curvature of a fully-developed turbulent pipe-flow***." Physics of Fluids, 1 (8): 1387-1397.

ASABE (2007). ***Method of determining and expressing particle size of chopped forage materials by screening***. Standard ANSI/ASAE S424.1. American Society of Agricultural and Biological Engineers, St. Joseph, MI, US.

ASABE (2008). ***Moisture measurement for forages***. Standard S358.2 American Society of Agricultural and Biological Engineers, St. Joseph, MI, US.

ASTM (2012). **Standard test method for density, relative density, and absorption of coarse aggregate**. ASTM, Designation C127. American Society for Testing and Materials, West Conshohocken, PA, US.

Bain, A.J. and Bonnington, S.T. (1970). ***The hydraulic transport of solids by pipeline***. Pergamon Press, New York, NY, US.

Bates, S. and Edwards, K. (2014). "***Pipeline transportation rates***." http://www.enbridge.com/~/media/www/Site%20Documents/Delivering%20Energy/Shippers/US/Toledo/Toledo-FERC-No-37-3-0.pdf. Accessed: May 2014.

Bitra, V.S.P., Womac, A.R., Yang, Y.C.T., Miu, P.I., Igathinathane, C., Chevanan, N. and Sokhansanj, S. (2011). "***Characterization of wheat straw particle size distributions as affected by knife mill operating factors***." Biomass and Bioenergy, 35 (8): 3674-3686.

Bitra, V.S.P., Womaca, A.R., Yang, Y.T., Miu, P.I., Igathinathane, C., Chevanan, N. and Sokhansanj, S. (2011). "***Characterization of wheat straw particle size distributions as affected by knife mill operating factors***." Biomass and Bioenergy, 35: 3674-3687.

Blott, S.J. and Pye, K. (2001). "***GRADISTAT: A grain size distribution and statistics package for the analysis of unconsolidated sediments***." Earth Surface Processes and Landforms, 26 (11): 1237-1248.

Bobkowic, A. and Gauvin, W.H. (1965). "***Turbulent flow characteristics of model fibre suspensions***." Canadian Journal of Chemical Engineering, 43 (2): 87-91.

Bodenheimer, V.B. (1969). "***Channeling in bleach towers and friction losses in pulp stock lines***." Southern Pulp and Paper Manufacture, 32 (9): 42.

Bowen, R.L. (1961). "Series of articles." Journal of Chemical Engineering.

Brebner, A. (1964). "***On Pumping of Wood Chips through 4-Inch Aluminum Pipe-Line***." Canadian Journal of Chemical Engineering, 42 (3): 139-142.

Brecht, W. and Heller, H. (1950). "***A study of the friction losses of paper stock suspensions***." Tappi, 33 (9).

British Standards Institution (1985). Testing aggregates part 103: ***Methods for determination of particle size distribution***, Sec. 103.1: Sieve tests.

Brown, N.P. and Heywood, N.I. (1991). ***Surry handling - Design of solid liquid systems***. New York, Elsevier.

Burgess, K.E. and Reizes, J.A. (1976). "***Effect of sizing, specific gravity, and concentration on the performance of the centrifugal slurry pump***." Institution of Mechanical Engineers (London), 190 (36): 391-399.

Bureau of Indian Standards (BIS). (1977). ***Technical requirements for rotodynamic special purpose pumps***, IS: 5120.

Cave, I. (1976). ***Effects of suspended solids on the performance of centrifugal pumps***. Hydrotransport 4, BHRA Fluid Engineering.

Center for Energy Efficiency and Renewable Energy (CEERE). (2006). ***Electric Motor Systems***. Industrial Assessment Center (IAC), University of Massachusetts, Amherst.

Chandler, H.M. (2000). ***RS Means Company - Heavy construction data***, 14th annual edition, Kingston, USA.

Chevanan, N., Womac, A.R., Bitra, V.S.P., Igathinathane, C., Yang, Y.T., Miu, P.I. and Sokhansanj, S. (2010). "***Bulk density and compaction behavior of knife mill chopped switchgrass, wheat straw, and corn stover***." Bioresource Technology, 101 (1): 207-214.

Churchill, S.W. (1977). "***Friction factor equation spans all fluid regimes***." Chemical Engineering, 84 (24): 91-92.

Colebrook, C.F. (1939). "***Turbulent flow in pipes, with particular reference to the transition region between the smooth and rough pipe laws***." Journal of the Institution of Civil Engineers, 11 (4): 133-156.

DeSmet, O. (2014). "***Bales R Us Co***.". http://balesrus.com/. Accessed: May 2014.

Dhuyvetter, K.C. (2014). ***2014 projected custom rates for Kansas***. Kansas State University, Department of Agricultural Economics.

Djalili-Moghaddam, M. and Toll, S. (2006). "***Fibre suspension rheology: effect of concentration, aspect ratio and fibre size***." Rheologica Acta, 45 (3): 315-320.

Dodge, D.W. and Metzner, A.B. (1959). "***Turbulent flow of non-Newtonian systems***." Aiche Journal, 5 (2): 189-204.

Duffy, G.G. (2006). "***Measurement, mechanisms, and models: some important insights into the mechanisms of flow of fibre suspensions***." Annula Transaction of Nordic Rheology Society, 14: 19-31.

Duffy, G.G. (1989). "***The optimum design of pipelines for transporting wood pulp fiber suspensions***." Appita Journal, 42 (5): 358-361.

Duffy, G.G. (1976). "***Review and evaluation of design methods for calculating friction loss in stock piping systems***." Tappi, 59 (8): 124-127.

Duffy, G.G. (2003). "***The significance of mechanistic-based models in fibre suspension flow***." Nordic Pulp and Paper Research Journal, 18 (1): 74-80.

Duffy, G.G. and Abdullah, L. (2003). "***Fibre suspension flow in small diameter pipes***." Appita Journal, 56 (4): 290-295.

Duffy, G.G., Kazi, S.N. and Chen, X.D. (2002). "***Monitoring pulp fibre quality by frictional pressure drop measurement***." Proceeding of 56th Appita Annual Conference: 119-126.

Duffy, G.G. and Lee, P.F.W. (1978). "***Drag reduction in turbulent flow of wood pulp suspensions***." Appita, 31 (4): 280-286.

Duffy, G.G., Moller, K., Lee, P.F.W. and Milne, S.W.A. (1974). "***Design correlations for groundwood pulps and effects of minor variables on pulp suspension flow***." Appita, 27 (5): 327-333.

Duffy, G.G., Moller, K. and Titchene.Al (1972). "***Determination of pipe friction loss***." Appita, 26 (3): 191-195.

Duffy, G.G. and Titchene.Al (1974). "***Design procedures for obtaining pipe friction loss for chemical pulps***." Tappi, 57 (5): 162-166.

Duffy, G.G., Titchener, A.L., Lee, P.F.W. and Moller, K. (1976). "***The mechanism of flow of pulp suspensions in pipes***." Appita, 29 (5): 363-370.

Duffy, M. (2008). "***Estimated costs for production, storage and transportation of switchgrass***." Ag Decision Maker: An agricultural economics and business. from https://www.extension.iastate.edu/agdm/crops/pdf/a1-22.pdf. Accessed: May 2014.

Durand, R. and Condolios, G. (1952). ***The hydraulic trasnport of coal and solids in pipes***. Colloquium on Hydraulic Transport Conference London.

Durst, R.E., Chase, A.J. and Jenness, L.C. (1952). "***An analysis of data on material flow in pipes***." Tappi, 35 (12): 529.

Elliott, D.R. (1960). "***The transportation of pulpwood chips in pipelines***." Pulp and Paper Magazine of Canada, 61 (5): 170-175.

Elliott, D.R. and de Montmorency, W.H. (1963). ***The transportation of pulpwood chips in pipelines.*** Report of an exploratory study. Montreal, Pulp and Paper Institute of Canada.

Ellis, H.S., Redberger, P.J. and Bolt, L.H. (1963). "***Slurries: basic principles and power requirements.***" Industrial and Engineering Chemistry, 55 (8): 18-26.

Engin, T. and Gur, M. (2003). "***Comparative evaluation of some existing correlations to predict head degradation of centrifugal slurry pumps***." Journal of Fluids Engineering-Transactions of the Asme, 125 (1): 149-157.

Engin, T. and Gur, M. (2001). "***Performance characteristics of a centrifugal pump impeller with running tip clearance pumping solid-liquid mixtures***." Journal of Fluids Engineering-Transactions of the Asme, 123 (3): 532-538.

Epplin, F.M. (1996). "***Cost to produce and deliver switchgrass biomass to an ethanol-conversion facility in the Southern Plains of the United States***." Biomass and Bioenergy, 11 (6): 459-467.

Epstein, B. (1948). "***Logarithmico-normal distribution in breakage of solids***." Industrial and Engineering Chemistry, 40 (12): 2289-2291.

European Blenders Association (EBA) (1997). **Handbook of solid fertilizer blending, code of good practices for quality**. Le Pontoury, Montviron, France.

Faddick, R.R. (1963). ***The aqueous transport of pulpwood chips in a four inch aluminum pipe***. Kingston, Ontario, Queen's University. M.Sc.

Faddick, R.R. (1970). ***Hydraulic transportation of solids in pipelines***. Bozeman, Montana State University. Ph.D. .

Fairbank, L.C. (1942). ***Effect on the characteristics of centrifugal pumps***. Solids in Suspension Symposium.

Fangary, Y.S., Ghani, A.S.A., ElHaggar, S.M. and Williams, R.A. (1997). "***The effect of fine particles on slurry transport processes.***" Minerals Engineering, 10 (4): 427-439.

Flügel, E. (2004). ***Microfacies of carbonate rocks: analysis, interpretation and application***. Springer.

Fock, H., Claesson, J., Rasmuson, A. and Wikstrom, T. (2011). "***Near wall effects in the plug flow of pulp suspensions***." Canadian Journal of Chemical Engineering, 89 (5): 1207-1216.

Folk, R.L. (1974). ***Petrology of sedimentary rocks***. Austin, Texas, Hemphill Publishing Co.

Folk, R.L. and Ward, W.C. (1957). "***Brazos river bar: a study in the significance of grain size parameters.***", Journal of sedimentary petrology, 27: 3-26.

Forrest, F. and Grierson, G.H.A. (1931). "***Friction losses in cast iron pipe carrying paper stock***", Paper Trade, 92: 39-41.

Gahlot, V.K., Seshadri, V. and Malhotra, R.C. (1992). "***Effect of density, size distribution, and concentration of solid on the characteristics of centrifugal pumps***." Journal of Fluids Engineering-Transactions of the Asme, 114 (3): 386-389.

Gandhi, B.K., Singh, S.N. and Seshadri, V. (2001). "***Performance characteristics of centrifugal slurry pumps***." Journal of Fluids Engineering-Transactions of the Asme, 123 (2): 271-280.

Gaudin, A.M. and Meloy, T.P. (1962). "***Model and a comminution distribution equation for single fracture.***" Transactions of the Society of Mining Engineers of Aime, 223 (1): 40-43.

Genić, S., Arandjelović, I., Kolendić, P., Jarić, M., Budimir, N. and Genić, V. (2011). "***A review of explicit approximations of Colebrook's equation***." FME Transactions, 39 (2): 67-71.

Gibert, R. (1960). ***Hydraulic transport and discharge of mixtures in pipes***, Report by Annals of Roads and Bridges.

Gillies, R.G. and Shook, C.A. (1991). "***A deposition velocity correlation for water slurries.***" Canadian Journal of Chemical Engineering, 69 (5): 1225-1228.

Glassner, D., Hettenhaus, J. and Schechinger, T. (1998). ***Corn stover collection project***. Bioenergy 1998 - Expanding Bioenergy Partnerships.

Gow, J.L. (1971). ***Hydraulic transport of woodchips in pipelines***. Bozeman, Montana State University.

Godwin Pumps. http://www.godwinpumps.com/en/index.php/godwin-products/cd-range/cd80m/, Accessed: Feb. 2014.

Gubba, S.R., Ingham, D.B., Larsen, K.J., Ma, L., Pourkashanian, M., Qian, X., Williams, A. and Yan, Y. (2012). "***Investigations of the transportation characteristics of biomass fuel particles in a horizontal pipeline through CFD modelling and experimental measurement***." Biomass and Bioenergy, 46: 492-510.

Gupta, A. and Yan, D. (2006). ***Mineral processing design and operation: An introduction***. Amsterdam, Netherlans, Elsevier.

Harada, T. (2002). "***Energy consumption in utilization of woody biomass***." Wood Industry, 57 (11): 480-483.

Hellstrom, L.H.O. and Smits, A.J. (2012). ***Turbulent pipe flow through a 90 degree bend***. Fluid Mechanics Meeting, 1000 Islands, Ontario, Canada.

Horo, K. and Niskanen, T. (1978). "***Centrifugal pumps - research on pumping paper stock.***" Tappi, 61 (1): 67-70.

Horo, K. and Niskanen, T. (1979). "***Pumping paper stock efficiently***." Pumps-Pompes-Pumpen, 156: 427-429.

Hunt, W.A. (1962). ***Continuous flow transport of low value forst products by hydraulic pipeline*** [Unpublished report to Intermountain Forest and Range Experiment Station]. Bozman, Montana.

Hunt, W.A. (1967). "***Economic analysis of wood chip pipeline***." Forest Products, 17 (9): 68-74.

Hunt, W.A. (1976). ***Friction factors for mixtures of wood chips and water flowing in pipelines***. 4th International Conference on the Hydraulic Transport of Solids in Pipes, Alberta, Canada.

Hwang, S.H., Lee, K.P., Lee, D.S. and Powers, S.E. (2002). "***Models for estimating soil particle-size distribution.***" Soil Science Society of America, 66: 1143-1150.

Igathinathane, C., Melin, S., Sokhansanj, S., Bi, X., Lim, C.J., Pordesimo, L.O. and Columbus, E.P. (2009). "***Machine vision based particle size and size distribution determination of airborne dust particles of wood and bark pellets***." Powder Technology, 196 (2): 202-212.

Igathinathane, C., Pordesimo, L.O. and Batchelor, W.D. (2008). ***Ground biomass sieve analysis simulation by image processing and experimental verification of particle size distribution.*** ASABE Annual International Meeting. Rhode Island Convention Center, ASABE.

Igathinathane, C., Pordesimo, L.O., Columbus, E.P., Batchelor, W.D. and Methuku, S.R. (2008). "***Shape identification and particles size distribution from basic shape parameters using ImageJ***." Computers and Electronics in Agriculture, 63 (2): 168-182.

Igathinathane, C., Pordesimo, L.O., Columbus, E.P., Batchelor, W.D. and Sokhansanj, S. (2009). "***Sieveless particle size distribution analysis of particulate materials through computer vision***." Computers and Electronics in Agriculture, 66 (2): 147-158.

Igathinathane, C., Prakash, V.S.S., Padma, U., Babu, G.R. and Womac, A.R. (2006). "***Interactive computer software development for leaf area measurement***." Computers and Electronics in Agriculture, 51 (1-2): 1-16.

Ingersoll-Rand Co. ***Cameron Hydraulic Data***. New York, NY.

Internatinal Standards Organization (ISO). (2010). ***Guidance for the use of repeatability, reproducibility and trueness estimates in measurement uncertainty estimation***, ISO 21748: 2010(E).

Scandinavian Pulp, Paper and Board Testing Committee. ***Standard SCAN CM 40:88***.

Jenkins, B.M., Dhaliwal, R.B., Summers, M.D., Bernheim, L.G., Lee, H., Huisman, W. and Yan, L. (2000). ***Equipment performance, costs, and constraints in the commercial harvesting of rice straw for industrial applications***. American Society of Agricultural Engineers (ASAE) Conference.

Kato, H. and Mizunuma, H. (1983). "***Frictional resistance in fiber suspensions (part 1): pipe-flow.***" Bulletin of the Jsme-Japan Society of Mechanical Engineers, 26 (212): 231-238.

Kazi, S.N., Duffy, G.G. and Chen, X.D. (1999). "***Heat transfer in the drag reducing regime of wood pulp fibre suspensions.***" Chemical Engineering Journal, 73 (3): 247-253.

Kazim, K.A., Maiti, B. and Chand, P. (1997). "***A correlation to predict the performance characteristics of centrifugal pumps handling slurries***." Proceedings of the Institution of Mechanical Engineers Part a-Journal of Power and Energy, 211 (2): 147-157.

Kazim, K.A., Maiti, B. and Chand, P. (1997). "***Effect of drag reducing polymers on the performance characteristics of centrifugal pumps handling slurries***." Journal of Polymer Materials, 14 (3): 245-250.

Kazim, K.A., Maiti, B. and Chand, P. (1997). "***Effect of particle size, particle size distribution, specific gravity and solids concentration on centrifugal pump performance***." Powder Handling and Processing, 9 (1): 27-32.

Kerekes, R.J. and Schell, C.J. (1995). "***Effects of fiber length and coarseness on pulp flocculation***." Tappi Journal, 78 (2): 133-139.

Kerekes, R.J.E. and Douglas, W.J.M. (1972). "***Viscosity properties of suspensions at limiting conditions for turbulent drag reduction***." Canadian Journal of Chemical Engineering, 50 (2): 228-231.

Kim, S. and Dale, B.E. (2004). "***Global potential bioethanol production from wasted crops and crop residues.***" Biomass and Bioenergy, 26 (4): 361-375.

Kumar, A., Cameron, J.B. and Flynn, P.C. (2003). "***Biomass power cost and optimum plant size in western Canada.***" Biomass and Bioenergy, 24 (6): 445-464.

Kumar, A., Cameron, J.B. and Flynn, P.C. (2005). "***Large-scale ethanol fermentation through pipeline delivery of biomass.***" Applied Biochemistry and Biotechnology, 121: 47-58.

Kumar, A., Cameron, J.B. and Flynn, P.C. (2005 (b)). "***Pipeline transport and simultaneous saccharification of corn stover.***" Bioresource Technology, 96 (7): 819-829.

Kumar, A., Cameron, J.B. and Flynn, P.C. (2004). "***Pipeline transport of biomass.***" Applied Biochemistry and Biotechnology, 113: 27-39.

Kwan, A.K.H., Mora, C.F. and Chan, H.C. (1999). "***Particle shape analysis of coarse aggregate using digital image processing***." Cement and Concrete Research, 29 (9): 1403-1410.

Kwan, A.K.H., Mora, C.F. and Chan, H.C. (1998). "***Particle size distribution analysis of coarse aggregate using digital image processing***." Cement and Concrete Research, 28 (6): 921-932.

Lee, P.F.W. and Duffy, G.G. (1976 (a)). "***Analysis of drag reducing regime of pulp suspension flow.***" Tappi, 59 (8): 119-122.

Lee, P.F.W. and Duffy, G.G. (1976). "***Relationships between velocity profiles and drag reduction in turbulent fiber suspension flow***." Aiche Journal, 22 (4): 750-753.

Lee, P.F.W. and Duffy, G.G. (1976 (b)). "***Velocity profiles in drag reducing regime of pulp suspension flow***." Appita, 30 (3): 219-226.

Li, Z., Hong, T.S., Wu, W.B. and Liu, M.J. (2007). "***A novel method of object identification and leaf area calculation in multi-leaf image***." ASABE Paper No: 073047.

Liu, H., Noble, J., Zuniga, R. and Wu, J. (1995). ***Economic analysis of coal log pipeline transportation of coal***. Report No. 95-1. Capsule Pipeline Research Center (CPRC), University of Missouri, Columbia, USA.

Lokon, H.B., Johnson, P.W. and Horsley, R.R. (1982). ***A scale-up model for predicting head loss gradients in iron ore slurry pipelines***. Hydrotransport 8. Johannesburg, South Africa.

Luk, J. (2010). ***Pipeline transport of wheat straw slurry***. University of Alberta.

Luk, J., Mohammadabadi, H.S. and Kumar, A. (2014). "***Pipeline transport of biomass: Experimental development of wheat straw slurry pressure loss gradients*** ", Biomass and Bioenergy.

Luthi, O. (1987). ***The flow of MC fibre suspensions***. TAPPI Engineering Conference, Atlanta.

Marrison, C.I. and Larson, E.D. (1995***). Cost versus scale for advanced plantation-based biomass energy systems in the US and Brazil***. Proceeding of Second Biomass Conference of the Americas: Energy, Environment, Agriculture, and Industry.

Matousek, V. (2002). "***Pressure drops and flow patterns in sand-mixture pipes***." Experimental Thermal and Fluid Science, 26 (6-7): 693-702.

McKendry, P. (2002). "***Energy production from biomass (part 1): overview of biomass***." Bioresource Technology, 83 (1): 37-46.

Metzner, A.B. and Reed, J.C. (1955). "***Flow of non-Newtonian fluids - correlation of the laminar, transition, and turbulent flow regions***." Aiche Journal, 1 (4): 434-440.

Meyer, H. (1964). "***An analytical treatment of the laminar flow of annulus forming fibrous suspensions in vertical pipes***." Tappi, 47: 78-84.

Mez, W. (1984). ***The influence of solids concentration, solids density and grain size distribution on the working behaviour of centrifugal pumps***. Hydrotransport 9, BHRA Fluid Engineering.

Mohamadabadi, H.S. (2009). ***Characterization and pipelining of biomass slurries***. University of Alberta. M.Sc.

Moller, K. (1976). "***Correlation of pipe friction data for paper pulp suspensions***." Industrial and Engineering Chemistry Process Design and Development, 15 (1): 16-19.

Moller, K. (1976). "***General correlations of pipe friction data for pulp suspensions***." Tappi, 59 (8): 111-114.

Moller, K., Duffy, G.G. and A., T. (1971). "***Laminar plug flow regime of paper pulp suspensions in pipes.***" Svensk Papperstidning-Nordisk Cellulosa, 74 (24): 829-834.

Moller, K., Duffy, G.G. and A.L., T. (1973). "***Design correlation for flow of pulp suspensions in pipes.***" Appita, 26 (4): 278-282.

Moody, L.F. (1947). "***An approximate formula for pipe friction factors***." Transactions of the ASME, 69: 1005-1006.

Nailen, R.L. (2002). ***Just how important is drive motor efficiency***? Chicago, Barker Publications, Inc.

Nardi, J. (1959). "***Pumping solids through a pipeline***." Pipeline News: 26-33.

National Electrical Manufacturer Association (NEMA). (2003). The NEMA Premium™ efficiency electric motor program. ***The NEMA Premium™ efficiency levels. MG 1-2003***, Tables 12-12 and 12-13, NEMA Standards Publication.

Natural Resources Canada (NRC). (2004).Technical fact sheet, Premium efficiency motors, Catalog No. M144-21/2003E.

Newitt, D.M. and Richardson, J.F. (1955). "***Hydraulic Conveying of Solids***." Nature, 175 (4462): 800-801.

O'donnell, J.P. (1964). "***Diversification of owners is common in products pipeline***.", Oil and Gas Journal, 62 (27): 88-100.

Pande, H., Rao, N.J., Kapoor, S.K. and Roy, D.N. (1999). "***Hydrodynamic behavior of nonwood fiber suspensions***." Tappi, 82 (6): 140-145.

Paul, T., Duffy, G. and Chen, D. (2001). "***New insights into the flow of pulp suspensions.***" Tappi Solutions, 1 (1).

Pearson, T.C. and Brabec, D.L. (2006). "***Camera attachment for automatic measurement of single-wheat kernel size on a perten SKCS 4100***." Applied Engineering in Agriculture, 22 (6): 927-933.

Perfect, E., Xu, Q. and Terry, D.L. (1998). "***Improved parameterization of fertilizer particle size distribution.***" Journal of Aoac International, 81 (5): 935-942.

Perlack, R.D. and Turhollow, A.F. (2002). ***Assessment of options for the collection, handling, and transport of corn stover***. http://bioenergy.ornl.gov/pdfs/ornltm-200244.pdf. Report no. ORNL/TM-2002/44. Accessed: 2002.

Peter, M.S. and Timmerhaus, K.D. (1991). ***Plant design and economics for chemical engineers***. New York, NY, USA, McGraw-Hill.

Powell, R.L., Morrison, T.G. and Milliken, W.J. (2001). "***Apparent viscosity of suspensions of rods using falling ball rheometry.***" Physics of Fluids, 13 (3): 588-593.

Quantitative Micro Software (QMS). (2010). EViews 7.1. IHS Global Inc., Irvine, CA, USA.

Radin, I., Zakin, J.L. and Patterson, G.K. (1975). "***Drag reduction in solid-fluid systems***." Aiche Journal, 21 (2): 358-371.

Rao, N.J. (1985). "***Process piping design for pulp suspensions*** ", IPPTA, 22 (4): 27-35.

Rasband, W.S. (2008). "http://rsb.info.nih.gov/ij/index.html, U.S. National Institutes of Health, Accessed September 2011."

Rasband, W.S. (2008). "***ImageJ***." http://rsb.info.nih.gov/ij/index.html. Accessed September 2011.

Riegel, P.S. (1966). Tappi, 49 (3): 32A.

Rodieck, B. (2007). ***Ellipsefitter class of ImageJ***, http://rsb.info.nih.gov/ij/developer/source/ij/process/EllipseFitter.java.html, Accessed: September 2011.

Rosin, P. and Rammler, E. (1933). "***The laws governing the fineness of powdered coal***." Journal of the Institute of Fuel, 7: 26-39.

Rowe, M. (1970). "***Measurements and computations of flow in pipe bends***." Journal of Fluid Mechanics, 43: 771-783.

Ruth, M. (1999). ***Large scale ethanol facilities and short cut for changing facility size***. Internal Report, National Renewable Energy Laboratory Technical Memo.

Sauermann, H.B. and Webster, I.W. (1975). ***Scaling-up slurry pressure gradients from test loop data***. CSIR Report No. ME 1415. Pretoria, Australia

Sawai, T., Kajimoto, T., Ohmasa, M., Shibue, T. and Nishi, K. (2011). ***Hydraulic transportation system of chips by Hilly Terrain Pipelines.*** 22nd International Symposium on Transport Phenomena. Delft, The Netherlands

Schaan, J., Sumner, R.J., Gillies, R.G. and Shook, C.A. (2000). "***The effect of particle shape on pipeline friction for Newtonian slurries of fine particles***." Canadian Journal of Chemical Engineering, 78 (4): 717-725.

Scheer, A.C. (1962). ***Survey on wood chips transportation charges*** [Unpublished report to Intermountain Forest and Range Experiment Station]. Bozman, Montana.

Schmidt, R.E. (1965). ***An investigation of the effects of pressure and time on the specific gravity, moisture content and volume of wood chips in a water slurry*** [dissertation]. Civil Engineering, Montana State University. M.Sc.

Sellers, D. (2013). "***Variable frequency drive system efficiency – part 1, facility dynamic engineering***, http://av8rdas.wordpress.com/2010/12/18/variable-frequence-drive-system-efficiency, Accessed: May, 2013."

Sellgren, A. (1979). "***Performance of a centrifugal pump when pumping ores and industrial minerals***.", Hydrotransport, 1: 291-304.

Sellgren, A. and Addie, G. (1989). ***Effect of solids on large centrifugal pump head and efficiency.*** CEDA Dredging Day. Netherlands.

Sellgren, A., Addie, G. and Scott, S. (2000). "***The effect of sand-clay slurries on the performance of centrifugal pumps***." Canadian Journal of Chemical Engineering, 78 (4): 764-769.

Sellgren, A. and Addie, G.R. (1993***). Solid effects on characteristics of centrifugal slurry pumps***. Hydrotransport 12, Belgium.

Shahin, M.A. and Symons, S.J. (2005). "***Seed sizing from images of non-singulated grain samples***.", Canadian Biosystems Engineering, 47: 49-55.

Shahin, M.A., Symons, S.J. and Poysa, V.W. (2006). "***Determining soya bean seed size uniformity with image analysis.***" Biosystems Engineering, 94 (2): 191-198.

Sheth, K.K., Morrison, G.L. and Peng, W.W. (1987). "***Slip factors of centrifugal slurry pumps.***" Journal of Fluids Engineering-Transactions of the Asme, 109 (3): 313-318.

Shook, C.A., Gillies, R.G. and Sanders, R.S. (2002***). Pipeline hydrotransport with applications in the oil sand industry***. Saskatoon, SK, SRC Publicatin.

Shook CA, S.R. (2002). ***Pipeline hydrotransport with application in oilsand industry***. SRC publication No. 11508-1E02.

SIL Industrial Minerals Inc. http://www.sil.ab.ca/images/stories/pdf/Products/playsand.pdf, Accessed: Jan, 2014.

Sokhansanj, S., Turhollow, A., Cushman, J. and Cundiff, J. (2002). "***Engineering aspects of collecting corn stover for bioenergy.***" Biomass and Bioenergy, 23 (5): 347-355.

Soucy, A. (1968). Data supplied to R.R. Faddick for Ph.D. thesis by Laval University. Quebec City, Quebec.

Sun, D.W. and Brosnan, T. (2002). "***Inspection and grading of agricultural and food products by computer vision systems - a review***." Computers and Electronics in Agriculture, 36 (2-3): 193-213.

Sulzer Pumps. (2010). Suzler Pumps - Chapter three - ***Acceptance tests with centrifugal pumps***. Centrifugal Pump Handbook (Third Edition). Oxford, Butterworth-Heinemann**:** 69-88.

TAPPI (2007). The Technical Association of the Pulp and Paper Industry (TAPPI). ***Generalized method for determining the pipe friction loss of flowing pulp suspensions***. TIP 0410-14. Atlanta, GA, USA.

Technical Association of the Pulp and Paper Industry (TAPPI) (2010). ***TAPPI usefull methods NO.21, SCAN CM 40:88***

Thomas, A.D. (1976). "***Scale-up methods for pipeline transport of slurries***." International Journal of Mineral Processing, 3 (1): 51-69.

TRAPIL. Petrolum pipeline transport company. ***How pipelines work***? Available from http://www.trapil.fr/uk/comcamarche4.asp. Accessed: April 2013.

UN (1991). ***Green energy: biomass fuels and the evironment***. Geneva, Switzerland United Nations.

U.S. Department of Energy, Advanced Manufacturing Office. (2012). ***Adjustable speed drive part-load efficiency - Motor systems tip sheet#11***. Washington, DC, US.

United States Department of Energy. (1992). ***Energy Policy Act of 1992***, https://www1.eere.energy.gov/femp/regulations/epact1992.html. Accessed: May, 2013.

Vaezi, M., Katta, A.K. and Kumar, A. (2014). "***Investigation into the mechanisms of pipeline transport of slurries of wheat straw and corn stover to supply a bio-refinery***." Biosystems Engineering, 118: 52-67.

Vaezi, M. and Kumar, A. (2014). "***Devevopment of correlations for the flow of agricultural waste biomass slurries in pipes*** ". Biosystems Engineering, XX (XX).

Vaezi, M. and Kumar, A. (2014). "***The flow of wheat straw suspensions in an open-impeller centrifugal pump.***" Biomass and Bioenergy, XX (XX).

Vaezi, M. and Kumar, A. (2014). "***Pipeline hydraulic transport of biomass materials: A review.***" Biomass and Bioenergy, XX (XX).

Vaezi, M., Pandey, V., Kumar, A. and Bhattacharyya, S. (2013). "***Lignocellulosic biomass particle shape and size distribution analysis using digital image processing for pipeline hydro-transportation.***" Biosystems Engineering, 114 (2): 97-112.

Vaezi, M.N., B. and Kumar, A. (2014). "***Is pipeline hydro-transport of wheat straw and corn stover to a biorefinery realistic?***" Biofuels, Bioproducts and Biorefining, XX (XX).

Vaseleski, R.C. and Metzner, B. (1974). "***Drag reduction in the turbulent flow of fiber suspensions.***" AlChE, 20 (2): 301-308.

Viamajala, S., McMillan, J.D., Schell, D.J. and Elander, R.T. (2009). "***Rheology of corn stover slurries at high solids concentrations - Effects of saccharification and particle size.***" Bioresource Technology, 100 (2): 925-934.

Visen, N.S., Paliwal, J., Jayas, D.S. and White, N.D.G. (2004). "***Image analysis of bulk grain samples using neural networks***." Canadian Agricultural Engineering, 46 (7): 11-15.

Vocadlo, J.J., Koo, J.K. and Prang, A.J. (1974). ***Performance of centrifugal pumps in slurry service.*** Hydrotransport 3, BHRA Fluid Engineering.

Wallace, B., Yancey, M. and Easterly, J. (2003). ***Bioethanol co-location with a coal-fired power plant.*** 25th Symposium on Biotechnology for Fuels and Chemicals Breckenridge, CO.

Wallbom-Carlson, A. (1998). "***Energy comparison. VFD vs. on-off controlled pumping stations.***" Scientific impeller, ITT Flygt AB: 29-32.

Wang, W. and Paliwal, J. (2006). "***Separation and identification of touching kernels and dockage components in digital images***." Canadian Biosystems Engineering, 48 (7): 1-7.

Wasp, E.J., Aude, T.C., Thompson, T.L. and Bailey, C.D. (1967). "***Economics of chip pipelining.***" Tappi, 50 (7): 313-318.

Wasp, E.J., Regan, T.J., Withers, J., Cook, P.A.C. and Clancey, J.T. (1963). "***Crosscountry coal pipeline hydraulics***." Pipeline News, 35 (7): 20-28.

Webster, I.W. and Sauermann, H.B. (1978). "***Pressure gradient scale-up methods for slurry pipelines.***" The South African Mechanical Engineer, 28: 312-317.

Weston, M.D. and Worthen, L. (1987). ***Chevron Phosphate slurry pipeline commissioning and start-up.*** 12th International Conference on Coal and Slurry Technology. Washington, DC.

White, F.M. (2011). ***Fluid mechanics***. New York, N.Y., McGraw Hill.

Wilson, G. (1987). ***Effect of slurries on centrifugal pump performance***. Fourth International Pump Symposium, Houston, TX, USA.

Wilson, K.C. (1989). ***Two mechanisms for drag reduction. Drag reduction in fluid flows : techniques for friction control***. Ed. Sellin H.R.J. and Moses, R.T.,. New York, NY, USA, Chichester .

Wilson, K.C., Addie, G.R., Sellgren, A. and Clift, R. (2006). ***Slurry transport using centrifugal pumps***. New York, NY, USA, Springer.

Womac, A.R., Igathinathane, C., Bitra, P., Miu, P., Yang, T. and Sokhansanj, S. (2007). ***Biomass pre-processing size reduction with instrumented mills***. ASABE Paper No. 076046.

Wood, D.J. (1966). "***An explicit friction factor relationship***." Civil Engineering, 36 (12): 60-61.

Worster, R.C. (1952). ***Hydraulic transport of solids***. Colloquim on hydraulic transport of coal conference London.

Yadeta, R. and Durst, R.E. (1970). ***The behavior of gas-water-fiber systems in centrifugal pumps***. Hydrotransport 1. Coventry, UK.

Zandi, I. and Govatos, G. (1967). "***Hetrogeneous flow of solids in pipelines***." ASCE Journal of the Hydraulic Devision, 93: 145-159.